Title
Discovery and Elucidation of Novel Regulators of Cell Division

Author
Clutario, Kevin Morales

Publication Date
2022

Peer reviewed|Thesis/dissertation

UNIVERSITY OF CALIFORNIA

Los Angeles

Discovery and Elucidation of Novel Regulators of Cell Division

A dissertation submitted in satisfaction of the requirements for the degree

Doctor of Philosophy in Biochemistry, Molecular and Structural Biology

by

Kevin Clutario

2022

ABSTRACT OF THE DISSERTATION

Discovery and Elucidation of Novel Regulators of Cell Division

by

Kevin Clutario

Doctor of Philosophy in Biochemistry, Molecular and Structural Biology

University of California, Los Angeles, 2022

Professor Margot Elizabeth Quinlan, Co-Chair

Professor Jorge Torres, Co-Chair

Mitotic cell division is a process requiring a highly coordinated dance between many enzymes, substrates and metabolites to result in the segregation of identical sets of daughter chromosomes. A hallmark of cancer is the ability to perturb this process in ways that increase the proliferation of cancer cells. We have studied several aspects of cellular division in order to further elucidate how cancer cell progression can occur in human disease. Mammalian cell division is a biological process that has been studied for decades and important discoveries often coincide with the development of novel tools and techniques. I have developed a new cell-based high-throughput screening

tool that combines CRISPR/Cas9 technology with the Fluorescence Ubiquitin Cell Cycle Indicator system (FUCCI) for assessing the cell cycle effects of knocking out genes of interest. This tool provides a genome-encoded cell cycle phase indicator system and dox-inducible Cas9 for use with guide RNA libraries for future screens.

Many of the proteins our lab studies were initially identified through either proteomic analysis or genomic screening. While these approaches have yielded interesting hits, they have focused exclusively on protein-based regulation of cell cycle progression and division. To this end we performed a high-throughput screen of 1,200 different naturally occurring metabolites in order to find novel affectors of the cell cycle and have identified 180 putative. These results will provide the basis for future projects analyzing these metabolites and their roles in cell cycle regulation.

Ribosome biogenesis has long been linked to cell proliferation and in my studies, I characterized Rexo4, an exonuclease responsible for processing nascent ribosomal RNA. Recent studies suggest that Rexo4 is a biomarker for cancer disease and is seen to be upregulated in cancer cells at both the mRNA and protein level. My work has determined that Rexo4 is a requirement for cell cycle progression in mammalian cells and that both its nucleolar localization and exonuclease activity are required for cell proliferation.

The dissertation of Kevin Clutario is approved.

Guillaume Chanfreau

James Akira Wohlschlegel

Margot Elizabeth Quinlan, Committee Co-Chair

Jorge Z. Torres, Committee Co-Chair

University of California, Los Angeles

2022

Dedication

I would like to dedicate this work to my mom, whose fight against cancer inspired my own.

Table of Contents

List of Tables and Figures

Appendix I

Acknowledgements

I have so many people to thank for getting me here. There is that idiom that says “it takes a village to raise a child” and for me it was more like a large city. I have to start by thanking my previous mentors who have been instrumental in my scientific upbringing: Dr. Magda Polymenidou, Dr. Clotilde Lagier-Tourenne, and Dr. Andrew Holland. I cannot overstate the amount of personal and intellectual growth I experienced under their wings. I would like to also thank Dr. Georges Siddiqi, who got me my first undergraduate research position, which coincidentally required skateboarding every weekend.

I would like to thank my friends for always being there for me, especially when I needed to get my mind away from lab and experiments. Balance is exceptionally hard to find in graduate school and adventures were always available when I needed I them. I would like to also thank Dr. Katie Baker, who was always there to listen to me gripe about science and knew where I was coming from.

I am thankful for all the Torres lab members past and present who made the lab a fun place to be, provided so much help with experimentation, and most importantly were willing to ingest similar levels of caffeine with me. I would like to specifically thank Dr. Yenni Garcia and Dr. Erick Velasquez, who encouraged me to get help when they recognized how dark of a place I had gotten to. I would not have made it through graduate school if I did not listen to them.

I would like to thank my mentor, Dr. Jorge Torres for everything. I am thankful for all of the scientific mentoring, but I am eternally grateful for the patience, kindness,

understanding and willingness to listen that Dr. Torres has shown me over these years. Dr. Torres has taught me not only how to be a better scientist but how to be a better person and I cannot explain how important that is to me. Once again, just thank you so much.

Now, I would like to thank my family for the endless support. I would like to thank my parents for always encouraging me to chase what makes me happy, I have only ever wanted to make them proud. I would like to thank my siblings Adrian and Matthew for always being a phone call or text away when I needed anything. Everything I do is because you believe I am capable.

Lastly, I would like to thank my wonderful partner, Nancy. It is hard for me to put into words how appreciative I am that she is in my life and the amount of support she has given me throughout this process. I have had so many bad times and rough patches during this PhD program and she has always been there to pick me up and put me back together. Regardless of how lab went for the day, it was always comforting knowing there was someone waiting at home excited to see me, regardless of what my western blots looked like. Thank you, I love you, and sorry it took so long, hun.

--Kevin

CURRICULUM VITAE

Kevin Morales Clutario

EDUCATION

University of California San Diego, La Jolla CA. September 2006 – June 2011

B.S., Biochemistry, GPA: 3.2/4.0

RESEARCH EXPERIENCE

Ph.D. Candidate: Biochemistry, Molecular and Structural Biology (Torres Lab)

Sep 2015– Dec 2022

- Performed proteomic analysis of protein domains to identify putative interacting proteins, elucidated role of exonuclease within cell division, developed high-throughput organic molecule screen to identify novel regulators of cell division.

Research Assistant: Johns Hopkins Medical Institute (Holland Lab)

Mar 2013 – Sep 2015

- Developed novel auxin-inducible degron system in human cancer cell lines, performed siRNA phosphatase screen to identify novel regulators of centrosome biogenesis, established and maintained mouse colony.

Research Assistant: UC San Diego, Ludwig Cancer Center (Cleveland Lab)

June 2010 –Mar 2013

- Analyzed human and mouse brain tissue gene expression and splicing changes of RNA binding proteins in amyotrophic lateral sclerosis. Optimized cell sample preparation for RNA-SEQ.

Research Assistant: **UC Berkeley, Department of Chemistry (Bell Lab)**

June 2009 – Sep 2009

- Synthesized catalyst supports and analyzed alternatives to platinum/tin catalysts via gas chromatography and mass spectrometry.

AWARDS AND RECOGNITION

NIH Tumor Cell Biology Training Fellowship (September 2017– National)

University Admission Fellowship (September 2015 – School)

PUBLICATIONS

Garcia Y.A**.**, Velasquez E.F., Gao L.W., Gholkar A.A., **Clutario K.M.**, Cheung K., Williams-Hamilton T., Whitelegge J.P., and Torres J.Z. “Mapping Proximity Associations of Core Spindle

Assembly Checkpoint Proteins." J Proteome Res. 2021 Jul 2;20(7):3414-3427. doi:10.1021/acs.jproteome.0c00941.

Park E.M., Scott P.M., **Clutario K.M.**, Cassidy K.B., Zhan K., Gerber S.A., Holland A.J. "WBP11 is required for splicing the TUBGCP6 pre-mRNA to promote centriole duplication." J Cell Biol. 2020 Jan 6:219(1)e.201904203. doi: 10.1083/jcb.201904203.

Lambrus B.G., Daggubati V., Uetake Y., Scott P.M., **Clutario K.M.**, Sluder G., Holland A.J. "A USP28-53BP1-p53-p21 signaling axis arrests growth after centrosome loss or prolonged mitosis." J Cell Biol. 2016 Jul 18;214(2):143-53. doi 10.1083/jcb.201604054.

Lambrus B.G., Uetake Y., **Clutario K.M.**, Daggubati V., Snyder M., Sluder G., Holland A.J. "p53 protects against genome instability following centriole duplication failure." J Cell Biol. 2015 Jul 6;210(1):63-77. Doi:10.1083/jcb.201502089

Moyer T.C., **Clutario K.M.**, Lambrus B.G., Daggubati V., Holland A.J. "Binding of STIL to Plk4 activates kinase activity to promote centriole assembly." J Cell Biol. 2015 Jun 22;209(6):863-78. doi: 10.1083/jcb.201502088.

Anorld E.S., Ling S.C., Huelga S.C., Lagier-Tourenne C., Polymenidou M., Ditsworth D., Kordasiewicz H.B., McAlonis-Downes M., Platoshyn O., Parone P.A., Da Cruz S., **Clutario K.M.**, Swing D., Tessarollo L., Marsala M., Shaw C.E., Yeo G.W., Cleveland D.W. "ALS-linked TDP-43 mutations produce aberrant RNA splicing and adult-onset motor neuron disease without aggregation or loss of nuclear TDP-43." Proc Natl Acad Sci U S A. 2013 Feb 19;110(8):E736-45. doi: 10.1073/pnas.1222809110.

Lagier-Tourenne C., Polymenidou M., Hutt K.R., Vu A.Q., Baughn M., Huelga S.C., **Clutario K.M.**, Ling S.C., Liang T.Y., Mazur C., Wancewicz E., Kim A.S., Watt A., Freier S., Hicks G.G., Donohue J.P., Shiue L., Bennet C.F., Ravits J., Cleveland D.W., Yeo G.W. "Divergent roles of ALS-linked proteins FUS/TLS and TDP-43 intersect in processing long pre-mRNAs." Nat Neurosci. 2012 Nov 15(11):1488-97. doi: 10.1038/nn.3230.

Academic Conferences/Presentations

Clutario, K.M. (2018). Analysis of STARD9 in Cancer Cell Division. Presentation given: Tumor Cell Biology T32 Grant Seminar; February 28, 2018; Los Angeles, CA.

Clutario K.M. (2018). Functional and Proteomic Analysis of STARD9 in Mitosis. Presentation given: Chem 268 Midstream Seminar Series; May 11, 2018; Los Angeles, CA. (Department-wide seminar)

Clutario, K.M & Torres, J.Z. (2018). Functional and Proteomic Characterization of STARD9. Poster presented at: 2018 Salk Cell Cycle Symposium; June 28, 2018; San Diego, CA (No Abstract # Given)

Clutario, K.M & Torres, J.Z. (2019). Proteomic and Functional Characterization of STARD9. Poster presented at: Experimental Biology 2019 American Society for Biochemistry and Molecular Biology; April 7, 2019; Orlando, FL. (Abstract #6731)

Clutario, K.M. (2019). Functional and Proteomic Analysis of STARD9. Presentation given: Tumor Cell Biology T32 Grant Seminar; May 13, 2020; Los Angeles, CA.

Clutario, K.M. (2020). Characterizing STARD9's role in Aneuploidy. Presentation given: Tumor Cell Biology T32 Grant Seminar; January 13, 2020; Los Angeles, CA

Chapter 1

Introduction to the cell cycle and proliferation

Cell cycle, checkpoints

Cell proliferation is the complex process of a cell replicating its DNA and necessary components, then separating both of these into identical daughter cells. In interphase, cells undergo growth and duplicate their DNA; interphase is separated into 3 separate phase: G1, S, G2 [1], [2]. Gap 1 (G1) is the period which the cell prepares for the DNA replication that occurs in synthesis phase (S phase). Gap 2 (G2) is the period which the cell prepares for mitosis (M phase), in which the DNA is equally separated into two new cells. Mitosis is separated into prophase, prometaphase, metaphase, telophase and anaphase; which are all defined relative to what is happening to the DNA [1]. In prophase, the nuclear envelope breaks down and DNA condenses into individual chromosomes. This is followed by prometaphase in which the chromosomes attach to the spindle and in metaphase, the chromosomes organize into a symmetric plate. During anaphase, chromosomes segregate to separate sides of the cell and once they are far enough from each other, individual nuclei form in telophase prior to cytokinesis, which forms two new cells that can repeat the cell cycle[3]. Regulation is required in every step of this cycle and the dysregulation of such is the basis of human cancers [4]. Tumor cells are the result of a mix of unscheduled proliferation, genomic instability and chromosomal instability [5]–[7].

Mammalian cell cycle progression is directly regulated through a subset of cyclin-dependent kinases, in interphase these are CDK2, CDK4 and CDK6, while CDK1 is the mitotic regulator, also known as cell division control protein 2 (CDC2) [4], [7]–[9]. Cyclins are a family of proteins that are required to activate kinase activity in CDKs, along with having roles in complex formation [10], [11]. Cyclin D1 is most abundant in G1,

associating with CDK4 and CDK6 to phosphorylate the major tumor suppressor retinoblastoma protein (Rb) [10], [12]. Cyclin C is also most abundant in G1, associating with CDK2 to phosphorylate Rb. Cyclin B is the mitotic cyclin that associates with Cdk1 in order to license spindle attachments and nuclear envelope breakdown [12]. Three major cell cycle checkpoints exist between different phase transitions in order to guarantee the cell has required components for the next phase of the cell cycle. The checkpoints in place are: the G1/S transition, the G2/M transition and the metaphase to anaphase transition [13]. The G1/S transition checkpoint confirms the cell has enough nutrients to undergo the metabolic stress of DNA replication and synthesis of proteins required for that replication [14], [15]. The majority of human cancer cells feature many mutated components in this checkpoint, allowing increased proliferation, a hallmark of cancer cells [16]. This checkpoint is also linked to the mammalian target of rapamycin (mTOR) which regulates cell growth via nutrient signaling pathways [17]. The G2/M transition checkpoint prevents entry into mitosis, based on DNA damage response (DDR) mechanisms in the cell that sense double stranded breaks in chromosomes [16], [18]. A major part of the DDR pathway is p53, which is a nuclear transcription factor responsible for activation of several target genes involved in proliferative arrest and capable of inducing cell apoptosis [19], [20]. Studies have shown that half of human cancers feature a mutation in the TP53 gene, resulting in the expression of mutant p53 that is able to accelerate tumor growth [19], [21]. A faulty DDR pathway is therefore able to drive genomic instability.

The last major checkpoint occurs at the metaphase to anaphase transition and checks for proper bipolar-spindle formation. This checkpoint relies on mechanisms that

depolymerize improperly attached microtubules and the spindle assembly checkpoint (SAC), which is a signaling cascade that monitors for proper kinetochore state [13], [22]. Human cancers often have a dysfunctional SAC that allows them to form defective spindles, which in turn leads to the majority of cancer cell types displaying aneuploidy or an abnormal number of chromosomes [6], [23]. Thusly, chromosomal instability typically stems from the disfunction of the metaphase to anaphase transition.

Ribosomes and cell proliferation

Ribosomes are the protein factories of the cell in which messenger RNAs (mRNA) are translated into protein. Cell growth is a prerequisite for cell proliferation, as proliferating cells essentially double their contents prior to mitosis [24]. Ribosomes have been seen to be the limiting factor in cell growth, as up to 80% of cellular building materials and 80% of the energy used in proliferation are required for synthesis and assembly of ribosomal components [25], [26]. Ribosomes are large complexes made of four ribosomal RNAs and about 80 proteins, with assembly requiring 200-plus additional proteins [27]–[29]. Since this process presents such a resource intensive endeavor, ribosome biogenesis is linked to the same nutrient sensing mechanisms as the G1 to S checkpoint via the TOR pathway [30], [31]. Studies report that mTOR directly binds to the promoters of RNA polymerase I and RNA polymerase III in mammalian cells, suggesting that there is transcriptional control over these genes essential for ribosome biogenesis[32]. For these reasons proliferative control and ribosome biogenesis are intricately and intimately linked. Another direct link ribosome biogenesis has to the cell cycle is its relationship with p53; studies have demonstrated that perturbating ribosome

biogenesis stabilizes p53 and causes a proliferative arrest. This happens through the binding and inhibition of Mdm2, a E3 ubiquitin-protein ligase that inhibits p53, by numerous ribosomal proteins [33]. In cancer cells, where increased cell proliferation is a hallmark, there is a mirrored increase in ribosome formation and in turn protein synthesis. There is growing evidence that this increase in ribosome biogenesis is due to a mix of faulty mTORC1 (mTOR complex 1) signaling, mutations in TP53 and Rb inactivaton [34].

References

[1] C. H. Golias, A. Charalabopoulos, and K. Charalabopoulos, “Cell proliferation and cell cycle control: A mini review,” *International Journal of Clinical Practice*, vol. 58, no. 12. pp. 1134–1141, Dec. 2004. doi: 10.1111/j.1742-1241.2004.00284.x.

[2] J. J. Tyson, A. Csikasz-Nagy, and B. Novak, “The dynamics of cell cycle regulation,” *BioEssays*, vol. 24, no. 12. pp. 1095–1109, Dec. 01, 2002. doi: 10.1002/bies.10191.

[3] J. Richard Mcintosh, “Mitosis,” *Cold Spring Harb Perspect Biol*, vol. 8, no. 9, Sep. 2016, doi: 10.1101/cshperspect.a023218.

[4] M. Malumbres and M. Barbacid, “Cell cycle, CDKs and cancer: A changing paradigm,” *Nature Reviews Cancer*, vol. 9, no. 3. pp. 153–166, Mar. 2009. doi: 10.1038/nrc2602.

[5] M. Malumbres and M. Barbacid, “To cycle or not to cycle: a critical decision in cancer,” Dec. 2001. doi: https://doi.org/10.1038/35106065.

[6] G. J. P. L. Kops, B. A. A. Weaver, and D. W. Cleveland, “On the road to cancer: Aneuploidy and the mitotic checkpoint,” *Nature Reviews Cancer*, vol. 5, no. 10. pp. 773–785, Oct. 2005. doi: 10.1038/nrc1714.

[7] M. Malumbres and M. Barbacid, “Mammalian cyclin-dependent kinases,” *Trends in Biochemical Sciences*, vol. 30, no. 11. pp. 630–641, Nov. 2005. doi: 10.1016/j.tibs.2005.09.005.

[8] D. O. Morgan, *Cell Cycle: Principles of Control*. McGraw-Hill, Medical Pub. Division, 2006.

[9] S. Lim and P. Kaldis, “Cdks, cyclins and CKIs: Roles beyond cell cycle regulation,” *Development (Cambridge)*, vol. 140, no. 15. pp. 3079–3093, Aug. 01, 2013. doi: 10.1242/dev.091744.

[10] M. C. Casimiro, M. Crosariol, E. Loro, Z. Li, and R. G. Pestell, “Cyclins and cell cycle control in cancer and disease,” *Genes Cancer*, vol. 3, no. 11–12, pp. 649–657, Nov. 2012, doi: 10.1177/1947601913479022.

[11] Z. Darzynkiewicz, J. Gong, G. Juan, B. Ardelt, and F. Traganos, “Cytometry of cyclin proteins,” *Cytometry*, vol. 25, no. 1. pp. 1–13, 1996. doi: 10.1002/(SICI)1097-0320(19960901)25:1<1::AID-CYTO1>3.0.CO;2-N.

[12] D. Martínez-Alonso and M. Malumbres, “Mammalian cell cycle cyclins,” *Seminars in Cell and Developmental Biology*, vol. 107. Elsevier Ltd, pp. 28–35, Nov. 01, 2020. doi: 10.1016/j.semcdb.2020.03.009.

[13] K. J. Barnum and M. J. O'Connell, "Cell cycle regulation by checkpoints," *Methods in Molecular Biology*, vol. 1170, pp. 29–40, 2014, doi: 10.1007/978-1-4939-0888-2_2.

[14] D. S. Peeper, A. J. van der Eb, and A. Zantema, "Biochi~ic~a et Biophysica AEta The G1/S cell-cycle checkpoint in eukaryotic cells," 1994.

[15] D. A. Foster, P. Yellen, L. Xu, and M. Saqcena, "Regulation of G1 cell cycle progression: Distinguishing the restriction point from a nutrient-sensing cell growth checkpoint(s)," *Genes and Cancer*, vol. 1, no. 11. SAGE Publications Inc., pp. 1124–1131, 2010. doi: 10.1177/1947601910392989.

[16] M. Molinari, "Cell cycle checkpoints and their inactivation in human cancer," 2000.

[17] D. C. Fingar, C. J. Richardson, A. R. Tee, L. Cheatham, C. Tsou, and J. Blenis, "mTOR Controls Cell Cycle Progression through Its Cell Growth Effectors S6K1 and 4E-BP1/Eukaryotic Translation Initiation Factor 4E," *Mol Cell Biol*, vol. 24, no. 1, pp. 200–216, Jan. 2004, doi: 10.1128/mcb.24.1.200-216.2004.

[18] M. Löbrich and P. A. Jeggo, "The impact of a negligent G2/M checkpoint on genomic instability and cancer induction," 2007. [Online]. Available: www.nature.com/reviews/cancer

[19] K. H. Vousden and X. Lu, "Live or let die: The cell's response to p53," *Nature Reviews Cancer*, vol. 2, no. 8. pp. 594–604, Aug. 2002. doi: 10.1038/nrc864.

[20] T. Ozaki and A. Nakagawara, “Role of p53 in cell death and human cancers,” *Cancers*, vol. 3, no. 1. pp. 994–1013, Mar. 2011. doi: 10.3390/cancers3010994.

[21] A. Sigal and V. Rotter, “Oncogenic Mutations of the p53 Tumor Suppressor: The Demons of the Guardian of the Genome,” 2000. [Online]. Available: http://aacrjournals.org/cancerres/article-pdf/60/24/6788/2482679/ch240006788.pdf

[22] N. London and S. Biggins, “Signalling dynamics in the spindle checkpoint response,” *Nature Reviews Molecular Cell Biology*, vol. 15, no. 11. Nature Publishing Group, pp. 735–747, Nov. 27, 2014. doi: 10.1038/nrm3888.

[23] A. J. Holland and D. W. Cleveland, “Boveri revisited: chromosomal instability, aneuploidy and tumorigenesis.,” *Nat Rev Mol Cell Biol*, vol. 10, no. 7, pp. 478–87, Jul. 2009, doi: 10.1038/nrm2718.

[24] R. J. DeBerardinis, J. J. Lum, G. Hatzivassiliou, and C. B. Thompson, “The Biology of Cancer: Metabolic Reprogramming Fuels Cell Growth and Proliferation,” *Cell Metabolism*, vol. 7, no. 1. pp. 11–20, Jan. 09, 2008. doi: 10.1016/j.cmet.2007.10.002.

[25] Y. Tanaka and M. Tsuneoka, “Control of Ribosomal RNA Transcription by Nutrients,” in *Gene Expression and Regulation in Mammalian Cells - Transcription Toward the Establishment of Novel Therapeutics*, InTech, 2018. doi: 10.5772/intechopen.71866.

[26] J. Warner, J. Vilardell, and J. H. Sohn, “Economics of Ribosome Biosynthesis,” *Cold Spring Harb Symp Quant Biol* , vol. 66, pp. 567–574, 2001, doi: doi:10.1101/sqb.2001.66.567.

[27] A. M. Anger *et al.*, “Structures of the human and Drosophila 80S ribosome,” *Nature*, vol. 497, no. 7447, pp. 80–85, 2013, doi: 10.1038/nature12104.

[28] J. L. Woolford and S. J. Baserga, “Ribosome biogenesis in the yeast Saccharomyces cerevisiae,” *Genetics*, vol. 195, no. 3, pp. 643–681, 2013, doi: 10.1534/genetics.113.153197.

[29] H. Lempiäinen and D. Shore, “Growth control and ribosome biogenesis,” *Current Opinion in Cell Biology*, vol. 21, no. 6. pp. 855–863, Dec. 2009. doi: 10.1016/j.ceb.2009.09.002.

[30] V. Iadevaia, R. Liu, and C. G. Proud, “MTORC1 signaling controls multiple steps in ribosome biogenesis,” *Seminars in Cell and Developmental Biology*, vol. 36. Academic Press, pp. 113–120, Dec. 01, 2014. doi: 10.1016/j.semcdb.2014.08.004.

[31] H. Li, C. K. Tsang, M. Watkins, P. G. Bertram, and X. F. S. Zheng, “Nutrient regulates Tor1 nuclear localization and association with rDNA promoter,” *Nature*, vol. 442, no. 7106, pp. 1058–1061, Aug. 2006, doi: 10.1038/nature05020.

[32] C. Kwan Tsang, H. Liu, and X. F. S. Zheng, “mTOR binds to the promoters of RNA polymerase I-and III-transcribed genes,” 2010.

[33] G. Donati, L. Montanaro, and M. Derenzini, “Ribosome biogenesis and control of cell proliferation: p53 is not alone,” *Cancer Research*, vol. 72, no. 7. pp. 1602–1607, Apr. 01, 2012. doi: 10.1158/0008-5472.CAN-11-3992.

[34] L. Montanaro, D. Treré, and M. Derenzini, “Changes in ribosome biogenesis may induce cancer by down-regulating the cell tumor suppressor potential,” *Biochimica et*

Biophysica Acta - Reviews on Cancer, vol. 1825, no. 1. pp. 101–110, Jan. 2012. doi: 10.1016/j.bbcan.2011.10.006.

Chapter 2

Developing new tools and assays to analyze the contribution of novel proteins and metabolites to cell cycle regulation

Abstract

The mammalian cell cycle is an intricate process that requires the coordination of many enzymes, substrates, post-translational modifications and metabolites. Due to this complexity, the discovery of new proteins of interest or elucidation of regulatory pathways often goes hand in hand with the utilization of novel techniques or tools. We have developed a new screening tool that combines the CRISPR/Cas9 gene editing technology with the fluorescent ubiquitin-based cell cycle indicator (FUCCI) system in HeLa cells. We believe this cell line can be a useful new tool for CRISPR-based screening because it does not rely on additional reagents for cell cycle phase determination.

Many of the mitotic proteins our lab studies were initially identified through either proteomic analysis or genomic screening. While these approaches have yielded interesting hits to further analyze, these screens focused exclusively on protein-based regulation of cell cycle progression and cell division. As such, we sought to expand the field's knowledge of cell cycle regulation and performed a cell cycle screen using a library of about 1,200 cellular metabolites and identified around 180 putative hits. These results will provide our lab a fresh avenue of study and will provide the basis for future projects analyzing these metabolites and their role in regulating the cell cycle.

Introduction

Mitotic cell division is a highly coordinated process requiring many enzymes, substrates and metabolites that results in two identical daughter cells. Genome-wide screening has been used countless times to study a variety of processes within cell division [35]–[37]. Furthermore, with the advent of CRISPR/Cas9 gene editing technology, genomic knockout screens became much more feasible and common to do in mammalian cell lines [38]–[40]. CRISPR/Cas9, short for Clustered Regularly Interspaced Short Palindromic Repeats and CRISPR-associated protein 9, has been a revolutionary tool that has unlocked genomic editing for nearly every existing gene target [41]–[44]. In addition to the vast difference in targetable sequences, CRISPR is far more efficient than older zinc finger nuclease (ZFN) or transcription activator-like effector nuclease (TALENs) technology, while being able to multiplex knockouts by simply adding different guide RNAs [41], [45], [46]. CRISPR genome editing takes advantage of an adaptive bacterial endonuclease that uses a guide sequence inside of an RNA complex. This complex binds to targeted DNA sites via Watson-Crick base-pairing and allows the Cas9 endonuclease to introduce a specific double-sided break in the DNA, inducing non-homologous end joining (NHEJ) and subsequent gene silencing if the coding sequence is knocked out of frame. Gene editing can also be accomplished with this system if a repair template is provided during Cas9 cleavage, allowing homology-directed repair (HDR) mechanisms to occur instead of NHEJ [47], [48]. Overall, CRISPR is an incredibly powerful and versatile tool for genomic screening purposes.

Our genomic screening schemes have typically used cell cycle phase as a phenotypic readout, since we are mostly interested in cell cycle progression as it relates to cancer division. As such, we choose to use the Fluorescent Ubiquitination-based Cell Cycle Indicator (FUCCI) in order to visualize any cell cycle phase via immunofluorescent imaging. FUCCI utilizes two fluorescently-labeled proteins that have cell cycle-dependent abundance, due to their differing ubiquitination schedules during the cell cycle, mCherry-labeled $CDT1_{30\text{-}120}$ is present throughout G1 and very early S phase, while mVenus-labeled $Geminin_{1\text{-}110}$ is present from S phase to the end of mitosis. This system allows for cells to fluoresce red from G1 to early S, green from S to mitosis, and orange during early S phase, providing a genome-encoded means for cell cycle phase detection in high-throughput fashion [49].

The metabolite library we are screening contains around 1,200 different commercially available, naturally occurring compounds and is arrayed in individual wells across 4 384-well plates at 1mM. The first 3 plates of metabolites are dissolved in DMSO and the last plate is composed of metabolites that better solubilized in water. The library is not limited to, but includes a mix of: amino acids, sugars, lipids, organic acids, and hormones. Several metabolic enzymes are known to regulate cell cycle dynamics and one example is that a proliferatively-committed cell, upregulates glycolytic pathways after the G1/S checkpoint and either a reduction of available glucose or blockage of glycolysis will arrest proliferation [50]–[52]. Lipids also play several roles in cell cycle progression and different classes of lipids fluctuate in abundance during the cell cycle. [53].

Results and Discussion

HeLa Fucci iCas9 is a powerful novel screening tool

To create a novel cell-based screening tool for assessing the cell cycle effects of knocking out genes of interest, we combined two existing technologies, CRISPR/Cas9 and the FUCCI reporter system (Figure 1A) [40], [42], [49], [54]. We performed two rounds of antibiotic selection for HeLa FUCCI cells that had a tetracycline repressor and a doxycycline-inducible Cas9 randomly integrated via lentiviral transduction. Next, we seeded 96-well plates for limiting dilution to isolate monoclonal cell lines and twelve different clones were analyzed via immunoblot for expression of Cas9 and Cas9 leakiness when not in the presence of doxycycline (Figure 1B). We identified clones 2, 6, and 11 as being suitable for screening purposes, as they all express high levels of Cas9 during dox-treatment with minimal leakiness in regular media. We then tested clone 11 for Cas9 protein stability after a single day of dox treatment, the results demonstrate that the majority of expressed Cas9 levels are present 48hrs after washing into non-dox containing media and a little under half of Cas9 is present after 72hrs post-media change.

High-throughput metabolite screen

To better understand if and how the cell cycle is influenced by metabolites, we designed a high-throughput metabolite screen in conjunction with the CNSI and tested about 1,200 commercially available metabolites for the ability to alter cell cycle kinetics in HeLa cells. Before we tested the metabolite library, we optimized our screening protocol and validated our screening methods. Throughout these experiments we used

Vybrant DyCycle Green Stain in order to visualize DNA content via plate-scanning cytometry. First, we determined optimal seeding density for imaging on the scanning cytometer while testing HeLa cell tolerance to DMSO, as the vast majority of the metabolites were suspended in DMSO. We determined that a cell density of 4,500 cells per well was the optimal density to image individual cells with minimal clumping. With this plate, we also determined that our screen should not exceed 1% total DMSO per well, as cells that received higher concentrations of DMSO displayed unwanted cell death. Next, we tested known cell cycle effectors to confirm that we were able to see cell cycle arrests using our methodology. We confirmed that thymidine and taxol were able to synchronize cells in their expected phases, G1 and G2/M respectively, giving us confidence that our screening protocol would properly identify metabolites that would alter the cell cycle (Figure 2A).

After treating HeLa cells in 384-well plates for 20 hours with 5uM of each metabolite, we added Vybrant DyCycle Green to stain for DNA content and incubated cells for 3 hours prior to analyzing each plate on the Acumen scanning cytometer. Several of the hits found in the library stood out immediately, as the initial readout displayed from the instrument are per-well images from each plate (Figure 2B). Wells from each plate that displayed a different shade of green were noted due to their clear differences in DNA content when compared to the untreated wells. Averages of percent of cells in each cell cycle phase and total cell count were calculated from the untreated wells in each plate. Standard deviations from the average were calculated for each compound and hits were defined as any compound that displayed a change in any cell cycle phase by at least 2

standard deviations (Table 1). In the library of roughly 1,200 compounds, 180 of these were hits. After comparison of our statistical analysis with our collaborators at the Molecular Screening Shared Resource (MSSR), we choose 22 of our top hits and obtained a “mini library” sample plate to analyze via immunofluorescence microscopy (Table 2). However, after a deeper literature search for each of these metabolites, it was evident that the majority of these identified compounds were known cancer drug candidates. Strikingly, the 4 hits in our mini library that were not already known cancer drugs were fructose, d-tagatose, perillartine, and l-(-)-sorbose. Due to the other 18 initial hits being well characterized in their effects on cancer cells, we focused on analyzing the remaining 4 sugars. We then treated cells with these 4 compounds at 5uM to mimic the screening protocol and imaged these coverslips via immunofluorescence microscopy, initially staining for alpha-tubulin and DNA only. Our goal for these set of experiments was to determine if we could observe any immediate cell cycle defects after overnight treatment; but after imaging, there were no immediately obvious defects to be seen (data not shown).

Conclusions

We have developed a cell-based screening tool in the HeLa FUCCI iCas9 cell line that is ready for use in high-throughput genome-wide screening studies. The dox-inducible Cas9 allows for gene knockouts using either pooled or arrayed gRNA libraries and the FUCCI system provides a convenient phenotypic readout for cell cycle-related studies.

Our metabolite library screen has produced 180 putative hits after treating cells overnight with 5uM of each metabolite and we chose 22 of these to study further. However, there seems to be oversight when compiling our initial mini library for further

study via immunofluorescence microscopy, as 18 of the 22 of these initial hits are already well characterized for their ability to cause a cell-cycle arrest and are all either in clinical trials as cancer treatments or are already being used as cancer drugs [55]–[72]. Curiously, the four remaining hits on the list were all sugar compounds, which is of note, because many cancer cell types are dependent on an increased glucose metabolism [73]. Fructose displayed a modest increase in S-phase cells and G2/M-phase cells, while having a larger decease in G1-phase cells. D-tagatose, perillartine, and L(-)-sorbose each had a similar pattern of a large decrease in cells in G2/M and large increase in Sub-G1 cells, but vary in each phase from compound to compound. Specifically in L(-)-sorbose, we observed a large increase in total cell count, a large decrease in G1 cells and a moderate to large increase in S cells. These are interesting results and according to a preprint journal, L(-)-sorbose may exhibit antitumor activity, inducing cell apoptosis and inhibiting tumor growth with or without other cancer drugs present [74]. Other sugars are known to affect proliferation in cells as well, mannose has been reported to inhibit cancer cell growth and increase efficacy of antitumor treatment, while fructose (also found with this screen) has recently been shown to increase tumor growth in mice [75], [76]. Considering we have shown this screen is capable of identifying known cancer therapeutics, these sugars should be further investigated for possible therapeutic purposes.

Future perspectives

The HeLa FUCCI iCas9 cell line we have developed is ready for use in high throughput genomic screens in conjunction with CRISPR gRNA libraries. Originally, we had developed this tool in conjunction with the MSSR to validate their arrayed gRNA library,

however the library they chose to develop was based off a GFP-tagged construct, making our cell line incompatible with their library. Future experimentation with this cell-based tool would therefore involve a gRNA library without any fluorescent tags to confound results. One way to immediately improve this tool, would be to redevelop it using one of the newest FUCCI technologies, FUCCI(CA), which is able to distinguish between G1, S and G2/M using 3 colors [77]. FUCCI4 takes this one step further and is able to distinguish between all 4 of these cell cycle phases, incorporating a far-red fluorescent tag [78].

There are a few future experiments we have in mind to advance the metabolite screening project. Considering our first mini-library of top hits included mostly known cancer drugs, the first thing we should do is to obtain more of the top hits and to verify their novelty before moving forward with them. Another alternate method is to classify the whole 180 metabolite hit list into metabolic pathways and choose a pathway or two to investigate further. As previously mentioned, the initial immunofluorescence microscopy performed on the sugars identified did not yield any striking observations. By choosing a full pathway to study, it would allow us to focus on the type of phenotypes we would like to explore. Other directions for this screen would be to rerun the metabolite library screen, but at a higher concentration. This could reveal novel cell cycle effectors that have a dose dependent response such that the original 5uM concentration would not be enough to change cell cycle dynamics meaningfully.

Once more target metabolites are identified, it would be interesting to synchronize the HeLa cells prior to metabolite treatment in order to observe if any cell cycle arrests

occur. While this screening data suggests where these cell cycle arrests may occur, we can fully confirm it through this experimental scheme.

With all this said, it would be in our best interest to further explore the sugars we identified in the initial screening run. Precedent does exist for sugars affecting cell cycle dynamics in cancer cell proliferation and new avenues of cancer therapy may be discovered. Although most of our 22 initial top hits were known and well-studied cancer drugs, this does give us confidence in the screens ability to identify cell cycle effectors.

Materials and Methods

Cell Culture

293T and HeLa cells were grown in F12:DMEM 50:50 (Gibco) with 10% FBS, 2mM L-glutamine and penicillin/streptomycin (Gibco) in 5% CO_2 at 37°C. Tetracycline-tested FBS was used when indicated.

Isolation of HeLa FUCCI iCas9 cell line

To develop our HeLa FUCCI dox-inducible Cas9 cell line, we first packaged a plasmid containing a tetracycline repressor driven by a CMV promotor (Addgene, Plasmid #:17492) into lentivirus using the Takara Lenti-X™ Packaging Single Shot system (Takara, Cat #: 631276). A 10cm dish of 293T cells in 8mL of tetracycline-free media was transfected at 80% confluency with a 600uL solution containing 7ug of our tet-repressor plasmid combined with the lyophilized Lenti-X nanoparticle mix. After overnight incubation at 37°C with 5% CO_2, 6mL of fresh media was added to the plate and incubated for an additional 48hrs at 37°C. Afterwards, 14mLs of the lentivirus containing media was collected, and centrifuged gently at 500g to pellet any cells. The

clarified media was incubated at 4°C prior to concentration using a Lenti-X concentrator kit (Takara, Cat #: 631232). After concentrating lentivirus into a pellet, it was resuspended in 1mL of complete media. Presence of lentivirus was confirmed using a Takara Lenti-X GoStix™ kit (Takara, Cat #: 621280). 6-well plates of HeLa FUCCI cells were seeded at $2x10^5$ cells/well in 2mL of complete media prior to transduction with 850uL of complete media with 12ug/mL of Polybrene (Millipore Sigma, Cat #: TR-1003-G) combined with 150uL of 1:25 diluted lentivirus, for a total of 1mL per well. Virus-containing media was aspirated after overnight incubation and replaced with fresh growth media and cells were incubated for another two days prior to transferring them into a 10cm plate. We selected with media containing 5ug/mL of blasticidin (Millipore Sigma, Cat #: 203351-10ML-M), replacing media every 2 to 3 days until all the cells in the non-transduced control plate were dead. The selected HeLa FUCCI cells were then grown in complete media without selection agent until plate reached 50% confluency.

Monoclonal HeLa FUCCI TRex cell lines were then isolated by limiting dilution. We seeded multiple 96-well plates with 100uL of media containing 5 cells/mL, then incubated until colonies could be transferred to 12-well plates. When confluent enough, cells were collected and analyzed via immunoblot for the presence of the tetracycline repressor. A single clone was chosen and the same protocol was performed using a Cas9 lentivirus vector (Addgene, Plasmid #110837) and clones were selected with puromycin at 2ug/mL. Multiple clones were isolated and tested further.

Immunoblotting

For analysis of different HeLa FUCCI iCas9 clones, each clone was seeded in 2 separate wells of a 6-well plate at 25% confluency and incubated overnight in 5% CO_2 at 37°C overnight. The following day, one well was induced with 0.2ug/mL of doxycycline (Sigma Aldritch, Cat # D5207) in tet-free media, the other corresponding well was used as a non-induced control. Cells were incubated for 16hrs, then collected, lysed and extracts were resolved on a 4-20% SDS-PAGE gel before transferring onto a PVDF membrane. Membranes were incubated with indicated antibodies and imaged using a LI-COR Odyssey. Cell extracts were prepared as previously described (Gholkar et. al 2016).

For determination of post-induction Cas9 protein stability, 2 10-cm plates were seeded, and one plate was induced with 0.2ug/mL of doxycycline in tet-free media for 24hrs. Uninduced control and induced samples were collected and saved for later lysate extraction. Induced plate was washed into non-doxycycline tet-free media and samples were taken at the times indicated post-wash. All samples were lysed and cell extracts were analyzed as previously described. Band intensities were quantified using ImageJ and normalized to the sample collected after 24hrs of doxycycline induction.

Metabolite Library Screening

To determine correct seeding density and maximum DMSO concentration for the library screen, DMSO diluted in 25uL of complete media as previously described, with the exception of using F12:DMEM 50:50 with no phenol red (Gibco, Cat #: 21041025), was added to 384-well plates for final concentrations of either: 0% 0.5%, 1.0%, or 2.0%

using a Thermofisher Multidrop™ liquid handler. Cells were then seeded in similar fashion in 25uL of media at either: $3.0x10^3$, $4.5x10^3$, or $6.0x10^3$ cells per well, prio to incubation at 37°C and 5% CO_2 for 20hrs. After overnight incubation, 50uL of 10uM Vybrant™ DyeCycle™ Green diluted in complete media was added with the Multidrop, for a final concentration of 5uM of staining solution, the plate was incubated with dye for 3 hours at 37°C and imaged using an Acumen© EX3 scanning cytometer with laser power at 6mW (TTP Labtech, discontinued). All data acquisition was done via Acumen's Cellista software and exported to Excel spreadsheets and tiff images.

To test validity of our screening protocol we seeded a 384-well plate as previously described except wells were treated with a final concentration of either 5mM of Thymidine or 1uM of Taxol, instead of adding DMSO.

To screen the metabolite library, we added 25ul of complete media to each well of four 384-well plates. We transferred 0.25uL of each 1mM metabolite solution from the drug stock plates into our four 384-well plates on a Beckman BioMek™ FX liquid handler. We added 4,500 cells to each well of these plates, left them at room temperature for an hour to settle the cells, and then placed them in the incubator at 37°C and 5% CO_2 for 20hrs. After overnight incubation, DyeCycle Green was added as previously described and the plates were incubated for another 3 hours prior to scanning each plate with the Acumen EX3. Raw data was exported from Cellista into Excel spreadsheets and tiffs were exported for the plate images. Averages and standard deviations were calculated from untreated wells per plate of each recorded statistic: live cell count, and % of live cells in G1, S, or G2/M. Then, we calculated each metabolite's deviation from the untreated average for each recorded data point and defined any metabolite that caused

a shift of 2 standard deviations or greater, a hit.

A sample mini library of our chosen 22 initial hitlist was obtained and used for phenotypic analysis.

Fixed-cell immunofluorescence microscopy

Fixed-cell immunofluorescence microscopy was performed as previously described (Garcia et. al 2021), except substituting blocking buffer with an alternate buffer comprised of: 0.2M Glycine, 2.5% FBS, and 0.1% Triton-X-100 in PBS. Cells were fixed with 4% paraformaldehyde, permeabilized with 0.1% Triton-X-100 in PBS, and costained with 0.5ug/mL Hoechst 33342 and anti-α-tubulin. Imaging of cells was carried out using a Leica DMI6000 microscope (Leica DFC360 FX Camera, 6x 1.4-0.60 NA oil objective, Leica AF6000 software).

References

[1] A. E. Carpenter and D. M. Sabatini, “Systematic genome-wide screens of gene function,” *Nature Reviews Genetics*, vol. 5, no. 1. pp. 11–22, Jan. 2004. doi: 10.1038/nrg1248.

[2] J. Dobbelaere, F. Josué, S. Suijkerbuijk, B. Baum, N. Tapon, and J. Raff, “A genome-wide RNAi screen to dissect centriole duplication and centrosome maturation in Drosophila,” *PLoS Biol*, vol. 6, no. 9, pp. 1975–1990, Sep. 2008, doi: 10.1371/journal.pbio.0060224.

[3] “Genome-wide view of mitosis”.

[4] X. Yan *et al.*, “High-content imaging-based pooled CRISPR screens in mammalian cells,” *Journal of Cell Biology*, vol. 220, no. 2, Feb. 2021, doi: 10.1083/JCB.202008158.

[5] K. J. Condon *et al.*, “Genome-wide CRISPR screens reveal multitiered mechanisms through which mTORC1 senses mitochondrial dysfunction”, doi: 10.1073/pnas.2022120118/-/DCSupplemental.

[6] M. Kampmann, “CRISPRi and CRISPRa Screens in Mammalian Cells for Precision Biology and Medicine,” *ACS Chem Biol*, vol. 13, no. 2, pp. 406–416, Feb. 2018, doi: 10.1021/acschembio.7b00657.

[7] L. Cong *et al.*, “Multiplex genome engineering using CRISPR/Cas systems,” *Science (1979)*, vol. 339, no. 6121, pp. 819–823, Feb. 2013, doi: 10.1126/science.1231143.

[8] G. J. Knott and J. A. Doudna, “CRISPR-Cas guides the future of genetic engineering.” [Online]. Available: https://www.science.org

[9] J. A. Doudna and E. Charpentier, “The new frontier of genome engineering with CRISPR-Cas9.” [Online]. Available: https://www.science.org

[10] S. Ruiz *et al.*, “A Genome-wide CRISPR Screen Identifies CDC25A as a Determinant of Sensitivity to ATR Inhibitors,” *Mol Cell*, vol. 62, no. 2, pp. 307–313, Apr. 2016, doi: 10.1016/j.molcel.2016.03.006.

[11] J. C. Miller *et al.*, “A TALE nuclease architecture for efficient genome editing,” *Nat Biotechnol*, vol. 29, no. 2, pp. 143–150, Feb. 2011, doi: 10.1038/nbt.1755.

[12] J. C. Miller *et al.*, “An improved zinc-finger nuclease architecture for highly specific genome editing,” *Nat Biotechnol*, vol. 25, no. 7, pp. 778–785, Jul. 2007, doi: 10.1038/nbt1319.

[13] K. Li, G. Wang, T. Andersen, P. Zhou, and W. T. Pu, “Optimization of genome engineering approaches with the CRISPR/Cas9 system,” *PLoS One*, vol. 9, no. 8, Aug. 2014, doi: 10.1371/journal.pone.0105779.

[14] B. Pardo, B. Gómez-González, and A. Aguilera, “DNA double-strand break repair: How to fix a broken relationship,” *Cellular and Molecular Life Sciences*, vol. 66, no. 6. pp. 1039–1056, Mar. 2009. doi: 10.1007/s00018-009-8740-3.

[15] A. Sakaue-Sawano and A. Miyawaki, “Visualizing spatiotemporal dynamics of multicellular cell-cycle progressions with fucci technology,” *Cold Spring Harb Protoc*, vol. 2014, no. 5, pp. 525–531, Mar. 2014, doi: 10.1101/pdb.prot080408.

[16] S. Tudzarova, S. L. Colombo, K. Stoeber, S. Carcamo, G. H. Williams, and S. Moncada, “Two ubiquitin ligases, APC/C-Cdh1 and SKP1-CUL1-F (SCF)-β-TrCP, sequentially regulate glycolysis during the cell cycle,” *Proc Natl Acad Sci U S A*, vol. 108, no. 13, pp. 5278–5283, Mar. 2011, doi: 10.1073/pnas.1102247108.

[17] A. Almeida, J. P. Bolaños, and S. Moncada, “E3 ubiquitin ligase APC/C-Cdh1 accounts for the Warburg effect by linking glycolysis to cell proliferation,” *Proc Natl Acad Sci U S A*, vol. 107, no. 2, pp. 738–741, 2010, doi: 10.1073/pnas.0913668107.

[18] J. Kalucka *et al.*, “Metabolic control of the cell cycle,” *Cell Cycle*, vol. 14, no. 21, pp. 3379–3388, 2015, doi: 10.1080/15384101.2015.1090068.

[19] G. E. Atilla-Gokcumen *et al.*, “Dividing cells regulate their lipid composition and localization,” *Cell*, vol. 156, no. 3, pp. 428–439, Jan. 2014, doi: 10.1016/j.cell.2013.12.015.

[20] J. S. L. Yu and K. Yusa, “Genome-wide CRISPR-Cas9 screening in mammalian cells,” *Methods*, vol. 164–165. Academic Press Inc., pp. 29–35, Jul. 15, 2019. doi: 10.1016/j.ymeth.2019.04.015.

[21] J.-L. Roh, E. H. Kim, J. Y. Park, J. W. Kim, M. Kwon, and B.-H. Lee, “Piperlongumine selectively kills cancer cells and increases cisplatin antitumor activity in head and neck cancer.” [Online]. Available: www.impactjournals.com/oncotarget/

[22] M. yi Lv *et al.*, “Urolithin B suppresses tumor growth in hepatocellular carcinoma through inducing the inactivation of Wnt/β-catenin signaling,” *J Cell Biochem*, vol. 120, no. 10, pp. 17273–17282, Oct. 2019, doi: 10.1002/jcb.28989.

[23] B. C. Jang *et al.*, “Sanguinarine induces apoptosis in A549 human lung cancer cells primarily via cellular glutathione depletion,” *Toxicology in Vitro*, vol. 23, no. 2, pp. 281–287, Mar. 2009, doi: 10.1016/j.tiv.2008.12.013.

[24] J. S. Lee, W. K. Jung, M. H. Jeong, T. R. Yoon, and H. K. Kim, “Sanguinarine induces apoptosis of HT-29 human colon cancer cells via the regulation of Bax/Bcl-2 ratio and caspase-9-dependent pathway,” *Int J Toxicol*, vol. 31, no. 1, pp. 70–77, Jan. 2012, doi: 10.1177/1091581811423845.

[25] H. Y. Lim *et al.*, “Celastrol in cancer therapy: Recent developments, challenges and prospects,” *Cancer Letters*, vol. 521. Elsevier Ireland Ltd, pp. 252–267, Nov. 28, 2021. doi: 10.1016/j.canlet.2021.08.030.

[26] D. Kashyap, A. Sharma, H. S. Tuli, K. Sak, T. Mukherjee, and A. Bishayee, “Molecular targets of celastrol in cancer: Recent trends and advancements,” *Critical Reviews in Oncology/Hematology*, vol. 128. Elsevier Ireland Ltd, pp. 70–81, Aug. 01, 2018. doi: 10.1016/j.critrevonc.2018.05.019.

[27] D. dong Wang *et al.*, “Synthesis of MeON-neoglycosides of digoxigenin with 6-deoxy- and 2,6-dideoxy-D-glucose derivatives and their anticancer activity,” *Bioorg Med Chem Lett*, vol. 27, no. 15, pp. 3359–3364, 2017, doi: 10.1016/j.bmcl.2017.06.008.

[28] T. L. Tinley *et al.*, “Novel 2-Methoxyestradiol Analogues with Antitumor Activity 1,” 2003. [Online]. Available: http://aacrjournals.org/cancerres/article-pdf/63/7/1538/2512675/ch0703001538.pdf

[29] K. Hu and X. Yao, “The cytotoxicity of methyl protodioscin against human cancer cell lines in vitro,” *Cancer Invest*, vol. 21, no. 3, pp. 389–393, 2003, doi: 10.1081/CNV-120018230.

[30] D. Floryk and E. Huberman, “Mycophenolic acid-induced replication arrest, differentiation markers and cell death of androgen-independent prostate cancer cells DU145,” *Cancer Lett*, vol. 231, no. 1, pp. 20–29, Jan. 2006, doi: 10.1016/j.canlet.2005.01.006.

[31] S. Suresh, D. Raghu, and D. Karunagaran, “Menadione (Vitamin K3) induces apoptosis of human oral cancer cells and reduces their metastatic potential by modulating the expression of epithelial to mesenchymal transition markers and inhibiting migration,” *Asian Pacific Journal of Cancer Prevention*, vol. 14, no. 9, pp. 5461–5465, 2013, doi: 10.7314/APJCP.2013.14.9.5461.

[32] J. E. Cortes and R. Pazdur, “Docetaxel,” 1995.

[33] C. C. Lin *et al.*, “Casticin inhibits human prostate cancer DU 145 cell migration and invasion via Ras/Akt/NF-κB signaling pathways,” *J Food Biochem*, vol. 43, no. 7, Jul. 2019, doi: 10.1111/jfbc.12902.

[34] X. Lin, J. Liu, Y. Zou, C. Tao, and J. Chen, “Xanthotoxol suppresses non-small cell lung cancer progression and might improve patients’ prognosis,” *Phytomedicine*, vol. 105, Oct. 2022, doi: 10.1016/j.phymed.2022.154364.

[35] K. Tsuchida *et al.*, “Halofuginone enhances the chemo-sensitivity of cancer cells by suppressing NRF2 accumulation,” *Free Radic Biol Med*, vol. 103, pp. 236–247, Feb. 2017, doi: 10.1016/j.freeradbiomed.2016.12.041.

[36] N. Wakimoto *et al.*, “Cucurbitacin B has a potent antiproliferative effect on breast cancer cells in vitro and in vivo,” *Cancer Sci*, vol. 99, no. 9, pp. 1793–1797, 2008, doi: 10.1111/j.1349-7006.2008.00899.x.

[37] K. Rajpoot and S. K. Jain, “Irinotecan hydrochloride trihydrate loaded folic acid-tailored solid lipid nanoparticles for targeting colorectal cancer: development, characterization, and in vitro cytotoxicity study using HT-29 cells,” *J Microencapsul*, vol. 36, no. 7, pp. 659–676, Oct. 2019, doi: 10.1080/02652048.2019.1665723.

[38] N. Dogra, A. Kumar, and T. Mukhopadhyay, “Fenbendazole acts as a moderate microtubule destabilizing agent and causes cancer cell death by modulating multiple cellular pathways,” *Sci Rep*, vol. 8, no. 1, Dec. 2018, doi: 10.1038/s41598-018-30158-6.

[39] M. v. Liberti and J. W. Locasale, “The Warburg Effect: How Does it Benefit Cancer Cells?,” *Trends in Biochemical Sciences*, vol. 41, no. 3. Elsevier Ltd, pp. 211–218, Mar. 01, 2016. doi: 10.1016/j.tibs.2015.12.001.

[40] X.-D. Gao *et al.*, “Rare sugar L-sorbose exerts antitumor activity by impairing glucose metabolism,” 2022, doi: 10.21203/rs.3.rs-1694501/v1.

[41] M. D. Goncalves *et al.*, “High-fructose corn syrup enhances intestinal tumor growth in mice.” [Online]. Available: https://www.science.org

[42] P. S. Gonzalez *et al.*, “Mannose impairs tumour growth and enhances chemotherapy,” *Nature*, vol. 563, no. 7733, pp. 719–723, Nov. 2018, doi: 10.1038/s41586-018-0729-3.

[43] A. Sakaue-Sawano *et al.*, “Genetically Encoded Tools for Optical Dissection of the Mammalian Cell Cycle,” *Mol Cell*, vol. 68, no. 3, pp. 626-640.e5, Nov. 2017, doi: 10.1016/j.molcel.2017.10.001.

[44] B. T. Bajar *et al.*, “Fluorescent indicators for simultaneous reporting of all four cell cycle phases,” *Nature Methods*, vol. 13, no. 12. Nature Publishing Group, pp. 993–996, Dec. 01, 2016. doi: 10.1038/nmeth.4045.

Figures

1

A

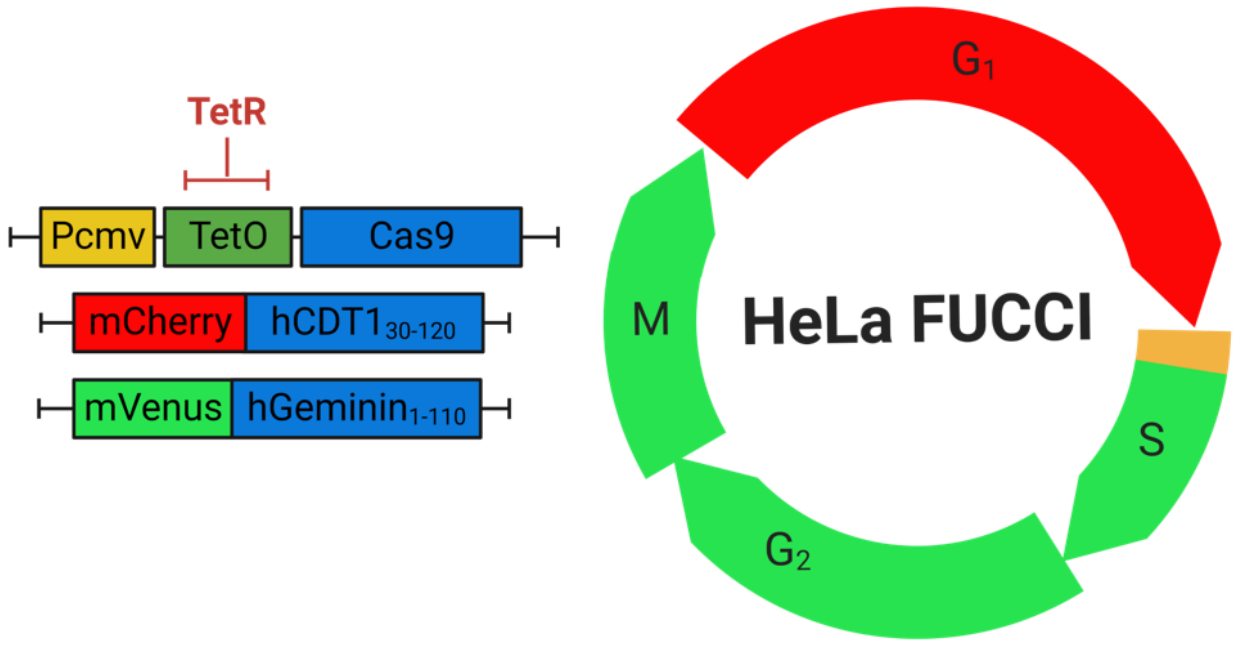

B

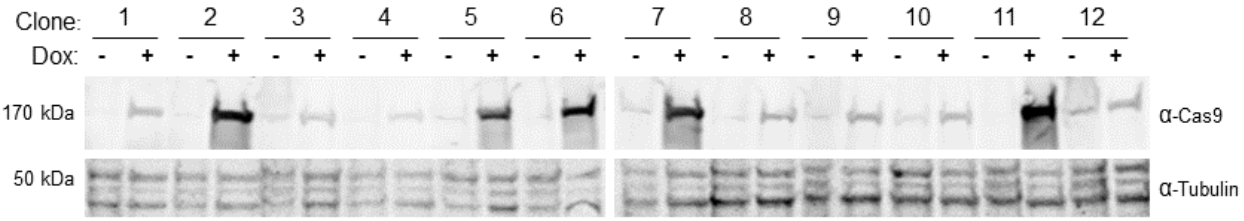

C

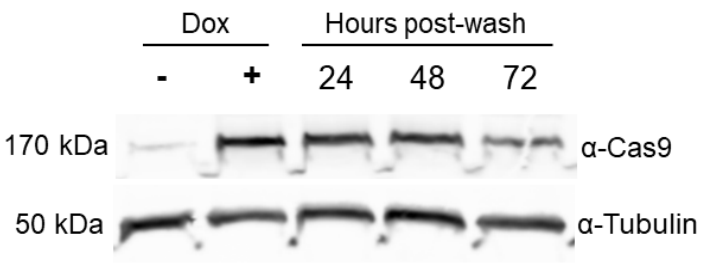

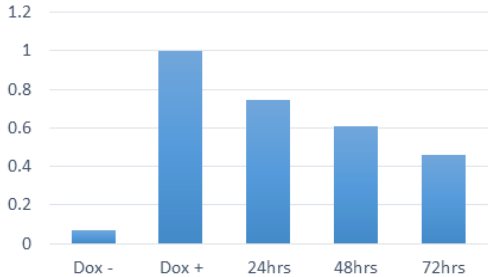

Figure 1. HeLa FUCCI iCas9 system. (A) A tet-repressor and Cas9 were randomly integrated into HeLa FUCCI cells through sequential rounds of lentiviral transduction. (B) A monoclonal tet-R containing HeLa FUCCI cell line was transduced with lentivirus containing tetO controlled Cas9. Post-selection, limiting dilution was performed and individual clones were analyzed for clean expression of Cas9. Cells were collected after 24 hours of doxycycline induction. (C) HeLa FUCCI iCas9 cell line was dox-induced for 24 hours, then dox was washed out with regular growth media and samples were collected for analysis via western blot every 24 hours for 3 days post-wash. Graph shows quantification of Cas9 bands normalized to 24 hours after dox-induction (Dox +).

A

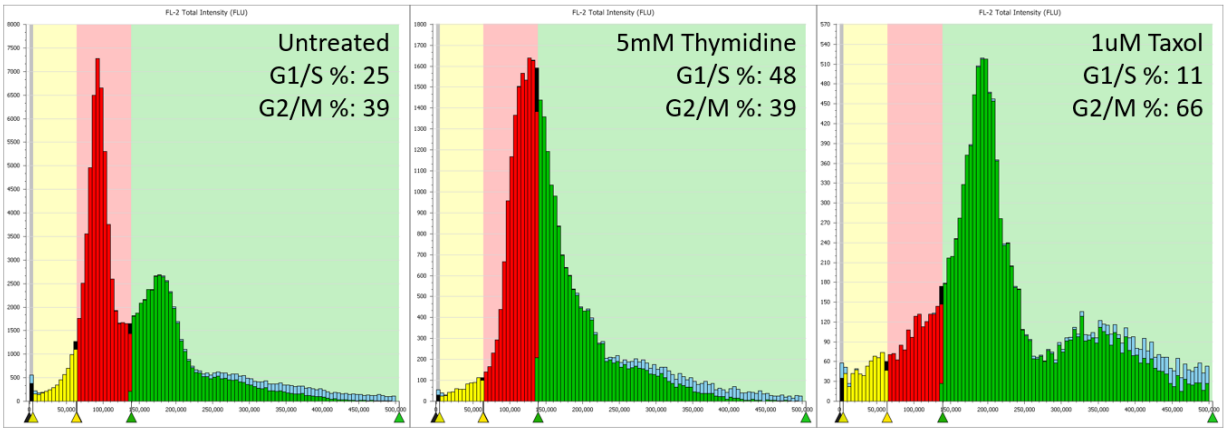
FL-2 Total Intensity (FLU)
Untreated
G1/S %: 25
G2/M %: 39
FL-2 Total Intensity (FLU)
5mM Thymidine
G1/S %: 48
G2/M %: 39
FL-2 Total Intensity (FLU)
1uM Taxol
G1/S %: 11
G2/M %: 66

B

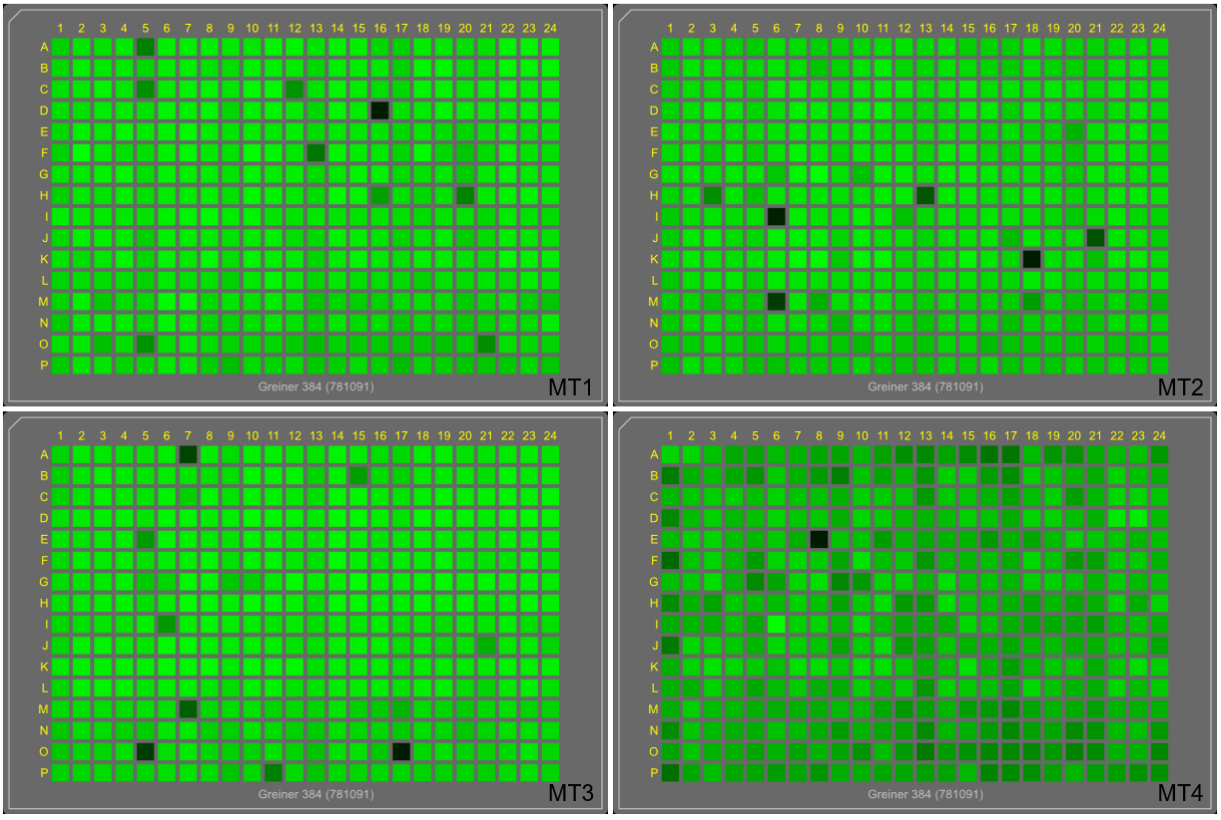
Greiner 384 (781091)
MT1
Greiner 384 (781091)
MT2
Greiner 384 (781091)
MT3
Greiner 384 (781091)
MT4

Figure 2. Metabolite library screening. (A) Screening protocol was validated using thymidine and taxol as known cell cycle effectors. Percent of total cells are an average of 16 wells for the treated conditions and 32 wells for the untreated cells. (B) Visual representation of each scanned metabolite library plate, shade/brightness of green represents average DNA content of the imaged cells in each well.

Table 1 Metabolite Library Screen Hits

Cells	SubG1%	G1%	S%	G2/M%	PLATE	WELL	COMPOUND
1.33	1.24	1.11	1.05	-2.12	MT1	C08	Oleic Acid
1.82	0.62	3.95	-0.86	-2.93	MT1	C11	Medroxyprogesterone acetate
-6.26	7.74	0.48	2.24	-1.52	MT1	C12	Trenbolone acetate
1.46	5.44	0.71	1.00	-3.13		D08	D-3-Phenyllactic acid
0.82	1.57	1.52	1.03	-2.53	MT1	D12	Eicosapentaenoic Acid
-16.07	3.64	-8.62	0.21	4.43	MT1	D16	2-Methoxyestradiol (2-MeOE2)
0.71	2.14	1.29	1.58	-2.78	MT1	D20	Syringic acid
-0.45	0.94	-2.13	-0.86	1.10	MT1	E19	Histamine
-1.10	4.09	-1.86	0.93	-2.78	MT1	E20	Stearic acid
-2.21	1.49	-2.04	0.51	-0.96	MT1	F20	Methyl Vanillate
1.23	2.86	1.16	0.88	-2.37	MT1	G06	Protirelin
1.20	4.19	0.84	1.81	-2.98	MT1	G16	Pyridoxal phosphate
0.36	5.45	0.35	-0.81	-2.07	MT1	G19	Pyridoxine
-1.78	4.68	-1.91	0.45	-2.47	MT1	G20	Citric acid
0.88	1.21	1.38	1.81	-2.47	MT1	H08	Undecanedioic acid
0.52	1.98	0.84	3.49	-2.83	MT1	H12	3beta-hydroxy-delta5-cholenic acid
1.34	2.89	0.71	1.43	-2.37	MT1	H15	3,5-Dihydroxybenzoic acid
-5.32	9.34	0.62	5.24	-3.53	MT1	H16	Ethinyl Estradiol
-0.81	1.37	1.29	3.14	-2.42	MT1	H18	Equol
-7.71	6.58	0.71	1.13	-3.03	MT1	H20	6-Hydroxyflavone (6-HF)
1.71	2.08	1.16	0.83	-2.73	MT1	I08	Lauric Acid
0.14	1.85	2.19	0.33	-1.57	MT1	I11	Dehydroepiandrosterone (DHEA)
0.17	2.05	0.71	1.54	-2.22	MT1	I12	Tryptophol
0.06	1.01	1.88	0.53	-2.53	MT1	I16	2-Phenylethylamine
0.63	0.36	0.53	-2.31	0.40	MT1	I22	Imidazole
1.41	1.17	1.88	0.10	-2.17	MT1	K04	6-Benzylaminopurine
-0.89	1.38	-0.06	2.35	-1.11	MT1	K05	Vitamin B12
1.75	1.69	6.02	-1.14	-4.99	MT1	K08	Corticosterone
0.82	2.21	0.48	2.18	-1.67	MT1	K12	Indole-3-carboxylic acid
-1.12	0.10	-0.10	-2.30	0.90	MT1	K13	Quinolinic acid

<-2	-2 to -1	-1 to 1	1 to 2	>2	Standard Deviation Key

Cells	SubG1%	G1%	S%	G2/M%	PLATE	WELL	COMPOUND
0.56	3.02	0.03	1.95	-2.17	MT1	K16	7-Dehydrocholesterol
-1.28	1.99	2.91	-0.62	-2.17	MT1	L18	Ethisterone
-1.83	0.41	3.18	-0.11	-1.57	MT1	M03	Estrone
-0.53	1.73	3.14	-0.87	-2.53	MT1	M05	Pregnenolone
-1.75	-0.80	-2.31	1.00	1.36	MT1	N17	N-Acetyl-L-methionine
-1.16	-0.66	-2.27	1.46	1.10	MT1	N21	Hydrocinnamic acid
-2.78	0.69	-0.51	4.24	-0.66	MT1	O03	Hydrocortisone
-6.45	-0.24	-4.16	-1.27	6.14	MT1	O05	Menadione
-2.78	-0.74	-1.19	2.88	1.61	MT1	O13	Tryptamine
-1.84	-1.18	2.33	-0.01	-0.46	MT1	O15	Cholic acid
-6.89	1.44	2.55	0.40	-0.71	MT1	O21	Deoxycorticosterone acetate
-1.69	0.50	2.01	0.65	-1.37	MT1	P08	(+)-Delta-Tocopherol
-1.56	-0.83	0.98	-2.23	1.10	MT1	P19	Ethyl pyruvate
-2.14	-1.81	-0.73	2.46	1.41	MT1	P22	Astaxanthin
-0.10	0.38	0.03	2.07	0.20	MT2	A10	Thioguanine
-1.77	2.54	2.67	-1.14	-2.06	MT2	B08	Urolithin A
-0.50	0.46	-2.19	-0.90	1.08	MT2	B09	Pinocembrin
-0.35	0.11	-2.14	-0.37	2.06	MT2	B16	Zerumbone
-1.09	0.02	-2.87	2.62	1.13	MT2	B17	(-)Epicatechin
1.81	3.07	1.38	0.90	-2.40	MT2	C12	Bilobalide
1.41	1.71	-0.59	2.08	-1.52	MT2	D04	Sorbic acid
1.61	2.45	0.86	3.27	-2.55	MT2	D08	Dihydrojasmone
0.23	5.27	1.95	1.10	-3.29	MT2	D12	3-Hydroxycinnamic acid
1.55	2.65	2.10	2.88	-3.14	MT2	D16	Cyclohexaneacetic acid
1.13	9.73	-0.02	1.66	-4.03	MT2	E08	Ginkgolide B
0.92	5.16	-0.12	1.66	-2.36	MT2	E09	Erucic acid
1.38	3.96	2.16	0.44	-2.40	MT2	E10	Daidzein
-0.04	2.74	0.91	2.43	-2.21	MT2	E16	Silibinin
0.40	2.56	-0.23	2.18	-1.42	MT2	E17	(S)-2-Hydroxysuccinic acid
-3.39	3.62	-2.71	3.43	-0.74	MT2	E20	Betulinic acid

<-2	-2 to -1	-1 to 1	1 to 2	>2	Standard Deviation Key

Cells	SubG1%	G1%	S%	G2/M%	PLATE	WELL	COMPOUND
1.17	-0.56	2.73	-1.02	-1.32	MT2	F11	Desloratadine
2.44	5.19	0.39	2.03	-2.31	MT2	G07	2,3-Dihydroxybenzoic acid
3.32	3.89	2.52	1.02	-2.94	MT2	G08	Calcitriol
0.80	2.65	0.39	0.91	-2.16	MT2	G09	D-Tagatose
-2.01	2.20	2.05	-1.53	-2.26	MT2	G10	Fluticasone propionate
2.00	1.47	0.76	2.23	-1.67	MT2	G11	Monomyristin
1.95	2.80	1.43	2.03	-2.31	MT2	G12	Cinchonidine
2.09	3.11	2.57	0.07	-2.36	MT2	G14	Myricetin
1.36	4.65	1.43	1.92	-3.19	MT2	G16	Tangeretin
0.50	2.16	-0.64	2.55	-1.13	MT2	G19	Malic acid
-6.65	1.38	-5.92	14.05	1.43	MT2	H03	Protodioscin
1.04	1.55	1.07	2.34	-1.82	MT2	H04	Nomilin
1.00	4.70	0.86	1.05	-2.50	MT2	H08	Nerolidol
1.55	4.47	2.10	3.30	-3.14	MT2	H11	Cyclamic acid
1.64	3.83	0.71	4.81	-2.65	MT2	H12	(1S)-(-)-α-Pinene
-11.68	9.17	2.83	6.33	-6.97	MT2	H13	Digoxigenin
1.34	1.42	1.48	2.21	-1.86	MT2	H14	Monobutyl phthalate
1.58	3.98	2.05	2.74	-2.94	MT2	H15	Etonogestrel
0.40	2.82	1.17	2.80	-2.90	MT2	H16	4-Methyl-n-octanoic Acid
0.13	2.13	-0.38	2.34	-1.47	MT2	H17	Betulin
-0.39	3.94	-0.49	2.41	-2.75	MT2	H20	(-)-Citronellal
-16.52	2.89	-14.94	-3.88	7.76	MT2	I06	Docetaxel
0.87	4.00	1.43	1.77	-3.04	MT2	I08	Natamycin
1.41	2.14	-0.59	2.50	-1.13	MT2	I11	5-Methyl-2'-deoxycytidine
-1.98	4.40	1.53	5.64	-3.24	MT2	I12	Dihydroartemisinin (DHA)
1.31	5.76	0.71	2.54	-2.65	MT2	I16	Troxerutin
-1.39	3.05	0.14	2.32	-1.32	MT2	I20	Carbendazim
-0.24	-0.56	-2.35	0.77	1.72	MT2	J05	Brassinolide
-2.64	2.36	3.92	-1.94	-2.50	MT2	J17	Dihydrotestosterone (DHT)
-12.06	4.25	-4.32	10.33	0.05	MT2	J21	SN-38

<-2	-2 to -1	-1 to 1	1 to 2	>2	Standard Deviation Key

Cells	SubG1%	G1%	S%	G2/M%	PLATE	WELL	COMPOUND
0.55	1.91	0.08	2.72	-1.82	MT2	K04	3-Hydroxybutyric acid
2.79	2.24	1.43	0.35	-2.11	MT2	K07	Aleuritic Acid
2.78	6.52	-0.02	4.26	-2.99	MT2	K08	Mesalamine
0.19	0.15	2.26	3.57	-2.80	MT2	K12	Glycyrrhizin (Glycyrrhizic Acid)
2.26	2.89	1.33	2.25	-2.90	MT2	K15	Ammonium formate
1.17	2.07	2.26	2.98	-2.40	MT2	K16	Ursolic Acid
-16.97	3.81	-15.71	-1.99	8.59	MT2	K18	Fenbendazole
0.59	3.96	1.48	1.71	-3.19	MT2	K20	Tyrosol
0.72	9.46	-0.12	2.40	-3.78	MT2	L08	Decyl aldehyde
0.60	1.20	0.96	2.08	-2.31	MT2	L12	Rhodamine B
-0.57	4.00	0.34	2.55	-2.50	MT2	L20	Allyl Methyl Sulfide
-1.56	-0.58	3.30	-1.27	-1.28	MT2	M03	Flavone
-14.05	40.80	2.16	-3.28	-10.41	MT2	M06	Celastrol
-5.43	-0.65	-7.58	23.02	1.28	MT2	M18	Mycophenolic acid
-1.09	-0.71	-1.68	2.15	1.33	MT2	N05	(-)-Arctigenin
-2.28	-1.30	-2.35	0.76	1.52	MT2	N17	4-Hydroxychalcone
-1.54	0.78	-2.19	0.07	-0.10	MT2	N20	Diethyl malonate
-2.34	-0.32	3.92	-0.12	-1.62	MT2	O10	Aloe-emodin
-1.23	-1.43	2.31	-0.43	0.44	MT2	O19	Undecanoic acid
-1.30	-1.96	0.19	-2.34	1.57	MT2	P11	Dinitolmide
-0.51	-0.78	-2.04	0.35	1.28	MT2	P22	Tricarballylic acid
2.31	1.92	1.46	4.39	-3.04	MT3	H07	1-Hydroxy-2-naphthoic acid
0.70	1.12	3.05	1.53	-2.86	MT3	I12	2,5-Dimethylpyrazine
0.67	-0.35	2.11	-0.75	-0.97	MT3	G03	2,6-Dimethoxybenzoic acid
1.22	5.43	0.41	3.65	-2.86	MT3	G16	2'-Deoxycytidine 5'-monophosphate
1.16	0.65	2.23	-0.51	-0.60	MT3	L07	3-Hydroxybenzoic acid
-1.18	-1.00	2.34	-0.67	-0.38	MT3	O12	3-Methyl-2-buten-1-ol
0.47	0.78	1.76	2.15	-1.69	MT3	C04	3-Methylxanthine
-1.00	2.61	-2.17	1.23	-0.24	MT3	G06	4',5,7-Trimethoxyflavone
0.88	2.97	2.75	2.87	-2.59	MT3	D08	5a-Pregnane-3,20-dione

<-2	-2 to -1	-1 to 1	1 to 2	>2	Standard Deviation Key

Cells	SubG1%	G1%	S%	G2/M%	PLATE	WELL	COMPOUND
1.07	14.92	-2.34	0.71	-2.41	MT3	I05	Abscisic Acid (Dormin)
1.46	1.08	2.11	1.44	-2.73	MT3	G08	Acetic acid octyl ester
1.71	1.52	1.17	2.82	-1.37	MT3	H11	Adipic acid
-1.48	-0.81	0.64	3.40	0.39	MT3	C07	Alantolactone
-1.48	1.22	-2.52	0.35	0.39	MT3	B17	Amcinonide
-1.99	2.29	-2.52	0.35	-1.73	MT3	G05	Anacardic Acid
-1.36	0.63	-2.05	1.36	0.03	MT3	B13	Benzophenone
2.40	3.20	1.23	2.93	-2.28	MT3	G15	Beta-Elemonic
1.24	1.01	0.29	2.16	-1.60	MT3	G04	Capric acid
1.24	1.01	0.29	2.16	-1.60	MT3	G04	Capric acid
-17.03	3.60	-19.30	-1.28	7.35	MT3	O17	Casticin
1.84	3.01	3.16	2.24	-2.77	MT3	H15	Cinacalcet
-13.60	17.19	6.32	4.89	-8.74	MT3	A07	Cucurbitacin B
0.70	2.07	0.53	2.99	-1.10	MT3	I14	D-(-)-Tartaric acid
-2.13	-0.64	2.34	1.51	-1.28	MT3	M16	Diethyl phosphate
1.27	0.18	0.23	2.39	-0.97	MT3	H04	Dihydrocholesterol
1.47	0.40	1.05	2.09	-1.64	MT3	C08	Dihydroxyfumaric acid hydrate
1.24	2.80	0.12	2.52	-1.24	MT3	G20	D-Mannosamine hydrochloride
2.01	4.05	0.70	3.12	-2.64	MT3	G12	D-Pyroglutamic acid
-8.55	7.00	2.52	5.01	-3.41	MT3	P11	Dydrogesterone
-1.18	1.42	-2.58	-0.86	0.53	MT3	P17	Eicosapentaenoic acid ethyl ester
-14.22	32.50	8.08	-1.10	-11.09	MT3	O05	Halofuginone
-1.98	-1.01	-2.52	0.12	0.53	MT3	N13	Iohexol
-5.78	-0.33	-19.86	0.87	14.94	MT3	B15	Irinotecan hydrochloride
-3.78	2.01	2.99	1.38	-1.42	MT3	M17	Isorhamnetin
2.03	4.83	0.59	3.28	-2.23	MT3	K08	Maleic acid
1.41	2.82	0.53	2.73	-1.91	MT3	I08	Malonic acid
-0.34	0.89	-2.34	0.54	0.53	MT3	B09	Maltopentaose
1.25	3.86	1.17	3.77	-2.59	MT3	G14	N-Acetyl-D-galactosamine
1.78	2.24	2.46	2.08	-3.18	MT3	K12	N-Acetyl-L-leucine

<-2	-2 to -1	-1 to 1	1 to 2	>2	Standard Deviation Key

Cells	SubG1%	G1%	S%	G2/M%	PLATE	WELL	COMPOUND
1.60	1.18	0.00	2.35	-0.74	MT3	D07	N-Acetyl-L-phenylalanine
1.74	3.33	4.39	1.80	-3.77	MT3	G07	Perillartine
-6.10	0.89	-7.09	3.16	6.17	MT3	E05	Piperlongumine
-1.82	-1.11	-2.11	-0.28	0.75	MT3	N17	Purine
-0.72	0.16	2.34	1.06	-1.06	MT3	M12	Pyridoxal hydrochloride
-11.26	66.71	0.06	-3.17	-11.54	MT3	M07	Sanguinarine
1.34	1.73	0.64	2.03	-1.69	MT3	C10	trans-Aconitic acid
1.66	2.94	2.11	1.05	-2.00	MT3	D11	Triolein
-6.19	31.74	-9.37	-1.22	-1.82	MT3	I06	Urolithin B
0.65	2.33	4.63	1.35	-3.09	MT3	G11	Xanthotoxol
0.61	-0.20	2.58	-0.23	-1.28	MT3	C12	δ-Valerolactone
0.47	3.35	-0.01	0.53	-2.04	MT4	C08	Spermine
-5.62	0.14	-6.67	21.13	-4.39	MT4	E08	Cytarabine
-0.99	0.62	3.08	0.17	-2.04	MT4	G10	D-Alanine
1.09	1.12	1.98	0.61	-2.04	MT4	G11	Spermine Tetrahydrochloride
1.13	1.84	1.64	1.75	-2.68	MT4	G12	L-Histidine monohydrochloride monohydrate
1.53	3.31	1.83	0.67	-2.41	MT4	G14	Phospho(enol)pyruvic acid monopotassium salt
0.62	3.67	2.26	1.74	-3.51	MT4	G16	Sodium etidronate
2.70	11.74	-2.41	1.88	-2.77	MT4	I06	L(-)-Sorbose
1.55	2.50	1.84	0.49	-2.27	MT4	K07	Creatine phosphate disodium salt
1.51	0.87	0.63	1.88	-2.27	MT4	K08	Citicholine
0.77	0.40	0.33	2.15	-1.35	MT4	K12	1-Aminocyclopropanecarboxylic acid
-0.43	-1.32	-0.40	-1.56	2.20	MT4	M11	Creatine
-0.22	-0.48	2.26	-0.01	-0.52	MT4	O04	D-glutamine
-0.02	-1.26	2.19	-1.36	0.64	MT4	O06	Goserelin Acetate
-0.95	-0.83	3.23	-1.05	-0.84	MT4	O12	L-Anserine nitrate salt
-2.13	-1.28	-0.15	-0.21	2.06	MT4	O13	L-Hydroxyproline

<-2	-2 to -1	-1 to 1	1 to 2	>2	Standard Deviation Key

Table 1 Metabolite library screening hits.

HeLa cells were treated with 5uM of each metabolite for 20 hours prior to addition of DyeCycle Vybrant Green DNA stain and analyzed with a scanning cytometer. Each metabolite was analyzed for deviation from the mean of untreated cells in their respective plate. List is of every metabolite shown to alter cell cycle percentages by at least 2 or more standard deviations.

Table 2 Metabolite Library Screen Initial Hit List

Metabolite Library - Initial Hit List							
Cells	**SubG1%**	**G1%**	**S%**	**G2/M%**	**PLATE**	**WELL**	**COMPOUND**
1.82	0.62	3.95	-0.86	-2.93	MT1	C11	Medroxyprogesterone acetate
1.75	1.69	6.02	-1.14	-4.99	MT1	K08	Corticosterone
-16.07	3.64	-8.62	0.21	4.43	MT1	D16	2-Methoxyestradiol (2-MeOE2)
-6.45	-0.24	-4.16	-1.27	6.14	MT1	O05	Menadione
-6.65	1.38	-5.92	14.05	1.43	MT2	H03	Protodioscin
-5.43	-0.65	-7.58	23.02	1.28	MT2	M18	Mycophenolic acid
-0.52	0.20	-1.83	1.53	1.08	MT2	A09	Fructose
0.80	2.65	0.39	0.91	-2.16	MT2	G09	D-Tagatose
-16.52	2.89	-14.94	-3.88	7.76	MT2	I06	Docetaxel
-11.68	9.17	2.83	6.33	-6.97	MT2	H13	Digoxigenin
-14.05	40.80	2.16	-3.28	-10.41	MT2	M06	Celastrol
-16.97	3.81	-15.71	-1.99	8.59	MT2	K18	Fenbendazole
-11.26	66.71	0.06	-3.17	-11.54	MT3	M07	Sanguinarine
-6.10	0.89	-7.09	3.16	6.17	MT3	E05	Piperlongumine
-6.19	31.74	-9.37	-1.22	-1.82	MT3	I06	Urolithin B
-5.78	-0.33	-19.86	0.87	14.94	MT3	B15	Irinotecan hydrochloride
-14.22	32.50	8.08	-1.10	-11.09	MT3	O05	Halofuginone
-13.60	17.19	6.32	4.89	-8.74	MT3	A07	Cucurbitacin B
1.74	3.33	4.39	1.80	-3.77	MT3	G07	Perillartine
0.65	2.33	4.63	1.35	-3.09	MT3	G11	Xanthotoxol
-17.03	3.60	-19.30	-1.28	7.35	MT3	O17	Casticin
2.70	11.74	-2.41	1.88	-2.77	MT4	I06	L(-)-Sorbose

<-2	-2 to -1	-1 to 1	1 to 2	>2	Standard Deviation Key

Table 2

Table of initial hits chosen for further study via immunofluorescence microscopy.

Supplemental Data

Table 1A Metabolite Library - Plate 1 List

MT1-WELL	COMPOUND
A03	Melatonin
A04	Serotonin HCl
A05	Progesterone
A06	Dehydrocholic acid
A07	Uridine
A08	2-Deoxy-D-glucose
A09	5-hydroxytryptophan (5-HTP)
A10	L-5-Hydroxytryptophan
A11	Isoprenaline HCl
A12	N-Acetylneuraminic acid
A13	4-Aminohippuric Acid
A14	cis-Aconitic acid
A15	Vitamin E Acetate
A16	Taurocholic acid sodium salt hydrate
A17	Betaine
A18	2'-deoxyuridine
A19	Taurochenodeoxycholic acid
A20	Glyceryl tridecanoate
A21	cholecalciferol (Vitamin D3)
A22	Pyrrole-2-carboxylic acid
B03	Methyloxalacetic acid diethyl ester
B04	N-Acetylglucosamine
B05	2-Naphthol
B06	3,3-Dimethylglutaric acid
B07	Phenylglyoxylic acid
B08	5-Methoxytryptamine
B09	Glycodeoxycholic acid sodium salt
B10	NADH, disodium salt hydrate
B11	L-Hydroorotic acid
B12	Docosahexaenoic Acid
B13	(±)-α-Bisabolol
B14	Homogentisic Acid
B15	2-Hydroxyphenylacetic acid
B16	(–)-Norepinephrine
B17	N-Isovaleroylglycine

MT1-WELL	COMPOUND
F10	Ac-Arg-OH
F11	D-Arabitol
F12	Isohomovanillic acid
F13	16-Dehydroprogesterone
F14	5'-Adenylic acid
F15	5-Methyluridine
F16	Alprostadil
F17	N-Methylhydantoin
F18	Forskolin
F19	β-Alanine methyl ester hydrochloride
F20	Methyl Vanillate
F21	L-Lactic acid
F22	Cinnamaldehyde
G03	Ursodiol
G04	17-Hydroxyprogesterone
G05	Chenodeoxycholic Acid
G06	Protirelin
G07	Xylose
G08	Kynurenic acid
G09	Guanosine
G10	Cortodoxone
G11	L-Thyroxine
G12	3-Indolepropionic acid
G13	Vitamin C
G14	Skatole
G15	2,6-Dihydroxypurine
G16	Pyridoxal phosphate
G17	Gentisic acid
G18	Vitamin A
G19	Pyridoxine
G20	Citric acid
G21	1-Hexadecanol
G22	Cortisone
H03	D-(–)-Pantolactone
H04	Dodecanedioic acid

MT1-WELL	COMPOUND
K17	D-Galactose
K18	Hippuric acid
K19	(+)-α-Lipoic acid
K20	Glycochenodeoxycholic acid
K21	Azaguanine-8
K22	Bisphenol A
L03	3-(3-Methoxyphenyl)propionic acid
L04	4-Methylvaleric acid
L05	3-Oxopentanedioic acid
L06	N-Acetyl-L-tyrosine
L07	5-Hydroxymethyl-2-furancarboxylic acid
L08	D-Glucuronic acid
L09	(±)-α-Tocopherol
L10	1,5-Diaminopentane dihydrochloride
L11	5-Hydroxymethyluracil
L12	(R)-(-)-Mandelic acid
L13	Glycoursodeoxycholic acid
L14	Thymine
L15	2-Methyl-4-pentenoic Acid
L16	Caffeic Acid
L17	Dimethylamine hydrochloride
L18	Ethisterone
L19	2-Ketoglutaric acid
L20	Tauroursodeoxycholic Acid (TUDCA)
L21	H-D-Trp-OH
L22	Phloretic acid
M03	Estrone
M04	i-Inositol
M05	Pregnenolone
M06	D panthenol
M07	Orotic acid (6-Carboxyuracil)
M08	2,4-Dihydroxyacetophenone
M09	Dopamine HCl
M10	L-α-Phosphatidylcholine
M11	3-Methyladenine (3-MA)

MT1-WELL	COMPOUND
B18	Kinetin
B19	Phthalic acid
B20	Rosmarinic acid
B21	N-Acetylglutamic acid
B22	Cinnamic acid
C03	Isotretinoin
C04	DL-Mevalonic Acid Lactone
C05	Estradiol
C06	DL-Panthenol
C07	Cytidine
C08	Oleic Acid
C09	L-carnitine
C10	Adrenosterone
C11	Medroxyprogesterone acetate
C12	Trenbolone acetate
C13	Prostaglandin E2 (PGE2)
C14	Nonanoic acid
C15	Methylmalonate
C16	Protoporphyrin IX
C17	2'-Deoxyinosine
C18	D-Ribose
C19	3,5-Diiodotyrosine Dihydrate
C20	Sebacic acid
C21	Histamine 2HCl
C22	SDMA
D03	3-Methoxyphenylacetic acid
D04	1,2-Propanediol
D05	2,3-Butanediol (mixture of isomers)
D06	Octanoic acid
D07	2-Ethylbutyric Acid
D08	D-3-Phenyllactic acid
D09	cis,cis-Muconic acid
D10	Androsterone
D11	Oxalacetic acid
D12	Eicosapentaenoic Acid

MT1-WELL	COMPOUND
H05	(S)-Leucic acid
H06	Methylguanidine HCl
H07	Monomethyl glutarate
H08	Undecanedioic acid
H09	5-Phenylvaleric Acid
H10	Glycochenodeoxycholic acid sodium salt
H11	Pyridoxal 5′-phosphate hydrate
H12	3beta-hydroxy-delta5-cholenic acid
H13	Ureidopropionic acid
H14	ADP
H15	3,5-Dihydroxybenzoic acid
H16	Ethinyl Estradiol
H17	Arachidonic acid
H18	Equol
H19	Methylamine hydrochloride
H20	6-Hydroxyflavone (6-HF)
H21	Terephthalic acid
H22	Stachydrine
I03	Adenosine
I04	4-Aminobenzoic acid
I05	Nicotinamide (Vitamin B3)
I06	Vitamin E
I07	3-Indolebutyric acid (IBA)
I08	Lauric Acid
I09	Inosine
I10	Menadiol Diacetate
I11	Dehydroepiandrosterone (DHEA)
I12	Tryptophol
I13	Biotin (Vitamin B7)
I14	3,4,5-Trimethoxycinnamic acid
I15	Glucosamine hydrochloride
I16	2-Phenylethylamine
I17	Trigonelline Hydrochloride
I18	4-Methylcatechol
I19	L-Tryptophan

MT1-WELL	COMPOUND
M12	Cytosine
M13	Tyramine
M14	Vitamin K2
M15	Boldenone Undecylenate
M16	2-Hydroxycaprylic acid
M17	Allantoin
M18	3,4-Dihydroxyphenylacetic acid
M19	Lithocholic acid
M20	Allopregnanolone
M21	Cysteamine HCl
M22	p-Hydroxybenzaldehyde
N03	2,6-Dihydroxybenzoic acid
N04	Cyclohexanecarboxylic Acid
N05	1,3-Dimethyluracil
N06	2,5-Furandicarboxylic acid
N07	DL-Dopa
N08	Tetradecanedioic acid
N09	trans-3-Indoleacrylic acid
N10	Glucosamine
N11	2-Oxo-3-phenylpropanoic acid
N12	2'-Deoxyguanosine monohydrate
N13	Hexadecanedioic acid
N14	Urocanic acid
N15	trans-trans-Muconic acid
N16	Enoxolone
N17	N-Acetyl-L-methionine
N18	Vanillin
N19	β-D-Glucose pentaacetate
N20	Thymopentin
N21	Hydrocinnamic acid
N22	Royal jelly acid
O03	Hydrocortisone
O04	Xylitol
O05	Menadione
O06	Vitamin K1

MT1-WELL	COMPOUND
D13	5-Methylcytidine
D14	Phenylacetaldehyde
D15	H-Trp-NH2.HCl
D16	2-Methoxyestradiol (2-MeOE2)
D17	L-Gulono-1,4-lactone
D18	Oleanolic Acid
D19	o-Toluic acid
D20	Syringic acid
D21	Picolinic acid (PCL 016)
D22	4-Hydroxybenzoic acid
E03	Acetylcysteine
E04	Calcium D-Panthotenate
E05	Nicotinic Acid
E06	Benzyl alcohol
E07	Dextrose
E08	Palmitoylethanolamide
E09	Sorbitol
E10	Xanthurenic Acid
E11	Phenylephrine HCl
E12	Thymidine
E13	Pyridoxine HCl
E14	Glycocholic acid
E15	Urea
E16	Adenosine 5'-monophosphate monohydrate
E17	Palmitic acid
E18	Benzoic aldehyde
E19	Histamine
E20	Stearic acid
E21	Benzoic Acid
E22	L-Kynurenine
F03	Isonicotinic acid
F04	Ureidosuccinic acid

MT1-WELL	COMPOUND
I20	D-Mannose
I21	Uracil
I22	Imidazole
J03	α-D-Glucose anhydrous
J04	2-(4-Methoxyphenyl)acetic acid
J05	Lactose
J06	Dimethyl Trisulfide
J07	Phenylacetylglutamine
J08	3-(Methylthio)propionic acid
J09	3-Furoic acid
J10	2-Methylsuccinic acid
J11	3-Hydroxyisovaleric acid
J12	NMDA (N-Methyl-D-aspartic acid)
J13	O-Acetylserine
J14	Xanthosine Dihydrate
J15	2-Octenoic acid
J16	Acetylcholine Chloride
J17	N-(5-Aminopentyl)acetamide
J18	5-Aminolevulinic acid HCl
J19	Pentadecanoic acid
J20	4-Amino-5-imidazolecarboxamide
J21	3-Hydroxypicolinic acid
J22	Succinic acid
K03	Tretinoin
K04	6-Benzylaminopurine
K05	Vitamin B12
K06	Deoxycholic acid
K07	Hyodeoxycholic acid (HDCA)
K08	Corticosterone
K09	Estriol
K10	Nicotinamide N-oxide
K11	Ribitol

MT1-WELL	COMPOUND
O07	Synephrine
O08	Melibiose
O09	Cortisone acetate
O10	3-Hydroxyflavone
O11	Epiandrosterone
O12	D-Glucurone
O13	Tryptamine
O14	Stachyose
O15	Cholic acid
O16	O-Acetyl-L-carnitine hydrochloride
O17	Dulcitol
O18	Homovanillic acid
O19	Vitamin D2
O20	L-Pyroglutamic acid
O21	Deoxycorticosterone acetate
O22	Acetamide
P03	2-Aminobenzenesulfonic acid
P04	Sodium Thiocyanate
P05	Phenyl-ac-Gly-OH
P06	2-Phenylpropionic acid
P07	6-(Dimethylamino)purine
P08	(+)-Delta-Tocopherol
P09	2-Methylpentanedioic acid
P10	Nervonic acid
P11	All trans-Retinal
P12	2'-Deoxyadenosine monohydrate
P13	3-Methyl-2-oxobutanoic acid
P14	Uridine 5'-monophosphate
P15	trans-2-Butene-1,4-dicarboxylic Acid
P16	Ferulic Acid
P17	Ethanolamine hydrochloride
P18	(+,-)-Octopamine HCl

MT1-WELL	COMPOUND
F05	L-Arabinitol
F06	4-Hydroxy-3-methylbenzoic acid
F07	trans-4-Hydroxycyclohexanecarboxylic Acid
F08	2-Oxobutanoic acid
F09	Quinoline-4-carboxylic acid

MT1-WELL	COMPOUND
K12	Indole-3-carboxylic acid
K13	Quinolinic acid
K14	Methylcobalamin
K15	Dihydrothymine
K16	7-Dehydrocholesterol

MT1-WELL	COMPOUND
P19	Ethyl pyruvate
P20	Umbelliferone
P21	Isocytosine
P22	Astaxanthin

Table 1B Metabolite Library - Plate 2 List

MT2-WELL	COMPOUND
A03	Guaiacol
A04	Vanillylmandelic acid
A05	Thioctic acid
A06	Sevoflurane
A07	Indole-3-acetic acid
A08	Costunolide
A09	Fructose
A10	Thioguanine
A11	γ-Linolenic acid
A12	Arbutin
A13	2-Phenylbutyric acid
A14	Indole-3-carbinol
A15	Isethionic acid sodium salt
A16	Sclareol
A17	Methyl 3-indolyacetate
A18	Naringenin
A19	L-(+)-Arabinose
A20	Dimethyl Fumarate
A21	Madecassic acid
A22	Notoginsenoside R1
B03	Glycitin
B04	Nerol
B05	Perillyl alcohol
B06	Geranyl acetate
B07	Tetrahydrocurcumin
B08	Urolithin A
B09	Pinocembrin
B10	Aucubin
B11	Ketoisophorone
B12	Citronellal
B13	Cyromazine
B14	Methyl Stearate
B15	Triacetin
B16	Zerumbone
B17	(-)Epicatechin
B18	(+)-(S)-Carvone
B19	Gibberellic acid

MT2-WELL	COMPOUND
F10	Juglone
F11	Desloratadine
F12	3-Carene
F13	Carbadox
F14	Cinnamyl alcohol
F15	Gallic acid
F16	Ethyl acetoacetate
F17	Ganoderic acid A
F18	cis-3-Hexen-1-ol
F19	Harmaline
F20	Traumatic acid
F21	2-Furoic acid
F22	2-Acetylpyrazine
G03	4',7-Dimethoxyisoflavone
G04	Trifluoperazine
G05	Aceglutamide
G06	Rapamycin (Sirolimus)
G07	2,3-Dihydroxybenzoic acid
G08	Calcitriol
G09	D-Tagatose
G10	Fluticasone propionate
G11	Monomyristin
G12	Cinchonidine
G13	Tridecanoic acid
G14	Myricetin
G15	Tartaric acid
G16	Tangeretin
G17	2,4-Dihydroxybenzoic acid
G18	Geniposidic acid
G19	Malic acid
G20	Asiaticoside
G21	Phenprocoumon
G22	Guggulsterone E&Z
H03	Protodioscin
H04	Nomilin
H05	Harmine
H06	Methyl Dihydrojasmonate

MT2-WELL	COMPOUND
K17	2-Methyllactic acid
K18	Fenbendazole
K19	D-(+)-Raffinose pentahydrate
K20	Tyrosol
K21	Hydrocortisone butyrate
K22	Angelic acid
L03	Madecassoside
L04	p-Anisaldehyde
L05	Protopine
L06	7-Methoxycoumarin
L07	Liquiritin
L08	Decyl aldehyde
L09	(-)-Borneol
L10	6-Paradol
L11	Mequinol
L12	Rhodamine B
L13	Urethane
L14	3-(4-Hydroxyphenyl)-1-propanol
L15	(-)-Menthol
L16	4-Ethyloctanoic acid
L17	Thymoquinone
L18	2-Methylheptanoic Acid
L19	Cedryl acetate
L20	Allyl Methyl Sulfide
L21	Maltol
L22	4-Pentenoic acid
M03	Flavone
M04	Sphingosine
M05	Gluconolactone
M06	Celastrol
M07	Sodium erythorbate
M08	Prednisolone
M09	Arachidic acid
M10	Esculin
M11	Trimethylamine N-oxide dihydrate
M12	Gynostemma Extract
M13	3-Methyladipic acid

MT2-WELL	COMPOUND
B20	2-Hydroxybutyric acid
B21	TriacetonaMine
B22	Indole-2-carboxylic acid
C03	Pyrogallol
C04	Maltotetraose
C05	Guanidine HCl
C06	Nicotinamide Riboside Chloride (NIAGEN)
C07	4-Hydroxyphenylacetic acid
C08	Edaravone
C09	Behenic Acid
C10	Oxfendazole
C11	Sodium Dehydrocholate
C12	Bilobalide
C13	Imidazole-4(5)-acetic Acid Hydrochloride
C14	Kaempferol
C15	Levulinic acid
C16	Shikimic Acid
C17	6-Hydroxynicotinic acid
C18	Chrysophanic Acid
C19	2-Aminoethanethiol
C20	N6-methyladenosine (m6A)
C21	p-Hydroxy-cinnamic Acid
C22	Carvacrol
D03	Hydroxytyrosol
D04	Sorbic acid
D05	4-Hydroxybenzyl alcohol
D06	Tylosin
D07	4',7-Dimethoxy-5-Hydroxyflavone
D08	Dihydrojasmone
D09	Mesterolone
D10	Monotropein
D11	Guaiazulene
D12	3-Hydroxycinnamic acid
D13	Sucralose
D14	Methyl linoleate
D15	Butylparaben
D16	Cyclohexaneacetic acid

MT2-WELL	COMPOUND
H07	Ginsenoside Rb1
H08	Nerolidol
H09	(+)-Borneol
H10	Galangin
H11	Cyclamic acid
H12	(1S)-(-)-α-Pinene
H13	Digoxigenin
H14	Monobutyl phthalate
H15	Etonogestrel
H16	4-Methyl-n-octanoic Acid
H17	Betulin
H18	2-Methylhexanoic acid
H19	Xanthoxyline
H20	(-)-Citronellal
H21	Trans-Zeatin
H22	Glycerol Tributyrate
I03	N-Sulfo-glucosamine sodium salt
I04	Apraclonidine HCl
I05	Salicylic acid
I06	Docetaxel
I07	Fumaric acid
I08	Natamycin
I09	Propylparaben
I10	Ginkgolide A
I11	5-Methyl-2'-deoxycytidine
I12	Dihydroartemisinin (DHA)
I13	Maltotriose
I14	Nobiletin
I15	Senecioic acid
I16	Troxerutin
I17	2-Methoxybenzoic acid
I18	20-Hydroxyecdysone
I19	S-(-)-Cotinine
I20	Carbendazim
I21	3-Methylbutanoic acid
I22	Rebaudioside A
J03	Amentoflavone

MT2-WELL	COMPOUND
M14	Piperine
M15	(S)-2-Hydroxy-3-phenylpropanoic acid
M16	Vanillylacetone
M17	4-Ethylphenol
M18	Mycophenolic acid
M19	D-(+)-Turanose
M20	Ginkgolide C
M21	(±)-Equol
M22	Stevioside
N03	Eupatilin
N04	4-Isopropylbenzaldehyde
N05	(-)-Arctigenin
N06	(-)-Ambroxide
N07	Ginsenoside Rd
N08	Fenchyl Alcohol
N09	Caryophyllene oxide
N10	Benzyl acetate
N11	Vitamin A Acetate
N12	Hydroxyhexamide
N13	Ethylvanillin
N14	Apocarotenal
N15	Benzamide
N16	Dibutyl sebacate
N17	4-Hydroxychalcone
N18	1-Furfurylpyrrole
N19	6-Methylcoumarin
N20	Diethyl malonate
N21	Linalool
N22	(–)-β-Pinene
O03	Batyl alcohol
O04	Isopropyl myristate
O05	p-Coumaric Acid
O06	Mercaptopurine (6-MP)
O07	Pyrithioxin
O08	Oxytetracycline (Terramycin)
O09	Indole-3-acetamide
O10	Aloe-emodin

MT2-WELL	COMPOUND
D17	Rebaudioside C
D18	β-Caryophyllene
D19	alpha-Asarone
D20	DL-Benzylsuccinic acid
D21	Squalene
D22	Methyl nicotinate
E03	Quinic acid
E04	Josamycin
E05	Erythritol
E06	Myristic Acid
E07	Farnesol
E08	Ginkgolide B
E09	Erucic acid
E10	Daidzein
E11	Linoleic acid
E12	Chlorogenic Acid
E13	2-Hydroxy-3-methylbutanoic acid
E14	Limonin
E15	Octanedioic acid
E16	Silibinin
E17	(S)-2-Hydroxysuccinic acid
E18	Genipin
E19	Salicylamide
E20	Betulinic acid
E21	Eriodictyol
E22	Tiglic acid
F03	Isoalantolactone
F04	TBHQ
F05	Vanillyl Alcohol
F06	Safflower Yellow
F07	Ginsenoside Rg1
F08	Vanillic acid
F09	Hydroumbellic acid

MT2-WELL	COMPOUND
J04	Imazalil
J05	Brassinolide
J06	D-(+)-Melezitose
J07	Liquiritigenin
J08	Ethyl Oleate
J09	Acetylvanillin
J10	Geraniol
J11	Valdecoxib
J12	Methyl furan-2-carboxylate
J13	Ethylparaben
J14	Citronellyl acetate
J15	Esculetin
J16	Methyl p-tert-butylphenylacetate
J17	Dihydrotestosterone(DHT)
J18	3-Methylvaleric acid
J19	Phloracetophenone
J20	DL-6,8-Thioctamide
J21	SN-38
J22	γ-caprolactone
K03	Homoveratrumic acid
K04	3-Hydroxybutyric acid
K05	Azelaic acid
K06	Fluorouracil (5-Fluoracil, 5-FU)
K07	Aleuritic Acid
K08	Mesalamine
K09	Hydrocortisone acetate
K10	(-)-Epigallocatechin Gallate
K11	3-Methoxybenzoic acid
K12	Glycyrrhizin (Glycyrrhizic Acid)
K13	Glycerol trilinoleate
K14	Phloretin
K15	Ammonium formate
K16	Ursolic Acid

MT2-WELL	COMPOUND
O11	1,11-Undecanedicarboxylic acid
O12	Hesperidin
O13	2-Hydroxy-2-methylbutanoic acid
O14	Rutin
O15	Glycolic acid
O16	Diosmetin
O17	Glycerol Tri-n-octanoate
O18	L-Ascorbyl 6-palmitate
O19	Undecanoic acid
O20	Obacunone
O21	Cyclothiazide
O22	Ginsenoside Re
P03	Panaxatriol
P04	4-Isopropylbenzyl Alcohol
P05	Ursonic acid
P06	Canrenone
P07	Nonivamide
P08	1,4-Cineole
P09	Methyl 4-hydroxybenzoate
P10	Cinnamyl acetate
P11	Dinitolmide
P12	Methyl Eugenol
P13	Hexylresorcinol
P14	4'-Methoxychalcone
P15	(+)-Catechin
P16	3-Indoleacetonitrile
P17	Melezitose
P18	Terpinen-4-ol
P19	Saccharin
P20	10-Undecen-1-ol
P21	Jasmone
P22	Tricarballylic acid

Table 1C Metabolite Library - Plate 3 List

MT3-WELL	COMPOUND
A03	2,5-Dimethyl-2,3-dihydrofuran-3-one
A04	Caftaric acid
A05	Glycyrrhetinic acid
A06	Trans-Anethole
A07	Cucurbitacin B
A08	Nα-Acetyl-L-asparagine
A09	Maslinic acid
A10	12-Hydroxydodecanoic acid
A11	Pulegone
A12	N-Acetylglycine
A13	Isochlorogenic acid A
A14	N-Formylglycine
A15	1-Naphthaleneacetic acid
A16	Glutaric acid
A17	2-Undecanol
A18	N-Acetyl-L-arginine dihydrate
A19	Ginsenoside F2
A20	N-Formyl-L-methionine
A21	Rebaudioside D
A22	3-(2-Hydroxyphenyl)propionic acid
B03	Lithium acetoacetate
B04	Hypoxanthine
B05	3-Hydroxyphenylacetic acid
B06	Norfloxacin
B07	3-Amino-4-hydroxybenzoic acid
B08	Uvaol
B09	Maltopentaose
B11	Spermidine
B13	Benzophenone
B15	Irinotecan hydrochloride
B17	Amcinonide
B19	amdinocillin
C03	Methyl cyclohexanecarboxylate
C04	3-Methylxanthine
C05	n-Butylidenephthalide
C06	Maltose
C07	Alantolactone
C08	Dihydroxyfumaric acid hydrate
C09	Hydroxy safflor yellow A
C10	trans-Aconitic acid
C11	Rhapontigenin

MT3-WELL	COMPOUND
E21	Tracheloside
E22	Petroselinic acid
F03	Phosphonoacetic acid
F04	Bilibubin
F05	Monoethyl malonic acid
F06	Paliperidone
F07	3-Hydroxybenzyl alcohol
F08	Retinyl (Vitamin A) Palmitate
F09	Ginsenoside Rc
F11	Benzenebutyric acid
F13	Dimercaprol
F15	Cefpiramide acid
F17	Propafenone
G03	2,6-Dimethoxybenzoic acid
G04	Capric acid
G05	Anacardic Acid
G06	4',5,7-Trimethoxyflavone
G07	Perillartine
G08	Acetic acid octyl ester
G09	Pogostone
G10	Glyoxylic acid monohydrate
G11	Xanthotoxol
G12	D-Pyroglutamic acid
G13	Alnustone
G14	N-Acetyl-D-galactosamine
G15	Beta-Elemonic
G16	2'-Deoxycytidine 5'-monophosphate
G17	AKBA
G18	N-Methylnicotinamide
G19	TFAP
G20	D-Mannosamine hydrochloride
G21	Absinthin
G22	Methyl β-D-Galactopyranoside
H03	Elaidic acid
H04	Dihydrocholesterol
H05	N-Acetyl-D-mannosamine
H06	Lornoxicam
H07	1-Hydroxy-2-naphthoic acid
H09	2-Pentylfuran
H11	Adipic acid
H13	Pipobroman

MT3-WELL	COMPOUND
K12	N-Acetyl-L-leucine
K13	D-(+)-Trehalose Anhydrous
K14	2-Amino-1-phenylethanol
K15	Bergaptol
K16	Myosmine
K17	Morin
K18	2-Hydroxycaproic acid
K19	Veratraldehyde (3,4-Dimethoxybenzaldehyde)
K20	Glycolaldehyde dimer
K21	Cyperotundone
K22	3-Methylglutaric acid
L03	Bis(2-ethylhexyl) phthalate
L04	Beta Carotene
L05	Hemin
L06	Enrofloxacin
L07	3-Hydroxybenzoic acid
L09	Succinic anhydride
L11	3-Phenoxybenzoic acid
L13	Quinine
L15	Loxapine
L17	Amitriptyline
M03	Coniferyl alcohol
M04	D-Mannitol
M05	Licochalcone A
M06	N-Acetyl-5-hydroxytryptamine
M07	Sanguinarine
M08	N-Acetyl-DL-methionine
M09	Tectorigenin
M10	Itaconic acid
M11	(+)-Isocorynoline
M12	Pyridoxal hydrochloride
M13	Ethyl 4-Methoxycinnamate
M14	Pyruvic acid
M15	Dihydrokavain
M16	Diethyl phosphate
M17	Isorhamnetin
M18	Sodium 2-(1H-indol-3-yl)acetate
M19	Trigonelline
M20	L-Histidinol dihydrochloride
M21	Medicagenic acid
M22	O-Acetyl-L-serine hydrochloride

MT3-WELL	COMPOUND
C12	δ-Valerolactone
C13	Ginsenoside F1
C14	Sodium 2-hydroxybutanoate
C15	2',5'-Dihydroxyacetophenone
C16	Citraconic acid
C17	Pomolic acid
C18	Levoglucosan
C19	(20S)Ginsenoside Rg2
C20	(L)-Dehydroascorbic acid
C21	Steviol (Hydroxydehydrostevic acid)
C22	Palmitoleic acid
D03	3-Hydroxyanthranilic acid
D04	Folic acid
D05	(S)-(-)-1-Phenylethanol
D06	Methyldopa
D07	N-Acetyl-L-phenylalanine
D08	5a-Pregnane-3,20-dione
D09	Esculentoside A
D11	Triolein
D13	2-Phenylacetamide
D15	Levobupivacaine
D17	Megestrol
D19	Chloroquine
E03	trans-2-Hexenal
E04	Monomethyl Fumarate
E05	Piperlongumine
E06	Ethyl palmitate
E07	L-Fucose
E08	Isophorone
E09	Nootkatone
E10	Methyl acetoacetate
E11	Curdione
E12	2-Deoxy-D-ribose
E13	Cryptochlorogenic acid
E14	2,4-Dihydroxypyrimidine-5-carboxylic acid
E15	2'-Hydroxyacetophenone
E16	2'-Deoxyadenosine 5'-monophosphate
E17	(-)-Fenchone
E18	(R)-3-Hydroxybutanoic acid
E19	Didymin
E20	Maleamic acid

MT3-WELL	COMPOUND
H15	Cinacalcet
H17	Bisoprolol
I03	2-Ethyl-3-hydroxy-4H-pyran-4-one
I04	Neohesperidin Dihydrochalcone (Nhdc)
I05	Abscisic Acid (Dormin)
I06	Urolithin B
I07	20S-Ginsenoside Rg3
I08	Malonic acid
I09	Orientin
I10	Pyrazole
I11	Steviolbioside
I12	2,5-Dimethylpyrazine
I13	Sequoyitol
I14	D-(-)-Tartaric acid
I15	Diosbulbin B
I16	D-(+)-Galacturonic acid monohydrate
I17	Dihydrocapsaicin
I18	Nicotinuric acid
I19	Glycerol
I20	(2R,3R)-(-)-2,3-Butanediol
I21	Cynarin
I22	Serotonin creatinine sulfate monohydrate
J03	4-Acetamidobutyric acid
J04	6-Biopterin
J05	Oxiglutatione
J06	Diosmin
J07	Quinaldic acid
J09	1-Undecanol
J11	D-Gluconic acid
J13	Tetracycline
J15	Promethazine
J17	Alverine
K03	3,4-Dihydroxyhydrocinnamic acid
K04	Neohesperidin
K05	4-Hydroxytamoxifen
K06	Adenine
K07	20S-Ginsenoside Rh2
K08	Maleic acid
K09	1-Kestose
K10	N-Acetyl-L-alanine
K11	α-Cyperone

MT3-WELL	COMPOUND
N03	D-Gulonic acid γ-lactone
N04	Tritetradecanoin
N05	Indole
N06	6-Aminopenicillanic acid
N07	S-Adenosyl-L-homocysteine (SAH)
N09	Crotamiton
N11	Sucrose
N13	Iohexol
N15	Oxytetracycline hydrochloride
N17	Purine
O03	Damascenone
O04	Asaraldehyde
O05	Halofuginone
O06	4-Methyl-2-oxovaleric acid
O07	Isochlorogenic acid C
O08	(±)-Methyl Jasmonate
O09	20(S)-Ginsenoside Rh1
O10	5,6-Dimethylbenzimidazole
O11	Isochlorogenic acid B
O12	3-Methyl-2-buten-1-ol
O13	Oxalic acid
O14	Pimelic acid
O15	10-Undecenoic acid
O16	cis-3-Hexenyl hexanoate
O17	Casticin
O18	L-Cysteic acid monohydrate
O19	Rebaudioside B
O20	D-(-)-Lyxose
O21	Galangin 3-methyl ether
O22	Tricosanoic acid
P03	DL-Mandelic acid
P04	Ellagic acid
P05	2-Hydroxypyridine
P06	Ginsenoside Rb2
P07	Ginsenoside Ro
P09	4-Hydroxyphenylpyruvic acid
P11	Dydrogesterone
P13	Balsalazide
P15	Allylestrenol
P17	Eicosapentaenoic acid ethyl ester

Table 1D Metabolite Library - Plate 4 List

MT4 -WELL	COMPOUND
A03	L-Glutamine
A04	Adenosine 5′-diphosphate sodium salt
A05	Thiamine HCl (Vitamin B1)
A06	Sodium Demethylcantharidate
A07	Glutathione
A08	Estramustine phosphate sodium
A09	L-Threonine
A10	Bicine
A11	L-carnosine
A12	L-DAB HBR
A13	L-Proline
A14	Phytic acid dipotassium salt
A15	D-Proline
A16	Uridine-5'-diphosphate disodium salt
A17	8-Aminooctanoic acid
A19	Aminomalonic acid
A21	(S)-Glutamic acid
B03	D-Phenylalanine
C03	ATP disodium
C04	DL-Norvaline
C05	Citicoline sodium
C06	Calcium Gluceptate
C07	L-Ornithine hydrochloride
C08	Spermine
C09	Agmatine sulfate
C10	Oxytocin (Syntocinon)
C11	β-Nicotinamide
C12	Isocitric acid trisodium salt
C13	L-lysine
C14	Disodium 5'-inosinate monohydrate
C15	5-Methylcytosine

MT4 -WELL	COMPOUND
E13	L-Alanine
E14	2-Aminoethylphosphonic acid
E15	Creatine monohydrate
E16	Gadobutrol
E17	Inosine 5′-triphosphate trisodium salt
E19	3-Amino-2-methylpropanoic acid
E21	D-Fructose-1,6-diphosphate trisodium salt octahydrate
G03	Taurine
G04	O-Phosphoethanolamine
G05	L-Leucine
G06	Calcium folinate
G07	Sarcosine
G08	Phytic acid
G09	Flavin mononucleotide
G10	D-Alanine
G11	Spermine Tetrahydrochloride
G12	L-Histidine monohydrochloride monohydrate
G13	L-aspartic Acid
G14	Phospho(enol)pyruvic acid monopotassium salt
G15	H-Tyr(3-I)-OH
G16	Sodium etidronate
G17	3-Chloro-L-tyrosine
G19	4-Guanidinobutanoic acid
G21	L(-)-Pipecolinic acid
I03	Chondroitin sulfate
I04	L-serine
I05	L-Citrulline
I06	L(-)-Sorbose
I07	D-(+)-Cellobiose
I08	DL-Glutamine
I09	Sodium L-ascorbyl-2-phosphate

MT4 -WELL	COMPOUND
K08	Citicholine
K09	DL-Citrulline
K10	Thiamine monophosphate chloride dihydrat
K11	L-Asparagine
K12	1-Aminocyclopropanecarboxylic acid
K13	L-arginine
K14	1-Methylnicotinamide chloride
K15	N-Methylsarcosine
K16	Cytidine 5′-triphosphate (disodium salt)
K17	N-Acetylornithine
K19	L-Leucyl-L-alanine Hydrate
K21	L-Threonic acid Calcium Salt
M03	Creatinine
M04	Adenosine disodium triphosphate
M05	L-Hisidine
M06	D(-)-2-Aminobutyric acid
M07	Glycylglycine
M08	Ala-Gln
M09	O-Phospho-L-serine
M10	Sodium mesoxalate monohydrate
M11	Creatine
M12	Thymidine 5'-monophosphate disodium salt
M13	L-cysteine
M14	Phosphocholine chloride calcium salt tetrahydrate
M15	DL-m-Tyrosine
M17	Glycyl-L-valine
M19	H-Abu-OH
M21	Sodium phytate hydrate
O03	L-Arginine HCl (L-Arg)
O04	D-glutamine
O05	Sodium Gluconate

MT4 -WELL	COMPOUND
C16	Zoledronic Acid
C17	Thiamine pyrophosphate hydrochloride
C19	H-Gly-Pro-OH
C21	2-Aminoisobutyric acid
D03	Sodium Hyaluronate
E03	Sodium butyrate
E04	Triphosphopyridine nucleotide disodium salt
E05	isoleucine
E06	Homotaurine
E07	4-Aminobutyric acid
E08	Cytarabine
E09	Choline Glycerophosphate
E10	Hyaluronic acid
E11	L-Homoarginine hydrochloride
E12	Calcium 2-hydroxy-4-(methylthio)butanoate

MT4 -WELL	COMPOUND
I10	DL-5-Hydroxylysine hydrochloride
I11	β-Alanine
I12	L-Homoserine
I13	L-methionine
I14	Nα-Acetyl-L-lysine
I15	Glycyl-L-leucine
I16	ATP
I17	H-HoArg-OH
I19	3-Amino-4-methylpentanoic acid
I21	Guanosine 5'-monophosphate disodium salt
K03	NAD+
K04	Disodium uridine-5'-monophosphate
K05	L-SelenoMethionine
K06	Anserine
K07	Creatine phosphate disodium salt

MT4 -WELL	COMPOUND
O06	Goserelin Acetate
O07	Glycine
O08	scyllo-Inositol
O09	D-Pantethine
O10	D-Saccharic acid potassium salt
O11	L-Valine
O12	L-Anserine nitrate salt
O13	L-Hydroxyproline
O14	cis-4-Hydroxy-D-proline
O15	Nepsilon-Acetyl-L-lysine
O17	L-Homocitrulline
O19	(R)-Serine
O21	Pipecolic acid

Table 2A Raw Metabolite Screen Results – Objects/Live Cells

MT1	Objects			Average		2827.1875		S.D.	107.72936														
	1	2	3	4	5	6	7	8	9	10	11	12	13	14	15	16	17	18	19	20	21	22	23	24
A	-1.44	0.27	-0.06	0.48	-8.06	1.02	0.93	0.90	0.60	0.43	1.37	1.40	0.15	1.20	1.08	-0.91	-1.47	0.76	0.58	-0.35	-0.18	1.39	1.32	1.08
B	-0.87	0.95	0.38	0.46	-0.79	0.78	0.92	-0.15	-0.34	1.08	0.86	0.64	-0.87	0.79	0.77	0.45	-1.46	1.49	1.44	-0.14	-0.10	1.62	1.35	1.40
C	-0.23	0.35	1.54	0.38	-6.72	0.74	1.20	1.33	0.24	1.67	1.82	-6.26	-0.07	1.44	0.80	-0.35	-0.87	1.30	1.25	0.36	0.90	1.61	0.81	1.12
D	-0.44	-0.19	0.70	0.62	-0.05	1.46	1.11	1.46	-0.77	1.15	1.35	0.82	-0.87	1.45	0.84	-16.07	-0.09	0.76	1.49	0.71	0.61	0.74	1.04	0.69
E	-0.88	1.16	0.61	1.32	0.56	1.13	1.68	0.80	0.19	0.78	0.38	0.95	-0.55	0.39	0.36	0.11	-0.88	0.38	-0.45	-1.10	0.01	0.71	-0.14	0.14
F	-1.36	2.22	0.77	-0.28	-0.50	1.07	1.72	0.55	-0.08	2.13	1.34	0.34	-8.72	1.36	0.79	0.50	-1.15	1.85	-0.78	-2.21	-0.72	1.35	0.18	-0.36
G	-0.12	0.54	1.20	1.48	-0.22	1.23	0.90	0.83	0.17	1.46	0.74	1.08	-0.58	0.41	1.41	1.20	-0.55	-0.08	0.36	-1.78	0.58	1.43	0.45	0.45
H	-1.56	0.33	0.19	0.69	-0.35	0.62	0.68	0.88	-0.13	1.43	1.07	0.52	-0.56	1.74	1.34	-5.32	-0.27	-0.81	-0.09	-7.71	0.56	1.24	1.22	0.33
I	0.71	0.56	0.57	0.39	0.02	1.07	1.31	1.71	0.83	1.30	0.14	0.17	0.37	0.11	-0.01	0.06	-0.28	-0.58	0.10	-0.11	-0.85	0.63	-0.10	-0.57
J	-0.82	1.15	1.15	0.45	-1.60	1.01	0.75	0.45	-0.01	0.62	0.96	-0.30	-0.92	1.17	0.78	0.07	-1.11	0.24	0.74	-1.69	-0.60	0.79	0.23	-0.12
K	-0.10	-0.41	0.35	1.41	-0.89	1.29	0.47	1.75	-0.30	1.25	0.98	0.82	-1.12	0.56	1.26	0.56	-0.14	1.08	0.74	0.00	-0.24	1.69	1.10	1.04
L	-0.99	-0.47	-0.43	-0.27	-1.26	0.63	-0.28	-0.15	-1.45	0.32	1.43	0.63	-0.89	0.26	-0.30	-0.36	-0.70	-1.28	-0.04	-0.54	0.17	-0.32	0.83	0.26
M	-1.12	1.03	-1.83	-0.47	-0.53	1.85	1.83	-0.80	0.15	0.02	0.65	0.21	-2.17	-1.17	-1.63	-1.29	-0.65	-0.20	-0.26	-1.80	-0.84	-0.04	-1.43	-2.23
N	-2.03	0.45	1.06	0.80	-0.65	1.37	0.78	-0.84	-1.00	-0.15	0.52	-0.12	-1.12	0.22	-0.73	-0.36	-1.75	-0.57	-0.45	-1.71	-1.16	-0.13	-0.66	0.76
O	-0.25	0.50	-2.78	-0.41	-6.45	-0.26	0.69	-0.50	-1.29	-1.00	-0.95	-1.88	-2.78	-1.48	-1.84	-1.85	-2.28	-2.10	-2.50	-1.64	-6.89	-0.24	-0.82	-1.29
P	-1.93	0.06	0.25	-1.11	-0.99	0.49	0.50	-1.69	-3.01	-0.61	-1.20	-0.39	-2.13	-1.73	-0.66	-1.55	-3.25	-1.06	-1.56	-2.31	-2.29	-2.14	-0.90	-2.28

MT2	Objects			Average		2838.45313		S.D.	110.04803														
	1	2	3	4	5	6	7	8	9	10	11	12	13	14	15	16	17	18	19	20	21	22	23	24
A	-1.19	0.49	0.25	-0.46	-1.15	0.87	0.22	-0.82	-0.52	-0.10	0.62	0.94	0.05	0.98	-0.80	-0.54	-0.97	0.81	0.39	-0.41	-0.61	0.03	0.19	0.22
B	-1.35	0.90	1.11	0.27	0.32	1.11	0.48	-1.77	-0.50	0.90	1.70	-0.18	-0.12	0.84	0.24	-0.35	-1.09	0.65	-0.45	-0.91	-0.76	0.72	0.74	-0.28
C	-0.88	0.58	0.53	1.06	-0.17	1.87	1.96	0.84	0.30	1.37	1.89	1.81	0.85	1.21	2.01	0.63	1.04	0.59	1.38	0.74	0.02	1.18	0.86	0.54
D	-0.79	0.71	2.00	1.41	-0.40	1.03	2.13	1.61	0.17	1.64	2.34	0.23	0.25	0.52	2.00	1.55	-0.92	1.61	0.61	0.17	-0.35	0.51	1.21	0.14
E	0.74	0.50	0.91	0.70	0.47	1.01	1.45	1.13	0.92	1.38	0.81	0.49	0.33	0.73	0.47	-0.04	0.40	-0.29	-0.39	-3.39	0.53	1.17	1.30	-0.01
F	0.20	1.33	-0.52	1.56	-0.39	1.15	2.47	1.24	-0.04	1.50	1.17	1.50	0.27	1.79	1.77	0.03	-0.75	0.64	-0.19	-1.39	0.52	1.39	0.70	-0.61
G	0.89	1.59	0.84	1.21	1.35	-1.43	2.44	3.32	0.80	-2.01	2.00	1.95	0.87	2.09	2.18	1.36	0.47	0.99	0.50	-0.70	1.22	1.09	0.81	0.59
H	-0.51	0.90	-6.65	1.04	-1.98	1.10	1.16	1.00	0.72	0.81	1.55	1.64	-11.68	1.34	1.58	0.40	0.13	1.60	1.08	-0.39	0.16	1.26	1.50	0.98
I	-1.11	0.38	0.76	0.35	0.64	-16.52	1.62	0.87	0.62	1.87	1.41	-1.98	0.03	1.15	0.43	1.31	0.51	0.60	0.02	-1.39	0.26	1.40	-0.06	-0.52
J	-1.08	1.20	1.83	0.12	-0.24	2.22	1.85	1.56	-0.20	1.67	0.98	0.95	-0.47	0.88	0.97	1.11	-2.64	1.18	0.52	0.48	-12.06	1.02	0.52	-0.69
K	-0.06	1.36	1.11	0.55	0.92	1.70	2.79	2.78	-1.37	2.30	2.62	0.19	0.89	0.90	2.26	1.17	-0.33	-16.97	0.59	0.59	-1.97	1.50	1.60	0.30
L	-1.57	0.69	1.29	1.19	-0.37	1.46	1.17	0.72	0.31	0.78	0.75	0.60	-0.39	0.88	1.00	0.05	-0.09	1.42	1.10	-0.57	0.18	0.08	0.55	0.91
M	-0.89	-0.23	-1.56	-0.74	-1.49	-14.05	1.17	-3.68	0.48	0.76	0.96	-0.28	-0.92	0.16	-0.41	-0.35	-1.09	-5.43	-0.46	-1.80	-1.16	-0.23	-1.50	-2.63
N	-1.14	0.20	1.08	-0.02	-1.09	0.70	0.58	-0.01	-2.64	0.31	0.45	-0.69	-1.54	-0.05	0.34	-0.48	-2.28	-0.65	-0.29	-1.54	-1.24	0.12	0.02	-0.48
O	-1.66	-0.98	0.15	-0.36	-1.52	-0.19	-0.85	-0.49	-1.52	-2.34	-0.33	-1.39	-1.70	0.00	-0.28	-2.48	-1.88	-1.53	-1.23	-1.43	-0.36	-1.49	-1.52	-0.62
P	-2.07	0.60	0.10	-0.21	-1.77	-1.95	-0.89	-1.15	-1.13	-0.09	-1.30	-1.60	-1.48	-0.39	-0.99	0.04	-1.79	-0.99	-1.54	-0.48	-1.66	-0.51	-1.13	-1.41

MT3	Objects			Average		2881.25		S.D.	123.47251														
	1	2	3	4	5	6	7	8	9	10	11	12	13	14	15	16	17	18	19	20	21	22	23	24
A	-1.19	0.68	0.39	0.07	0.01	0.85	-13.60	0.86	-0.54	1.15	1.15	0.55	0.16	1.42	0.74	-0.20	-0.78	1.09	1.16	0.02	0.09	0.63	0.92	0.18
B	-1.74	0.16	1.33	0.56	0.14	0.69	0.22	-0.11	-0.34	1.49	1.32	1.38	-1.36	0.99	-5.78	-0.65	-1.48	0.53	0.48	0.44	-0.47	1.41	0.44	0.74
C	-1.53	0.22	1.33	0.47	0.10	1.34	-1.48	1.47	0.01	1.34	1.09	0.61	-0.36	1.69	1.68	0.65	0.03	1.11	1.40	0.91	1.19	1.41	0.95	1.42
D	-0.13	0.79	1.27	1.00	0.15	1.55	1.60	0.88	0.95	2.06	1.66	1.50	0.52	1.83	1.80	1.17	0.04	2.00	1.41	1.42	0.82	1.60	1.81	1.50
E	0.01	0.08	0.69	0.77	-6.10	1.60	1.15	0.49	0.19	1.36	1.33	0.65	0.34	1.56	1.06	0.14	0.30	1.33	0.70	0.42	0.31	1.09	0.58	0.59
F	-0.76	0.91	0.73	0.87	-0.16	1.03	0.99	1.70	-0.17	1.33	1.43	0.64	-0.30	2.12	1.21	0.31	0.81	1.03	1.45	0.31	0.21	0.17	1.14	0.26
G	-0.63	0.22	0.67	1.24	-1.99	-1.00	1.74	1.46	-2.30	-1.59	0.65	2.01	0.87	1.25	2.40	1.22	0.98	1.53	1.92	1.24	1.59	1.04	1.36	0.73
H	-0.24	0.55	1.05	1.27	-0.35	0.95	2.31	1.62	0.95	2.06	1.71	1.33	-0.23	1.80	1.84	1.16	0.79	1.82	1.22	1.42	0.64	1.00	1.70	0.99
I	-1.01	-0.19	0.30	0.08	1.07	-6.19	1.12	1.41	0.79	0.85	0.23	0.70	-0.50	0.70	0.52	0.86	0.08	0.67	-0.29	0.61	0.34	1.02	-0.36	-0.24
J	-1.01	1.20	1.43	0.73	0.25	1.94	1.76	1.04	0.69	0.98	0.77	0.08	-0.21	1.09	1.28	1.16	-0.18	0.63	-0.27	0.14	-4.27	0.37	0.64	-1.20
K	0.39	1.22	1.28	1.12	1.12	1.77	1.63	2.03	0.57	1.71	1.37	1.78	-0.39	0.78	1.04	0.84	0.06	0.90	0.73	0.64	0.61	1.35	1.10	0.99
L	-1.08	0.95	1.43	0.96	0.18	0.99	1.16	0.30	-0.38	1.25	1.17	-0.04	-0.07	0.69	0.85	0.77	0.14	1.26	1.19	-0.59	-1.21	0.45	1.01	-0.21
M	-0.72	-0.30	-0.20	-0.61	-0.13	0.08	-11.26	-0.76	-0.42	0.03	-1.19	-0.72	-1.13	0.17	-1.44	-2.13	-3.78	-0.56	-0.97	-1.95	-0.81	-0.21	-1.14	-1.22
N	-2.40	-0.39	-0.43	-1.45	-1.85	0.33	0.55	-1.61	-1.67	0.22	-0.68	-1.52	-1.98	-0.34	-1.03	-1.03	-1.82	-0.40	-1.11	-2.29	-1.13	-0.26	-0.18	-0.60
O	-2.32	-1.08	-1.02	-0.30	-14.22	-0.29	0.50	-0.91	-1.56	-1.21	-0.09	-1.18	-2.66	-0.27	-0.04	-2.21	-17.03	-0.78	-0.15	-1.25	-1.27	-0.84	0.33	-1.01
P	-1.47	-1.01	-0.56	-1.28	-1.06	-0.27	0.04	-0.56	-2.58	-0.93	-8.55	-0.75	-2.54	-0.86	-1.11	-0.96	-1.18	-1.24	-1.30	-1.14	-1.68	-0.74	-0.20	-1.16

MT4	Objects			Average		2917.25		S.D.	130.22605														
	1	2	3	4	5	6	7	8	9	10	11	12	13	14	15	16	17	18	19	20	21	22	23	24
A	1.17	1.27	0.47	-0.37	-0.40	0.23	0.01	-0.52	-0.54	0.17	-0.65	-1.35	-1.56	-0.65	-1.53	-2.30	-2.26	0.27	-1.14	-1.11	-0.27	0.23	0.52	-0.98
B	-2.11	-0.18	0.46	-0.45	-1.14	0.88	-0.12	-0.93	-1.93	0.47	-0.52	0.18	-1.05	0.91	0.93	-0.84	-1.44	1.04	0.64	0.11	-0.34	1.07	0.44	-0.21
C	0.12	0.70	1.01	1.00	0.42	1.16	0.54	0.47	-0.04	0.92	0.87	0.67	-0.97	0.70	0.58	-0.09	-0.68	0.40	0.97	-0.82	0.06	1.22	1.15	0.62
D	-1.60	0.29	1.06	0.24	0.47	1.24	0.69	0.73	-0.22	1.24	0.92	0.34	0.04	0.37	1.06	0.59	-0.27	1.15	1.10	0.40	-0.16	1.89	2.03	0.29
E	0.23	1.02	1.24	0.40	0.10	0.87	-0.22	-5.62	0.59	0.50	-0.86	0.13	-0.33	0.01	0.01	-1.00	-0.10	-0.46	0.22	1.13	0.70	0.67	0.07	0.44
F	-2.79	0.56	1.17	0.27	-0.88	1.19	1.27	0.87	-0.49	1.70	0.36	0.86	-1.05	0.23	0.16	0.44	-0.26	1.30	0.60	-0.93	-0.73	0.87	0.82	0.01
G	0.46	0.81	1.49	0.14	-1.55	-0.55	1.21	1.56	-1.60	-0.99	1.09	1.13	0.31	1.53	0.54	0.62	0.04	0.97	0.94	0.69	0.02	0.84	0.30	0.50
H	-1.42	0.00	-0.61	0.73	0.43	0.29	1.00	0.51	-0.60	0.85	1.53	-0.92	-0.80	1.46	0.71	0.36	-0.22	-0.39	0.16	-0.33	-0.23	1.21	-0.27	1.10
I	-0.29	0.04	-0.02	0.73	-0.26	2.70	1.07	1.17	0.28	1.54	0.37	-0.29	-0.27	-0.15	1.23	0.61	-0.22	-0.40	-0.38	-0.41	-0.82	0.22	0.53	0.00
J	-2.14	1.23	1.17	0.75	0.02	1.33	1.00	0.60	-0.43	0.97	1.56	-0.76	-0.50	0.67	-0.09	-0.01	-0.44	0.17	0.28	-0.11	-0.13	0.63	0.60	-0.45
K	-0.23	1.09	1.73	1.26	0.83	0.54	1.55	1.51	0.75	1.70	1.54	0.77	-0.10	0.53	1.68	0.20	-0.82	0.27	0.71	0.65	-0.29	0.73	1.43	0.90
L	-0.16	-0.14	1.07	0.21	-0.46	0.24	0.85	-0.16	-0.25	1.07	0.37	0.93	-1.02	1.02	0.79	0.42	-0.56	1.33	0.49	0.00	-0.32	1.09	0.23	0.87
M	-0.27	0.94	0.29	0.15	-0.22	-0.22	-0.19	-0.30	0.24	0.24	-0.43	-1.08	-0.68	0.07	-0.79	-1.00	-1.61	-0.60	-0.09	-0.37	-0.76	-0.06	-0.16	-0.22
N	-1.41	0.59	0.17	-0.21	-0.26	0.52	0.20	-0.33	-0.87	-0.09	-0.41	-0.59	-1.53	0.06	-0.18	-0.97	-1.60	-0.73	-0.53	-1.52	-1.28	0.17	0.32	-1.08
O	-0.64	0.55	-0.01	-0.22	-0.54	-0.02	-0.59	0.00	-0.59	-1.21	0.24	-0.95	-2.13	-0.90	-1.27	-1.69	-1.64	-1.66	-1.06	-1.79	-1.56	-0.14	-0.15	-1.69
P	-2.57	-0.43	0.33	-0.45	-0.52	-0.86	-0.52	-1.14	-0.31	-0.20	-0.45	-0.49	-0.78	-0.65	0.14	-1.77	-1.58	-1.38	-0.69	0.02	-0.82	-0.86	-1.26	-1.36

S.D.	neg 2 or less	neg 1 to neg 2	neg 1 to 1	1 to 2	2 or more

Table 2B Raw Metabolite Screen Results – Sub G1%

MT1	% SubG1			Average			2.41328125		S.D.	0.6909783													
	1	2	3	4	5	6	7	8	9	10	11	12	13	14	15	16	17	18	19	20	21	22	23	24
A	-0.67	0.41	-1.13	-0.38	2.72	1.10	-0.03	1.60	0.62	-0.47	-0.03	1.27	-0.38	0.47	-0.93	0.43	-0.73	-0.90	-0.79	-0.84	-0.82	-1.25	-0.28	0.55
B	0.43	-0.28	0.99	-0.28	0.57	-0.02	0.66	0.27	-0.48	-0.25	0.82	1.46	0.15	2.08	-0.06	1.49	-0.19	0.53	2.04	0.78	0.52	1.43	-0.24	-0.48
C	0.28	0.60	1.24	0.55	3.53	1.04	-0.41	1.24	0.41	1.95	0.62	7.74	1.12	2.33	-0.37	-0.02	0.00	0.99	0.91	1.30	1.31	0.95	-0.12	0.53
D	0.88	0.11	4.18	3.16	2.46	1.25	2.64	5.44	2.21	1.76	1.72	1.57	1.11	3.15	1.12	3.64	0.88	1.08	4.06	2.14	0.96	2.59	4.13	0.15
E	-0.68	-0.31	0.01	3.14	1.37	-0.06	0.69	2.02	1.04	0.49	0.69	0.81	1.01	0.75	0.40	1.40	0.69	2.25	0.94	4.09	0.50	0.94	0.27	0.43
F	-0.74	-0.09	-1.00	0.59	0.47	0.44	1.07	0.31	1.12	0.91	0.69	0.91	4.79	2.30	0.08	0.57	0.63	1.34	1.36	1.49	-0.08	1.08	0.63	0.14
G	0.31	1.07	1.21	1.93	1.98	2.86	3.09	1.67	0.27	1.36	1.89	3.15	0.69	2.46	4.42	4.19	1.47	2.25	5.45	4.68	1.41	1.46	1.14	0.39
H	-0.87	0.85	0.47	1.10	0.04	0.60	1.40	1.21	1.40	1.12	1.18	1.98	1.95	0.55	2.89	9.34	1.67	1.37	0.52	6.58	1.33	0.41	1.93	0.20
I	-0.31	-0.44	0.17	1.30	1.62	1.04	1.24	2.08	2.37	1.67	1.85	2.05	0.79	0.59	0.40	1.01	0.34	-0.25	0.95	2.06	0.63	0.36	-0.21	-0.09
J	0.26	-0.45	-0.74	1.08	-0.66	1.04	1.14	0.73	0.91	0.70	1.44	-0.44	1.12	1.56	0.34	1.66	0.04	0.46	1.04	0.66	0.28	-0.16	-0.29	0.15
K	-1.08	0.78	0.91	1.17	1.38	2.12	2.74	1.69	1.73	1.20	1.40	2.21	0.10	2.61	3.05	3.02	1.24	1.82	1.93	1.47	0.17	0.17	-0.40	0.26
L	-1.15	-1.05	-0.47	0.23	1.14	1.21	0.75	1.92	0.02	1.25	0.83	0.70	0.65	0.31	0.39	2.33	0.60	1.99	2.61	1.57	0.17	-0.28	4.05	0.05
M	0.10	0.30	0.41	0.47	1.73	0.95	0.14	0.73	1.04	2.18	1.46	0.17	-1.15	-0.82	0.55	-0.42	0.70	0.17	-0.24	0.73	0.69	-0.06	-1.00	-0.41
N	-1.16	-0.63	0.30	-0.90	-0.45	0.20	-0.11	0.26	-0.03	-1.08	0.07	0.88	-0.87	0.52	-0.76	-0.95	-0.80	-0.03	0.36	-0.58	-0.66	1.76	-0.76	-0.66
O	-0.34	-0.18	0.69	0.56	-0.24	-0.24	-0.40	-0.25	-0.48	-0.99	-0.31	-0.29	-0.74	-1.32	-1.18	-1.12	-0.63	-1.50	-1.18	-0.71	1.44	-1.22	-1.22	-0.53
P	-0.73	-1.65	-0.35	0.36	-1.05	-0.22	-0.38	0.50	-0.77	-1.08	-0.11	-0.22	-1.54	-0.70	-0.71	0.53	-1.34	-1.73	-0.83	-0.35	-0.58	-1.81	-1.48	-0.41

MT2	% SubG1			Average			2.22875		S.D.	0.550819													
	1	2	3	4	5	6	7	8	9	10	11	12	13	14	15	16	17	18	19	20	21	22	23	24
A	-1.03	0.73	1.40	2.47	1.24	1.09	-0.05	2.24	0.20	0.38	-0.42	1.20	1.18	-1.03	0.24	-1.23	0.20	-0.58	-0.65	-0.34	1.33	-0.72	0.71	1.78
B	-0.20	-0.83	0.55	-0.05	0.00	-0.36	-0.27	2.54	0.46	0.53	0.27	0.00	-0.45	-0.89	-1.00	0.11	0.02	0.13	0.31	1.33	-0.69	0.62	0.00	1.38
C	0.26	0.02	-0.22	2.78	2.65	1.09	1.00	1.65	1.64	1.65	3.58	3.07	-0.40	1.20	0.29	0.20	1.24	0.84	3.00	0.80	-0.27	1.09	0.29	1.91
D	0.57	0.18	0.58	1.71	5.45	0.20	1.27	2.45	1.24	1.36	3.34	5.27	4.58	0.96	2.18	2.65	-0.60	0.17	-0.31	1.67	0.69	2.54	0.60	-0.36
E	0.11	-0.22	0.27	0.37	1.36	1.62	0.86	9.73	5.16	3.96	0.86	0.35	2.27	0.87	0.17	2.74	2.56	0.35	2.00	3.62	1.09	-0.02	-0.14	1.27
F	-0.69	-0.89	-0.40	1.80	0.31	-0.49	0.75	1.15	-0.98	0.96	-0.56	-0.12	1.02	1.22	-0.03	0.42	0.04	1.94	0.07	1.96	2.22	1.06	0.62	-1.03
G	1.09	1.20	0.42	2.44	4.21	2.38	5.19	3.89	2.65	2.20	1.47	2.80	2.76	3.11	3.85	4.65	2.62	1.07	2.16	1.94	0.35	1.11	1.16	0.40
H	-0.52	-0.40	1.38	1.55	2.05	0.75	1.27	4.70	3.62	1.91	4.47	3.83	9.17	1.42	3.98	2.82	2.13	1.25	4.00	3.94	1.49	3.03	3.09	0.33
I	-1.30	0.67	-1.00	0.87	1.13	2.89	2.45	4.00	3.02	3.65	2.14	4.40	3.56	0.00	1.18	5.76	3.16	1.02	0.82	3.05	0.46	0.62	0.57	-0.45
J	0.29	0.35	0.96	1.87	-0.56	0.96	1.02	0.78	0.91	2.14	0.95	1.94	1.24	0.35	1.13	2.20	2.36	1.58	0.96	1.55	4.25	0.33	-0.09	-0.03
K	-0.65	0.69	0.44	1.91	1.07	2.13	2.24	6.52	2.36	2.53	3.45	0.15	0.40	1.02	2.89	2.07	-0.16	3.81	3.02	3.96	0.73	0.00	1.13	-0.45
L	-1.25	0.62	1.31	2.13	0.75	0.67	1.22	9.46	2.40	1.60	1.29	1.20	0.82	1.40	1.25	0.62	3.72	1.11	0.49	4.00	-0.11	0.98	-0.16	1.51
M	-1.12	-1.01	-0.58	2.22	0.29	40.80	2.07	-0.32	0.98	0.67	0.09	0.75	0.93	-0.67	2.71	1.47	2.56	-0.65	-0.72	2.83	0.17	-0.23	-0.58	-0.42
N	-1.43	-0.11	-0.72	-0.40	-0.71	-0.12	-0.11	1.07	-1.69	-1.14	-1.29	-0.63	-1.20	-0.20	0.00	0.46	-1.30	-0.96	-0.81	0.78	-1.16	-0.61	2.22	-1.43
O	-1.38	-1.12	0.27	0.17	-1.05	0.07	-0.80	-1.63	0.04	-0.32	-1.90	-0.52	-1.80	0.75	-1.27	-0.65	-1.21	0.04	-1.43	-0.40	-0.74	-0.52	-1.20	-1.36
P	-1.27	-0.72	-0.29	-1.47	-1.09	-1.07	-1.27	-0.09	-0.91	-1.29	-1.96	-0.43	-0.58	-1.00	-0.45	1.31	-1.58	-1.00	-1.87	-1.63	-0.98	-0.78	-0.76	-1.14

MT3	% SubG1			Average			2.20671875		S.D.	0.5290754													
	1	2	3	4	5	6	7	8	9	10	11	12	13	14	15	16	17	18	19	20	21	22	23	24
A	0.12	-0.22	-0.56	-0.32	0.29	1.52	17.19	4.81	0.72	2.27	-0.73	1.67	1.42	0.16	-0.86	0.67	-0.71	0.84	0.27	2.39	-0.37	1.57	0.37	0.71
B	-0.05	1.18	0.29	3.71	2.16	-0.03	0.84	1.03	0.89	0.57	0.37	2.63	0.63	0.55	-0.33	0.14	1.22	0.12	1.05	0.54	1.46	1.08	1.42	-1.32
C	0.95	-0.79	1.92	0.78	2.56	0.97	-0.81	0.40	-0.24	1.73	0.59	-0.20	0.37	0.54	0.61	0.80	0.08	1.71	0.48	0.69	1.14	0.54	1.95	0.40
D	1.63	0.97	0.50	2.88	4.11	2.95	1.18	2.97	3.01	2.46	2.94	4.71	2.44	0.76	0.71	0.46	-0.11	1.14	5.98	2.14	1.16	1.48	1.18	1.93
E	-0.96	0.99	1.12	-0.16	0.89	1.97	1.52	2.44	1.37	0.91	-0.01	1.57	-0.09	1.48	-0.47	1.05	1.33	1.42	-0.28	1.82	-0.09	0.46	-0.79	-0.15
F	-0.45	-0.26	0.86	0.06	-0.73	-0.60	0.86	0.23	0.86	0.67	1.76	0.55	0.69	1.37	0.82	-0.03	0.14	0.80	1.08	2.10	0.44	-0.79	1.71	0.31
G	-0.47	0.38	-0.35	1.01	2.29	2.61	3.33	1.08	1.37	0.55	2.33	4.05	1.46	3.86	3.20	5.43	0.55	4.50	2.37	2.80	2.71	2.37	2.27	1.29
H	0.48	-0.20	0.86	0.18	1.95	0.69	1.92	2.95	3.20	3.24	1.52	7.93	2.92	1.80	3.01	3.01	2.29	3.31	2.18	5.03	1.25	1.31	0.54	0.61
I	-0.67	-0.67	0.42	0.21	14.92	31.74	0.27	2.82	2.56	0.25	0.63	1.12	0.93	2.07	0.52	3.99	0.27	0.67	0.48	3.31	0.29	1.75	-0.45	-0.47
J	-1.15	0.14	-0.09	-0.35	7.06	0.55	0.89	1.05	0.16	0.23	0.59	-0.13	-0.13	0.59	1.48	2.90	0.78	1.06	1.27	0.40	-1.45	0.74	-0.28	-1.20
K	-0.81	-0.24	1.48	0.84	1.14	0.59	2.58	4.83	1.97	2.01	1.46	2.24	-0.56	0.78	1.29	0.71	1.65	0.50	0.91	1.90	0.04	0.23	0.54	0.99
L	-1.15	0.23	0.35	0.42	0.25	0.99	0.65	0.88	0.57	0.01	0.76	2.60	0.18	-1.18	1.22	1.86	0.33	0.44	1.39	1.69	1.63	-0.05	1.42	0.14
M	-1.13	-0.26	0.40	0.54	-1.73	-0.37	66.71	0.44	0.04	-0.11	-0.84	0.16	-0.66	-0.52	-1.45	-0.64	2.01	-0.07	-0.62	0.91	-0.56	-0.13	-0.73	1.44
N	-2.05	-1.17	-0.16	-0.47	-0.39	-0.03	-0.64	1.75	-1.49	-1.18	-0.73	-0.66	-1.01	0.42	0.01	-1.43	-1.11	-0.90	0.52	-1.11	-0.58	-0.58	-0.86	-0.86
O	-1.77	-0.81	-1.35	0.42	32.50	0.27	-0.64	1.22	-0.86	-0.64	-0.67	-1.00	-1.73	-0.92	0.37	-0.84	3.60	-0.03	-0.73	0.33	-0.64	-1.32	-0.81	-1.30
P	-0.88	-0.47	-0.15	0.20	-0.73	-1.66	-1.41	-0.07	-1.66	-1.71	7.00	-0.45	-1.81	-1.17	-1.35	0.76	1.42	-1.96	-0.90	0.93	-0.64	-0.71	-1.00	0.52

MT4	% SubG1			Average			2.64421875		S.D.	0.7626558													
	1	2	3	4	5	6	7	8	9	10	11	12	13	14	15	16	17	18	19	20	21	22	23	24
A	0.64	1.59	2.79	1.65	1.16	0.31	-0.06	0.31	-0.15	-0.61	-0.23	1.03	0.49	0.28	-0.19	-0.41	-0.77	-0.32	-0.82	-1.53	-0.37	0.36	0.31	1.57
B	-0.19	-1.02	-0.16	-0.62	-0.62	1.24	-0.25	-0.94	-1.36	-0.43	-0.02	-0.44	-0.31	0.94	-0.53	-0.29	0.03	0.06	-0.75	0.07	-0.36	-0.12	-0.56	-0.20
C	-0.29	0.55	1.44	0.23	1.21	-0.35	-0.44	3.35	-0.18	-0.32	-0.04	0.24	-0.18	-0.11	0.69	1.27	-0.08	0.02	2.70	0.31	-0.11	0.58	0.13	0.43
D	0.85	-0.84	0.65	1.83	1.73	-0.36	0.37	1.41	0.79	0.36	1.45	3.26	0.61	-0.46	2.12	0.87	-0.10	-0.01	2.11	1.74	-0.75	2.63	4.03	2.30
E	0.72	-0.24	-0.23	0.34	-0.24	0.03	1.16	0.14	0.26	-0.57	-0.52	0.43	-1.19	0.09	-0.28	0.11	-1.21	-0.81	0.23	1.88	2.72	-0.24	0.65	1.61
F	-0.95	-0.83	-0.39	-1.07	-1.59	-0.35	0.32	0.13	0.11	-0.54	0.24	-1.08	1.53	1.33	-1.02	2.62	-0.24	0.65	-0.92	0.14	0.39	-0.27	1.57	0.26
G	0.45	-0.65	0.83	0.19	1.02	0.18	3.01	-0.19	0.69	0.62	1.12	1.84	1.80	3.31	1.10	3.67	-0.63	1.40	-0.06	2.85	-0.23	4.20	-0.19	-0.31
H	0.28	-0.60	-0.46	0.45	0.77	-0.14	-0.50	-0.70	-0.46	-0.04	-0.40	-0.01	-0.71	0.87	0.41	1.97	0.26	0.15	0.06	0.60	0.94	3.23	0.68	2.24
I	-0.56	-0.91	-0.67	-0.03	3.26	11.74	2.93	1.23	1.02	-0.10	1.84	-0.14	0.40	-0.62	0.02	1.08	1.35	-1.32	-1.28	-0.08	0.69	3.65	-0.44	-0.45
J	-0.14	-0.53	0.37	0.01	0.09	2.22	0.19	0.61	-0.44	-0.66	0.78	-0.49	-0.84	-0.67	-0.08	0.44	-0.58	-0.98	0.13	0.23	1.06	-0.36	0.13	0.06
K	-0.70	0.18	0.62	1.00	0.78	0.35	2.50	0.87	0.36	-0.54	1.20	0.40	-0.40	-1.32	0.01	-0.57	-0.99	-0.84	0.45	-0.11	-0.96	1.41	1.06	0.81
L	-0.39	-0.84	-0.29	-0.18	-0.16	-0.94	-0.27	0.15	0.03	0.52	0.11	1.84	0.39	-0.58	0.48	5.53	-0.33	-0.28	-0.29	0.27	-0.28	-0.43	0.14	-0.18
M	-0.87	-1.19	-0.90	-0.79	-0.06	-0.98	-0.79	0.58	0.27	-0.18	-1.32	-0.82	-0.78	-1.32	-1.04	-0.32	-1.09	-1.53	-1.71	0.83	-1.28	-1.12	0.24	0.39
N	-1.21	-0.62	-1.28	-0.88	-1.11	-1.00	-0.70	-1.24	-1.37	-0.62	-1.54	-2.08	-1.74	-0.46	-1.07	0.30	-0.81	-1.05	-1.54	-0.57	-0.84	-1.02	-0.10	-0.22
O	-0.14	-1.28	-1.17	-0.48	-0.57	-1.26	-1.40	-0.60	-0.37	-0.52	-0.36	-0.83	-1.28	-1.12	-0.99	-1.28	-1.24	-1.28	-0.73	-1.03	-1.25	-0.03	-0.71	-1.53
P	-1.28	-1.26	-1.29	-0.67	-0.98	-1.59	-1.17	-0.01	-0.96	-0.98	-0.99	-0.20	-0.35	-1.99	-0.96	-0.20	-1.09	-1.64	-0.82	-0.73	-0.99	-0.62	-0.90	-0.54

S.D.	neg 2 or less	neg 1 to neg 2	neg 1 to 1	1 to 2	2 or more

Table 2C Raw Metabolite Screen Results – G1%

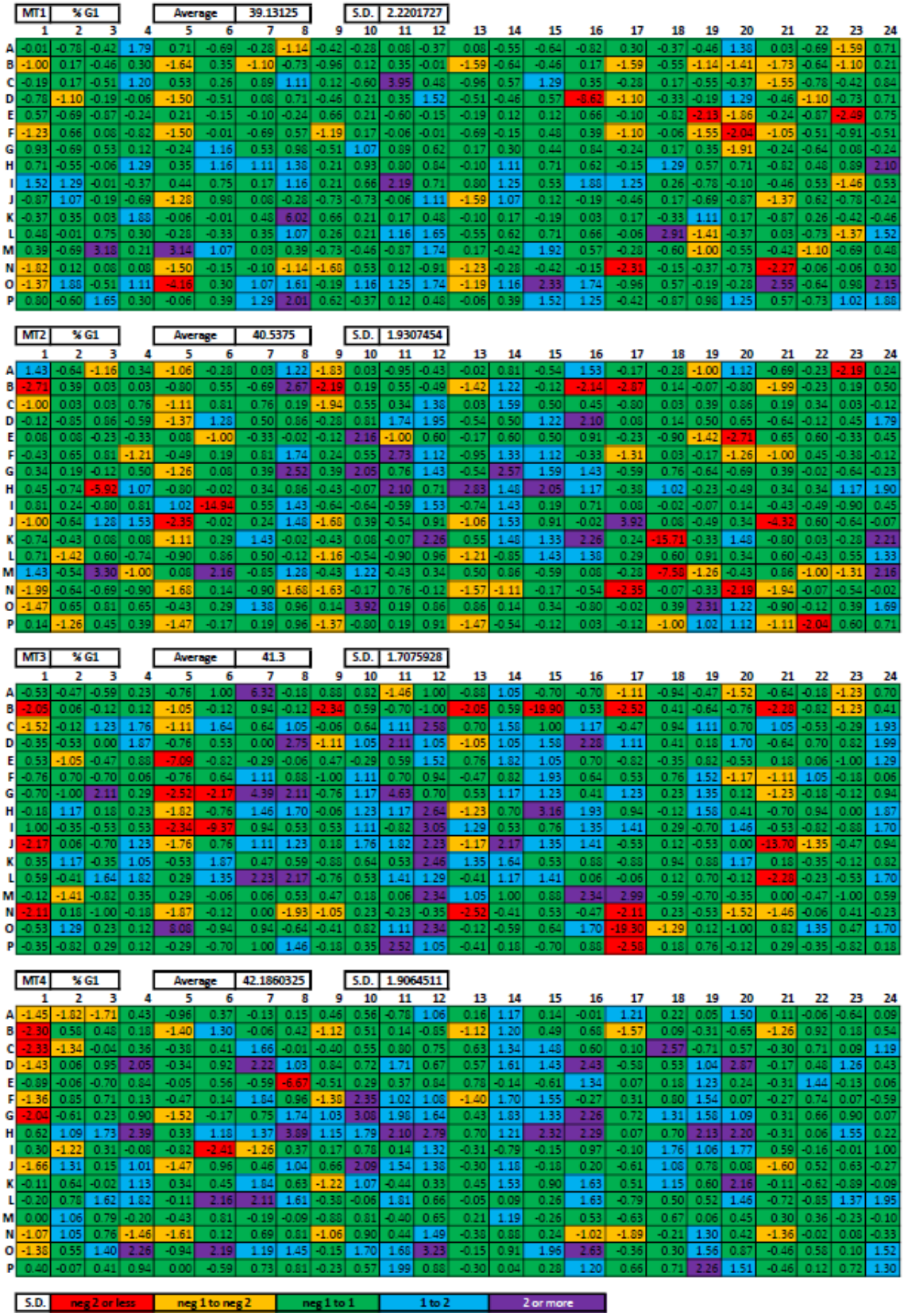

MT1	% G1			Average	39.13125			S.D.	2.2201727														
	1	2	3	4	5	6	7	8	9	10	11	12	13	14	15	16	17	18	19	20	21	22	23	24
A	-0.01	-0.76	-0.42	1.79	0.71	-0.69	-0.28	-1.14	-0.42	-0.28	0.08	-0.37	0.08	-0.55	-0.64	-0.82	0.30	-0.37	-0.46	1.38	0.03	-0.69	-1.59	0.71
B	-1.00	0.17	-0.46	0.30	-1.64	0.35	-1.10	-0.73	-0.96	0.12	0.35	-0.01	-1.59	-0.64	-0.46	0.17	-1.59	-0.55	-1.14	-1.41	-1.73	-0.64	-1.10	0.21
C	-0.19	0.17	-0.51	1.20	0.53	0.26	0.89	1.11	0.12	-0.60	3.95	0.48	-0.96	0.57	1.29	0.35	-0.28	0.17	-0.55	-0.37	-1.55	-0.78	-0.42	0.84
D	-0.78	-1.10	-0.19	-0.06	-1.50	-0.51	0.08	0.71	-0.46	0.21	0.35	1.52	-0.51	-0.46	0.57	-8.62	-1.10	-0.33	-0.19	1.29	-0.46	-1.10	-0.73	0.71
E	0.57	-0.69	-0.87	-0.24	0.21	-0.15	-0.10	-0.24	0.66	0.21	-0.60	-0.15	-0.19	0.12	0.12	0.66	-0.10	-0.82	-2.13	-1.86	-0.24	-0.87	-2.49	0.75
F	-1.23	0.66	0.08	-0.82	-1.50	-0.01	-0.69	0.57	-1.19	0.17	-0.06	-0.01	-0.69	-0.15	0.48	0.39	-1.10	-0.06	-1.55	-2.04	-1.05	-0.51	-0.91	-0.51
G	0.93	-0.69	0.53	0.12	-0.24	1.16	0.53	0.98	-0.51	1.07	0.89	0.62	0.17	0.30	0.44	0.84	-0.24	0.17	0.35	-1.91	-0.24	-0.64	0.08	-0.24
H	0.71	-0.55	-0.06	1.29	0.35	1.16	1.11	1.38	0.21	0.93	0.80	0.84	-0.10	1.11	0.71	0.62	-0.15	1.29	0.57	0.71	-0.82	0.48	0.89	2.10
I	1.52	1.29	-0.01	-0.37	0.44	0.75	0.17	1.16	0.21	0.66	2.19	0.71	0.80	1.25	0.53	1.88	1.25	0.26	-0.78	-0.10	-0.46	0.53	-1.46	0.53
J	-0.87	1.07	-0.19	-0.69	-1.28	0.98	0.08	-0.28	-0.73	-0.73	-0.06	1.11	-1.59	1.07	0.12	-0.19	-0.46	0.17	-0.69	-0.87	-1.37	0.62	-0.78	-0.24
K	-0.37	0.35	0.03	1.88	-0.06	-0.01	0.48	6.02	0.66	0.21	0.17	0.48	-0.10	0.17	-0.19	0.03	0.17	-0.33	1.11	0.17	-0.87	0.26	-0.42	-0.46
L	0.48	-0.01	0.75	0.30	-0.28	-0.33	0.35	1.07	0.26	0.21	1.16	1.65	-0.55	0.62	0.71	0.66	-0.06	2.91	-1.41	-0.37	0.03	-0.73	-1.37	1.52
M	0.39	-0.69	3.18	0.21	3.14	1.07	0.03	0.39	-0.73	-0.46	-0.87	1.74	0.17	-0.42	1.92	0.57	-0.28	-0.60	-1.00	-0.55	-0.42	-1.10	-0.69	0.48
N	-1.82	0.12	0.08	0.08	-1.50	-0.15	-0.10	-1.14	-1.68	0.53	0.12	-0.91	-1.23	-0.28	-0.42	-0.15	-2.31	-0.15	-0.37	-0.73	-2.27	-0.06	-0.06	0.30
O	-1.37	1.88	-0.51	1.11	-4.16	0.30	1.07	1.61	-0.19	1.16	1.25	1.74	-1.19	1.16	2.38	1.74	-0.96	0.57	-0.19	-0.28	2.55	-0.64	0.98	2.15
P	0.80	-0.60	1.65	0.30	-0.06	0.39	1.29	2.01	0.62	-0.37	0.12	0.48	-0.06	0.39	1.52	1.25	-0.42	-0.87	0.98	1.25	0.57	-0.73	1.02	1.88

MT2	% G1			Average	40.5375			S.D.	1.9307454														
	1	2	3	4	5	6	7	8	9	10	11	12	13	14	15	16	17	18	19	20	21	22	23	24
A	1.43	-0.64	-1.16	0.34	-1.06	-0.28	0.03	1.22	-1.83	0.03	-0.95	-0.43	-0.02	0.81	-0.54	1.53	-0.17	-0.28	-1.00	1.12	-0.69	-0.23	-2.19	0.24
B	-2.71	0.39	0.03	0.03	-0.80	0.55	-0.69	2.67	-2.19	0.19	0.55	-0.49	-1.42	1.22	-0.12	-2.14	-2.87	0.14	-0.07	-0.80	-1.99	-0.23	0.19	0.50
C	-1.00	0.03	0.03	0.76	-1.11	0.81	0.76	0.19	-1.94	0.55	0.34	1.38	0.03	1.59	0.50	0.45	-0.80	0.03	0.39	0.86	0.19	0.34	0.03	-0.12
D	-0.12	-0.85	0.86	-0.59	-1.37	1.28	0.50	0.86	-0.28	0.81	1.74	1.95	-0.54	0.50	1.22	2.10	0.08	0.14	0.50	0.65	-0.64	-0.12	0.45	1.79
E	0.08	0.08	-0.23	-0.33	0.08	-1.00	-0.33	-0.02	-0.12	2.16	-1.00	0.60	-0.17	0.60	0.50	0.91	-0.23	-0.90	-1.42	-2.71	0.65	0.60	-0.33	0.45
F	-0.43	0.65	0.81	-1.21	-0.49	0.19	0.81	1.74	0.24	0.55	2.73	1.12	-0.95	1.33	1.12	-0.33	-1.31	0.03	-0.17	-1.26	-1.00	0.45	-0.38	-0.12
G	0.34	0.19	-0.12	0.50	-1.26	0.08	0.39	2.52	0.39	2.05	0.76	1.43	-0.54	2.57	1.59	1.43	-0.59	0.76	-0.64	-0.69	0.39	-0.02	-0.64	-0.23
H	0.45	-0.74	-5.92	1.07	-0.80	-0.02	0.34	0.86	-0.43	-0.07	2.10	0.71	2.83	1.48	2.05	1.17	-0.38	1.02	-0.23	-0.49	0.34	0.34	1.17	1.90
I	0.81	0.24	-0.80	0.81	1.02	-14.94	0.55	1.43	-0.64	-0.64	-0.59	1.53	-0.74	1.43	0.19	0.71	0.08	-0.02	-0.07	0.14	-0.43	-0.49	-0.90	0.45
J	-1.00	-0.64	1.28	1.53	-2.35	-0.02	0.24	1.48	-1.68	0.39	-0.54	0.91	-1.06	1.53	0.91	-0.02	3.92	0.08	-0.49	0.34	-4.32	0.60	-0.64	-0.07
K	-0.74	-0.43	0.08	0.08	-1.11	0.29	1.43	-0.02	-0.43	0.08	-0.07	2.26	0.55	1.48	1.33	2.26	0.24	-15.71	-0.33	1.48	-0.80	0.03	-0.28	2.21
L	0.71	-1.42	0.60	-0.74	-0.90	0.86	0.50	-0.12	-1.16	-0.54	-0.90	0.96	-1.21	-0.85	1.43	1.38	0.29	0.60	0.91	0.34	0.60	-0.43	0.55	1.33
M	1.43	-0.54	3.30	-1.00	0.08	2.16	-0.85	1.28	-0.43	1.22	-0.43	0.34	0.50	0.86	-0.59	0.08	-0.28	-7.58	-1.26	-0.43	0.86	-1.00	-1.31	2.16
N	-1.99	-0.64	-0.69	-0.90	-1.68	0.14	-0.90	-1.68	-1.63	-0.17	0.76	-0.12	-1.57	-1.11	-0.17	-0.54	-2.35	-0.07	-0.33	-2.19	-1.94	-0.07	-0.54	-0.02
O	-1.47	0.65	0.81	0.65	-0.43	0.29	1.38	0.96	0.14	3.92	0.19	0.86	0.86	0.14	0.34	-0.80	-0.02	0.39	2.31	1.22	-0.90	-0.12	0.39	1.69
P	0.14	-1.26	0.45	0.39	-1.47	-0.17	0.19	0.96	-1.37	-0.80	0.19	0.91	-1.47	-0.54	-0.12	0.03	-0.12	-1.00	1.02	1.12	-1.11	-2.04	0.60	0.71

MT3	% G1			Average	41.3			S.D.	1.7075928														
	1	2	3	4	5	6	7	8	9	10	11	12	13	14	15	16	17	18	19	20	21	22	23	24
A	-0.53	-0.47	-0.59	0.23	-0.76	1.00	6.32	-0.18	0.88	0.82	-1.46	1.00	-0.88	1.05	-0.70	-0.70	-1.11	-0.94	-0.47	-1.52	-0.64	-0.18	-1.23	0.70
B	-2.05	0.06	-0.12	0.12	-1.05	-0.12	0.94	-0.12	-2.34	0.59	-0.70	-1.00	-2.05	0.59	-19.90	0.53	-2.52	0.41	-0.64	-0.76	-2.28	-0.82	-1.23	0.41
C	-1.52	-0.12	1.23	1.76	-1.11	1.64	0.64	1.05	-0.06	0.64	1.11	2.58	0.70	1.58	1.00	1.17	-0.47	0.94	1.11	0.70	1.05	-0.53	-0.29	1.93
D	-0.35	-0.53	0.00	1.87	-0.76	0.53	0.00	2.75	-1.11	1.05	2.11	1.05	-1.05	1.05	1.58	2.28	1.11	0.41	0.18	1.70	-0.64	0.70	0.82	1.99
E	0.53	-1.05	-0.47	0.88	-7.09	-0.82	-0.29	-0.06	0.47	-0.29	0.59	1.52	0.76	1.82	1.05	0.70	-0.82	-0.35	0.82	-0.53	0.18	0.06	-1.00	1.29
F	-0.76	0.70	-0.70	0.06	-0.76	0.64	1.11	0.88	-1.00	1.11	0.70	0.94	-0.47	0.82	1.93	0.64	0.53	0.76	1.52	-1.17	-1.11	1.05	-0.18	0.06
G	-0.70	-1.00	2.11	0.29	-2.52	-2.17	4.39	2.11	-0.76	1.17	4.63	0.70	0.53	1.17	1.23	0.41	1.23	0.23	1.35	0.12	-1.23	-0.18	-0.12	0.94
H	-0.18	1.17	0.18	0.23	-1.82	-0.76	1.46	1.70	-0.06	1.23	1.17	2.64	-1.23	0.70	3.16	1.93	0.94	-0.12	1.58	0.41	-0.70	0.94	0.00	1.87
I	1.00	-0.35	-0.53	0.53	-2.34	-9.37	0.94	0.53	0.53	1.11	-0.82	3.05	1.29	0.53	0.76	1.35	1.41	0.29	-0.70	1.46	-0.53	-0.82	-0.88	1.70
J	-2.17	0.06	-0.70	1.23	-1.76	0.76	1.11	1.23	0.18	1.76	1.82	2.23	-1.17	2.17	1.35	1.41	-0.53	0.12	-0.53	0.00	-13.70	-1.35	-0.47	0.94
K	0.35	1.17	-0.35	1.05	-0.53	1.87	0.47	0.59	-0.88	0.64	0.53	2.46	1.35	1.64	0.53	0.88	-0.88	0.94	0.88	1.17	0.18	-0.35	-0.12	0.82
L	0.59	-0.41	1.64	1.82	0.29	1.35	2.23	2.17	-0.76	0.53	1.41	1.29	-0.41	1.17	1.41	0.06	-0.06	0.12	0.70	-0.12	-2.28	-0.23	-0.53	1.70
M	-0.12	-1.41	-0.82	0.35	0.29	-0.06	0.06	0.53	0.47	0.18	0.06	2.34	1.05	1.00	0.88	2.34	2.99	-0.59	-0.70	-0.35	0.00	-0.47	-1.00	0.59
N	-2.11	0.18	-1.00	-0.18	-1.87	-0.12	0.00	-1.93	-1.05	0.23	-0.23	-0.35	-2.52	-0.41	0.53	-0.47	-2.11	0.23	-0.53	-1.52	-1.46	-0.06	0.41	-0.23
O	-0.53	1.29	0.23	0.12	8.08	-0.94	0.94	-0.64	-0.41	0.82	1.11	2.34	-0.12	-0.59	0.64	1.70	-19.30	-1.29	0.12	-1.00	0.82	1.35	0.47	1.70
P	-0.35	-0.82	0.29	0.12	-0.29	-0.70	1.00	1.46	-0.18	0.35	2.52	1.05	-0.41	0.18	-0.70	0.88	-2.58	0.18	0.76	-0.12	0.29	-0.35	-0.82	0.18

MT4	% G1			Average	42.1860325			S.D.	1.9064511														
	1	2	3	4	5	6	7	8	9	10	11	12	13	14	15	16	17	18	19	20	21	22	23	24
A	-1.45	-1.82	-1.71	0.43	-0.96	0.37	-0.13	0.15	0.46	0.56	-0.78	1.06	0.16	1.17	0.14	-0.01	1.21	0.22	0.05	1.50	0.11	-0.06	-0.64	0.09
B	-2.30	0.58	0.48	0.18	-1.40	1.30	-0.06	0.42	-1.12	0.51	0.14	-0.85	-1.12	1.20	0.49	0.68	-1.57	0.09	-0.31	-0.65	-1.26	0.92	0.18	0.54
C	-2.33	-1.34	-0.04	0.36	-0.38	0.41	1.66	-0.01	-0.40	0.55	0.80	0.75	0.63	1.34	1.48	0.60	0.10	2.57	-0.71	0.57	-0.30	0.71	0.09	1.19
D	-1.43	0.06	0.95	2.05	-0.34	0.92	2.22	1.03	0.84	0.72	1.71	0.67	0.57	1.61	1.43	2.43	-0.58	0.53	1.04	2.87	-0.17	0.48	1.26	0.43
E	-0.89	-0.06	-0.70	0.84	-0.05	0.56	-0.59	-6.67	-0.51	0.29	0.37	0.84	0.78	-0.14	-0.61	1.34	0.07	0.18	1.23	0.24	-0.31	1.44	-0.13	0.06
F	-1.36	0.85	0.71	0.13	-0.47	0.14	1.84	0.96	-1.36	2.35	1.02	1.08	-1.40	1.70	1.55	-0.27	0.31	0.80	1.54	0.07	-0.27	0.74	0.07	-0.59
G	-2.04	-0.61	0.23	0.90	-1.52	-0.17	0.75	1.74	1.03	3.08	1.98	1.64	0.43	1.83	1.33	2.26	0.72	1.31	1.58	1.09	0.31	0.66	0.90	0.07
H	0.62	1.09	1.73	2.39	0.33	1.18	1.37	3.89	1.15	1.79	2.10	2.79	0.70	1.21	2.32	2.29	0.07	0.70	2.13	2.20	-0.31	0.06	1.55	0.22
I	0.30	-1.22	0.31	-0.08	-0.82	-2.41	-1.26	0.37	0.17	0.78	0.14	1.32	-0.31	-0.79	-0.15	0.97	-0.10	1.76	1.06	1.77	0.59	-0.16	-0.01	1.00
J	-1.66	1.31	0.15	1.01	-1.47	0.96	0.48	1.04	0.66	2.09	1.54	1.38	-0.30	1.16	-0.18	0.20	-0.61	1.08	0.78	0.08	-1.60	0.52	0.63	-0.27
K	-0.11	0.64	-0.02	1.13	0.34	0.45	1.84	0.63	-1.22	1.07	-0.44	0.33	0.45	1.53	0.90	1.63	0.51	1.15	0.60	2.16	-0.11	-0.62	-0.89	-0.09
L	-0.20	0.78	1.62	1.82	-0.11	2.16	2.11	1.61	-0.38	-0.06	1.81	0.66	-0.05	0.09	0.26	1.63	-0.79	0.50	0.52	1.46	-0.72	-0.85	1.37	1.95
M	0.00	1.06	0.79	-0.20	-0.43	0.81	-0.19	-0.09	-0.88	0.81	-0.40	0.65	0.21	1.19	-0.26	0.53	-0.63	0.67	0.06	0.45	0.30	0.36	-0.23	-0.10
N	-1.07	1.05	0.76	-1.46	-1.61	0.12	0.69	0.81	-1.06	0.90	0.44	1.49	-0.38	0.88	0.24	-1.02	-1.89	-0.21	1.30	0.42	-1.36	-0.02	0.08	-0.33
O	-1.38	0.55	1.40	2.26	-0.94	2.19	1.19	1.45	-0.15	1.70	1.68	3.23	-0.15	0.91	1.96	2.63	-0.36	0.30	1.56	0.87	-0.46	0.58	0.10	1.52
P	0.40	-0.07	0.41	0.94	0.00	-0.59	0.73	0.81	-0.23	0.57	1.99	0.88	-0.30	0.04	0.28	1.20	0.66	0.71	2.26	1.51	-0.46	0.12	0.72	1.30

S.D.	neg 2 or less	neg 1 to neg 2	neg 1 to 1	1 to 2	2 or more

Table 2D Raw Metabolite Screen Results – S%

MT1	% S			Average	7.309375			S.D.	0.7996128														
	1	2	3	4	5	6	7	8	9	10	11	12	13	14	15	16	17	18	19	20	21	22	23	24
A	0.04	1.76	-0.54	-0.80	1.39	-0.50	-0.17	0.65	0.38	0.18	-1.57	1.31	-0.91	-0.51	-0.09	0.99	-0.15	-1.19	1.20	0.23	-0.67	-0.52	-1.26	-1.29
B	1.79	-0.22	0.15	-1.80	-0.11	-1.45	-1.27	0.20	-0.76	-0.60	-0.02	0.61	0.70	1.13	-0.11	-0.87	1.21	-0.72	-0.67	-1.00	-0.17	-0.60	-0.77	-1.20
C	-0.21	-0.67	-0.49	-1.25	-0.22	-1.31	-0.81	1.05	0.38	0.59	-0.86	2.24	-1.69	0.25	-1.24	-0.26	-1.14	-1.05	1.16	0.50	-0.07	-0.56	0.04	-0.66
D	0.44	0.79	-1.09	0.75	-0.72	-0.42	0.70	1.00	-1.07	-0.57	0.61	1.03	-0.36	-0.89	-0.27	0.21	-0.09	1.14	0.95	1.58	-0.32	-0.36	1.24	1.80
E	-0.12	-0.32	-0.02	1.56	0.48	0.95	0.34	1.55	-0.10	0.05	0.15	1.03	0.66	-0.16	0.15	1.30	0.24	1.10	-0.86	0.93	-1.27	-0.91	-0.74	-0.91
F	1.83	-0.25	0.83	-0.02	0.33	-0.26	0.41	0.83	-0.40	-0.02	0.11	0.29	1.26	-0.01	-0.55	-0.24	-0.59	0.20	0.44	0.51	-0.22	0.91	-0.84	0.59
G	1.84	-0.04	0.59	1.86	0.40	0.88	-0.20	1.91	0.49	0.50	1.74	1.83	0.71	1.31	0.73	1.81	1.11	-0.27	-0.81	0.45	1.33	0.76	-0.19	-0.54
H	0.50	0.73	0.25	0.25	-0.54	0.66	0.90	1.81	-0.25	0.34	1.06	3.49	-0.55	0.36	1.43	5.24	0.60	3.14	1.20	1.13	0.69	-0.61	-1.54	0.99
I	-1.74	-0.91	-0.26	0.66	-0.04	0.13	-0.84	0.83	1.10	0.13	0.33	1.54	0.63	-0.95	0.50	0.53	0.03	-0.36	0.29	1.93	-1.51	-2.31	0.50	-0.24
J	1.18	-1.17	0.23	-0.75	0.56	-1.35	0.54	0.55	-0.46	0.15	-0.40	0.84	0.58	-1.14	-0.04	0.21	-0.79	0.55	0.93	-0.54	-0.64	-0.64	0.24	-0.47
K	-0.61	-0.15	-0.89	0.10	2.35	0.98	1.08	-1.14	1.10	0.40	1.81	2.18	-2.30	1.21	1.33	1.95	-0.47	1.05	0.93	-0.25	1.40	-0.70	-0.44	-0.07
L	-0.45	1.04	0.49	1.31	-0.31	-0.11	0.20	1.85	-0.10	-0.54	-0.12	1.23	-0.85	-1.26	0.93	1.23	-0.10	-0.62	1.14	1.03	0.18	0.58	1.40	1.64
M	-1.51	0.81	-0.11	-0.22	-0.87	0.20	-1.11	0.71	0.84	-1.05	1.14	-0.15	0.55	-0.66	-1.41	0.86	-0.02	-1.25	0.11	0.64	0.00	-0.10	-0.54	-0.64
N	1.79	-1.66	-0.97	-0.42	0.16	-0.74	-0.16	-0.19	0.51	-0.69	-0.04	-0.52	0.15	0.08	0.23	-0.94	1.00	0.80	-0.86	-1.52	1.46	0.81	-0.11	-1.19
O	1.71	-1.06	4.24	0.48	-1.27	-0.61	-1.21	0.69	1.09	0.61	-0.70	-0.95	2.88	0.28	-0.01	0.04	0.50	1.44	1.41	-1.59	0.40	-0.04	-0.10	0.44
P	-0.07	0.61	-0.55	0.84	0.33	-1.20	-0.50	0.65	0.10	0.50	0.83	1.23	0.78	0.66	-0.29	-0.11	1.00	0.31	-2.23	-1.09	0.01	2.46	-1.21	0.40

MT2	% S			Average	7.40984375			S.D.	0.7250692														
	1	2	3	4	5	6	7	8	9	10	11	12	13	14	15	16	17	18	19	20	21	22	23	24
A	0.58	-0.54	-0.07	-1.12	-0.76	-0.97	0.23	0.22	1.53	2.07	-0.50	1.88	0.59	0.41	-0.19	-0.04	-0.79	0.10	-1.03	0.84	-0.22	-0.76	-0.72	-1.74
B	3.06	-0.92	-0.62	-0.55	-0.58	-0.30	0.28	-1.14	-0.90	-0.08	0.54	-0.33	1.54	0.14	-1.46	-0.37	2.62	-1.31	-0.18	-0.15	-0.76	-0.34	-1.14	0.19
C	-0.97	-0.29	-0.08	0.57	-0.73	0.21	0.30	0.74	-0.99	1.09	0.73	0.90	-1.14	1.66	-0.08	0.73	-0.22	1.09	-1.50	-0.63	-0.76	0.51	-1.48	-1.32
D	-0.10	0.04	0.47	2.08	-0.65	0.39	1.81	3.27	-0.03	-0.95	1.14	1.10	-0.26	-0.08	0.92	2.88	0.32	0.35	0.98	1.71	-0.28	-0.17	0.69	1.57
E	-0.17	0.46	0.52	-0.15	-0.68	1.14	0.59	1.66	1.66	0.44	0.80	1.89	-0.05	1.59	1.67	2.43	2.18	-0.73	-0.15	3.43	0.54	-0.55	-0.65	1.89
F	-1.35	-0.47	1.13	-0.45	-0.69	0.80	-0.25	-0.48	0.54	-0.03	-1.02	-0.21	-1.46	0.73	0.10	0.26	1.14	1.72	-1.06	0.72	-0.26	0.35	0.52	-0.17
G	0.03	0.58	0.51	0.92	1.92	0.48	2.03	1.02	0.91	-1.53	2.23	2.03	1.16	0.07	1.83	1.92	0.23	1.57	2.55	0.92	0.22	0.59	1.37	-0.05
H	-0.85	-0.63	14.05	2.34	0.51	0.59	1.92	1.05	1.03	0.86	3.30	4.81	6.33	2.21	2.74	2.80	2.34	1.08	1.43	2.41	-0.95	-0.21	0.80	2.70
I	-2.00	-0.17	0.92	-0.63	-0.12	-3.88	0.48	1.77	-0.07	1.79	2.50	5.64	1.63	1.17	0.48	2.54	1.21	0.32	-0.70	2.32	0.84	-0.40	-0.48	1.13
J	0.28	0.55	1.35	1.24	0.77	1.37	1.02	-1.10	-1.35	0.83	0.59	-0.47	-1.50	0.54	0.69	0.17	-1.94	-0.69	0.44	0.84	10.33	-0.63	-1.12	0.41
K	-0.87	-0.11	0.22	2.72	-0.08	1.49	0.35	4.26	1.17	1.82	1.30	3.57	0.58	1.56	2.25	2.98	0.46	-1.99	1.46	1.71	0.46	0.52	0.66	-0.57
L	-0.97	-1.42	0.61	1.43	1.02	-0.92	0.47	2.40	-0.28	0.21	0.97	2.08	0.69	0.30	0.36	0.88	-0.12	-0.36	1.34	2.55	-1.14	0.44	0.35	0.86
M	-1.06	1.26	-1.27	1.59	0.14	-3.28	0.10	-1.16	-0.21	1.16	0.69	1.42	0.26	-0.80	-0.04	0.72	-1.64	23.02	-0.12	0.44	-0.50	0.18	-0.47	0.33
N	1.63	0.48	-0.23	-0.30	2.15	0.76	-0.23	-0.05	0.39	0.19	-1.34	-0.68	-0.14	0.54	-0.63	-0.76	0.76	-1.14	0.10	0.07	1.63	0.76	-0.26	0.22
O	0.28	-0.37	-1.05	1.12	1.14	-1.46	-1.02	0.83	0.77	-0.12	-0.72	0.21	-0.50	-0.11	-0.44	-0.01	0.52	-0.19	-0.43	-0.50	-1.45	-0.47	0.68	0.48
P	-0.23	-1.10	-0.48	-1.06	0.11	0.50	-0.91	0.87	0.40	-1.54	-2.34	0.04	-0.37	-1.09	-0.41	1.19	0.17	-1.28	-2.00	0.22	-0.10	0.35	-0.11	0.79

MT3	% S			Average	7.454375			S.D.	0.806814														
	1	2	3	4	5	6	7	8	9	10	11	12	13	14	15	16	17	18	19	20	21	22	23	24
A	-0.17	-0.46	-0.95	0.89	-0.38	-0.35	4.89	0.47	-1.00	0.32	-1.08	0.34	-0.44	-1.01	-0.95	0.87	0.28	-0.28	-0.84	0.52	-0.97	-1.20	-0.84	-1.08
B	0.48	-0.70	-0.98	-0.63	-0.34	1.00	-0.97	-0.43	0.54	0.66	0.53	1.04	1.36	-0.82	0.87	0.09	0.35	0.39	0.29	-1.13	-1.07	-0.23	-1.01	-0.53
C	0.06	1.16	0.94	2.15	-0.07	-0.09	3.40	2.09	1.04	2.03	0.25	-0.23	-0.81	1.23	0.91	0.73	0.08	0.54	-0.43	1.32	0.54	1.02	-0.02	0.70
D	-1.46	-0.34	1.00	1.20	-0.53	0.64	2.35	2.87	0.18	0.89	1.05	2.24	0.94	0.94	0.83	1.37	-0.56	0.35	1.27	2.08	-0.85	0.06	0.70	3.13
E	0.01	-0.71	-0.92	1.13	3.16	-0.27	1.05	1.93	-0.87	0.60	0.24	1.06	-1.06	-0.65	-0.64	0.43	-0.91	1.10	-0.94	0.09	0.19	0.04	0.42	0.75
F	-0.66	-1.21	-0.86	0.75	-0.53	1.18	0.29	0.54	1.90	1.79	-0.15	0.23	-0.44	1.73	0.83	0.74	0.28	0.60	0.56	0.44	0.61	-0.18	0.85	-0.30
G	-1.59	1.07	-0.75	2.16	0.35	1.23	1.80	1.44	-1.51	-0.38	1.35	3.12	0.92	3.77	2.93	3.65	-1.11	1.58	1.37	2.52	1.92	1.75	0.44	2.31
H	-0.64	-1.68	1.38	2.39	1.54	0.92	4.39	4.02	1.26	2.42	2.82	2.72	-0.15	1.83	2.24	2.44	1.28	1.62	1.75	3.53	0.30	0.37	1.27	2.65
I	-0.07	0.65	-1.51	0.07	0.71	-1.22	-0.25	2.73	0.42	-0.44	0.30	1.53	0.69	2.99	-0.23	1.79	0.11	1.63	0.78	1.99	0.85	0.16	-0.36	-0.24
J	-0.38	0.33	-0.81	-0.14	-0.77	-0.14	1.12	-0.34	-1.29	1.00	0.96	0.92	-1.12	-0.24	-0.02	1.13	-1.48	0.73	-0.58	-0.01	-1.77	0.16	0.02	-1.44
K	-0.53	-0.36	0.55	1.84	-1.03	-0.13	1.82	3.28	0.08	1.54	1.89	2.08	-1.49	1.54	1.30	1.89	-0.44	-0.20	1.78	1.15	-0.65	1.87	0.83	0.63
L	-0.35	-1.01	1.33	1.79	-0.44	0.47	-0.51	1.68	-0.66	0.89	1.94	1.71	0.90	0.17	0.89	4.15	0.34	-0.46	1.20	1.48	0.19	-0.13	0.61	0.66
M	-0.32	-0.65	-0.56	1.63	-0.28	-0.19	-3.17	0.59	-0.35	0.29	0.78	1.06	-0.60	0.16	0.02	1.51	1.38	-0.12	0.73	0.48	0.21	0.40	1.79	0.12
N	0.49	-0.75	0.75	-1.53	0.11	-0.12	0.25	0.42	-0.12	-0.63	-1.53	-0.54	0.12	-0.98	0.44	-1.10	-0.28	-0.14	0.21	-0.65	0.89	0.03	-0.48	-1.11
O	0.32	-1.12	-0.19	-0.70	-1.10	0.25	-0.74	0.52	-0.76	0.33	-1.33	-0.67	-0.20	0.29	-0.28	-1.02	-1.28	-0.51	-0.58	-0.06	-1.01	-0.81	0.04	0.43
P	-1.57	-0.25	0.24	-0.28	-0.50	-0.19	-0.22	-0.46	0.68	-0.36	5.01	0.94	-0.27	0.81	0.38	0.18	-0.86	-0.84	-0.49	-0.79	-0.71	0.32	-0.25	1.72

MT4	% S			Average	7.59109375			S.D.	1.122025														
	1	2	3	4	5	6	7	8	9	10	11	12	13	14	15	16	17	18	19	20	21	22	23	24
A	-0.14	-0.58	-1.02	-0.18	0.83	0.89	-0.75	0.55	0.00	0.57	-0.72	0.81	0.03	0.63	-0.30	0.31	-0.41	-0.37	0.06	0.34	1.18	-0.21	-1.28	0.42
B	1.70	-1.01	-0.60	0.09	-0.01	-1.12	-0.22	-1.00	0.28	0.15	-0.42	-0.16	0.12	1.10	-0.61	-0.61	0.93	0.19	-0.50	-0.07	0.19	-0.32	-0.47	-1.34
C	-1.08	0.82	0.11	0.69	-0.20	0.00	0.01	0.53	-0.77	0.69	0.29	1.18	-0.15	0.37	0.74	0.75	0.13	-0.58	0.76	0.40	-0.37	-0.60	0.33	0.16
D	0.04	-0.71	0.61	0.46	-0.57	-0.83	0.70	1.49	-0.38	0.12	0.60	1.60	-0.24	-0.33	-0.05	0.65	-0.77	0.24	0.52	0.95	-1.20	0.14	0.12	1.68
E	0.10	0.30	-0.48	0.41	-0.44	0.14	0.73	21.13	-0.19	-0.29	-0.45	1.74	-1.99	0.81	-0.17	1.23	-0.41	-0.34	0.65	1.58	-0.19	-0.21	1.12	0.54
F	1.09	-0.74	-0.09	-1.12	0.90	0.66	-0.09	-0.30	0.29	0.78	0.42	0.24	-1.03	1.10	0.24	0.43	-0.83	1.09	0.13	0.37	-0.51	0.47	1.10	0.41
G	-0.51	0.52	0.03	0.82	-0.11	0.85	0.39	1.66	-0.19	0.17	0.61	1.75	0.83	0.67	0.93	1.74	0.46	0.70	1.92	1.21	0.65	0.12	-0.05	1.34
H	-0.38	-1.36	-0.01	1.55	0.13	0.05	0.78	2.01	-0.02	0.39	1.07	1.67	-0.18	0.23	0.67	2.41	0.95	0.20	1.18	1.36	0.92	0.92	1.09	3.04
I	-0.92	-0.33	-1.20	0.69	0.19	1.88	0.15	0.99	-0.04	0.12	0.18	-0.45	-0.14	0.83	0.68	1.11	-0.41	0.08	0.88	-0.32	-0.11	0.20	-0.62	1.30
J	-0.89	0.10	-0.30	-0.64	-0.38	0.53	0.14	0.61	-0.94	-0.32	1.06	0.57	0.52	-0.60	0.11	0.93	-0.25	-0.06	0.38	0.54	-0.22	0.13	-0.49	0.19
K	-1.49	-0.01	0.19	1.10	-0.72	1.52	0.49	1.88	0.44	0.42	1.90	2.15	-0.32	-0.11	0.93	0.99	-0.52	0.18	0.04	0.30	-0.08	0.36	1.88	-0.16
L	-1.75	-0.87	0.14	0.93	0.16	-0.75	-0.53	1.35	0.12	0.00	1.20	1.98	0.37	-0.37	0.50	0.11	-0.31	-0.54	-0.19	1.06	-0.63	0.61	0.68	1.03
M	-1.23	-1.17	-0.97	-0.57	-0.56	0.18	-0.61	1.01	0.28	-0.99	-1.56	0.68	-0.37	-0.34	0.39	0.04	0.14	-1.28	-0.72	-0.71	-0.66	-0.39	-1.22	0.30
N	-0.05	-0.28	-0.82	-0.69	-0.30	0.04	-1.35	-1.31	-0.38	-0.76	-0.70	-1.18	-1.32	-1.10	-0.14	-1.14	-0.62	-0.48	-1.42	-0.87	-0.29	-0.24	0.64	-0.86
O	-0.41	-0.87	-0.65	-0.01	-0.95	-1.36	-0.24	-0.75	-1.36	-0.28	-0.96	-1.05	-0.21	-1.10	-0.06	0.18	-0.44	-0.56	-0.58	-0.26	-1.09	-1.17	-1.38	1.36
P	1.21	-0.97	-0.50	0.66	-0.98	-0.98	-0.38	0.54	-0.38	-0.26	-0.09	1.19	-0.97	-0.31	0.10	-0.83	-1.04	-0.91	-0.84	0.47	-0.55	0.06	-0.42	1.40

S.D.	neg 2 or less	neg 1 to neg 2	neg 1 to 1	1 to 2	2 or more

Table 2E Raw Metabolite Screen Results – G2/M%

MT1	% G2/M			Average			39.7109375		S.D.	1.9843129													
	1	2	3	4	5	6	7	8	9	10	11	12	13	14	15	16	17	18	19	20	21	22	23	24
A	1.41	0.75	1.3	-0.4	-0.66	0.246	0.196	-1	0.04	0.8	0.25	-1.1	0.549	-0.3	1.1	-0.26	0.448	1.204	0.65	-0.5	0.246	1.76	1.66	-0.8
B	-0.1	0.45	0.15	0.5	0.347	0.347	1.254	0.15	0.04	-0.1	-0.5	-0.7	0.045	-1.2	0.55	-0.86	-0.51	0.146	0.7	0.15	0.952	0.15	0.95	-0.4
C	-0.4	-0.1	0.95	-0.3	-0.06	0.196	-0.76	-2.1	-0.7	-0.5	-2.9	-1.5	-0.31	-1.6	0.2	0.246	-0.01	0.045	-0.2	-0.9	-0.16	0.25	-0.4	-0.8
D	-0.7	0.8	-1.6	-1.5	-0.01	-0.26	-0.91	-3.1	-0.6	-1.1	-1.3	-2.5	0.095	-1.1	-0.7	4.429	-0.21	-0.66	-1.7	-2.8	-0.46	-0.7	-1.9	-0.9
E	-0.1	0.75	1.05	-1.9	-1.01	-0.16	-0.46	-1.2	-0.9	-0.6	-0.7	-0.7	-1.06	-0.9	-0.2	-1.67	-0.66	-1.52	1.1	-2.8	-0.86	0.25	1.76	-1.8
F	1.15	-0.6	0.5	1	0.347	0.7	0.246	-0.5	-0.2	-0.3	-0.2	-0.2	-0.01	-1	0.45	-1.32	0.498	-0.41	-1.2	-1	-0.91	-0.6	0.5	-0.6
G	-1.6	0.2	-1.4	-1.5	-1.21	-2.37	-1.27	-2	-0.3	-0.8	-1.3	-2	-0.56	-1.4	-1.6	-2.98	-0.91	-0.71	-2.1	-2.5	-1.57	-0.9	-1	-0.8
H	-0.3	-0.3	-0	-1.7	0.448	-0.76	-0.81	-2.5	-1.4	-1.4	-1.6	-2.8	-0.11	-1.3	-2.4	-3.53	-1.27	-2.42	-1.3	-3	-0.11	0.04	-1.2	-2.8
I	-0.9	-0.4	0.3	-0.8	-1.52	-1.16	-1.01	-2.7	-1.5	-1	-1.6	-2.2	-1.42	-0.2	-0.6	-2.53	-1.62	1.305	-0.2	-1.5	0.801	0.4	1.41	-0.9
J	0.3	-0.2	0.85	0.65	0.902	0.095	-0.11	-0.1	0.4	0.9	-0.2	0.1	0.7	-0.6	-0.1	-0.96	0.196	0.297	-0.6	0.5	0.448	0.35	0.55	0.04
K	0.95	0.25	0.5	-2.2	-1.11	-0.31	-1.97	-5	-1.3	-0.7	-1.3	-1.7	0.902	-1.6	-1.6	-2.17	-0.66	-0.91	-1.7	-1.1	0.851	0.4	0.6	-0.5
L	1.15	1.05	0.04	-0.1	0.095	0.599	0.549	-1.4	-0.2	0.25	-0.2	-0.9	0.398	0.4	-0.7	-1.72	-1.01	-2.17	-0.5	-1.8	-0.41	0.8	-0.8	-2.2
M	0.9	0.55	-1.6	-0.4	-2.53	-1.21	-0.36	-0.7	-0.8	-0.8	-0.1	-1.8	1.254	0.85	-1.1	-0.86	0.045	0.297	0.95	-0.3	-0.11	1.61	1.86	0.15
N	0.75	0.85	0.8	0.85	0.7	0.549	0.246	0.55	0.6	1.66	0.4	-0.5	1.406	-0.2	1.25	1.103	1.355	0.196	0.55	0.8	1.103	-1.4	1.1	-0.1
O	0.95	-0.3	-0.7	-0.6	6.143	0.952	0.045	-0.6	0.55	0.45	1.25	-0	1.607	0.9	-0.5	-0.06	1.456	-0.01	1.71	1.36	-0.71	1.66	-0.2	-1.2
P	0.6	1.46	-0.8	0.15	1.355	-0.11	0.448	-1.4	0.85	1.61	1.41	-0.6	1.456	0.8	-0.4	-0.06	0.801	1.809	1.1	-0.2	0.801	1.41	-0	-1.3

MT2	% G2/M			Average			39.096875		S.D.	2.03649													
	1	2	3	4	5	6	7	8	9	10	11	12	13	14	15	16	17	18	19	20	21	22	23	24
A	-1	0.79	0.59	-0.7	0.542	0.198	0.149	-0.8	1.08	0.2	1.23	-1	-0.83	-0.3	0.89	-0.19	0.493	1.426	1.92	-0.5	0.984	0.74	1.62	-0.1
B	1.72	0.59	0.35	0.2	0.1	0.149	0.738	-2.1	1.08	-0.6	-0.4	0.49	0.149	-0.4	1.33	2.064	1.131	0.394	0.89	0.05	1.671	0.79	0.74	-0.4
C	0.79	0.05	0.84	-1.2	-0.64	-0.83	-0.49	-1	0.35	-1.5	-1	-2.4	0.051	-2	0.05	-0.93	-0.19	-0.44	-0.3	-0.4	0.149	-0.3	0.05	0.15
D	-0.3	0.25	-1.1	-1.5	-0.64	-0.49	-1.86	-2.6	-0.9	-0	-2	-3.3	-1.23	-0.5	-1.4	-3.14	-0.59	-0.39	-0.2	-1.5	-0.44	-1.3	-1	-1.4
E	-0.9	-0.5	-0.6	-0.3	-0.69	-0.98	-0.29	-4	-2.4	-2.4	-0.6	-1.1	-1.42	-0.2	-0.2	-2.21	-1.42	0.885	-0.7	-0.7	-0.15	-0.4	0.15	-2
F	0.69	0.25	0.84	0.39	0.394	0.738	-0.19	-1.2	0.05	-0.2	-1.3	-0.9	0.345	-0.7	-0.4	0.787	-0.39	-1.77	-0.1	-1.4	-0.59	-0.9	-1.1	-0
G	-1.3	-0.5	0.1	-1.2	-1.32	-1.23	-2.31	-2.9	-2.2	-2.3	-1.7	-2.3	-0.69	-2.4	-2	-3.19	-1.03	-1.57	-1.1	-0.7	-0.93	0.05	-0.1	-1
H	-0.3	1.43	1.43	-1.8	0.394	-0.49	-0.44	-2.5	-1.7	-0.5	-3.1	-2.7	-6.97	-1.9	-2.9	-2.9	-1.47	-1.86	-1.1	-2.7	-0.1	-2	-2.3	-3.2
I	0.54	-0.2	0.39	-0.9	-1.28	7.76	-0.78	-3	-0.5	-1.2	-1.1	-3.2	-1.42	-1.1	-0.7	-2.65	-1.96	-0.44	0.39	-1.3	0.394	-0.2	0.79	-0.6
J	0.44	-0.3	-1.4	-0.8	1.72	-0.54	-0.69	-1.1	1.23	-0.8	0.59	-0.8	-0.1	-1.3	-0.7	-0.83	-2.5	-0.49	0	-1.3	0.051	-0.7	-0	-0.1
K	0.25	0.44	-0.1	-1.8	-0.19	-0.93	-2.11	-3	-1.8	-1.7	-1.9	-2.8	-0.93	-1	-2.9	-2.4	0.345	8.595	-1.4	-3.2	-0.83	-0	-0.6	-0.5
L	0.1	0.84	-1.2	-0.8	-0.44	-1.03	-0.74	-3.8	-0.2	0.44	0.44	-2.3	-0.24	0.49	-1.7	-1.91	-1.52	-0.39	-0.9	-2.5	-0.05	0.59	-0.2	-2.5
M	0.25	0.44	-1.3	-0.6	0.296	-10.4	-0.39	-1.7	-0.8	-1.2	0.05	-0.6	0.051	0.3	0.84	-1.23	-0.19	1.278	1.18	-1	0.296	0.79	1.47	-0.8
N	1.43	0.35	1.47	1.13	1.327	-0.49	0.984	-0.1	1.23	-0.1	0.15	-0.1	1.131	0.74	-0.1	-0.1	1.524	1.229	0.35	-0.1	0.787	0.15	-0.1	0.44
O	1.62	0.69	0.15	-0.2	0.738	1.131	0.394	0.1	0.25	-1.6	1.18	0.59	0.885	0.69	1.57	1.426	-0.15	-0.15	0.44	-0.8	1.327	1.38	1.18	0.3
P	1.52	1.23	-0.1	0.74	1.72	1.671	1.524	-0.2	1.28	0.84	1.57	-0.1	1.229	1.47	0.44	-0.69	0.051	1.769	1.28	-0.6	1.524	1.28	0.54	-0.5

MT3	% G2/M			Average			38.4375		S.D.	2.2135585													
	1	2	3	4	5	6	7	8	9	10	11	12	13	14	15	16	17	18	19	20	21	22	23	24
A	0.12	0.48	0.57	0.25	1.022	-1.19	-8.74	-1.3	-0.2	-0.6	1.34	-1.4	0.164	-0.1	1.47	0.525	1.474	0.119	0.98	0.62	1.067	0.16	1.47	0.34
B	0.66	-0	0.71	-1.1	-0.88	-0.06	0.254	0.03	0.53	-0.6	0.21	-0.6	0.028	0.39	14.9	-0.56	0.39	-0.02	-0	0.21	0.977	0.39	0.53	0.53
C	-0.6	-0.4	-1.4	-1.7	-0.29	-0.88	0.39	-1.6	-0.2	-1.7	-0.2	-1.3	-0.42	-1.2	-0.8	-0.92	0.344	-1.37	-0.1	-0.8	-0.97	-0.4	-0.6	-1.7
D	-0.4	0.48	0.34	-2.6	-1.1	-1.06	-0.74	-2.6	-0.8	-1.9	-2	-2.5	-1.46	-0.7	-0.8	-2.41	-1.06	-0.24	-1.5	-2.6	-0.33	-1.1	-0.6	-2.7
E	0.21	0.93	0.39	-1.3	6.172	-0.06	-0.74	-1.6	-0.3	-0.6	-0.6	-1.8	0.028	-0.8	-0.1	-0.51	0.119	-0.88	0.07	-0.1	0.028	-0.4	1.56	-1.6
F	0.8	0.43	0.53	-1.1	1.022	-0.38	-1.06	-1.1	-0.2	-0.9	-0.3	-0.9	0.028	-1.1	-0.8	-0.06	-0.15	-0.56	-1	0.12	-0.11	0.21	-0.8	-0.6
G	0.62	-0.6	-1	-1.6	-1.73	-0.24	-3.77	-2.7	-0	-1.5	-3.1	-2.6	-1.01	-2.6	-2.3	-2.86	-0.38	-1.91	-1.9	-1.2	-0.88	-0.7	-0.5	-2.4
H	-0.3	0.75	-0.9	-1	-1.28	-0.56	-3.04	-3.2	-1.6	-2.5	-1.4	-4.5	0.344	-0.7	-2.8	-2.82	-1.82	-1.01	-1.9	-2	-0.24	-0.6	-0.5	-2.6
I	-0.4	0.89	0.43	-1.1	-2.41	-1.82	-0.24	-1.9	-1.6	-0.2	0.89	-2.9	-0.47	-1.1	0.16	-2.82	-0.56	-0.69	0.12	-2.2	0.344	-0.4	0.57	-0.5
J	1.93	-0.2	0.57	-0.1	-1.19	0.073	-0.88	-0.4	-0.1	-0.9	-0.9	-1	1.022	-0.4	-0.6	-2.14	-0.15	-0.06	0.43	-0.4	10.37	0.71	0.57	0.16
K	-0.3	-0.6	-0	-1	0.616	-0.65	-1.6	-2.2	-0.2	-1.1	-1.3	-3.2	0.254	-0.4	-0.7	-1.37	-0.6	-0.06	-0.6	-1.6	0.073	-0.2	0.03	-1.8
L	-0.4	0.48	-1.5	-1.8	-0.51	-0.74	-0.6	-1.6	0.07	-0.6	-1.3	-2.4	-0.2	-0.3	-0.2	-2.1	-0.11	-0.56	-0.9	-1.2	-0.11	0.39	-0.6	-1.7
M	0.43	0.84	1.11	-1.2	0.616	0.39	-11.5	-0.6	-0.6	0.16	-0.1	-1.1	-0.2	-0.5	0.48	-1.28	-1.42	0.344	0.53	-0.5	0.119	-0.2	0.89	-1
N	1.16	0.57	0.71	0.66	0.706	-0.38	-0.15	0.34	0.25	1.16	0.8	0.75	0.525	0.21	0.21	0.932	0.751	0.028	0.25	1.07	0.344	0.71	-0.1	0.89
O	1.47	0.39	0.62	-0.3	-11.1	0.254	0.164	-0.4	0.71	0.62	0.34	-0.4	1.158	1.29	-0.1	0.525	7.347	0.073	0.03	-0.2	1.158	0.39	0.53	-0.2
P	0.8	0.98	0.12	0.16	0.661	1.248	0.57	-1.3	1.34	1.11	-3.4	-1.1	1.384	0.39	0.53	-0.92	0.525	1.022	0.71	-0.5	0.57	1.2	1.7	-0.6

MT4	% G2/M			Average			37.2203125		S.D.	2.1705226													
	1	2	3	4	5	6	7	8	9	10	11	12	13	14	15	16	17	18	19	20	21	22	23	24
A	-0.1	0.41	0.41	-1	-0.33	-0.42	0.359	-0.4	-0.2	-0	1.42	-1.3	-0.15	-1.5	0.87	0.774	0.497	1.05	1.33	-0.1	-0.06	0.5	1.42	-0.8
B	0.73	0.96	0.41	0.08	0.82	-0.42	0.912	0.17	1.05	0.27	0.41	0.45	0.59	-1.4	0.68	0.221	0.175	0.037	0.82	0.45	0.728	-0.3	0.08	0.17
C	0.91	-0.2	-0	-0.7	-1.12	-0.33	-0.93	-2	0.5	-0.6	-0.9	-1.3	-0.79	-0.8	-1.1	-0.98	-0.29	-0.93	-0.9	-0.1	0.59	-0.1	0.22	-0.6
D	0.41	1.37	-0.8	-2.2	-0.06	-0.06	-1.35	-2.3	-0.4	-0.5	-2.1	-2.9	-0.47	-0.2	-1.2	-1.71	0.59	-0.65	-1.1	-2.8	1.281	-1.3	-2.5	-2.5
E	-0.3	0.08	0.64	-1.3	0.129	0.129	-0.52	-4.4	-0.6	0.04	1.19	-1.9	0.497	-0.6	0.31	-1.94	0.451	1.004	-0.7	-1.8	-0.52	-0.7	-1.1	-0.7
F	0.87	0.87	-0.1	1.14	1.05	-0.01	-0.56	-0.8	0.27	-1.1	-0.4	-0.3	1.004	-1.7	-0.3	-0.93	-0.1	-0.93	-0	-0.1	0.175	-0.7	-1.9	-0
G	0.17	0.45	0.04	-1.6	-0.88	-0.52	-1.58	-1.9	-1.5	-2	-2	-2.7	-0.98	-2.4	-1.6	-3.51	-0.24	-1.62	-1.6	-2.3	-0.29	-2.2	-0.2	-0.3
H	-0.3	0.68	0.08	-2.6	-0.7	-0.47	-0.06	-2.7	-0.3	-0.2	-1.3	-2.3	-0.29	-1	-1.6	-2.82	-0.19	-1.16	-1.1	-1.8	-0.29	-1.7	-1.1	-2.8
I	0.31	1.74	-0.2	-0.9	-0.61	-2.77	-0.19	-1.8	-1	-0.7	-0.7	-0.7	0.544	0.82	-0.4	-0.79	-0.47	0.451	-0.1	-0.2	-0.42	-1.2	0.22	-0.6
J	1	-0.4	-0	-0.3	0.636	-0.75	-0.65	-1.8	0.22	-0.2	-2.1	-0.6	0.359	0.41	0.64	-0.79	0.59	0.221	-0.7	-0.6	0.497	0.13	-0.7	-0.6
K	0.73	-0.1	-1.1	-1.5	-0.38	-1.16	-2.27	-2.3	-0.2	-0.7	-1.7	-1.3	0.129	-0.3	-1.1	-1.02	0.313	0.221	-0.4	-1.3	0.866	-1	-1.3	-0.1
L	0.82	0.64	-0.6	-1.3	0.037	-0.19	-0.88	-1.1	-0.3	-0	-0.9	-2.6	-0.15	0.31	0.04	-2.82	-0.24	-0.24	-0.1	-1.6	0.82	0.13	-1.5	-1.5
M	0.96	0.22	0.87	0.77	0.359	0.497	0.682	-0.8	0.54	-0.1	2.2	-0.1	0.359	-0.3	1.79	-0.15	0.636	1.05	1.37	-0.4	0.912	1.19	0.22	-0.1
N	1.14	0.22	0.91	1.6	2.064	1.05	0.175	0.17	1.51	0.45	0.73	0.59	1.281	0.36	0.41	0.636	1.649	1.235	0.87	0.04	1.235	0.87	-0.8	1
O	1.19	1.33	0.77	-0.5	1.834	0.636	1.05	-0	1	0.17	0.36	-0.8	2.064	0.96	-0.1	-0.33	1.235	1.004	0.73	0.64	1.373	-0.1	1.14	-0.3
P	-0.5	1.56	0.73	-0.1	1.142	1.603	0.912	-0.4	0.22	1.19	-0.6	-1.1	1.05	0.91	0.22	0.129	0.728	0.958	0.08	-1	1.281	0.96	0.54	-0.8

S.D.	neg 2 or less	neg 1 to neg 2	neg 1 to 1	1 to 2	2 or more

Chapter 3

Functional characterization of Rexo4 in cell cycle progression

Abstract

The ribosome is the macromolecular factory in cells responsible for synthesizing protein from strands of messenger RNA (mRNA) by catalyzing the formation of peptide bonds. Due to the complexity of this structure, ribosome biogenesis is an intricate process involving many different processing and maturation steps in multiple subcellular compartments. These steps include: the co-transcriptional assembly between ribosomal RNA (rRNA) and protein, rRNA modification, protein and ribosome precursor shuttling into and out of the nucleus, and multiple rRNA cleavage steps. In this work, we characterized the human Rexo4 protein, predicted to be an RNA exonuclease involved in the processing of nascent ribosomes. We determined that it localizes to the nucleolus through an N-terminal nucleolar localization signal and that its function in the nucleolus is required for cell cycle progression. Ribosome biogenesis has recently received more attention as an avenue for possible cancer treatments and this work sets the foundation for future work on an essential protein within this pathway.

Introduction

Ribosomes are large ribonucleoprotein complexes that are responsible for the translation of messenger RNA (mRNA) into protein, providing a catalytic site for forming peptide bonds. A fully matured ribosome is a complex made of four ribosomal RNAs (rRNA) and about 80 ribosomal proteins [27], [28]. Human ribosome biogenesis is an incredibly complex process which involves an additional 200-plus proteins and non-coding RNAs that modify, process, export and assemble the mature ribosome in various locations in the cell [29]. This endeavor starts in the subnuclear compartment known as the nucleolus, where RNA polymerase I (RNA Pol I) synthesizes the large polycistronic

47S precursor rRNA which contains what eventually is processed into the 18S, 5.8S and 28S rRNAs[79]. These rRNA precursors are surrounded by a 5' and a 3' external transcribed spacer (ETS) and are separated by internal transcribed spacers (ITS1 and ITS2). Simultaneously, ribosomal proteins (made in the cytoplasm by mature ribosomes and imported to the nucleus) and pre-ribosomal factors associate with the 47S precursor to form a 90S particle, which includes a 5S rRNA subunit that is transcribed in the nucleoplasm by RNA polymerase III (RNA Pol III) [80]. Other early modifications to the 90S particle include the association of box C/D class small nuclear RNAs (snoRNA) that mediate 2'-O-methylation and psuedouridinylation of the pre-rRNAs as they are being synthesized by RNA Pol I [81]–[83]. The 5'ETS and 3'ETS are cleaved from the ends of the 90S pre-rRNA in the nucleolus, separating the 90S particle into a pre-40S complex containing a 18S pre-rRNA and a pre-60S complex containing 5.8S pre-rRNA, 28S pre-rRNA, and 5S rRNA [84]. Here is where the distinction between ribosomal protein small subunits (RPS) and ribosomal protein large subunits (RPL) is made, RPSs associate with the pre-40S particle and RPLs associate with pre-60S particle [85], [86]. The 40S and 60S undergo several processing steps prior to being exported into the cytoplasm by different proteins. In the cytoplasm, final maturation steps of these complexes occur and they associate with each other to form a mature 80S ribosome, necessary for the translating mRNA into protein. The 40S half is responsible for binding, unwinding and scanning mRNA, while the 60S half is responsible for peptide bond formation and nascent peptide quality control [85], [87].

Cell-cycle progression requires the synthesis of many proteins for both the production of necessary proteins in mitosis and the regulation of mitosis itself. Ribosomes are thusly required for cell growth and are directly linked to nutrient availability in cells [88]–[90].

Rexo4 was originally identified as a cell division regulatory protein in *Xenopus* as *Xenopus* mitotic catastrophe (XPMC) due to its ability to prevent mitotic catastrophe in *S. pombe* deficient in both *wee1* and *mik1* kinases (Su 1995). Wee1 and Mik1 both act as inhibitors of the G2 to M transition in *S. pombe* via Cdc2 phosphorylation and the lack of both of these kinases results in premature mitotic entry in yeast [91]. Early work on the homologous *S. cerevisae* gene, REX4, demonstrates that though it is not an essential gene, it plays some role in pre-rRNA processing through interaction with rrp2-1 (RNAse for mitochondrial RNA processing), as processing of 35S to 27S pre-rRNA is greatly diminished when rrp2-1 is depleted but this phenotype is reversed upon inactivation of REX4 [92], [93]. Along with 35S to 27S processing, there is a change in ratio of mature $5.8S_S$ to $5.8S_L$ rRNAs when rrp2-1 is depleted, but again is restored to what is observed in wild-type yeast when REX4 is inactivated, suggesting that it plays a role in ITS1 cleavage/processing [94]. These phenotypes are unsurprising as REX4 does contain a predicted RNA exonuclease domain. Another RNA exonuclease in its family, Rexo5, was shown to cleave the 3' ends of 28S pre-rRNA, 5S pre-rRNA, and snoRNA precursor in *Drosophila* [95]. A direct human homolog hPMC2 (renamed to Rexo4) was discovered, but it remains relatively uncharacterized regarding its cellular role [96]. More recently, there have been several studies that demonstrate Rexo4 plays a role in cancer progression and promotion [97]. Rexo4 has been found to have

increased expression in cancer cell models founding claims that it can be used as a biomarker for hepatocellular carcinomas [98]. These claims make sense in the context that Rexo4 is likely involved in ribosome biogenesis/pre-rRNA processing, as there is ever growing sentiment that a link exists between upregulation of ribosome biogenesis and cancer risk [86], [99], [100].

Results and Discussion

Rexo4 localizes to the nucleolus and requires L32 to L35 for localization

Previously, our lab had performed proteomic studies on Rexo4 using a doxycycline-inducible LAP-tagged (GFP-tev-S-protein tag) Rexo4 stably integrated into Hek293 Flp-In T-Rex cells (Figure 1A). This tagged version of Rexo4 was overexpressed overnight and purified via sequential rounds of affinity purification with anti-GFP beads followed by S-protein agarose. SDS-PAGE was performed and ten excised bands were sent to the Harvard microchemistry and proteomics analysis facility for analysis via tandem mass spectrometry. After receiving the results, we performed gene ontology analysis on this list of purified proteins/putative interactors, using GOnet, an easy-to-use, interactive tool that visualizes the functional similarities of the entered proteins [101]. This allowed us to determine that Rexo4 is most likely involved within the process of ribosome biogenesis, which takes place inside of the nucleolus (Figure 1B). This theory is supported by the fact that many of the identified proteins were either large or small ribosomal proteins (RPLs and RPSs) or other proteins involved in ribosome biogenesis. For example, Bystin (BYSL), is a protein required for the processing of 40S rRNA to 18S rRNA and TSR1 is an assembly factor with a similar role, involved in the trimming of 20S pre-rRNA to 18S rRNA [102], [103]. Nucleolar protein 2 (NOP2) is a regulator of

pre-rRNA through complex formation with box C/D snoRNAs [104]. These are only a few of the nucleolar ribosomal biogenesis proteins that were identified in this LAP-Tag purification of Rexo4.

Using the nucleolar marker NPM1, we confirmed via immunofluorescence (IF) microscopy that during interphase, Rexo4 primarily localizes to the nucleoli (Figure 2A). In mitosis, Rexo4 primarily colocalizes generically to the chromosomes, with no specific localization (Sup. Figure 1). Proteins highly enriched in the nucleolus usually require a nucleolar localization sequence (NoLS) as nucleoli are subnuclear area typically dense with proteins [105]–[107](choose paper). We used the Nucleolar localization sequence Detector (NoD) in order to find the putative NoLSs in Rexo4 [107]. According to this tool, Rexo4 has 3 different predicted NoLSs, between residues 16 to 53, 92 to 112, and 336 to 358 (Sup. Figure 1). To investigate if these NoLSs are responsible for Rexo4's localization, we made Rexo4 truncation mutants, dividing the recombinant Rexo4 coding sequence into N-terminal (NT,a.a.1-243), exonuclease with C-terminal (Exo-CT, a.a. 244-422), and exonuclease only regions (Exo, a.a. 244-394) (Figure 2B). The wildtype gene and these mutants, were cloned into our pgLAP1 plasmid, transiently transfected into HeLa cells and visualized via IF microscopy. The wild-type localization confirmed our initial observation that primary localization was in the nucleoli, while the NT mutant also localized strongly to the nucleoli (Figure 2D). However, truncation mutants lacking the N-terminal region, Exo-CT and Exo, were observed to lose all ability to localize to the nucleoli and were broadly dispersed throughout the cytoplasm in cells. These results suggest that the predicted NoLS found in the exonuclease was not responsible for localization to the nucleoli, and that at least one of the two predicted

NoLSs found in the N-terminal region is necessary and sufficient for proper Rexo4 localization. We expected the NoLSs predicted between residues 16 to 53 be the most likely needed site, as it scored highest on NoD. Taking this into account, we targeted the four consecutive lysines found in amino acid positions 32 to 35. We performed the *in-silico* version of this experiment, changing each of these lysines to alanines to see how it affected the predicted NoLS score on NoD. According to this method, it requires mutating at least three of these lysines until the predicted score drops below the threshold for NoLS prediction (Sup. Figure 1).

After mutating one, two, or three of these lysines in position 32 to 35 to alanines, we observed via IF microscopy that Rexo4 nucleolar localization is not affected by up to three lysine-to-alanine mutations in the predicted NoLS (Figure 3). This was quite surprising, considering the predicted NoLS score for Rexo4$^{\Delta K323334A}$ and Rexo4$^{\Delta K333435A}$ indicated otherwise. Taking the rest of the predicted NoLS into consideration, there are 8 other lysines we can mutate in order to create a full-length Rexo4 mutant that will not localize to the nucleolus. This could be expected, as we posit Rexo4 is an essential gene required for proper ribosome biogenesis, one could imagine Rexo4 has evolved to safeguard its ability to localize to its subcellular home by having many redundant lysines in this region.

Rexo4 is required for cell proliferation

Next, we used siRNA treatment to investigate Rexo4's possible role in cell division. Western blotting revealed that acute knockdown of Rexo4 occurred after 72 hours post

siRNA treatment and this knockdown was validated via IF microscopy, where we see endogenous Rexo4 absent from nucleoli in transfected cells (Figure 3A). A clear lack of mitotic cells was observed in the coverslips treated with siRNAs against Rexo4 and this begged the question if Rexo4 depletion caused a cell cycle arrest. We then performed a cell proliferation assay over 96 hours and remarkably, we observed a near-to-complete stop in cell growth (Figure 3B). This result was further corroborated by using scanning cytometry, which provided cell counts suggesting similar growth kinetics (Figure 3C). In the plate read after 3 days of treatment, the wells that received Rexo4 siRNA treatment had slightly lower cell counts than the untreated or transfection reagent only conditions. However, in the plate treated for 4 days, the cell counts for the siRNA-treated wells were about half of the control conditions, indicating that cells had stopped growing for about 24 hours. These experiments also provided generic insight regarding when in the cell cycle this arrest was occurring, with the vast majority of cells pausing sometime between G1 and S. With what we have observed regarding depletion timing of anti-Rexo4 siRNA treatment and the growth kinetics post-depletion of Rexo4, we can deduce that in human cancer cells, the Rexo4 protein is required for cell proliferation. There is precedent for this, as multiple ribosomal proteins have been reported as necessary for cell proliferation [108], [109].

Next, we overexpressed Rexo4 full length and truncation mutants to see if an abundance of Rexo4 was sufficient to drive proliferation forward and if localization to the nucleolus was required for this change in cell cycle kinetics (Figure 3D). Surprisingly, overexpression of full-length Rexo4 did not drive increased proliferation but halted

proliferation for 48 hours, at which point the cells resumed a reasonably normal growth curve. However, overexpression of a Rexo4 truncation mutant lacking either the predicted exonuclease domain or the ability to localize to the nucleolus led to a complete halt in cell growth from 24 hours and onward.

Conclusion

Rexo4 is an important regulator in ribosome biogenesis which is gaining more and more attention in its role in the proliferative upregulation found in many cancer cell types. Though Rexo4's exonuclease activity is required for proper pre-rRNA processing in the early stages of ribosome biogenesis, there has been surprisingly little work performed to study its function in human cell division. Our proteomic studies using LAP-tagged Rexo4 in Hek293 cells suggested that Rexo4's function was at least similar to what was seen in previous work performed in yeast on its homologous protein, Rex4 [94]. After expression of the different truncations, it was clear that proper localization of Rexo4 is reliant on at least one of the nucleolar localization sequences predicted to be in the N-terminal region prior to the exonuclease domain. This result was not surprising as the highest scoring putative NoLS was the region located between amino acids 16 to 53. The mis-localization of the exonuclease domain with or without the C-terminal tail supports this and more investigation using GFP-labeled Rexo4 NoLS can further confirm this theory. So far, we have shown Rexo4 still localizes to the nucleolus even after half of the lysines in the purported NoLS are mutated to alanines.

We have shown that Rexo4's localization to the nucleolus is critical for cell proliferation, as overexpression of Rexo4^{ExoCT} causes a dominant-negative effect that leads to cell

cycle arrest. Interestingly, the reverse is true as well, as overexpression of Rexo4^{NT}, which localizes to the nucleolus, but presumably does not have exonuclease activity, we see the same dominant-negative effect that arrests stops the cell cycle in its tracks. These results suggest both localization and exonuclease activity/function of Rexo4 are necessary for cell proliferation in mammalian cells. This is a departure from what is reported with the homologous REX4 in *S. cerevisiae*, as inactivation of just REX4 does not lead to any obvious growth defects or changes in pre-rRNA processing [94]. This could be contributed to mammalian mitosis being more susceptible to perturbation due to having an open mitosis or simply because yeast may have more redundant mechanisms/functional overlap for pre-rRNA processing via Rex1, Rex2, and Rex3 [92], [110]. Furthermore, other studies in ribosome biogenesis have revealed an extra step in the processing of 21S to 18S pre-rRNA not found in yeast pre-rRNA processing [103]. Any number of these reasons could explain Rexo4's elevated importance in human cell division.

Future perspectives

While we have performed preliminary characterization of Rexo4, plenty of work still remains in order to elucidate Rexo4's function. Currently, studies in our lab are ongoing to identify a Rexo4 NoLS mutant unable to localize to the nucleolus. This work entails mutating more of the positively charged lysines in the predicted NoLS to hydrophobic alanines. Afterwards, it would be interesting to reperform the overexpression experiment to see if a full-length Rexo4 construct with a nonfunctional NoLS will reproduce the dominant-negative effect seen with Rexo^{NT} and Rexo^{ExoCT} truncations. This will further confirm Rexo4 localization to the nucleolus is a requirement for cell

cycle progression. To confirm that Rexo4's exonuclease activity is also required for progression, the same experiments could be performed using a catalytically-dead construct that has critical residues for activity mutated, this can be done by identifying the highly conserved charged residues in the exonuclease domain [111], [112]. A more elegant version of this experiment would be to make siRNA-resistant versions of the aforementioned constructs and perform addback experiments, once again looking at cell proliferation over time.

These experiments address cell proliferation, but Rexo4's actual function in the mammalian cell has not yet been elucidated. To this end, total RNA-sequencing experiments are underway, in which we have performed siRNA depletion of Rexo4 in HeLa cells and extracted total RNA. We have given these total RNA samples to a collaborator for analysis via a MiniSeq™ platform and expect to observe differences in the ratios of different rRNA precursors from sample to sample. Observing which pre-rRNA species is enriched in the siRNA-treated samples would inform us where Rexo4 is implicated in ribosome biogenesis. An alternative experiment to determine this would be to purify early ribosomal complexes from Rexo4-depleted cells and perform northern blots using existing probes against ITS1 [113]. Once again, increased accumulation of a precursor rRNA would reveal which processing step Rexo4 is involved in. If neither of these protocols yield results, a less direct method is to use classic sucrose gradient and fractioning protocol to see which ribosome precursor Rexo4 associates with. These studies regarding Rexo4's function would also benefit from the use of previously described mutant-NoLS Rexo4 or the exonuclease-dead Rexo4. We would be able to

determine if overexpression or addback after endogenous depletion of these constructs would change any observed phenotypes. Addback experiments especially would confirm which processing steps require Rexo4's exonuclease activity in HeLa cells.

Currently, our proteomic analysis of Rexo4 is from a tandem-affinity experiment performed from Hek293 cells. Since then, our lab has started to utilize modern proximity-labeling methods to screen for protein-protein interactions, such as BioID2, in conjunction with our home-grown analysis and visualization program, CANVS [114]–[116] Though BioID2 is a powerful tool, TurboID is a newer version of this promiscuous biotin ligase has been developed that allows for much faster labeling . We have cloned a Rexo4 construct into a Flp-In compatible vector with a TurboID tag and have began isolating a pseudo-monoclonal stable HeLa cell line with a dox-inducible TurboID tagged-Rexo4. TurboID allows for reported biotin-labeling times of as short as 10 minutes compared to 15 to 18 hour labeling time using a BioID/BioID2 tag [117]. Since ribosomes are made constantly throughout the cell cycle (~4,000 ribosomes per minute), this type of temporal resolution may not be necessary for Rexo4 studies, but it is a nice to have, considering the time saved [118]. Overall, further proteomic studies on Rexo4 may reveal novel protein-protein interactions, through the use of TurboID, our CANVS pipeline, and any other advances in mass spectrometry detection that have occurred since the original studies were performed over a decade ago.

Materials and Methods

Cell Culture

Hek293 and HeLa cells were grown in F12:DMEM 50:50 with 10% FBS, 2mM L-glutamine and penicillin/streptomycin (Gibco) in 5% CO_2 at 37°C. The following siRNAs were used for siRNA transfections; Thermo Fisher Silencer Select: anti-Rexo4 (Cat #: 4392420 Assay IDs: s224450, s32694), anti-POLR1A (Cat # 4427037 Assay IDs: s223665, s223666). All transient transfections and siRNA transfections were carried out with Mirus TransIT-X2® (Cat# MIR6000, Fisher Scientific) according to stock protocol found in the product literature.

Generation of Rexo4 truncations and mutants

To generate Rexo4 truncation derivatives and mutants, Rexo4 in pDONR221 (Clone #: HsCD000439084, DNASU, Tempe, AZ) was used as a template. Primers were designed for the indicated truncations, amplified using Phusion polymerase and flipped into empty pDONR221 with BP Clonase (Thermofisher). The truncation-containing pDONRs were then flipped into pgLAP1 (Plasmid #: 19702, Addgene) with LR Clonase (Thermofisher) for transient transfection in HeLa cells. To generate Rexo4 NoLS mutants, appropriate primers were designed and pDONR221-Rexo4 was subjected to site-directed mutagenesis via a Agilent QuikChange Lightning kit (Cat #:210518). After sequencing verification, mutants were flipped into pgLAP1 for transient transfection.

Immunoblots

For pgLAP1 construct expression confirmation, HeLa cells were seeded at 40% confluency in 6-well plates and transfected the next day with 400ng of the indicated

pgLAP1 plasmid with Mirus TransIT-X2 transfection reagent. Cells were collected, lysed and extracts were resolved on a 4-20% SDS-PAGE gel before transferring onto a PVDF membrane. Membranes were incubated with indicated antibodies and imaged using a LI-COR Odyssey. Cell extracts were prepared as previously described (Gholkar et. al 2016).

Fixed-cell immunofluorescence microscopy

Fixed-cell immunofluorescence microscopy was performed as previously described (Garcia et. al 2021), except substituting blocking buffer with an alternate buffer comprised of: 0.2M Glycine, 2.5% FBS, and 0.1% Triton-X-100 in PBS. Cells were fixed with 4% paraformaldehyde, permeabilized with 0.1% Triton-X-100 in PBS, and costained with 0.5ug/mL Hoechst 33342 and any indicated antibodies. Imaging of cells was carried out using a Leica DMI6000 microscope (Leica DFC360 FX Camera, 6x 1.4-0.60 NA oil objective, Leica AF6000 software). Images were subjected to Leica Application Suite 3D Deconvolution Software, cropped and exported as TIFF files.

References

[1] A. M. Anger *et al.*, “Structures of the human and Drosophila 80S ribosome,” *Nature*, vol. 497, no. 7447, pp. 80–85, 2013, doi: 10.1038/nature12104.

[2] J. L. Woolford and S. J. Baserga, “Ribosome biogenesis in the yeast Saccharomyces cerevisiae,” *Genetics*, vol. 195, no. 3, pp. 643–681, 2013, doi: 10.1534/genetics.113.153197.

[3] H. Lempiäinen and D. Shore, “Growth control and ribosome biogenesis,” *Current Opinion in Cell Biology*, vol. 21, no. 6. pp. 855–863, Dec. 2009. doi: 10.1016/j.ceb.2009.09.002.

[4] S. J. Goodfellow and J. C. B. M. Zomerdijk, “Basic mechanisms in RNA polymerase I transcription of the ribosomal RNA genes,” *Subcell Biochem*, vol. 61, pp. 211–236, 2013, doi: 10.1007/978-94-007-4525-4_10.

[5] D. M. Stults, M. W. Killen, H. H. Pierce, and A. J. Pierce, “Genomic architecture and inheritance of human ribosomal RNA gene clusters,” *Genome Res*, vol. 18, no. 1, pp. 13–18, Jan. 2008, doi: 10.1101/gr.6858507.

[6] T. Kiss, “Small nucleolar RNA-guided post-transcriptional modification of cellular RNAs,” *EMBO Journal*, vol. 20, no. 14. pp. 3617–3622, Jul. 16, 2001. doi: 10.1093/emboj/20.14.3617.

[7] D. Tollervey and T. Kiss, “Function and synthesis of small nucleolar RNAs,” *Curr Opin Cell Biol*, vol. 9, pp. 337–342, 1997.

[8] T. Bratkovič and B. Rogelj, “The many faces of small nucleolar RNAs,” *Biochimica et Biophysica Acta - Gene Regulatory Mechanisms*, vol. 1839, no. 6. Elsevier B.V., pp. 438–443, 2014. doi: 10.1016/j.bbagrm.2014.04.009.

[9] K. E. Bohnsack and M. T. Bohnsack, “Uncovering the assembly pathway of human ribosomes and its emerging links to disease,” *EMBO J*, vol. 38, no. 13, Jul. 2019, doi: 10.15252/embj.2018100278.

[10] P. S. Shen *et al.*, “Rqc2p and 60S ribosomal subunits mediate mRNA-independent elongation of nascent chains,” *Science (1979)*, vol. 347, no. 6217, pp. 75–78, Jan. 2015, doi: 10.1126/science.1259724.

[11] A. Gentilella, S. C. Kozma, and G. Thomas, “A liaison between mTOR signaling, ribosome biogenesis and cancer,” *Biochimica et Biophysica Acta - Gene Regulatory Mechanisms*, vol. 1849, no. 7. Elsevier, pp. 812–820, Jul. 01, 2015. doi: 10.1016/j.bbagrm.2015.02.005.

[12] C. L. Simms, E. N. Thomas, and H. S. Zaher, “Ribosome-based quality control of mRNA and nascent peptides,” *Wiley Interdisciplinary Reviews: RNA*, vol. 8, no. 1. Blackwell Publishing Ltd, Jan. 01, 2017. doi: 10.1002/wrna.1366.

[13] C. Mayer and I. Grummt, “Ribosome biogenesis and cell growth: mTOR coordinates transcription by all three classes of nuclear RNA polymerases,” *Oncogene*, vol. 25, no. 48. pp. 6384–6391, Oct. 16, 2006. doi: 10.1038/sj.onc.1209883.

[14] R. Santoro, J. Li, and I. Grummt, “The nucleolar remodeling complex NoRC mediates heterochromatin formation and silencing of ribosomal gene transcription,” *Nat Genet*, vol. 32, no. 3, pp. 393–396, Nov. 2002, doi: 10.1038/ng1010.

[15] R. N. Laribee, A. Hosni-Ahmed, J. J. Workman, and H. Chen, “Ccr4-Not Regulates RNA Polymerase I Transcription and Couples Nutrient Signaling to the Control of Ribosomal RNA Biogenesis,” *PLoS Genet*, vol. 11, no. 3, Mar. 2015, doi: 10.1371/journal.pgen.1005113.

[16] A. Blasina, E. S. Paegle, and C. H. Mcgowan, “The Role of Inhibitory Phosphorylation of CDC2 following DNA Replication Block and Radiation-induced Damage in Human Cells,” 1997.

[17] A. van Hoof, P. Lennertz, and R. Parker, “Three conserved members of the RNase D family have unique and overlapping functions in the processing of 5S, 5.8S, U4, U5, RNase MRP and RNase P RNAs in yeast,” 2000.

[18] N. A. Eppens *et al.*, “Deletions in the S1 domain of Rrp5p cause processing at a novel site in ITS1 of yeast pre-rRNA that depends on Rex4p.”

[19] A. W. Faber, J. C. Vos, H. R. Vos, G. Ghazal, S. A. Elela, and H. A. Raué, “The RNA catabolic enzymes Rex4p, Rnt1p, and Dbr1p show genetic interaction with trans-acting factors involved in processing of ITS1 in Saccharomyces cerevisiae pre-rRNA,” *RNA*, vol. 10, no. 12, pp. 1946–1956, Dec. 2004, doi: 10.1261/rna.7155904.

[20] S. Gerstberger *et al.*, “The Conserved RNA Exonuclease Rexo5 Is Required for 3′ End Maturation of 28S rRNA, 5S rRNA, and snoRNAs,” *Cell Rep*, vol. 21, no. 3, pp. 758–772, Oct. 2017, doi: 10.1016/j.celrep.2017.09.067.

[21] J. Kwiatkowska, R. Slomski, S. Jozwiak, M. P. Short, and D. J. Kwiatkowski, “Human XPMC2H: cDNA Cloning, Mapping to 9q34, Genomic Structure, and Evaluation as TSC1,” 1997.

[22] W. Chen, C. Gao, J. Shen, L. Yao, X. Liang, and Z. Chen, “The expression and prognostic value of REXO4 in hepatocellular carcinoma,” *J Gastrointest Oncol*, vol. 12, no. 4, pp. 1704–1717, Aug. 2021, doi: 10.21037/jgo-21-98.

[23] Y. Ruan *et al.*, “REXO4 acts as a biomarker and promotes hepatocellular carcinoma progression,” *J Gastrointest Oncol*, vol. 13, no. 6, pp. 3093–3106, Dec. 2021, doi: 10.21037/jgo-21-819.

[24] M. Penzo, L. Montanaro, D. Treré, and M. Derenzini, “The ribosome biogenesis-cancer connection,” *Cells*, vol. 8, no. 1. MDPI, Jan. 01, 2019. doi: 10.3390/cells8010055.

[25] “Ribosome biogenesis in cancer new players and therapeutic avenues”.

[26] M. Pomaznoy, B. Ha, and B. Peters, “GOnet: A tool for interactive Gene Ontology analysis,” *BMC Bioinformatics*, vol. 19, no. 1, Dec. 2018, doi: 10.1186/s12859-018-2533-3.

[27] M. Miyoshi, T. Okajima, T. Matsuda, M. N. Fukuda, and D. Nadano, “Bystin in human cancer cells: Intracellular localization and function in ribosome biogenesis,” *Biochemical Journal*, vol. 404, no. 3, pp. 373–381, Jun. 2007, doi: 10.1042/BJ20061597.

[28] C. Carron, M. F. O’Donohue, V. Choesmel, M. Faubladier, and P. E. Gleizes, “Analysis of two human pre-ribosomal factors, bystin and hTsr1, highlights differences in evolution of ribosome biogenesis between yeast and mammals,” *Nucleic Acids Res*, vol. 39, no. 1, pp. 280–291, Jan. 2011, doi: 10.1093/nar/gkq734.

[29] H. Liao *et al.*, “Human NOP2/NSUN1 regulates ribosome biogenesis through non-catalytic complex formation with box C/D snoRNPs,” *Nucleic Acids Res*, Oct. 2022, doi: 10.1093/nar/gkac817.

[30] L. Stenström *et al.*, “Mapping the nucleolar proteome reveals a spatiotemporal organization related to intrinsic protein disorder,” *Mol Syst Biol*, vol. 16, no. 8, Aug. 2020, doi: 10.15252/msb.20209469.

[31] S. P. Kenney and X. J. Meng, “Identification and fine mapping of nuclear and nucleolar localization signals within the human ribosomal protein S17,” *PLoS One*, vol. 10, no. 4, Apr. 2015, doi: 10.1371/journal.pone.0124396.

[32] M. S. Scott, F. M. Boisvert, M. D. McDowall, A. I. Lamond, and G. J. Barton, “Characterization and prediction of protein nucleolar localization sequences,” *Nucleic Acids Res*, vol. 38, no. 21, pp. 7388–7399, Nov. 2010, doi: 10.1093/nar/gkq653.

[33] A. Lerch-Gaggl, J. Haque, J. Li, G. Ning, P. Traktman, and S. A. Duncan, “Pescadillo is essential for nucleolar assembly, ribosome biogenesis, and mammalian cell proliferation,” *Journal of Biological Chemistry*, vol. 277, no. 47, pp. 45347–45355, Nov. 2002, doi: 10.1074/jbc.M208338200.

[34] C. D. Castle, E. K. Cassimere, J. Lee, and C. Denicourt, “Las1L Is a Nucleolar Protein Required for Cell Proliferation and Ribosome Biogenesis,” *Mol Cell Biol*, vol. 30, no. 18, pp. 4404–4414, Sep. 2010, doi: 10.1128/mcb.00358-10.

[35] B. Boettcher and Y. Barral, “The cell biology of open and closed mitosis,” *Nucleus (United States)*, vol. 4, no. 3, pp. 160–165, 2013, doi: 10.4161/nucl.24676.

[36] A. Barbas, R. G. Matos, M. Amblar, E. López-Viñas, P. Gomez-Puertas, and C. M. Arraiano, “Determination of key residues for catalysis and RNA cleavage specificity. One mutation turns RNase II Into a ‘super-enzyme,’” *Journal of Biological Chemistry*, vol. 284, no. 31, pp. 20486–20498, Jul. 2009, doi: 10.1074/jbc.M109.020693.

[37] M. J. Longley, P. A. Ropp, S. E. Lim, and W. C. Copeland, “Characterization of the Native and Recombinant Catalytic Subunit of Human DNA Polymerase γ: Identification of Residues Critical for Exonuclease Activity and Dideoxynucleotide Sensitivity,” 1998. [Online]. Available: https://pubs.acs.org/sharingguidelines

[38] B. Nieto *et al.*, “Efficient fractionation and analysis of ribosome assembly intermediates in human cells,” *RNA Biol*, vol. 18, no. S1, pp. 182–197, 2021, doi: 10.1080/15476286.2021.1965754.

[39] D. I. Kim *et al.*, “An improved smaller biotin ligase for BioID proximity labeling,” *Mol Biol Cell*, vol. 27, no. 8, pp. 1188–1196, Apr. 2016, doi: 10.1091/mbc.E15-12-0844.

[40] E. F. Velasquez, Y. A. Garcia, I. Ramirez, A. A. Gholkar, and J. Z. Torres, “CANVS: an easy-to-use application for the analysis and visualization of mass spectrometry- based protein-protein interaction/association data,” *Mol Biol Cell*, vol. 32, no. 21, Nov. 2021, doi: 10.1091/mbc.E21-05-0257.

[41] K. J. Roux, D. I. Kim, B. Burke, and D. G. May, “BioID: A Screen for Protein-Protein Interactions,” *Curr Protoc Protein Sci*, vol. 91, no. 1, pp. 19.23.1-19.23.15, Jan. 2018, doi: 10.1002/cpps.51.

[42] D. G. May, K. L. Scott, A. R. Campos, and K. J. Roux, “Comparative Application of BioID and TurboID for Protein-Proximity Biotinylation,” *Cells*, vol. 9, no. 5, Apr. 2020, doi: 10.3390/cells9051070.

[43] J. D. Lewis and D. Tollervey, “Like Attracts Like: Getting RNA Processing Together in the Nucleus.” [Online]. Available: https://www.science.org

Figures

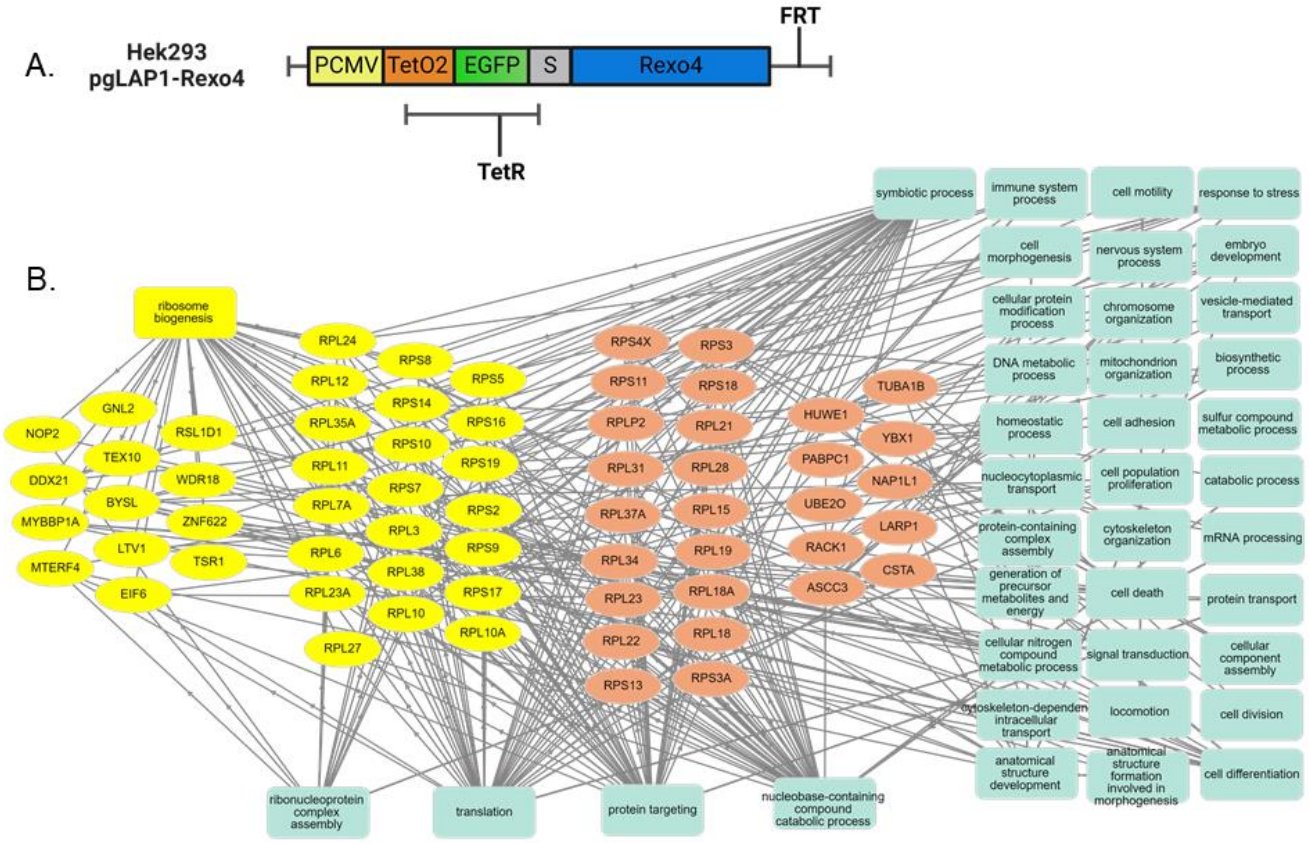

Figure 1. (A) Schematic of LAP-tagged Rexo4 expressed in Hek293 FLP-In TRex cells. (B) GOnet analysis of previous Rexo4 LAP-tag purification from Hek293 cells. Protein hits were organized by function, RPLs and RPSs grouped together. Proteins involved in ribosome biogenesis are highlighted in yellow. Proteins without associated pathways were excluded for simplicity.

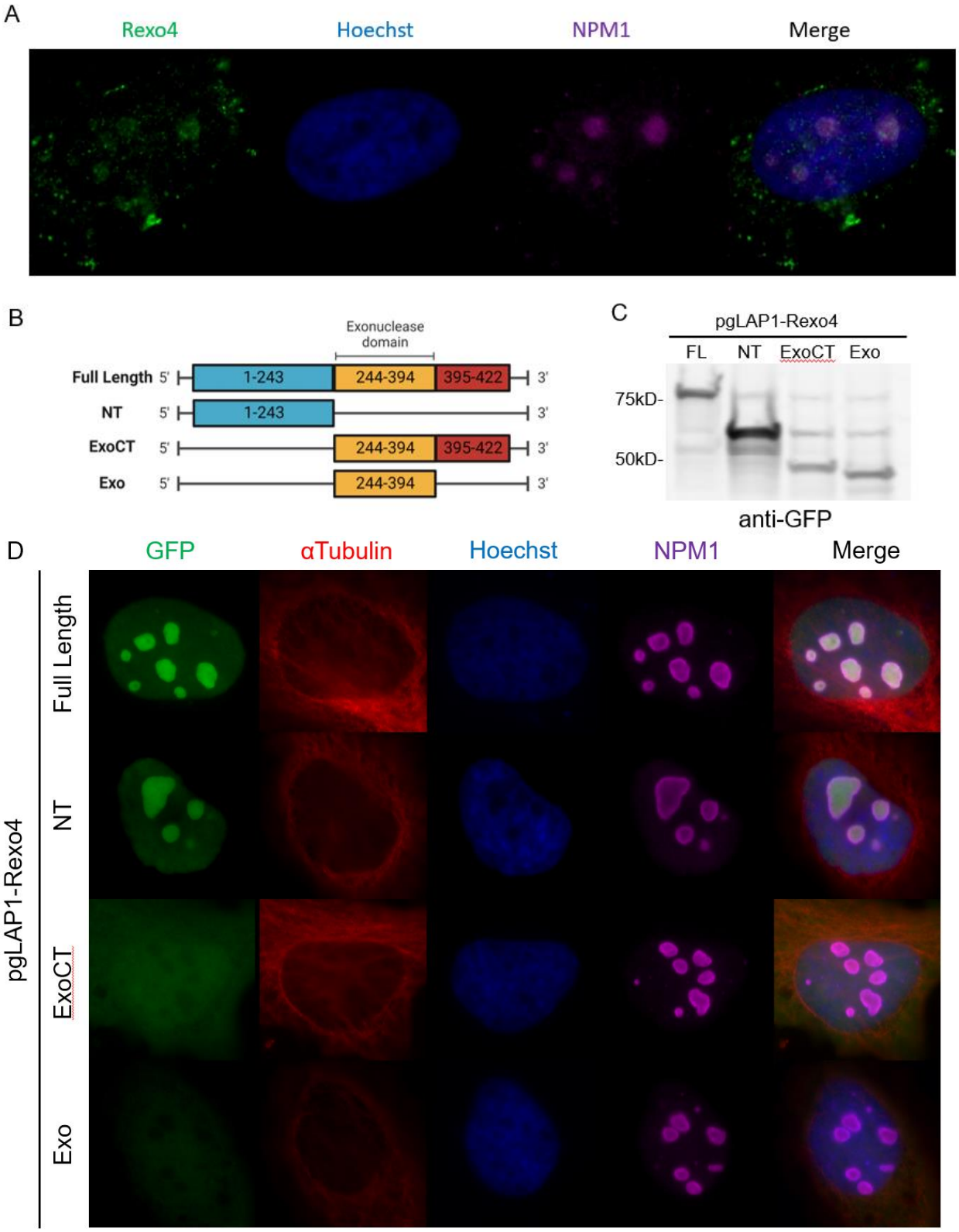
A
Rexo4
Hoechst
NPM1
Merge
B
Exonuclease domain
Full Length 5' 1-243 244-394 395-422 3'
NT 5' 1-243 3'
ExoCT 5' 244-394 395-422 3'
Exo 5' 244-394 3'
C
pgLAP1-Rexo4
FL NT ExoCT Exo
75kD-
50kD-
anti-GFP
D
GFP
αTubulin
Hoechst
NPM1
Merge
pgLAP1-Rexo4
Full Length
NT
ExoCT
Exo

Figure 2. Rexo4 localization during interphase. (A) HeLa cells were fixed and stained with Hoechst 33342 DNA dye, anti-alpha-Tubulin, anti-NPM1 and anti-Rexo4. These cells were then imaged by IF microscopy to show Rexo4's colocalization with nucleolar marker NPM1 during interphase. (B) Schematic of Rexo4 truncation mutants used to analyze putative NoLSs in Rexo4. These truncation mutants were cloned into pgLAP1 vector in order to determine which regions are required for Rexo4 nucleolar localization. (C) Expression test of pgLAP1-Rexo4 constructs. Each pgLAP1-Rexo4 construct was transiently transfected in Hela cells for 20 hours before cells were collected, lysed and prepared for immunoblot analysis. Blot was stained with anti-EGFP antibody to confirm presence of exogenous GFP-tagged Rexo4. (D) HeLa cells were transfected with each pgLAP1-Rexo4 construct, fixed 20 hours post-transfection, then imaged by IF microscopy. Cells were stained with anti-EGFP, anti-alpha-Tubulin, Hoechst 33342 DNA stain, and NPM1 antibodies.

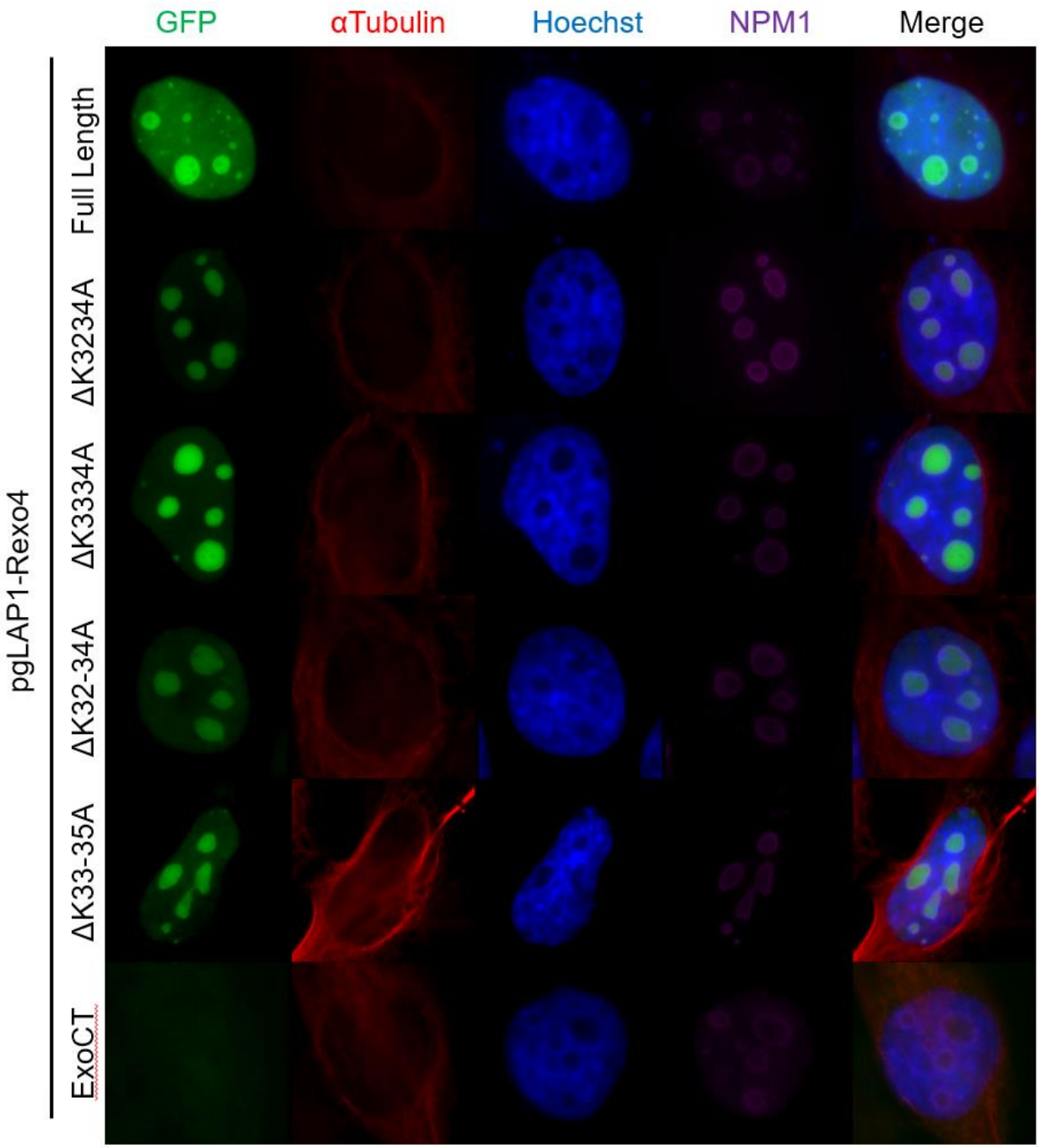
GFP
αTubulin
Hoechst
NPM1
Merge
pgLAP1-Rexo4
Full Length
ΔK3234A
ΔK3334A
ΔK32-34A
ΔK33-35A
ExoCT

Figure 3. Rexo4 NoLS Mutant Localization. (A) HeLa cells were transiently transfected with pgLAP1-Rexo4 mutants and fixed 20 hours post-transfection. Coverslips were stained with Hoechst 33342 DNA dye, anti-alpha-Tubulin, anti-NPM1 and anti-EGFP. Rexo4^{FL} was used a positive control for localization and Rexo4^{ExoCT} was used as a negative control for nucleolar localization. Rexo4 mutant constructs had either two or three lysines mutated to alanines in Rexo4's putative NoLS.

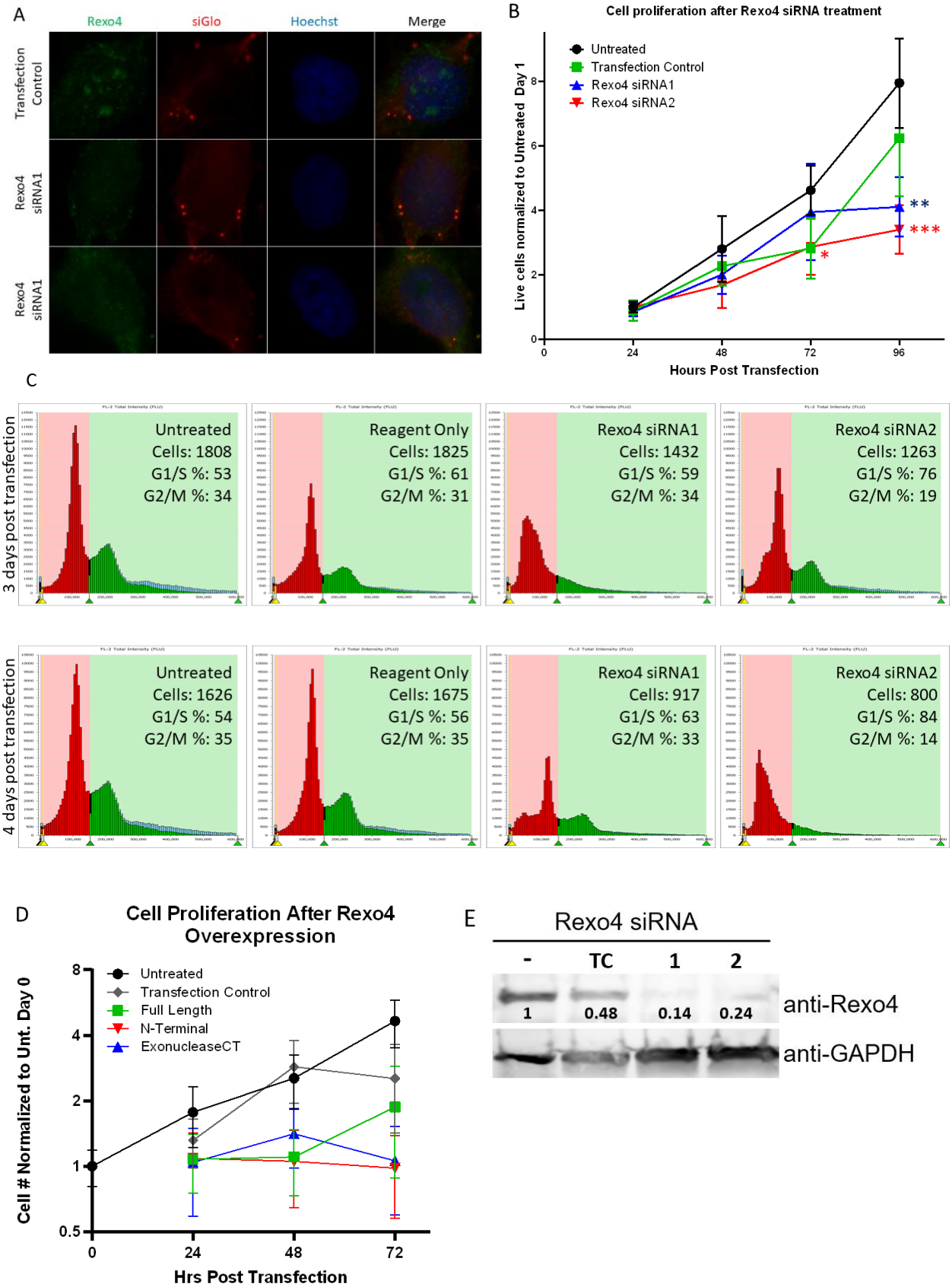
A
Rexo4
siGlo
Hoechst
Merge
Transfection Control
Rexo4 siRNA1
Rexo4 siRNA1
B
Cell proliferation after Rexo4 siRNA treatment
Untreated
Transfection Control
Rexo4 siRNA1
Rexo4 siRNA2
Live cells normalized to Untreated Day 1
Hours Post Transfection
C
3 days post transfection
Untreated
Cells: 1808
G1/S %: 53
G2/M %: 34
Reagent Only
Cells: 1825
G1/S %: 61
G2/M %: 31
Rexo4 siRNA1
Cells: 1432
G1/S %: 59
G2/M %: 34
Rexo4 siRNA2
Cells: 1263
G1/S %: 76
G2/M %: 19
4 days post transfection
Untreated
Cells: 1626
G1/S %: 54
G2/M %: 35
Reagent Only
Cells: 1675
G1/S %: 56
G2/M %: 35
Rexo4 siRNA1
Cells: 917
G1/S %: 63
G2/M %: 33
Rexo4 siRNA2
Cells: 800
G1/S %: 84
G2/M %: 14
D
Cell Proliferation After Rexo4 Overexpression
Untreated
Transfection Control
Full Length
N-Terminal
ExonucleaseCT
Cell # Normalized to Unt. Day 0
Hrs Post Transfection
E
Rexo4 siRNA
-
TC
1
2
1
0.48
0.14
0.24
anti-Rexo4
anti-GAPDH

Figure 4 Rexo4 depletion by siRNA leads to cell cycle arrest. (A) HeLa cells were treated with siRNA against Rexo4, fixed 72 hours post transfection and imaged by IF microscopy. Cells were stained with anti-Rexo4, anti-alpha-Tubulin, and Hoechst 33342 DNA stain. Cells were also co-transfected with siGlo to differentiate transfected vs. non-transfected cells. (B) HeLa cells were seeded into 6-well plates and either treated with siRNAs against Rexo4, transfection reagent alone or untreated. Each well was collected and counted every 24 hours for 4 days. Data represents the average cell count from 2 duplicate wells for each condition over 3 runs. Live cell counts were normalized to the cell counts for the untreated 24-hour post-transfection time point. Error bars represent standard deviation. * indicates p-value<0.01, ** indicates p-value<0.005, and *** indicates p-value<<0.0001. (C) Scanning cytometry histograms from Rexo4 cell cycle experiments. Y-axis represents cell count and X-axis represents fluorescence intensity of Vybrant DyeCycle green stain. (D) HeLa cells were seeded into 12-well plates and transfected with various pgLAP1-Rexo4 truncation mutants. Wells were collected and counted every 24 hours for 3 days. Data represents average cell count from 3 duplicate wells from 3 runs. (E) HeLa cells were treated with siRNA against Rexo4, transfection reagent alone or untreated for 3 days. Cell extracts were analyzed via immunoblot after 3 days of treatment. Membrane was incubated with antibodies against Rexo4 or GAPDH. All band intensities were normalized to untreated sample.

Supplemental Material

Sup. Figure 1

Rexo4 NoLS predictions by NoD: Nucleolar localization sequence Detector

A NoLS prediction for wild-type Rexo4

3 NoLSs are predicted in this protein:

PVAKPGPVKTLTRKKNKKKKRFWKSKAREVSKKPASGP (between positions 16 and 53)

SQMGSKKKPKIIQQNKKETSP (between positions 92 and 112)

FLDHPKKKIRDTQKYKPFKSQVK (between positions 336 and 358)

Position in full-length protein (NoLSs shown in red):

MGKAKVPASKRAPSSPVAKPGPVKTLTRKKNKKKKRFWKSKAREVSKKPASGPGAVVRPP
KAPEDFSQNWKALQEWLLKQKSQAPEKPLVISQMGSKKKPKIIQQNKKETSPQVKGEEMP
AGKDQEASRGSVPSGSKMDRRAPVPRTKASGTEHNKKGTKERTNGDIVPERGDIEHKKRK
AKEAAPAPPTEEDIWFDDVDPADIEAAIGPEAAKIARKQLGQSEGSVSLSLVKEQAFGGL
TRALALDCEMVGVGPKGEESMAARVSIVNQYGKCVYDKYVKPTEPVTDYRTAVSGIRPEN
LKQGEELEVVQKEVAEMLKGRILVGHALHNDLKVLFLDHPKKKIRDTQKYKPFKSQVKSG
RPSLRLLSEKILGLQVQQAEHCSIQDAQAAMRLYVMVKKEWESMARDRRPLLTAPDHCSD
DA

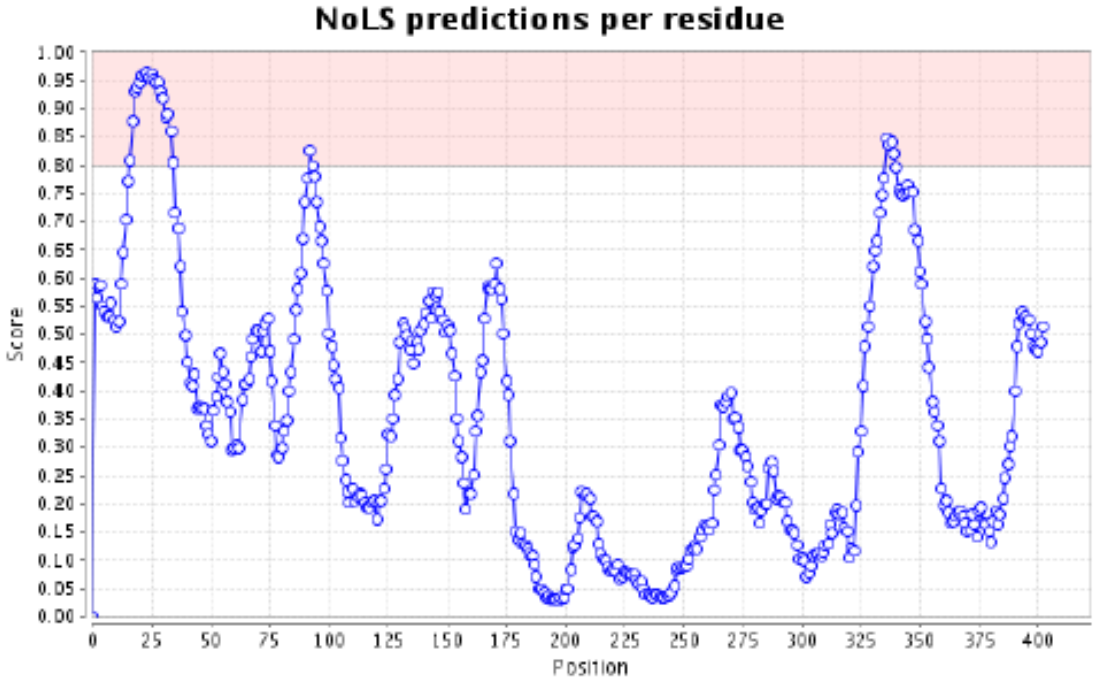

Predicative scores in graph show likelihood that a predicted sequence in protein is a NoLS. Sequences with scores above 0.80 are most likely NoLS.

B NoLS prediction for 2 of 3 mutated lysines

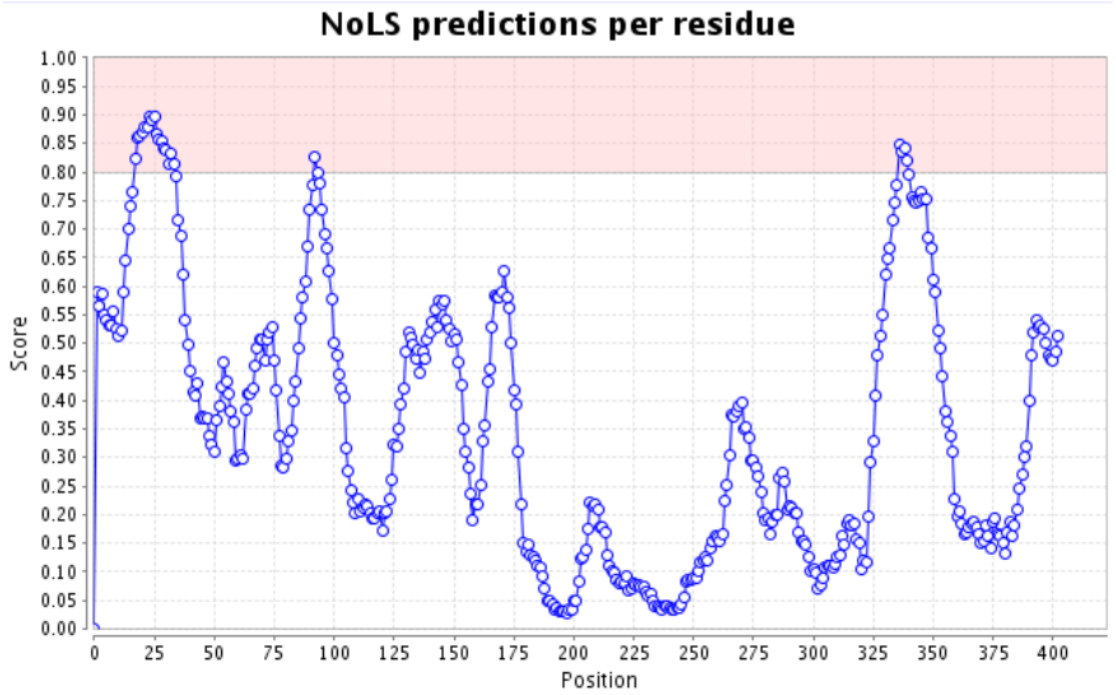

C NoLS prediction for 3 of 4 mutated lysines.

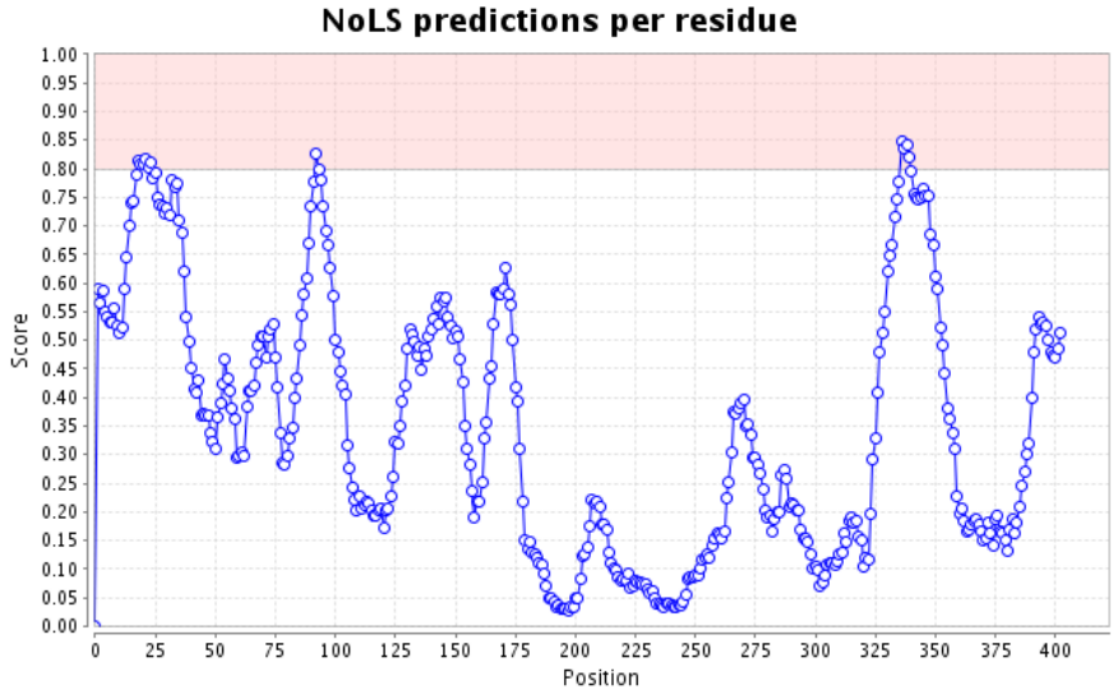

Sup. Table 1 Raw MS/MS Data from pgLAP1-Rexo4 purification, with spectral counts

Peptide Spectra Count		Fxn										
Description	Reference	01	02	03	04	05	06	07	08	09	10	Total
40S ribosomal protein S24.	sp|p62847|rs24_human								6	6	2	14
40S ribosomal protein S26.	sp|p62854|rs26_human								7	7	3	17
40S ribosomal protein S27-like protein.	sp|q71um5|rs27l_human									3	2	5
40S ribosomal protein S29.	sp|p62273|rs29_human							1	3	2	4	10
40S ribosomal protein S3.	sp|p23396|rs3_human						4	20	48	16	9	97
40S ribosomal protein S30.	sp|p62861|rs30_human							1	3	5	2	11
40S ribosomal protein S3a.	sp|p61247|rs3a_human					2	1	17	48	17	3	88
40S ribosomal protein S4, X isoform (Single copy abundant mRNA protein) (SCR10).	sp|p62701|rs4x_human						1	6	38	26	9	80
40S ribosomal protein S5.	sp|p46782|rs5_human								7	10	5	22
40S ribosomal protein S7.	sp|p62081|rs7_human							1	11	12	7	31
40S ribosomal protein S8.	sp|p62241|rs8_human			2	1	1	3	7	14	23	10	61
40S ribosomal protein S9.	sp|p46781|rs9_human							1	15	21	7	44
60S acidic ribosomal protein P1.	sp|p05386|rla1_human								2	1		3
60S acidic ribosomal protein P2 (Renal carcinoma antigen NY-REN-44).	sp|p05387|rla2_human			1		2	3	5	25	23	8	67
60S ribosomal protein L10 (QM protein) (Tumor suppressor QM) (Laminin receptor homolog).	sp|p27635|rl10_human			1		1	1	5	12	28	5	53
60S ribosomal protein L10a (CSA-19) (Protein NEDD6) (Neural precursor cell expressed developmentally d	sp|p62906|rl10a_human						3	8	21	28	17	77
60S ribosomal protein L11 (CLL-associated antigen KW-12).	sp|p62913|rl11_human			2	2	1	1	3	5	11	7	32
60S ribosomal protein L12.	sp|p30050|rl12_human		1	2	1	2	3	5	11	18	8	51
60S ribosomal protein L15.	sp|p61313|rl15_human	1	1	1		1	1	10	20	24	11	70
60S ribosomal protein L18.	sp|q07020|rl18_human			1			2	3	8	13	7	34
60S ribosomal protein L18a.	sp|q02543|rl18a_human							2	11	20	10	43
60S ribosomal protein L19.	sp|p84098|rl19_human							3	15	20	7	45
60S ribosomal protein L21.	sp|p46778|rl21_human					1		4	17	23	13	58
60S ribosomal protein L22 (Epstein-Barr virus small RNA-associated protein) (EBER-associated protein) (E	sp|p35268|rl22_human		1	1			1	2	16	17	13	51
60S ribosomal protein L23 (Ribosomal protein L17).	sp|p62829|rl23_human		1	1			1	4	19	23	10	59
60S ribosomal protein L23a.	sp|p62750|rl23a_human						1	4	14	20	9	48
60S ribosomal protein L24 (Ribosomal protein L30).	sp|p83731|rl24_human			1			1	4	19	21	12	58
60S ribosomal protein L26.	sp|p61254|rl26_human						2	4	17	42	24	89
60S ribosomal protein L26-like 1.	sp|q9unx3|rl26l_human									1		1
60S ribosomal protein L27.	sp|p61353|rl27_human			1				3	15	12	10	41
60S ribosomal protein L28.	sp|p46779|rl28_human							1	7	17	7	32
60S ribosomal protein L3 (HIV-1 TAR RNA-binding protein B) (TARBP-B).	sp|p39023|rl3_human				3	8	8	94	2			115
60S ribosomal protein L31.	sp|p62899|rl31_human		1						6	15	8	30
60S ribosomal protein L34.	sp|p49207|rl34_human							1	2	9	6	18
60S ribosomal protein L35a.	sp|p18077|rl35a_human			1	1	1	1	4	9	14	14	45
60S ribosomal protein L36.	sp|q9y3u8|rl36_human								5	8	4	17
60S ribosomal protein L36a (60S ribosomal protein L44) (Cell migration-inducing gene 6 protein).	sp|p83881|rl36a_human							1	5	6	3	15
60S ribosomal protein L37a.	sp|p61513|rl37a_human								4	9	3	16
60S ribosomal protein L38.	sp|p63173|rl38_human								8	14	6	28
60S ribosomal protein L39.	sp|p62891|rl39_human										1	1
60S ribosomal protein L6 (TAX-responsive enhancer element-binding protein 107) (TAXREB107) (Neoplas	sp|q02878|rl6_human						4	27	28	1		60
60S ribosomal protein L7a (Surfeit locus protein 3) (PLA-X polypeptide).	sp|p62424|rl7a_human				1		3	15	38	21	12	90
60S ribosomal protein L9.	sp|p32969|rl9_human								8	6	4	18
60S ribosome subunit biogenesis protein NIP7 homolog (KD93).	sp|q9y221|nip7_human									1		1
78 kDa glucose-regulated protein precursor (GRP 78) (Heat shock 70 kDa protein 5) (Immunoglobulin hea	sp|p11021|grp78_human			4	11	59	32					106
Activating signal cointegrator 1 (ASC-1) (Thyroid receptor-interacting protein 4) (TRIP-4).	sp|q15650|trip4_human						4					4
Activating signal cointegrator 1 complex subunit 2 (ASC-1 complex subunit p100) (Trip4 complex subunit	sp|q9h1i8|ascc2_human				1	4						5
Activating signal cointegrator 1 complex subunit 3 (EC 3.6.1.-) (ASC-1 complex subunit p200) (Trip4 comp	sp|q8n3c0|helc1_human			53								53
A-kinase anchor protein 13 (AKAP 13) (Protein kinase A-anchoring protein 13) (Breast cancer nuclear rece	sp|q12802|akp13_human	1			1							2
A-kinase anchor protein 8 (A-kinase anchor protein 95 kDa) (AKAP 95).	sp|o43823|akap8_human					3						3

Peptide Spectra Count		Fxn										
Description	Reference	01	02	03	04	05	06	07	08	09	10	Total
(X99140) type II intermediate filament of hair keratin [Homo sapiens]	uc|1903218|gnl|pid|e255345				1							1
REV Armadillo repeat-containing protein 5.	r-sp|q96c12|armc5_human	1										1
REV Bardet-Biedl syndrome 10 protein.	r-sp|q8tam1|bbs10_human								1	1		2
REV Brefeldin A-inhibited guanine nucleotide-exchange protein 1 (Brefeldin A-inhibited GEP 1) (p200 A	r-sp|q9y6d6|big1_human	1										1
REV Centrosome-associated protein CEP250 (Centrosomal protein 2) (Centrosomal Nek2-associated pr	r-sp|q9bv73|cp250_human						1					1
REV Dermatan-sulfate epimerase-like protein precursor.	r-sp|q8izu8|dsel_human			1								1
REV Dynamin-like protein DYNIV-11 variant (Fragment).	r-sp|q59gn9|q59gn9_human								1			1
REV Endonuclease domain-containing 1 protein precursor (EC 3.1.30.-).	r-sp|o94919|endd1_human			1								1
REV Euchromatic histone-lysine N-methyltransferase 1.	r-sp|q5vt56|q5vt56_human					1				1		2
REV Extracellular matrix protein FRAS1 precursor.	r-sp|q86xx4|fras1_human						1					1
REV FACT complex subunit SPT16 (Facilitates chromatin transcription complex subunit SPT16) (hSPT16	r-sp|q9y5b9|spt16_human										1	1
REV Histidyl-tRNA synthetase, cytoplasmic (EC 6.1.1.21) (Histidine--tRNA ligase) (HisRS).	r-sp|p12081|syhc_human									1	1	2
REV Homeobox even-skipped homolog protein 1 (EVX-1).	r-sp|p49640|evx1_human						1					1
REV Protein transport protein Sec23A (SEC23-related protein A).	r-sp|q15436|sc23a_human								1			1
REV Serologically defined colon cancer antigen 8 (Antigen NY-CO-8) (Centrosomal colon cancer autoan	r-sp|q86sq7|sdcg8_human			1								1
REV Synaptojanin-2 (EC 3.1.3.36) (Synaptic inositol-1,4,5-trisphosphate 5- phosphatase 2).	r-sp|o15056|synj2_human							1				1
REV T-complex protein 1 subunit epsilon (TCP-1-epsilon) (CCT-epsilon).	r-sp|p48643|tcpe_human								1			1
REV Tetratricopeptide repeat protein 29 (TPR repeat protein 29) (Testis development protein NYD-SP1	r-sp|q8na56|ttc29_human							1	1			2
REV TFIIH basal transcription factor complex helicase subunit (EC 3.6.1.-) (DNA-repair protein complem	r-sp|p18074|ercc2_human									1		1
REV Thyroid receptor-interacting protein 11 (TRIP-11) (Golgi-associated microtubule-binding protein 2	r-sp|q15643|tripb_human									1		1
REV Tubby-related protein 1 (Tubby-like protein 1).	r-sp|o00294|tulp1_human					1						1
REV Tudor domain-containing protein 3.	r-sp|q9h7e2|tdrd3_human							2	1			3
REV Type-2 angiotensin II receptor (AT2).	r-sp|p50052|agtr2_human			1								1
REV Tyrosine-protein phosphatase non-receptor type 7 (EC 3.1.3.48) (Protein-tyrosine phosphatase LC	r-sp|p35236|ptn7_human								1	1		2
REV Uncharacterized protein C3orf63 (Retinoblastoma-associated protein RAP140) (CTCL tumor antige	r-sp|q9uk61|cc063_human								2	1		3
REV Uncharacterized protein C8orf45.	r-sp|q4g0z9|ch045_human										1	1
REV Uncharacterized protein FAM22B.	r-sp|a6ncl3|a6ncl3_human							1				1
REV Uncharacterized protein HEPHL1 (Fragment).	r-sp|a6nd83|a6nd83_human							1				1
REV Zinc finger protein 469.	r-sp|q96jg9|zn469_human					1						1
14-3-3 protein epsilon (14-3-3E).	sp|p62258|1433e_human								1			1
26S proteasome non-ATPase regulatory subunit 3 (26S proteasome regulatory subunit S3) (Proteasome s	sp|o43242|psmd3_human						2					2
28S ribosomal protein S18b, mitochondrial precursor (MRP-S18-b) (Mrps18b) (MRP-S18-2).	sp|q9y676|rt18b_human								1			1
28S ribosomal protein S26, mitochondrial precursor (MRP-S26) (MRP- S13).	sp|q9byn8|rt26_human								1	3		4
28S ribosomal protein S31, mitochondrial precursor (S31mt) (MRP-S31) (Imogen 38).	sp|q92665|rt31_human							4				4
28S ribosomal protein S7, mitochondrial precursor (S7mt) (MRP-S7) (bMRP27a) (bMRP-27a).	sp|q9y2r9|rt07_human								1	1		2
28S ribosomal protein S9, mitochondrial precursor (S9mt) (MRP-S9).	sp|p82933|rt09_human							4				4
39S ribosomal protein L38, mitochondrial precursor (L38mt) (MRP-L38).	sp|q96dv4|rm38_human							1				1
40S ribosomal protein S10.	sp|p46783|rs10_human								10	11	6	27
40S ribosomal protein S11.	sp|p62280|rs11_human							3	12	22	14	51
40S ribosomal protein S12.	sp|a6ncp0|a6ncp0_human								10	8	3	21
40S ribosomal protein S13.	sp|p62277|rs13_human								6	10	6	22
40S ribosomal protein S14.	sp|p62263|rs14_human							1	14	26	7	48
40S ribosomal protein S15a.	sp|p62244|rs15a_human							1	8	6	6	21
40S ribosomal protein S16.	sp|p62249|rs16_human			1		1	3	6	21	21	13	66
40S ribosomal protein S17.	sp|p08708|rs17_human								5	7	6	18
40S ribosomal protein S18 (Ke-3) (Ke3).	sp|p62269|rs18_human						1	2	12	24	15	54
40S ribosomal protein S19.	sp|p39019|rs19_human			1				3	9	18	13	44
40S ribosomal protein S2 (S4) (LLRep3 protein).	sp|p15880|rs2_human						3	13	19	7	3	45
40S ribosomal protein S20.	sp|p60866|rs20_human							2	2	7	6	17
40S ribosomal protein S21.	sp|p63220|rs21_human							1	10	12	4	27

Peptide Spectra Count		Fxn										
Description	Reference	01	02	03	04	05	06	07	08	09	10	Total
A-kinase anchor protein 8-like (AKAP8-like protein) (Neighbor of A- kinase-anchoring protein 95) (Neighb	sp|q9ulx6|akp8l_human					6						6
Alpha-S1-casein precursor - Bos taurus	uc|p02662|casa1_bovin				5	2						7
Alpha-S2-casein precursor - Bos taurus	uc|p02663|casa2_bovin				5							5
Annexin A2 (Annexin-2) (Annexin II) (Lipocortin II) (Calpactin I heavy chain) (Chromobindin-8) (p36) (Prote	sp|p07355|anxa2_human					1						1
Apoptosis-inducing factor, mitochondrion-associated, 1 (Programmed cell death 8 (Apoptosis-inducing fa	sp|a4qpb4|a4qpb4_human						4					4
ATP-dependent RNA helicase DDX54 (EC 3.6.1.-) (DEAD box protein 54) (ATP-dependent RNA helicase DP	sp|q8tdd1|ddx54_human					1						1
Beta-casein precursor - Bos taurus	uc|p02666|casb_bovin				1							1
Brefeldin A-inhibited guanine nucleotide-exchange protein 1 variant (Fragment).	sp|q59fy5|q59fy5_human			2								2
Brefeldin A-inhibited guanine nucleotide-exchange protein 2 (Brefeldin A-inhibited GEP 2).	sp|q9y6d5|big2_human			1								1
Bystin.	sp|q13895|byst_human						15	50				65
CAD protein [Includes: Glutamine-dependent carbamoyl-phosphate synthase (EC 6.3.5.5); Aspartate carb	sp|p27708|pyr1_human			27								27
Calmodulin-like skin protein variant (Fragment).	sp|q53h37|q53h37_human				3							3
Calumenin precursor (Crocalbin) (IEF SSP 9302).	sp|o43852|calu_human							3				3
Casein kinase II subunit alpha (EC 2.7.11.1) (CK II).	sp|p68400|csk21_human							1				1
Caspase-14 precursor (EC 3.4.22.-) (CASP-14) [Contains: Caspase-14 subunit p19; Caspase-14 subunit p10	sp|p31944|caspe_human				4							4
Cathepsin B precursor (EC 3.4.22.1) (Cathepsin B1) (APP secretase) (APPS) [Contains: Cathepsin B light ch	sp|p07858|catb_human				1							1
CDNA FLJ38626 fis, clone HEART2009599.	sp|q8n901|q8n901_human									1		1
CDNA FLJ43954 fis, clone TESTI4015600.	sp|q6zu73|q6zu73_human									1		1
cDNA FLJ75008, highly similar to Homo sapiens proline-, glutamic acid- , leucine-rich protein 1 (PELP1), m	sp|a8k548|a8k548_human		4	23	27							54
cDNA FLJ75127, highly similar to Homo sapiens heat shock 70kDa protein 1A, mRNA (Heat shock 70kDa p	sp|a8k5i0|a8k5i0_human			2	5	40	49	1	1			98
cDNA FLJ75154, highly similar to Homo sapiens heterogeneous nuclear ribonucleoprotein C (C1/C2), mR	sp|a8k9a4|a8k9a4_human							7	1			8
cDNA FLJ75163, highly similar to Homo sapiens heterogeneous nuclear ribonucleoprotein U-like 1 (HNRP	sp|a8k3w4|a8k3w4_human				2	13						15
cDNA FLJ75260, highly similar to H.sapiens p53-associated gene.	sp|a8k2s6|a8k2s6_human		1	5	9	28	18	7				68
cDNA FLJ75307 (KIAA0020).	sp|a8k804|a8k804_human						3					3
cDNA FLJ75549, highly similar to Homo sapiens ribosomal protein, large, P0 (RPLP0), transcript variant 1,	sp|a8k4z4|a8k4z4_human		1	1	1	1	5	28	31	4	1	73
cDNA FLJ75551, highly similar to Homo sapiens ribosomal protein L13a (RPL13A), mRNA (Ribosomal prot	sp|a8k505|a8k505_human			1				5	21	29	11	67
cDNA FLJ75605, highly similar to Homo sapiens CGI-115 protein (CGI- 115), mRNA.	sp|a8k201|a8k201_human							4	1			5
cDNA FLJ75749, highly similar to Homo sapiens MKI67 (FHA domain) interacting nucleolar phosphoprotei	sp|a8k788|a8k788_human								5			5
cDNA FLJ75796, highly similar to Homo sapiens RNA binding motif protein 34 (RBM34), mRNA.	sp|a8k8j7|a8k8j7_human						3	8				11
cDNA FLJ75823, highly similar to Homo sapiens dimethyladenosine transferase (HSA9761), mRNA.	sp|a8k9k8|a8k9k8_human								3			3
cDNA FLJ75871, highly similar to Homo sapiens staufen, RNA binding protein (STAU), transcript variant 1	sp|a8k622|a8k622_human						5	11				16
cDNA FLJ75925, highly similar to Homo sapiens keratin 16 (focal non- epidermolytic palmoplantar kerato	sp|a8k488|a8k488_human			8	17	33		1				59
cDNA FLJ76122, highly similar to Homo sapiens nucleophosmin (nucleolar phosphoprotein B23, numatrin	sp|a8k3n7|a8k3n7_human		1	8	3	1		4	1			18
cDNA FLJ76205, highly similar to Homo sapiens ribosomal protein L8 (RPL8), transcript variant 1,mRNA (R	sp|a8k094|a8k094_human			1	1	2	2	13	29	13	9	70
cDNA FLJ76395, highly similar to Homo sapiens ribosomal protein L35 (RPL35), mRNA.	sp|a8k4v7|a8k4v7_human						1	6	10	16	9	42
cDNA FLJ76585, highly similar to Homo sapiens brix domain containing 2 (BXDC2), mRNA (Brix domain co	sp|a8k0p5|a8k0p5_human							15	1			16
cDNA FLJ76726, highly similar to Homo sapiens eukaryotic translation elongation factor 1 alpha 1 (EEF1A	sp|a8k9c4|a8k9c4_human							2				2
cDNA FLJ76907, highly similar to Homo sapiens cyclin-dependent kinase 2 (CDK2), transcript variant 1, mI	sp|a8k7c6|a8k7c6_human								2			2
cDNA FLJ76924, highly similar to Homo sapiens brix domain containing 1 (BXDC1), mRNA.	sp|a8k800|a8k800_human							2	5			7
cDNA FLJ77328, highly similar to Homo sapiens NOL1/NOP2/Sun domain family, member 4 (NSUN4), mR	sp|a8k6s6|a8k6s6_human			5	4	1	5	29	28	2	1	75
cDNA FLJ77548, highly similar to Homo sapiens bin3, bicoid-interacting 3, homolog (Drosophila) (BCDIN3	sp|a8k5q1|a8k5q1_human					2						2
cDNA FLJ77754, highly similar to Homo sapiens keratin 8 (KRT8), mRNA.	sp|a8k4h3|a8k4h3_human						3					3
cDNA FLJ77849, highly similar to Homo sapiens keratin, hair, basic, 6 (monilethrix) (KRTHB6), mRNA.	sp|a8k872|a8k872_human				2							2
cDNA FLJ77921, highly similar to Homo sapiens ribosomal protein S23 (RPS23), mRNA (Ribosomal protein	sp|a8k517|a8k517_human							2	5	10	6	23
cDNA FLJ78110 (Putatative 28 kDa protein).	sp|a8k6q0|a8k6q0_human								12	7		19
cDNA FLJ78387.	sp|a8k008|a8k008_human			2	4	1	1	2				10
cDNA FLJ78483, highly similar to Homo sapiens elongation factor Tu GTP binding domain containing 2 (EF	sp|a8kap3|a8kap3_human				2							2
cDNA FLJ78488, highly similar to Homo sapiens ribosomal protein L7 (RPL7), mRNA.	sp|a8k504|a8k504_human			1		1	2	14	43	29	18	108
cDNA FLJ78508.	sp|a8k7c2|a8k7c2_human							5				5
cDNA FLJ78590 (Ribosomal protein L13, isoform CRA_a).	sp|a8k4c8|a8k4c8_human							9	33	29	18	89

Peptide Spectra Count		Fxn										
Description	Reference	01	02	03	04	05	06	07	08	09	10	Total
cDNA FLJ78645, highly similar to Homo sapiens DEAH (Asp-Glu-Ala-His) box polypeptide 30 (DHX30), tran	sp|a8k5f1|a8k5f1_human				16							16
cDNA FLJ78653, highly similar to Homo sapiens processing of 1, ribonuclease P/MRP subunit (POP1), mR	sp|a8k5w9|a8k5w9_human				6							6
CDW4/GRWD1 (Glutamate-rich WD repeat containing 1).	sp|a0mnn5|a0mnn5_human						3					3
Cell growth-regulating nucleolar protein.	sp|q9nx58|lyar_human						2	22	1			25
Centrosomal protein 170kDa.	sp|a6h8x9|a6h8x9_human			3								3
Centrosomal protein of 57 kDa (Cep57 protein) (Testis-specific protein 57) (Translokin) (FGF2-interacting	sp|q86xr8|cep57_human				1							1
Centrosomal protein of 78 kDa (Cep78).	sp|q5jtw2|cep78_human					2						2
Ceramide kinase-like protein.	sp|q49mi3|cerkl_human							1	1			2
Cerebral protein 1.	sp|o43159|huce1_human						1					1
Coiled-coil domain-containing protein 100 (Fragment).	sp|q8n960|q8n960_human				2							2
Coiled-coil domain-containing protein 86 (Cytokine-induced protein with coiled-coil domain).	sp|q9h6f5|ccd86_human						3					3
CSDA protein (Cold shock domain protein A, isoform CRA_b).	sp|q96b76|q96b76_human						3	2				5
Cullin-2 (CUL-2).	sp|q13617|cul2_human					2						2
CXXC-type zinc finger protein 6 (Leukemia-associated protein with a CXXC domain).	sp|q8nfu7|cxxc6_human										1	1
Cyclin-dependent kinase inhibitor 2A, isoform 4 (p14ARF) (p19ARF).	sp|q8n726|cd2a2_human								3	3	1	7
Cystatin-A (Stefin-A) (Cystatin-AS).	sp|p01040|cyta_human				14					1		15
DDX24 protein.	sp|q4v9l5|q4v9l5_human				3	2						5
DEAD (Asp-Glu-Ala-Asp) box polypeptide 50.	sp|q5vx37|q5vx37_human					3						3
DEAD (Asp-Glu-Ala-Asp) box polypeptide 56 (DEAD (Asp-Glu-Ala-Asp) box polypeptide 56, isoform CRA_b	sp|a4d2k9|a4d2k9_human						4					4
DENN domain-containing protein 2C.	sp|q68d51|den2c_human					1						1
Dermcidin isoform 2.	sp|a5jhp3|a5jhp3_human				10	6	1	2		2		21
Desmocollin-1 precursor (Desmosomal glycoprotein 2/3) (DG2/DG3).	sp|q08554|dsc1_human				2							2
Desmoglein-1 precursor (Desmosomal glycoprotein 1) (DG1) (DGI) (Pemphigus foliaceus antigen).	sp|q02413|dsg1_human				1	2						3
Desmoplakin (DP) (250/210 kDa paraneoplastic pemphigus antigen).	sp|p15924|desp_human					8						8
DNA polymerase subunit alpha B (DNA polymerase alpha 70 kDa subunit).	sp|q14181|dpoa2_human								1			1
DNA-binding protein A (Cold shock domain-containing protein A) (Single-strand DNA-binding protein NF-/	sp|p16989|dbpa_human					3	15	2				20
DNA-dependent protein kinase catalytic subunit (EC 2.7.11.1) (DNA-PK catalytic subunit) (DNA-PKcs) (DN	sp|p78527|prkdc_human		36									36
DnaJ homolog subfamily A member 1 (Heat shock 40 kDa protein 4) (DnaJ protein homolog 2) (HDJ-2) (HS	sp|p31689|dnja1_human							2				2
dTDP-D-glucose 4,6-dehydratase (EC 4.2.1.46).	sp|o95455|tgds_human								1			1
Dual specificity protein phosphatase 12 (EC 3.1.3.48) (EC 3.1.3.16) (Dual specificity tyrosine phosphatase	sp|q9uni6|dus12_human							2	4			6
E3 ubiquitin-protein ligase HUWE1 (EC 6.3.2.-) (HECT, UBA and WWE domain-containing protein 1) (URE-	sp|q7z6z7|huwe1_human	38	9									47
EBNA1BP2 protein (EBNA1 binding protein 2, isoform CRA_a) (EBNA1 binding protein 2 variant) (EBNA1 b	sp|q6ib29|q6ib29_human							15	1			16
Elongator complex protein 1 (ELP1) (IkappaB kinase complex-associated protein) (IKK complex-associated	sp|o95163|elp1_human				1							1
Elongator complex protein 3 (EC 2.3.1.48) (hELP3).	sp|q9h9t3|elp3_human						1					1
Enolase (EC 4.2.1.11).	sp|a6ng30|a6ng30_human								2			2
Envoplakin.	sp|a0auv5|a0auv5_human						1			2	1	4
Eukaryotic initiation factor 4A-III (EC 3.6.1.-) (Eukaryotic translation initiation factor 4A isoform 3) (ATP-d	sp|p38919|if4a3_human							2				2
Eukaryotic translation initiation factor 3 subunit A (Eukaryotic translation initiation factor 3 subunit 10) (e	sp|q14152|eif3a_human				1							1
Eukaryotic translation initiation factor 3 subunit B (Eukaryotic translation initiation factor 3 subunit 9) (eI	sp|p55884|eif3b_human				1							1
Eukaryotic translation initiation factor 3 subunit I (Eukaryotic translation initiation factor 3 subunit 2) (eIF	sp|q13347|eif3i_human							1				1
Eukaryotic translation initiation factor 6 (eIF-6) (B4 integrin interactor) (CAB) (p27(BBP)) (B(2)GCN homol	sp|p56537|if6_human				1		4	1	17	15	8	46
Fanconi anemia complementation group I isoform 3.	sp|a4zve4|a4zve4_human				4							4
Fanconi anemia group D2 protein (Protein FACD2).	sp|q9bxw9|facd2_human				5							5
Filaggrin.	sp|p20930|fila_human			1	1							2
FLJ11184 protein (Fragment).	sp|q0p6e4|q0p6e4_human								2			2
G patch domain-containing protein 4.	sp|q5t3i0|gptc4_human						3					3
G protein-binding protein CRFG variant (Fragment).	sp|q53gs0|q53gs0_human				2	34	9					45
GCN1 general control of amino-acid synthesis 1-like 1 (Yeast).	sp|a8kay1|a8kay1_human			3								3
GDNF-inducible zinc finger protein 1 (Zinc finger protein 336) (Zinc finger and BTB domain-containing pro	sp|q9h116|gzf1_human					1						1
General transcription factor 3C polypeptide 5 (Transcription factor IIIC subunit epsilon) (TF3C-epsilon) (TF	sp|q9y5q8|tf3c5_human						1					1

Peptide Spectra Count		Fxn										
Description	Reference	01	02	03	04	05	06	07	08	09	10	Total
Glyceraldehyde-3-phosphate dehydrogenase (EC 1.2.1.12) (GAPDH).	sp|p04406|g3p_human				1							1
Guanine nucleotide-binding protein G(s) subunit alpha isoforms XLas (Adenylate cyclase-stimulating G alp	sp|q5jwf2|gnas1_human							1				1
Guanine nucleotide-binding protein subunit beta-2-like 1 (Guanine nucleotide-binding protein subunit be	sp|p63244|gblp_human						4	12	34	9	3	62
Guanine nucleotide-binding protein-like 3 (Nucleolar GTP-binding protein 3) (Nucleostemin) (E2-induced	sp|q9bvp2|gnl3_human					1	12					13
Heat shock 70 kDa protein 6 (Heat shock 70 kDa protein B').	sp|p17066|hsp76_human			1	1	1	1					4
Heat shock cognate 71 kDa protein (Heat shock 70 kDa protein 8).	sp|p11142|hsp7c_human		1	2	10	57	55	2	1			128
Heat shock protein 75 kDa, mitochondrial precursor (HSP 75) (Tumor necrosis factor type 1 receptor-assc	sp|q12931|trap1_human					1						1
Heat shock protein HSP 90-alpha (HSP 86) (Renal carcinoma antigen NY- REN-38).	sp|p07900|hs90a_human					1						1
Heat shock protein HSP 90-beta (HSP 84) (HSP 90).	sp|p08238|hs90b_human					4						4
Heterogeneous nuclear ribonucleoprotein F (hnRNP F) (Nucleolin-like protein mcs94-1).	sp|p52597|hnrpf_human						1	8				9
Heterogeneous nuclear ribonucleoprotein H2 (H').	sp|a1l400|a1l400_human						2					2
Heterogeneous nuclear ribonucleoprotein M (hnRNP M).	sp|p52272|hnrpm_human					12	2					14
Heterogeneous nuclear ribonucleoprotein Q (hnRNP Q) (hnRNP-Q) (Synaptotagmin-binding, cytoplasmic	sp|o60506|hnrpq_human						2					2
Heterogeneous nuclear ribonucleoprotein U (hnRNP U) (Scaffold attachment factor A) (SAF-A) (p120) (pp	sp|q00839|hnrpu_human				2	3						5
Histone H1x.	sp|q92522|h1x_human							1	4			5
Histone H2A type 1-A (H2A/r).	sp|q96qv6|h2a1a_human									1		1
Histone H4 (Fragment).	sp|a2vcl0|a2vcl0_human									2		2
Hornerin.	sp|q5dt20|q5dt20_human				4	14	13					31
Hydrocephalus-inducing protein homolog.	sp|q4g0p3|hydin_human						1					1
Ifapsoriasin (Filaggrin 2).	sp|q5d862|q5d862_human					1						1
Ig alpha-1 chain C region.	sp|p01876|igha1_human				1							1
Importin subunit beta-1 (Karyopherin subunit beta-1) (Nuclear factor P97) (Importin 90).	sp|q14974|imb1_human					3						3
Importin subunit beta-3 (Karyopherin beta-3) (Ran-binding protein 5) (RanBP5).	sp|o00410|imb3_human				2							2
Insulin receptor substrate 4 (IRS-4).	sp|o14654|o14654_human			7	33	6						46
Insulin-like growth factor 2 mRNA-binding protein 1 (IGF2 mRNA-binding protein 1) (IGF-II mRNA-binding	sp|q9nzi8|if2b1_human					2	5					7
Insulin-like growth factor 2 mRNA-binding protein 3 (IGF2 mRNA-binding protein 3) (IGF-II mRNA-binding	sp|o00425|if2b3_human						3					3
Interferon-inducible double stranded RNA-dependent protein kinase activator A (Protein kinase, interferc	sp|o75569|prkra_human								1			1
Interferon-related developmental regulator 1 (Interferon-related developmental regulator 1, isoform CRA	sp|a4d0u1|a4d0u1_human						3	3				6
Interleukin-1 family member 9 (IL-1F9) (Interleukin-1 homolog 1) (IL- 1H1) (Interleukin-1 epsilon) (IL-1 eps	sp|q9nzh8|il1f9_human				2							2
Junction plakoglobin (Desmoplakin-3) (Desmoplakin III) (Catenin gamma).	sp|p14923|plak_human					2						2
Kappa-casein precursor - Bos taurus	uc|p02668|cask_bovin				3							3
Keratin 13 (Keratin 13, isoform CRA_a).	sp|a1a4e9|a1a4e9_human				1	1						2
keratin 4, type II, cytoskeletal - human (fragment) gi|34073 (X07695) cytokeratin 4 (408 AA) [Homo sapie	uc|88044|pir||s01068					1						1
Keratin 6A.	sp|a4qpc1|a4qpc1_human				3	2	5					10
keratin, 67K type II cytoskeletal - human (fragment) gi|386854 (M10938) type II keratin subunit protein [	uc|71536|pir||krhu2	1			1		4	1	1			8
Keratin, type I cuticular Ha1 (Hair keratin, type I Ha1) (Keratin-31).	sp|q15323|k1h1_human					2						2
Keratin, type I cytoskeletal 10 (Cytokeratin-10) (CK-10) (Keratin-10) (K10).	sp|p13645|k1c10_human			6	21	23	62	8	2	12	7	141
Keratin, type I cytoskeletal 14 (Cytokeratin-14) (CK-14) (Keratin-14) (K14).	sp|p02533|k1c14_human			1	4	5	20					30
Keratin, type I cytoskeletal 17 (Cytokeratin-17) (CK-17) (Keratin-17) (K17) (39.1).	sp|q04695|k1c17_human					3	9					12
Keratin, type I cytoskeletal 19 (Cytokeratin-19) (CK-19) (Keratin-19) (K19).	sp|p08727|k1c19_human							2				2
Keratin, type I cytoskeletal 9 (Cytokeratin-9) (CK-9) (Keratin-9) (K9).	sp|p35527|k1c9_human		13	27	37	82	9	2		3		173
Keratin, type II cytoskeletal 1 (Cytokeratin-1) (CK-1) (Keratin-1) (K1) (67 kDa cytokeratin) (Hair alpha prot	sp|p04264|k2c1_human	1	15	38	48	116	17	2	7	5		249
Keratin, type II cytoskeletal 2 epidermal (Cytokeratin-2e) (K2e) (CK 2e) (keratin-2).	sp|p35908|k22e_human		1	7	13	45	2		6	3		77
Keratin, type II cytoskeletal 5 (Cytokeratin-5) (CK-5) (Keratin-5) (K5) (58 kDa cytokeratin).	sp|p13647|k2c5_human			5	4	24						33
KERATIN, TYPE II CYTOSKELETAL 6F (CYTOKERATIN 6F) (CK 6F) (K6F KERATIN) gi|2119219|pir||I61771 ker	uc|1346349|sp|p48669|k2cf_human			6	13	19						38
Keratin-74 (Keratin-5c) (Keratin-K6irs4).	sp|q7rts7|q7rts7_human				1	4						5
Keratinocyte proline-rich protein (hKPRP).	sp|q5t749|kprp_human				2	4						6
KIAA0265 protein (KIAA0265 protein, isoform CRA_a).	sp|q6pid8|q6pid8_human							1	1			2
KIAA0543 protein (Fragment).	sp|o60290|o60290_human								1			1
Kinesin-like protein KIF14.	sp|q15058|kif14_human								1			1

Peptide Spectra Count		Fxn										
Description	Reference	01	02	03	04	05	06	07	08	09	10	Total
Kinesin-like protein KIFC1 (Kinesin-like protein 2) (Kinesin-related protein HSET).	sp|q9bw19|kifc1_human								1			1
KRR1 small subunit processome component homolog (HIV-1 Rev-binding protein 2) (Rev-interacting prot	sp|q13601|krr1_human							7				7
La-related protein 1 (La ribonucleoprotein domain family member 1).	sp|q6pkg0|larp1_human			9	46	3						58
La-related protein 7 (La ribonucleoprotein domain family member 7).	sp|q4g0j3|larp7_human					1						1
LAS1-like protein.	sp|q9y4w2|las1l_human			2	5	24						31
Leydig cell tumor 10 kDa protein homolog.	sp|q9unz5|l10k_human									1		1
Lin-9 homolog (huLin-9) (hLin-9) (Beta subunit-associated regulator of apoptosis) (Type I interferon recep	sp|q5tka1|lin9_human							1				1
Lipocalin-1 precursor (Von Ebner gland protein) (VEG protein) (Tear prealbumin) (TP) (Tear lipocalin) (TIC	sp|p31025|lcn1_human				2							2
Liver histone H1e.	sp|a3r0t7|a3r0t7_human							6	5	2		13
L-lactate dehydrogenase B chain (EC 1.1.1.27) (LDH-B) (LDH heart subunit) (LDH-H) (Renal carcinoma anti	sp|p07195|ldhb_human								3			3
LSG1 protein (Fragment).	sp|a0jlt4|a0jlt4_human				3	25						28
Lysosome-associated membrane glycoprotein 1 precursor (LAMP-1) (CD107a antigen).	sp|p11279|lamp1_human				1							1
Lysozyme C precursor (EC 3.2.1.17) (1,4-beta-N-acetylmuramidase C).	sp|p61626|lysc_human				2							2
Major centromere autoantigen B (Centromere protein B) (CENP-B).	sp|p07199|cenpb_human					4						4
MAP kinase-activating death domain protein (Differentially expressed in normal and neoplastic cells) (Ins	sp|q8wxg6|madd_human						1					1
MAP7 domain-containing protein 1 (Proline/arginine-rich coiled-coil domain-containing protein 1) (Argini	sp|q3kqu3|ma7d1_human				4							4
Mitochondrial 28S ribosomal protein S22 (S22mt) (MRP-S22).	sp|p82650|rt22_human							6	1			7
Mitochondrial 28S ribosomal protein S29 (S29mt) (MRP-S29) (Death- associated protein 3) (DAP-3) (Ioniz	sp|p51398|rt29_human							3				3
Mitochondrial 28S ribosomal protein S34 (S34mt) (MRP-S34).	sp|p82930|rt34_human									1		1
Mitochondrial ribosomal protein S27 (Mitochondrial ribosomal protein S27, isoform CRA_a).	sp|q6p1s1|q6p1s1_human							6				6
mRNA turnover protein 4 homolog.	sp|q9ukd2|mrt4_human								6	9		15
mTERF domain-containing protein 2.	sp|q7z6m4|mter2_human	1		6	2	4	5	77	50	7	4	156
Myb-binding protein 1A.	sp|q9bqg0|mbb1a_human			3	26							29
Myosin-9 (Myosin heavy chain 9) (Myosin heavy chain, non-muscle IIa) (Non-muscle myosin heavy chain	sp|p35579|myh9_human			1								1
Myosin-Va (Dilute myosin heavy chain, non-muscle) (Myosin-12) (Myosin heavy chain 12) (Myoxin).	sp|q9y4i1|myo5a_human								2	1		3
Myosin-XVIIIa (Myosin containing a PDZ domain) (Molecule associated with JAK3 N-terminus) (MAJN).	sp|q92614|myi18a_human										1	1
N-acetylgalactosaminyltransferase 7 (EC 2.4.1.-) (Protein-UDP acetylgalactosaminyltransferase 7) (UDP-G	sp|q86sf2|galt7_human				1							1
N-acetyltransferase 10 (EC 2.3.1.-).	sp|q9h0a0|nat10_human				2							2
Nascent polypeptide-associated complex subunit alpha (NAC-alpha) (Alpha-NAC) (Hom s 2.02).	sp|q13765|naca_human								1			1
Nischarin.	sp|q6pib4|q6pib4_human			20								20
NOL5A protein (Fragment).	sp|a0pj92|a0pj92_human						5					5
Novel protein (CGI-18) (Activating signal cointegrator 1 complex subunit 1, isoform CRA_a).	sp|q5sw07|q5sw07_human							4				4
Nuclease sensitive element-binding protein 1 (Y-box-binding protein 1) (Y-box transcription factor) (YB-1)	sp|p67809|ybox1_human					1	16	33				50
Nucleolar complex protein 2 homolog (Protein NOC2 homolog) (NOC2- like).	sp|q9y3t9|noc2l_human					1						1
Nucleolar GTP-binding protein 2 (Autoantigen NGP-1).	sp|q13823|nog2_human				10	27						37
Nucleolar phosphoprotein p130 (Nucleolar 130 kDa protein) (140 kDa nucleolar phosphoprotein) (Nopp1	sp|q14978|nolc1_human			1								1
Nucleolar protein 5 (Nucleolar protein NOP5) (NOP58).	sp|q9y2x3|nol5_human						4					4
Nucleolar protein 9 (cDNA FLJ75381, highly similar to Homo sapiens nucleolar protein 9 (NOL9), mRNA).	sp|q2nl84|q2nl84_human				2	17	2					21
Nucleolar RNA helicase 2 (EC 3.6.1.-) (Nucleolar RNA helicase II) (Nucleolar RNA helicase Gu) (RH II/Gu) (G	sp|q9nr30|ddx21_human				9	50						59
Nucleolin (Protein C23).	sp|p19338|nucl_human					2						2
Nucleosome assembly protein 1-like 1 (NAP-1-related protein) (hNRP).	sp|p55209|np1l1_human			1		4	37	14	1			57
p21-activated protein kinase-interacting protein 1 (PAK1-interacting protein 1) (PAK/PLC-interacting prot	sp|q9nwt1|pk1ip_human							2				2
PAI-1 mRNA-binding protein (PAI-RBP1).	sp|q5vu19|q5vu19_human						6	6				12
PAP-associated domain-containing protein 5 (EC 2.7.7.-) (Topoisomerase-related function protein 4-2) (TF	sp|q8ndf8|papd5_human					1						1
Pentatricopeptide repeat-containing protein 3, mitochondrial precursor (Transformation-related gene 15	sp|q96ey7|ptcd3_human					5	1					6
Pescadillo homolog 1.	sp|o00541|pesc_human					1	4					5
Phosphate carrier protein, mitochondrial precursor (PTP) (Solute carrier family 25 member 3).	sp|q00325|mpcp_human								2	1		3
Plakophilin-2.	sp|q99959|pkp2_human					1						1
Poly(A) binding protein, cytoplasmic 4 (Inducible form) (Poly(A) binding protein, cytoplasmic 4 (Inducible	sp|q5sps6|q5sps6_human					22	4					26
Poly(rC)-binding protein 1 (Alpha-CP1) (hnRNP-E1) (Nucleic acid- binding protein SUB2.3).	sp|q15365|pcbp1_human							2				2

Peptide Spectra Count		Fxn										
Description	Reference	01	02	03	04	05	06	07	08	09	10	Total
Polyadenylate-binding protein 1 (Poly(A)-binding protein 1) (PABP 1).	sp|p11940|pabp1_human				1	22	26					49
Possible J 56 gene segment (HCG2039797) (Fragment).	sp|a0n4v7|a0n4v7_human	1	1									2
Pre-mRNA-processing-splicing factor 8 (Splicing factor Prp8) (PRP8 homolog) (220 kDa U5 snRNP-specific	sp|q6p2q9|prp8_human			1								1
Pre-rRNA-processing protein TSR1 homolog.	sp|q2nl82|tsr1_human			11	21	63						95
PreS1 binding protein.	sp|q53yp0|q53yp0_human						2					2
Probable ATP-dependent RNA helicase DDX10 (EC 3.6.1.-) (DEAD box protein 10).	sp|q13206|ddx10_human			1		1						2
Probable ATP-dependent RNA helicase DDX17 (EC 3.6.1.-) (DEAD box protein 17) (RNA-dependent helicas	sp|q92841|ddx17_human						1					1
Probable ATP-dependent RNA helicase DDX20 (EC 3.6.1.-) (DEAD box protein 20) (DEAD box protein DP 1	sp|q9uhi6|ddx20_human					1						1
Probable ATP-dependent RNA helicase DDX27 (EC 3.6.1.-) (DEAD box protein 27).	sp|q96gq7|ddx27_human					7						7
Probable ATP-dependent RNA helicase DDX31 (EC 3.6.1.-) (DEAD box protein 31) (Helicain).	sp|q9h8h2|ddx31_human					6						6
Probable G-protein coupled receptor 21.	sp|q99679|gpr21_human				1							1
Probable ribosome biogenesis protein RLP24 (Ribosomal protein L24- like).	sp|q9uha3|rlp24_human									2		2
Protein BAP28 (FLJ10359).	sp|q5t3q7|q5t3q7_human			7								7
Protein FAM90A1.	sp|q86yd7|f90a1_human							1				1
Protein KRI1 homolog.	sp|q8n9t8|kri1_human					1						1
Protein LTV1 homolog.	sp|q96ga3|ltv1_human			2	7	19	31					59
Protein MON2 homolog (Protein SF21).	sp|q7z3u7|mon2_human			1								1
Protein NMD3 homolog (Nonsense-mediated mRNA decay protein 3 homolog).	sp|q96d46|q96d46_human						15	2				17
Protein S100-A7 (S100 calcium-binding protein A7) (Psoriasin).	sp|p31151|s10a7_human				5							5
Protein S100-A8 (S100 calcium-binding protein A8) (Calgranulin-A) (Migration inhibitory factor-related pr	sp|p05109|s10a8_human				1							1
Protein SDA1 homolog (SDA1 domain-containing protein 1) (hSDA) (Nucleolar protein 130).	sp|q9nvu7|sda1_human					8						8
Protein SMG7 (SMG-7 homolog) (EST1-like protein C).	sp|q92540|smg7_human				7							7
Protein transport protein Sec61 subunit alpha isoform 1 (Sec61 alpha- 1).	sp|p61619|s61a1_human							1				1
Protein VPRBP (HIV-1 Vpr-binding protein) (VprBP) (Vpr-interacting protein) (DDB1- and CUL4-associated	sp|q9y4b6|vprbp_human			1								1
Putative helicase MOV-10 (EC 3.6.1.-) (Moloney leukemia virus 10 protein).	sp|q9hce1|mov10_human				21	13						34
Putative pre-mRNA-splicing factor ATP-dependent RNA helicase DHX15 (EC 3.6.1.-) (DEAH box protein 15	sp|o43143|dhx15_human					1						1
Putative RNA methyltransferase NOL1 (EC 2.1.1.-) (Proliferating-cell nucleolar antigen p120) (Proliferatio	sp|p46087|nol1_human			9	35	40						84
Putative rRNA methyltransferase 3 (EC 2.1.1.-) (rRNA (uridine-2'-O-)- methyltransferase 3).	sp|q8iy81|rrmj3_human				5	4						9
Putative uncharacterized protein DKFZp686D15218 (Fragment).	sp|q7z377|q7z377_human								1		1	2
Putative uncharacterized protein DKFZp686H2338 (Fragment).	sp|q6aw89|q6aw89_human				19	3						22
Putative Xaa-Pro aminopeptidase 3 (EC 3.4.11.9) (X-Pro aminopeptidase 3) (Aminopeptidase P3) (APP3).	sp|q9nqh7|xpp3_human					1						1
RalBP1-associated Eps domain-containing protein 1 (RalBP1-interacting protein 1).	sp|q96d71|reps1_human					1						1
Receptor tyrosine-protein kinase erbB-3 precursor (EC 2.7.10.1) (c- erbB3) (Tyrosine kinase-type cell surfa	sp|p21860|erbb3_human						2					2
Replication protein A 70 kDa DNA-binding subunit (RP-A) (RF-A) (Replication factor-A protein 1) (Single-st	sp|p27694|rfa1_human						1					1
Reticulocalbin-1 precursor.	sp|q15293|rcn1_human							1				1
Retinal dehydrogenase 1 (EC 1.2.1.36) (RalDH1) (RALDH 1) (Aldehyde dehydrogenase family 1 member A	sp|p00352|al1a1_human						1					1
Retinoblastoma-like protein 2 (130 kDa retinoblastoma-associated protein) (p130) (PRB2) (RBR-2).	sp|q08999|rbl2_human				3							3
Ribonuclease inhibitor (Ribonuclease/angiogenin inhibitor 1) (RAI) (Placental ribonuclease inhibitor) (RNa	sp|p13489|rini_human							2				2
Ribosomal L1 domain-containing protein 1 (Cellular senescence- inhibited gene protein) (Protein PBK1) ((	sp|o76021|rl1d1_human					3	27	2				32
Ribosomal protein L14 variant (Fragment).	sp|q53g20|q53g20_human								2	5	2	9
Ribosomal protein L37 (Fragment).	sp|a6nfa3|a6nfa3_human									1	3	4
Ribosomal protein L5 (Ribosomal protein L5, isoform CRA_c).	sp|a2rum7|a2rum7_human					3	5	59	95	12	3	177
Ribosomal protein L7-like 1.	sp|q6dki1|rl7l_human								1			1
Ribosomal protein S15.	sp|a5d8v9|a5d8v9_human						1	1	3	7	4	16
Ribosomal protein S27.	sp|a6nk13|a6nk13_human							3	9	11	8	31
Ribosomal protein S27a.	sp|q5rkt7|q5rkt7_human								2			2
Ribosomal protein S6 (Ribosomal protein S6, isoform CRA_e) (cDNA FLJ78049, highly similar to Homo sap	sp|a2a3r6|a2a3r6_human					1	1	7	31	17	5	62
Ribosome biogenesis regulatory protein homolog.	sp|q15050|rrs1_human							4				4
RNA binding motif protein 28 (RNA binding motif protein 28, isoform CRA_a).	sp|a4d100|a4d100_human			2	3	19						24
RNA exonuclease 4 (EC 3.1.-.-) (Exonuclease XPMC2) (hPMC2) (Prevents mitotic catastrophe 2 protein hor	sp|q9gzr2|rexo4_human	15	17	47	56	95	236	135	71	47	31	750

Peptide Spectra Count		Fxn										
Description	Reference	01	02	03	04	05	06	07	08	09	10	Total
RNA-binding protein 39 (RNA-binding motif protein 39) (RNA-binding region-containing protein 2) (Hepat	sp|q14498|rbm39_human						1					1
RNA-binding protein NOB1 (Protein ART-4) (Phosphorylation regulatory protein HP-10).	sp|q9ulx3|nob1_human						9	12				21
RPL14 protein (Ribosomal protein L14 variant).	sp|q6iph7|q6iph7_human			1		1	2	7	21	25	16	73
rRNA 2'-O-methyltransferase fibrillarin (EC 2.1.1.-) (34 kDa nucleolar scleroderma antigen).	sp|p22087|fbrl_human							3	7			10
RRP12-like protein.	sp|q5jth9|rrp12_human		2	33	72							107
RRP1-like protein B.	sp|q14684|rrp1b_human						1	3				4
RuvB-like 1 (EC 3.6.1.-) (49 kDa TATA box-binding protein-interacting protein) (49 kDa TBP-interacting pro	sp|q9y265|ruvb1_human						1					1
RuvB-like 2 (EC 3.6.1.-) (48 kDa TATA box-binding protein-interacting protein) (48 kDa TBP-interacting pro	sp|q9y230|ruvb2_human							2				2
Salivary acidic proline-rich phosphoprotein 1/2 precursor (PRP-1/PRP- 2) (Parotid proline-rich protein 1/2	sp|p02810|prpc_human				2							2
SAPS domain family member 1 (Protein phosphatase 6, regulatory subunit 1).	sp|q9upn7|saps1_human				1							1
SEC16L.	sp|a1yca4|a1yca4_human			4								4
Sentrin-specific protease 3 (EC 3.4.22.-) (Sentrin/SUMO-specific protease SENP3) (SUMO-1-specific prote	sp|q9h4l4|senp3_human				1	3	15					19
Serine/threonine-protein kinase RIO2 (EC 2.7.11.1) (RIO kinase 2).	sp|q9bvs4|riok2_human					7	5					12
Serine/threonine-protein kinase RIO3 (EC 2.7.11.1) (RIO kinase 3) (sudD homolog).	sp|o14730|riok3_human						14					14
Serine/threonine-protein phosphatase 6 (EC 3.1.3.16) (PP6).	sp|o00743|ppp6_human								2			2
Serologically defined colon cancer antigen 1 (Antigen NY-CO-1).	sp|o60524|sdcg1_human				5							5
Serpin B3 (Squamous cell carcinoma antigen 1) (SCCA-1) (Protein T4-A).	sp|p29508|spb3_human				2							2
Serum albumin precursor.	uc|p02769|albu_bovin		1	5	1		2					9
	sp|p02768|albu_human		1	4	14	4	1					24
Similar to 60S ribosomal protein L15.	sp|a4d1q5|a4d1q5_human										1	1
Splicing factor 3B subunit 3 (Spliceosome-associated protein 130) (SAP 130) (SF3b130) (Pre-mRNA-splicin	sp|q15393|sf3b3_human				1							1
Sterile alpha motif domain-containing protein 4B.	sp|q5prf9|sam4b_human								1	1		2
Stress-70 protein, mitochondrial precursor (75 kDa glucose-regulated protein) (GRP 75) (Heat shock 70 kI	sp|p38646|grp75_human				4	25	12					41
Superoxide dismutase [Cu-Zn] (EC 1.15.1.1).	sp|p00441|sodc_human				1							1
Suppressor of SWI4 1 homolog (Ssf-1) (Peter Pan homolog).	sp|q9nq55|ssf1_human							9				9
Surfeit locus protein 6.	sp|o75683|surf6_human							13				13
TBC1 domain family member 1.	sp|q86ti0|tbcd1_human							1		1		2
T-complex protein 1 subunit alpha (TCP-1-alpha) (CCT-alpha).	sp|p17987|tcpa_human						1					1
T-complex protein 1 subunit delta (TCP-1-delta) (CCT-delta) (Stimulator of TAR RNA-binding).	sp|p50991|tcpd_human						1					1
T-complex protein 1 subunit theta (TCP-1-theta) (CCT-theta) (Renal carcinoma antigen NY-REN-15).	sp|p50990|tcpq_human						1					1
T-complex protein 1 subunit zeta (TCP-1-zeta) (CCT-zeta) (CCT-zeta-1) (Tcp20) (HTR3) (Acute morphine de	sp|p40227|tcpz_human						1					1
Testis-expressed sequence 10 protein.	sp|q9nxf1|tex10_human				5	27						32
Transcription elongation regulator 1 (TATA box-binding protein- associated factor 2S) (Transcription facto	sp|o14776|tcrg1_human								1			1
Transcription intermediary factor 1-beta (TIF1-beta) (Tripartite motif-containing protein 28) (Nuclear cor	sp|q13263|tif1b_human				3	8						11
Transcriptional activator protein Pur-alpha (Purine-rich single- stranded DNA-binding protein alpha).	sp|q00577|pura_human							4				4
Translocase of inner mitochondrial membrane 50 homolog (S. cerevisiae).	sp|q0vab1|q0vab1_human							4	3			7
Treacle protein (Treacher Collins syndrome protein).	sp|q13428|tcof_human			1								1
Tripartite motif-containing 26 (Fragment).	sp|a2ae48|a2ae48_human						2					2
TRM112-like protein.	sp|q9ui30|tr112_human								4	1		5
Tubulin alpha-1B chain (Tubulin alpha-ubiquitous chain) (Alpha-tubulin ubiquitous) (Tubulin K-alpha-1).	sp|p68363|tba1b_human					1	20	23				44
Tubulin alpha-4 chain (Alpha-tubulin 4).	sp|q9h853|q9h853_human						3	3				6
Tubulin beta chain (Tubulin beta-5 chain).	sp|p07437|tbb5_human					1	4	4				9
Tubulin, beta 2C.	sp|a2bfa2|a2bfa2_human						23	16				39
U3 small nucleolar RNA-associated protein 15 homolog.	sp|q8ted0|utp15_human						1					1
U5 small nuclear ribonucleoprotein 200 kDa helicase (EC 3.6.1.-) (U5 snRNP-specific 200 kDa protein) (U5	sp|o75643|u520_human			1								1
Ubiquitin A-52 residue ribosomal protein fusion product 1 (Ubiquitin A-52 residue ribosomal protein fusi	sp|q3mih3|q3mih3_human			3	4	6	4	4	2	4	1	28
Ubiquitin carboxyl-terminal hydrolase 11 (EC 3.1.2.15) (Ubiquitin thioesterase 11) (Ubiquitin-specific-pro	sp|p51784|ubp11_human				1	1						2
Ubiquitin-conjugating enzyme E2 O (EC 6.3.2.19) (Ubiquitin-protein ligase O) (Ubiquitin carrier protein O)	sp|q9c0c9|ube2o_human			35	3							38
Uncharacterized methyltransferase WBSCR22 (EC 2.1.1.-) (Williams- Beuren syndrome chromosomal regi	sp|o43709|wbs22_human								1			1
Uncharacterized protein AMY2B.	sp|a6njs5|a6njs5_human				4							4

Peptide Spectra Count		Fxn										
Description	Reference	01	02	03	04	05	06	07	08	09	10	Total
Uncharacterized protein C19orf22.	sp|q96d70|cs022_human								6	1		7
Uncharacterized protein C21orf70.	sp|q9nsi2|cu070_human								2	2		4
Uncharacterized protein C7orf24.	sp|o75223|cg024_human				2							2
Uncharacterized protein C7orf50.	sp|q9brj6|cg050_human									2		2
Uncharacterized protein CCT3.	sp|a6ne14|a6ne14_human						2					2
Uncharacterized protein DDB1.	sp|a6ng77|a6ng77_human				8							8
Uncharacterized protein ENSP00000267785.	sp|a6nei6|a6nei6_human								1	1	1	3
Uncharacterized protein ENSP00000275524 (HCG18290).	sp|a6nc28|a6nc28_human								8	11		19
Uncharacterized protein ENSP00000284293 (Fragment).	sp|a6nk96|a6nk96_human			1					2	11	3	17
Uncharacterized protein ENSP00000331275 (Fragment).	sp|a6nnt3|a6nnt3_human						1		8	6	2	17
Uncharacterized protein ENSP00000339488 (Fragment).	sp|a6nfe8|a6nfe8_human								5	1	2	8
Uncharacterized protein ENSP00000339522.	sp|a6nhq2|a6nhq2_human							1	1			2
Uncharacterized protein ENSP00000340469.	sp|a6np42|a6np42_human							1	6	2	7	16
Uncharacterized protein ENSP00000347049 (HCG2004593).	sp|a8msu5|a8msu5_human						1	2	13	21	12	49
Uncharacterized protein ENSP00000354495.	sp|a6nhx4|a6nhx4_human		1	3		1	7	17	7	1		37
Uncharacterized protein ENSP00000365743.	sp|a6np48|a6np48_human								1	1		2
Uncharacterized protein ENSP00000375262 (HCG2040224).	sp|a8my41|a8my41_human									1		1
Uncharacterized protein ENSP00000375546 (HCG21078).	sp|a8mwp1|a8mwp1_human		1	1	1		1	4	11	14	5	38
Uncharacterized protein ENSP00000380627 (Fragment).	sp|a8mv47|a8mv47_human	1	1		2		1			2	1	8
Uncharacterized protein ENSP00000382847 (Fragment).	sp|a8mve9|a8mve9_human								1			1
Uncharacterized protein GNL3L.	sp|a8mx10|a8mx10_human					1	1					2
Uncharacterized protein HP1BP3.	sp|a6ni71|a6ni71_human					3						3
Uncharacterized protein KIAA0776.	sp|o94874|k0776_human					1						1
Uncharacterized protein LARP5 (Fragment).	sp|a6nel6|a6nel6_human					3						3
Uncharacterized protein LRRIQ1.	sp|a8my60|a8my60_human			1								1
Uncharacterized protein MAGED2.	sp|a6nmx0|a6nmx0_human					6	1					7
Uncharacterized protein NAP1L4.	sp|a8mxh2|a8mxh2_human						5	1				6
Uncharacterized protein NEDD8 (Fragment).	sp|a8mua8|a8mua8_human					2						2
Uncharacterized protein NOC3L.	sp|a6njz9|a6njz9_human					2						2
Uncharacterized protein RCN2.	sp|a8mtg6|a8mtg6_human						2	5				7
Uncharacterized protein RPL30 (Fragment).	sp|a8mta6|a8mta6_human							2	11	18	10	41
Uncharacterized protein RPL4 (Fragment).	sp|a6nif7|a6nif7_human					4	16	69	1			90
Uncharacterized protein SET.	sp|a6ngv1|a6ngv1_human					3		1	1			5
Uncharacterized protein SQSTM1.	sp|a6nl52|a6nl52_human						2					2
UPF0384 protein CGI-117 (HBV pre-S2 trans-regulated protein 3).	sp|q9y3c1|u384_human								2	6		8
WD repeat-containing protein 18.	sp|q9bv38|wdr18_human						2	22				24
WD repeat-containing protein 43.	sp|q15061|wdr43_human					1						1
YTH domain family protein 2 (High-glucose-regulated protein 8) (CLL- associated antigen KW-14) (Renal c	sp|q9y5a9|ythd2_human						1					1
Zinc finger and BTB domain containing 11.	sp|q2nkp9|q2nkp9_human				3							3
Zinc finger CCCH type, antiviral 1.	sp|a4d1r2|a4d1r2_human					2						2
Zinc finger protein 593 (Zinc finger protein T86).	sp|o00488|zn593_human								1	4		5
Zinc finger protein 616.	sp|q08an1|zn616_human					2						2
Zinc finger protein 622 (Zinc finger-like protein 9).	sp|q969s3|zn622_human				3	14	42		2			61
Zinc-alpha-2-glycoprotein precursor (Zn-alpha-2-glycoprotein) (Zn- alpha-2-GP).	sp|p25311|za2g_human				15							15
Total		62	119	516	871	1424	1031	1249	1472	1260	616	8620

Proteomic analysis of LAP-tagged Rexo4 purifications from Hek293 cells. This study was previously performed in our lab. List of identified proteins was used to generate GOnet interactive graph shown in Figure 1B.

Sup. Figure 2 Rexo4 localization in mitosis

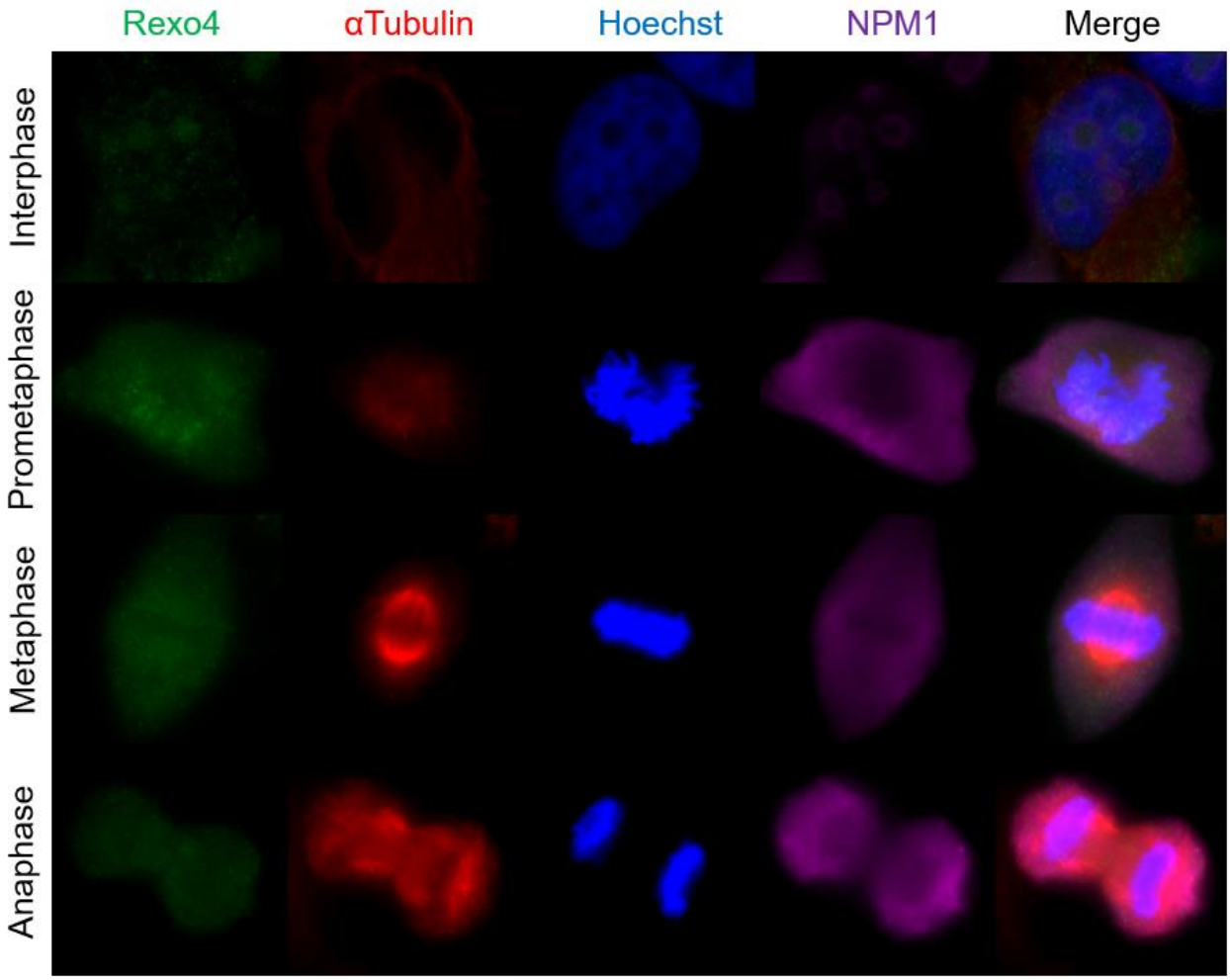

Supplemental Figure 2 Rexo4 localization during mitosis. (A) HeLa cells were fixed and stained with Hoechst 33342 DNA dye, anti-alpha-Tubulin, anti-NPM1 and anti-Rexo4. These cells were then imaged by IF microscopy to show Rexo4's colocalization with nucleolar marker NPM1 during interphase and the lack of any specific colocalization in several phases of mitosis.

Chapter 4

Final Thoughts

In this work, we have developed a new screening tool in the HeLa FUCCI iCas9 cell line that allows for inducible expression of Cas9 along with a built-in cell cycle phase indicator for use with common fluorescent imaging systems. This cell line is ready for use in conjunction with sgRNA libraries that are becoming more and more available. Improvements to this tool could be accomplished through substitution of FUCCI with FUCCI4 in order to individually resolve G1, S, G2 or M. However, we are excited to see its efficacy as a screening tool as is.

We have also designed and performed a high-throughput screen with roughly 1,200 naturally occurring metabolites, that we believe has identified novel cell cycle regulators amongst our 180 identified hits. Its identification of already known and well characterized cancer therapeutics gives us confidence that it has identified previously unknown and uncharacterized metabolites of interest. It is important to further classify and elucidate these results, as it is the first high-throughput metabolite screen of its size. Further analysis of more metabolite hits via immunofluorescence microscopy is needed, though initial attempts have proven unfruitful. After identification of a few more metabolites of interest, it would be of interest to the field to test how addition of these metabolites affect cell cycle regulation. Current studies mostly focus on glycolytic pathways (at time of writing, a Pubmed search for “glucose cancer” yields 50,812 results), but novel modes of regulation must exist and this screen attempts to begin the search for them.

We have begun work on the ribosome biogenesis protein, Rexo4, an RNA exonuclease that we believe is involved in the processing of rRNA. We have established is that Rexo4 nucleolar localization and exonuclease activity are required for proliferation in

HeLa cells. There are a few studies that suggest that Rexo4 is a biomarker for cancer, having shown upregulation of Rexo4 at both the mRNA and protein level of cancer cell types compared to their respective non-cancer cell types. It is important that we characterize exactly what Rexo4 is doing within the context of ribosome biogenesis, as there is growing interest in the field for cancer therapeutics targeting this biogenesis. In order to determine Rexo4's role, we are currently working on sequencing rRNAs isolated from Rexo4 depleted HeLa cells. We hope to see changes in rRNA precursor ratios to identify if and which rRNA precursor Rexo4 is cleaving. If this fails, there are other strategies we can employ, such as pulse-chase experiments or early ribosome purifications in order to accomplish this goal.

Appendix Chapter 1

Mapping Proximity Associations of Spindle Assembly Checkpoint Proteins

Mapping Proximity Associations of Spindle Assembly Checkpoint Proteins

Yenni A. Garcia[1], Erick F. Velasquez[1], Lucy W. Gao[2], Ankur A. Gholkar[1], Kevin M. Clutario[1], Keith Cheung[1], Taylor Williams-Hamilton[1], Julian P. Whitelegge[2,3,4] and Jorge Z. Torres[1, 3, 4*]

[1]Department of Chemistry and Biochemistry, University of California, Los Angeles, CA 90095, USA

[2]Pasarow Mass Spectrometry Laboratory, The Jane and Terry Semel Institute for Neuroscience

and Human Behavior, David Geffen School of Medicine, University of California, Los

Angeles, CA 90095, USA

[3]Molecular Biology Institute, University of California, Los Angeles, CA 90095, USA

[4]Jonsson Comprehensive Cancer Center, University of California, Los Angeles, CA 90095, USA

*Corresponding author:

Jorge Z. Torres

607 Charles E. Young Drive East

Los Angeles, CA 90095

Phone: 310-206-2092

Fax: 310-206-5213

torres@chem.ucla.edu

Reprinted (adapted) with permission from {Garcia YA, Velasquez EF, Gao LW, Gholkar AA, Clutario KM, Cheung K, Williams-Hamilton T, Whitelegge JP, Torres JZ. Mapping Proximity Associations of Core Spindle Assembly Checkpoint Proteins. J Proteome Res. 2021 Jul 2;20(7):3414-3427. doi: 10.1021/acs.jproteome.0c00941. Epub 2021 Jun 4. PMID: 34087075; PMCID: PMC8256817.}.

Abbreviations: BioID2, Biotin identification 2; SAC, Spindle assembly checkpoint

ABSTRACT

The spindle assembly checkpoint (SAC) is critical for sensing defective microtubule-kinetochore attachments and tension across the kinetochore and functions to arrest cells in prometaphase to allow time to repair any errors before proceeding into anaphase. Dysregulation of the SAC leads to chromosome segregation errors that have been linked to human diseases like cancer. Although much has been learned about the composition of the SAC and the factors that regulate its activity, the proximity associations of core SAC components have not been explored in a systematic manner. Here, we've taken a BioID2 proximity-labeling proteomic approach to define the proximity protein environment for each of the five core SAC proteins BUB1, BUB3, BUBR1, MAD1L1, and MAD2L1 in mitotic-enriched populations of cells where the SAC is active. These five protein association maps were integrated to generate a SAC proximity protein network that contains multiple layers of information related to core SAC protein complexes, protein-protein interactions, and proximity associations. Our analysis validated many known SAC complexes and protein-protein interactions. Additionally, it uncovered new protein associations, including the ELYS-MAD1L1 interaction that we have validated, that lend insight into the functioning of core SAC proteins and highlight future areas of investigation to better understand the SAC.

Key words: Spindle assembly checkpoint (SAC), BioID2, Proximity labeling, Protein associations, Protein networks, Cell division

INTRODUCTION

Human cell division is a highly coordinated set of events that ensures the proper transmission of genetic material from one mother cell to two newly formed daughter cells. Chromosome missegregation during cell division can lead to aneuploidy, an aberrant chromosomal number, which is a hallmark of many types of cancers and has been proposed to promote tumorigenesis (1). However, there is currently no consensus as to the pathways and factors that are deregulated to induce aneuploidy, why it is prevalent in cancer and how it contributes to tumorigenesis. Pivotal to cell division is the metaphase to anaphase transition, which is a particularly regulated process involving a multitude of protein-protein interactions that relies heavily on posttranslational modifications like phosphorylation and ubiquitination that function as switches to activate or inactivate protein function (2,3). For example, the multi-component spindle assembly checkpoint (SAC) is activated when unattached kinetochores or nonproductive (monotelic, syntelic, and merotelic) attachments are sensed and functions to arrest cells in metaphase to give time to correct these deficiencies and generate proper microtubule-kinetochore attachments (2) (Figure 1A). This ensures proper sister chromatid separation and minimizes segregation errors that lead to chromosomal instability, aneuploidy, and tumorigenesis (1). Core components of the SAC include BUB1, BUB3, BUBR1, MAD1L1, and MAD2L1(4). Critical to the SAC is the mitotic checkpoint complex (MCC, composed of MAD2L1, BUBR1, BUB3, and CDC20) that maintains the anaphase promoting complex/cyclosome (APC/C) ubiquitin ligase substrate adaptor protein CDC20 sequestered and thereby inactivates the APC/C (5,6). Upon proper microtubule-kinetochore attachment the SAC is satisfied and the inhibitory effect of the MCC on the APC/C is relieved (2) (Figure 1A). Active APC/C then ubiquitinates and targets Securin for degradation (2), which activates Separase, the protease that cleaves RAD21, a component of the cohesin complex that holds sister chromatids together (7). This releases sister chromatid cohesion and chromatids are pulled to opposing poles of the cell by spindle microtubules, marking the entry into anaphase.

Because understanding the SAC is critical to understanding tumorigenesis and the response of tumor cells to antimitotic drugs that activate the SAC and trigger apoptotic cell death, it has become an intensive area of research (8,9). Although decades of research have shed light on the SAC, we are far from elucidating the full complement of regulatory factors involved in this complex pathway and from understanding how misregulation of this pathway can lead to tumorigenesis and resistance to chemotherapeutic drugs like antimitotics (10). Furthermore, models of proximity associations of the core SAC proteins with themselves and with structural and signaling components that mediate the establishment and silencing of the SAC are still being defined (11-13). Recently, proximity-labeling approaches like BioID and APEX have been used effectively to determine association networks among proteins and for defining the architecture of the centrosome, centrosome-cilia interface, and other organelles within the cell (14-19). However, proximity labeling has not been applied to the SAC in a systematic fashion, which could help to interrogate current models of core SAC protein associations and regulation.

Here, we have engineered vectors for establishing inducible BioID2-tagged protein stable cell lines. This system was used to establish stable cell lines with inducible BioID2-tagged core SAC protein (BUB1, BUB3, BUBR1, MAD1L1, and MAD2L1) expression. These cell lines were utilized in BioID2-proximity biotin labeling studies, which were coupled to biotin biochemical purifications and mass spectrometry analyses to map the associations among the core SAC proteins and other proteins in close proximity. These analyses yielded a wealth of information with regards to the protein environment of the core SAC proteins in mitotic-enriched populations of cells where the SAC is active. In addition to validating well-established SAC protein complexes and protein-protein interactions, we defined new protein associations that warrant further investigation, including the ELYS-MAD1L1 interaction, to advance our understand SAC protein function and regulation.

EXPERIMENTAL PROCEDURES

Cell Culture and Cell Cycle Synchronization

All media and chemicals were purchased from ThermoFisher Scientific (Waltham, MA) unless otherwise noted. HeLa Flp-In T-REx BioID2-tagged stable cell lines and RPE cells were grown in F12:DMEM 50:50 medium with 10% FBS, 2 mM L-glutamine, in 5% CO_2 at 37^o C. Cells were induced to express the indicated BioID2-tagged proteins by the addition of 0.2 µg/ml doxycycline (Sigma-Aldrich, St. Louis, MO) for 16 hours. For synchronization of cells in mitosis, cells were treated with 100 nM Taxol (Sigma-Aldrich) for 16 hours. A list of all reagents used is provided in Table S1.

Cell siRNA and Chemical Treatments

HeLa cell siRNA treatments were performed as described previously (20), with control siRNA (siControl, D-001810-10) or BUB1-targeting siRNA (siBUB1, L-004102-00) from Dharmacon (Lafayette, CO) for 48 hours. For chemical treatments, RPE or HeLa cells were treated with control DMSO vehicle or the BUB1 inhibitor BAY 1816032 (HY-103020) (21) from MedChemExpress (Monmouth Junction, NJ) at 10 µM for five hours.

Generation of Inducible BioID2-tagging Vectors and Stable Cell Lines

For generating pGBioID2-27 or pGBioID2-47 vectors, the EGFP-S-tag was removed from pGLAP1 (22) by digestion with BstBI and AflII. BioID2-Myc-27 (27 amino acid linker) or BioID2-

Myc-47 (47 amino acid linker) were PCR amplified, digested with NheI and XhoI and cloned into BstBI and AflII digested pGLAP1 to generate pGBioID2-27 or pGBioID2-47 (Figure S1A). For full-length human SAC core gene *hBUB1, hBUB3, hBUBR1, hMAD1L1,* and *hMAD2L1* expression, cDNA corresponding to the full-length open reading frame of each gene was cloned into pDONR221 as described previously (22,23) (Figure S1B). SAC core genes were then transferred from pDONR221 to pGBioID2-47 using the Gateway cloning system (Invitrogen, Carlsbad, CA) as described previously (22,23) (Figure S1B). The pGBioID2-47-SAC protein vectors were then used to generate doxycycline inducible HeLa Flp-In T-REx BioID2 stable cell lines that expressed the fusion proteins from a specific single locus within the genome as described previously (22,23) (Figure S1C,D). All primers were purchased from ThermoFisher Scientific. A list of primers used is provided in Table S2. For a list of vectors generated in this study see Table S3. The pGBioID2-27 and pGBioID2-47 vectors have been deposited at Addgene (AddgeneIDs: 140276 and 140277 respectively) and are available to the scientific community.

Biotin Affinity Purifications

All media, chemicals, and beads were purchased from ThermoFisher Scientific unless otherwise noted. Biotin affinity purifications were conducted using previously described protocols with modifications (18,19). Briefly, 10% FBS was treated with 1 ml of MyOne streptavidin C1 Dynabeads overnight and passed through a 0.22 μm filter. The BioID2- BUB1, BUB3, BUBR1, MAD1L1, and MAD2L1, and BioID2 alone inducible stable cell lines were plated on six 150 mm tissue culture dishes, 24 hours post-plating, the cells were washed three times with PBS and once with DMEM without FBS, and shifted to the streptavidin Dynabead-treated 10% FBS DMEM. The cells were induced with 0.2 μg/ml Dox, and treated with 100 nM Taxol and 50 μM Biotin for 16 hours. Mitotic cells were collected by shake-off and centrifuged at 1,500 rpm for 5 minutes and washed twice with PBS. The pellet was lysed with 3 ml of lysis buffer (50 mM Tris-HCl pH 7.5,

150 mM NaCl, 1 mM EDTA, 1 mM EGTA, 1% Triton-X-100, 0.1% SDS, Halt Protease and Phosphatase Inhibitor Cocktail) and incubated with gentle rotation for 1 hour at 4 ° C, then centrifuged at 15,000 rpm for 15 minutes and transferred to a new 15 ml conical tube. The lysate was transferred to a TLA-100.3 tube (Beckman Coulter, Indianapolis, IN) and centrifuged at 45,000 rpm for 1 hour at 4 ° C. The lysate was then transferred to a new 15 ml conical tube and incubated with 300 ml of equilibrated streptavidin Dynabeads overnight with gentle rotation at 4 ° C. The beads were separated with a magnetic stand and washed twice with 2% SDS, followed by a wash with WB1 (0.1% sodium deoxycholate, 1% Triton X-100, 500 mM NaCl, 1 mM EDTA, 50 mM HEPES), a wash with WB2 (250 mM LiCl, 0.5% deoxycholate, 1 mM EDTA, 10 mM Tris-HCl pH 8.0), and a final wash with 50 mM Tris-HCl pH 7.5. The beads were then resuspended in 50 mM triethylammonium bicarbonate (TEAB), 12 mM sodium lauroyl sarcosine, 0.5% sodium deoxycholate. 10% of the beads were boiled with sample buffer and used for immunoblot analysis.

In Solution Tryptic Digestion

Streptavidin Dynabeads in 50 mM triethylammonium bicarbonate (TEAB), 12 mM sodium lauroyl sarcosine, 0.5% sodium deoxycholate were heated to 95 ° C for 10 minutes and then sonicated for 10 minutes to denature proteins. Protein disulfide bonds were reduced by treatment with 5 mM tris(2-carboxyethyl) phosphine (final concentration) for 30 minutes at 37° C. Protein alkylation was performed with 10 mM chloroacetamide (final concentration) and incubation in the dark for 30 minutes at room temperature. The protein solutions were diluted five-fold with 50 mM TEAB. Trypsin was prepared in 50 mM TEAB and added 1:100 (mass:mass) ratio to target proteins followed by a 4-hour incubation at 37 ° C. Trypsin was again prepared in 50 mM TEAB and added 1:100 (mass:mass) ratio to target proteins followed by overnight incubation at 37 ° C. A 1:1 (volume:volume) ratio of ethyl acetate plus 1% trifluoroacetic acid (TFA) was added to the samples and samples were vortexed for five minutes. Samples were centrifuged at 16,000 x *g* for

five minutes at room temperature and the supernatant was discarded. Samples were then lyophilized by SpeedVac (ThermoFisher Scientific) and desalted on C18 StageTips (ThermoFisher Scientific) as described previously (24).

Nano-liquid Chromatography with Tandem Mass Spectrometry (LC-MS/MS) Analysis Nano-LC-MS/MS with collision-induced dissociation was performed on a Q Exactive Plus Orbitrap (ThermoFisher Scientific) integrated with an Eksigent 2D nano-LC instrument. A laser-pulled reverse-phase column, 75 µm x 200 mm, containing 5-µm C18 resin with 300-Å pores (ThermoFisher Scientific) was used for online peptide chromatography. Electrospray ionization conditions using the nanospray source (ThermoFisher Scientific) for the Orbitrap were set as follows: capillary temperature at 200° C, tube lens at 110 V, and spray voltage at 2.3 kV. The flow rate for reverse-phase chromatography was 500 nl/min for loading and analytical separation (buffer A, 0.1% formic acid and 2% acetonitrile; buffer B, 0.1% formic acid and 98% acetonitrile). Peptides were loaded onto the column for 30 minutes and resolved by a gradient of 0–80% buffer B over 174 minutes. The Q Exactive Plus Orbitrap was operated in data-dependent mode with a full precursor scan time at 180 minutes at high resolution (70,000 at m/z 400) from 350-1,700 m/z and 10 MS/MS fragmentation scans at low resolution in the linear trap using charge-state screening excluding both unassigned and +1 charge ions. For collision-induced dissociation, the intensity threshold was set to 500 counts, and a collision energy of 40% was applied. Dynamic exclusion was set with a repeat count of 1 and exclusion duration of 15 seconds.

Experimental Design and Statistical Rationale

To enhance confidence in identifying core SAC protein proximity associations, we performed control and experimental purifications in biological replicates (3 biological purifications for each

core SAC proteins, except for BUB3 where 2 biological purifications were performed, and 2 technical replicates were performed for each biological purification). This approach allowed for downstream comparison of control and experimental purifications, where proteins identified in the control BirA only (empty vector) were deemed potential non-specific associations. See Figure S2 for experimental mass spectrometry data acquisition and analysis workflow. Database searches of the acquired spectra were analyzed with Mascot (v2.4; Matrix Science, Boston, MA) as described previously (25). The UniProt human database (October 10, 2018) was used with the following search parameters: trypsin digestion allowing up to 2 missed cleavages, carbamidomethyl on cysteine as a fixed modification, oxidation of methionine as a variable modification, 10-ppm peptide mass tolerance, and 0.02-Da fragment mass tolerance. With these parameters, an overall 5% peptide false discovery rate, which accounts for total false positives and false negatives, was obtained using the reverse UniProt human database as the decoy database. Peptides that surpassed an expectation cut-off score of 20 were accepted. See Table S4 for a list of all identified peptides and Table S5 for a list of all identified proteins. A list of all peptides that were used to identify proteins with one peptide sequence is provided in Table S6. All raw mass spectrometry files can be accessed at the UCSD Center for Computational Mass Spectrometry MassIVE datasets ftp://MSV000084975@massive.ucsd.edu. Peptides meeting the above criteria with information about their corresponding identified protein were further analyzed using in-house R scripts. All R scripts used in this study are freely available at GitHub https://github.com/uclatorreslab/MassSpecAnalysis. To increase precision and reduce error, a pseudo qualitative/quantitative approach was taken. Proteins identified in both the control and test purifications were assayed for significance, whereas proteins identified in test purifications but not present in control purifications were further considered. To handle proteins shared between test and control purifications, but only identified in less frequency, we measured the relative fold change or mean difference in a quantitative manner. To compare quantification between purifications, we used the Exponentially Modified Protein Abundance Index (emPAI)

(26). emPAI offers approximate relative quantitation of the proteins in a mixture based on protein coverage by the peptide matches in a database search result and can be calculated using the following equation (26).

$$emPAI = 10^{\frac{N_{Observed}}{N_{Observable}}} - 1$$

Where $N_{Observed}$ is the number of experimentally observed peptides and $N_{Observable}$ is the calculated number of observable peptides for each protein (26). To compare proteins across multiple replicates/baits each emPAI score was normalized to pyruvate carboxylase, a protein that readily binds to biotin (27), and was found in high abundance in all purifications. Using a normalized emPAI (NemPAI) as a relative quantification score, we calculated the mean difference (the mean NemPAI for a certain protein across test replicates minus the mean NemPAI). Resampling involved recreating or estimating the normal distribution around a test statistic, in this case the mean difference, by calculating that statistic many times under rearrangement of labels. We performed ten thousand simulations per test statistic, resulting in normal distributions of mean difference between values of proteins identified in the experimental and the control. Using this distribution, we related each individual mean difference to the mean difference observed in the overall population in order to get a relative idea of what might be significantly higher in value compared to the control, when taking what is observed in the entire population. Values that lied outside of the 95% confidence interval of the mean difference and showed a higher value in the experimental compared to the control were then considered for further analysis (see Table S7).

Protein Proximity Network Visualization and Integration of Systems Biology Databases

Visual renderings relating protein-protein interactions/associations were carried out using custom scripts in R. To incorporate protein-complex information, we integrated the Comprehensive Resource of Mammalian Protein Complexes (CORUM v. 3.0) (28). Protein-protein interaction

information was derived and integrated from the Biological General Repository for Interaction Datasets (BioGRID v. 3.5) (29). To create relational networks that associated proteins based on cellular mechanisms, Gene Ontology (GO) terms were incorporated into the search (Gene Ontology release June 2019) (30). For a list of GO terms used, see Table S8. Pathway information was derived from Reactome, an open source and peer-reviewed pathway database (31). All databases were individually curated into an in-house systems biology relational database using custom R scripts. Final visuals relating protein associations were constructed using RCytoscapeJS, a developmental tool used to develop Cytoscape renderings in an R and JavaScript environment (32,33).

Immunoprecipitations

For cell lysate immunoprecipitations (IPs), BioID2 (empty vector, EV), BioID2-MAD1L1, or BioID2-MAD2L1 HeLa stable cell lines were induced with 0.2 μg/ml Dox and treated with 100 nM Taxol for 16 hours to arrest cells in mitosis. Cells were collected by shake-off and lysed with lysis buffer (50 mM Tris-HCl pH 7.5, 150 mM NaCl, 1 mM EDTA, 1 mM EGTA, 1% Triton-X-100, 0.1% SDS, Halt Protease and Phosphatase Inhibitor Cocktail) and incubated with gentle rotation for one hour at 4 ° C, then centrifuged at 15,000 rpm for 30 minutes and the supernatant was transferred to a microcentrifuge tube. Myc magnetic beads were equilibrated and incubated with mitotic cell extracts for five hours at 4 ° □C with gentle rotation. The beads were then washed five times with wash buffer (50 mM Tris pH 7.4, 150 mM NaCl, 1 mM DTT, and Halt Protease and Phosphatase Inhibitor Cocktail) for five minutes each and bound proteins were eluted with 50 μL of 2X Laemmli SDS sample buffer. Ten percent of the sample inputs, and the entire eluates from the immunoprecipitations were used for immunoblot analysis.

In Vitro Binding Assays

For *in vitro* binding assays, Myc or FLAG-tagged GFP, MAD1L1, MAD2L1, or ELYS (N-terminal fragment) were *in vitro* transcribed and translated (IVT) using TNT® Quick Coupled Transcription/Translation System, (Promega, Madison, WI) in 10 µL reactions. Myc beads (MBL, Sunnyvale, CA) were washed three times and equilibrated with wash buffer (50 mM Tris pH 7.4, 200 mM KCl, 1 mM DTT, 0.5% NP-40, and Halt Protease and Phosphatase Inhibitor Cocktail). IVT reactions were added to the equilibrated Myc beads and incubated for 1.5 hours at 30o □C with gentle shaking and after binding, beads were washed three times with wash buffer and eluted by boiling for 10 minutes with 2X Laemmli SDS sample buffer. The samples were then resolved using a 4-20% gradient Tris gel with Tris-Glycine SDS running buffer, transferred to an Immobilon PVDF membrane (EMD Millipore, Burlington, MA), and the membranes were analyzed using a PharosFX Plus molecular imaging system (Bio-Rad, Hercules, CA).

Immunofluorescence Microscopy

Immunofluorescence microscopy was performed as described previously (34) with modifications described in (25). Briefly, HeLa inducible BioID2-tagged BUB1, BUB3, BUBR1, MAD1L1, and MAD2L1 stable cell lines were treated with 0.2 µg/ml doxycycline for 16 hours, fixed with 4% paraformaldehyde, permeabilized with 0.2% Triton X-100/PBS, and co-stained with 0.5 µg/ml Hoechst 33342 and the indicated antibodies. Imaging of mitotic cells was carried out with a Leica DMI6000 microscope (Leica DFC360 FX Camera, 63x/1.40-0.60 NA oil objective, Leica AF6000 software, Buffalo Grove, IL) at room temperature. Images were subjected to Leica Application Suite 3D Deconvolution software and exported as TIFF files. The quantification of immunofluorescence microscopy images from BUB1 RNAi and BUB1 inhibitor treated cells was performed by capturing intensity profiles in ImageJ for both a kinetochore section and a background section adjacent to the kinetochore. Each intensity value was normalized by the area

of the captured image and the background signal was subtracted. The values were compared using a student's t-test. The number of samples used varied by experiment; knock-down experiments: BUB1 (n=19), SGO2 (n=50), and PLK1 (n=13); inhibitor treatments: BUB1 (n=20), SGO2 (n=17), and PLK1 (n=17). All calculations were performed in R.

Antibodies

Immunofluorescence microscopy and immunoblotting were performed using the following antibodies: BioID2 (BioFront Technologies, Tallahassee, FL), GAPDH (Preoteintech, Rosemont, IL), □-tubulin (Serotec, Raleigh, NC), anti-centromere antibody (ACA, Cortex Biochem, Concord, MA), SGO2 (Bethyl, Montgomery, TX), PLK1, BUB1, and ELYS (Abcam, Cambridge, MA). Affinipure secondary antibodies labeled with FITC, Cy3, and Cy5 were purchased from Jackson Immuno Research (West Grove, PA). IRDye 680RD streptavidin was purchased from LI-COR Biosciences (Lincoln, NE). Immunoblot analyses were carried out using secondary antibodies conjugated to IRDye 680 and IRDye 800 from LI-COR Biosciences (Lincoln, NE) and blots were scanned using a LI-COR Odyssey infrared imager.

RESULTS AND DISCUSSION

Generation of Inducible BioID2-tagged SAC Protein Stable Cell Lines

The spindle assembly checkpoint is essential for ensuring the fidelity of chromosome segregation during cell division (35) (Figure 1A). To better understand how the SAC functions and is regulated, we sought to map the protein associations of the core SAC proteins BUB1, BUB3, BUBR1 (BUB1B), MAD1L1, and MAD2L1 using a BioID2 proximity labeling proteomic approach (18) (Figure 1B-F). The over-expression of critical cell division proteins often leads to cell division

defects that can preclude the generation of epitope-tagged stable cell lines. Therefore, we first sought to generate BioID2 Gateway-compatible vectors with a doxycycline (Dox) inducible expression functionality. To do this, we amplified BirA-Myc with linkers coding for 27 or 47 amino acid residues downstream of Myc (BirA-Myc-27/47) (Figure S1A, Table S2). These amplification products were cloned into the pGLAP1 vector (22), which had been previously modified by removal of its LAP-tag (EGFP-Tev-S-protein), to generate the pGBioID2-27 and pGBioID2-47 vectors (Figure S1A). Full-length human open reading frames encoding for BUB1, BUB3, BUBR1, MAD1L1, and MAD2L1 were cloned into the pGBioID2-47 vector. The pGBioID2-47-SAC protein vectors (Figure S1B, Table S3), were co-transfected with a vector expressing the Flp recombinase (pOG44) into HeLa Flp-In T-REx cells (Figure S1C). Hygromycin resistant clones were then selected (Figure S1D) and grown in the presence or absence of Dox for 16 hours. The Dox-induced expression of each BioID2-47-SAC protein was then assessed by immunoblot analysis (Figure 2A). All of the BioID2-tagged core SAC proteins were expressed only in the presence Dox (Figure 2A), indicating the successful establishment of inducible BioID2-tagged core SAC protein stable cell lines. Additionally, these BioID2-tagged core SAC proteins were expressed at lower levels than the untagged endogenous proteins (Figure S3A)

BioID2-SAC Proteins Localize Properly to Kinetochores During Prometaphase

Next the ability of BioID2-SAC proteins to properly localize to the kinetochores during prometaphase, a time when the SAC is active and core SAC proteins localize to the kinetochore region, was analyzed by immunofluorescence microscopy. BioID2-SAC protein HeLa inducible stable cells lines were treated with Dox for 16 hours, fixed, and stained with Hoechst 33342 DNA dye and anti-BioID2, anti-α-Tubulin and anti-centromere antibodies (ACA). The localization of BioID2-SAC proteins in prometaphase cells was then monitored by immunofluorescence microscopy. BioID2-tagged BUB1, BUB3, BUBR1, MAD1L1, and MAD2L1 localized to

kinetochores, overlapping fluorescence signal with anti-centromere antibodies (ACA) during prometaphase (Figure 2B). In contrast, the BioID2-tag alone showed no specific localization (Figure 2B). These results indicated that the BioID2-tag was not perturbing the ability of the SAC proteins to localize to kinetochores during the time when the SAC was active. Further, the addition of biotin did not perturb the localization of the BioID2-SAC proteins to the kinetochores (Figure S3B).

BioID2-SAC Protein Proximity Labeling, Purifications, and Peptide Identification

To define the protein proximity networks of core SAC proteins, the inducible BioID2-SAC protein HeLa stable cell lines were used to perform BioID2-dependent proximity biotin labeling and biotinylated proteins were purified with a streptavidin resin (Figures 1D and 2C). Briefly, inducible BioID2-SAC protein HeLa stable cells lines were treated with 0.2 μg/ml Dox, 100 nM Taxol, and 50 μM Biotin for 16 hours to induce the expression of BioID2-SAC proteins and to activate the SAC and arrest cells in prometaphase. Mitotic cells were collected by shake-off, lysed, and the cleared lysates were bound to streptavidin beads. Bound biotinylated proteins were trypsinized on the beads and the peptides were analyzed by 2D-LC MS/MS (for details see Experimental Procedures). A diagnostic immunoblot analysis of each purification, using anti-BioID2 antibodies, showed that BioID2-tagged BUB1, BUB3, BUBR1, MAD1L1, and MAD2L1 were present in the extracts and were purified with the streptavidin beads, indicating that they had been biotinylated (Figure 2C). Additionally, western blots of each purification were probed with streptavidin, which showed that biotinylated proteins were present and efficiently captured in each purification (Figure S4A). In-house R scripts were then used to analyze the mass spectrometry results (for details see Experimental Procedures), to draw significance between peptides shared between the experimental and the control, we estimated the distribution of the mean difference of normalized emPAI scores across proteins and selected proteins with a significant higher difference (for details

see Experimental Procedures). Proteins that showed significant higher values in test purifications compared to the controls (values that lied outside of 95% confidence interval of the population mean difference) were considered hits and further analyzed (Table S7).

Analysis of the Core SAC Protein Proximity Association Network

In-house R scripts were then used to integrate the identified proteins from the mass spectrometry analysis with the data visualization application RCytoscapeJS (32) to generate protein proximity association maps for each of the core SAC proteins (BUB1; BUB3; BUBR1; MAD1L1; MAD2L1) (Figure S5). These five maps were compiled to generate the SAC protein proximity network (Figure S6). To begin to digest the wealth of information within the SAC protein proximity network, we first analyzed the network with the CORUM database (28) and examined the proximal associations between each of the core SAC proteins. This analysis revealed many of the previously characterized core SAC component protein-protein interactions and the BUB1-BUB3, BUBR1-BUB3, BUBR1-BUB3-CDC20 (BBC subcomplex of the MCC) and MAD2L1-BUBR1-BUB3-CDC20 (MCC) complexes (Figures 3 and S6) (6,36-38). These SAC complexes are critical to the establishment and maintenance of the SAC (39) and their identification was an indication that our proximity-based labeling approach was robust. Of interest, BUB3 was present in all of the purifications, consistent with its central role in recruiting other SAC proteins to the kinetochore and coordinating the formation of SAC sub-complexes (Figure 3) (12). Although MAD1L1 and MAD2L1 had been previously determined to bind directly (40), our approach was unable to detect this association. However, previous proteomic analyses with N- or C- terminal BioID-tagged MAD1L1 were also unable to detect an association with MAD2L1, which was attributed to a low number of lysines on the surface of MAD2L1 that likely affected the efficiency of biotin labeling (41).

Analysis of Core SAC Protein-Kinetochore Protein Proximity Associations

To specifically analyze the kinetochore proteins identified in the core SAC protein proximity networks, we applied a kinetochore related Gene Ontology (GO) annotation analysis to the data sets. Briefly, R scripts were used to integrate the identified proteins with the bioinformatic databases CORUM (28), Gene Ontology (30), BioGRID (29), and Reactome (31) using kinetochore related GO terms (see Table S8 for a list of Kinetochore GO IDs) to reveal the kinetochore associated proteins. RCytoscapeJS (32) was then used to generate GO, BioGRID, and Reactome kinetochore protein proximity association maps for each of the core SAC proteins (BUB1; BUB3; BUBR1; MAD1L1; MAD2L1) (Figures S7-S11). The five kinetochore GO maps (one for each core SAC protein) were compiled to generate one core SAC protein kinetochore GO network that visualized the proteins within the network that were active at the kinetochore (Figure S12A). A similar process was repeated to generate one core SAC protein BioGRID network that displayed the verified associations between the proteins that were active at the kinetochore (Figure S12B) and one core SAC protein Reactome network that highlighted the cellular pathways that proteins in the SAC proximity association network have been linked to (Figure S12C). Additionally, we generated core SAC protein GO, BioGRID, and Reactome networks using mitotic spindle related GO annotations (Figure S13A-C) and centromere related GO annotations (Figure S14A-C), see Table S8 for a list of GO IDs. Finally, we generated core SAC protein GO, BioGRID, and Reactome networks using the kinetochore, mitotic spindle, and centromere related GO annotations (Figure 4A-C). Interestingly, of the proteins identified in the purifications, kinetochore associated proteins were enriched in comparison to mitochondrial proteins (Figure S15). Together, these networks not only visualized the associations of each core SAC protein with kinetochore components and more broadly proteins implicated in mitotic spindle

assembly, they also provided a holistic view of their interconnectedness (ie. associations among core SAC proteins and subcomplex and complex formation).

Numerous insights were derived from these networks and we highlight four here. First, we identified the Mis12 centromere complex components DSN1 and PMF1 in the BUB1 and MAD1L1 purifications (Figures 4A, S7A, and S10A). The Mis12 complex is comprised of PMF1, MIS12, DSN1, and NSL1 (42-44) and genetic and biochemical studies have shown that it coordinates communication from the outer kinetochore to the centromeric DNA in the inner kinetochore (44-46). Unexpectedly, PMF1 was also identified in the BUB3 purification (Figures 4A and S8A). To our knowledge there have been no previous reports of a direct association between BUB3 and the Mis12 complex. Therefore, this BUB3-PMF1 association could indicate a novel direct interaction or simply that these proteins reside within close proximity at the kinetochore. Of interest, the Mis12 complex recruits KNL1 to the kinetochore, which functions as a scaffold for the recruitment of BUB3 that subsequently recruits additional SAC components (4,38,47). Consistently, we observed the association of KNL1 with BUB1, BUB3, BUBR1, and MAD1L1 (Figure 4A). These associations were previously reported, as summarized in the Figure 4B BioGRID network, and had been established to have a role in checkpoint activation (41,48-50) (reviewed in (5)). Additionally, MAD2L1 was not found to associate with KNL1 and to our knowledge a KNL1-MAD2L1 interaction has not been reported.

Second, minor components of the Astrin-Kinastrin complex (PLK1, DYNLL1, and SGO2) (51) were found to associate with all of the core SAC proteins (Figures 4A, S7A, S8A, S9A, S10A, and S11A). The Astrin-Kinastrin complex is important for aligning and attaching microtubules to kinetochores (51-53). Previous studies showed that depletion of BUB1 led to the delocalization of PLK1 and SGO2 from the kinetochores during prometaphase (54,55). Additionally, the BUB1 kinase activity was shown to be important for SGO2 kinetochore localization (56) and for the proper localization of BUB1 to the kinetochore (55) and pharmacological inhibition of the BUB1

kinase activity led to delocalization of SGO2 away from kinetochores (57). However, whether the BUB1 kinase activity was required for PLK1 kinetochore localization remained unknown. To address this, we first sought to confirm that PLK1 and SGO2 were mislocalized in BUB1-depleted cells. HeLa cells were treated with control siRNA (siControl) or BUB1-targeting siRNA (siBUB1) capable of depleting BUB1 protein levels (Figure 5A). Immunofluorescence microscopy of these cells showed that BUB1was absent from kinetochores in siBUB1-treated cells (Figure 5B). Additionally, the siBUB1 treatment reduced the levels of kinetochore-localized PLK1 and SGO2 (Figure 5C,D). Next, we asked if the BUB1 kinase activity was required for PLK1 and SGO2 kinetochore localization. RPE cells were treated with control DMSO vehicle or the recently developed BUB1 kinase selective inhibitor BAY 1816032 (21) and the localization of PLK1 and SGO2 was assessed in mitotic cells. In comparison to the control DMSO treatment, treatment with BAY 1816032 led to a reduction in the levels of kinetochore-localized PLK1 and SGO2 (Figure 5E,F). Additionally, treatment of BioID2-BUB1 expressing HeLa cells with BAY 1816032 also led to a reduction in the levels of kinetochore-localized BioID2-BUB1 (Figure 5G). This data indicated that the BUB1 kinase activity was important for its proper localization to kinetochores and for the localization of the Astrin-Kinastrin minor complex components PLK1 and SGO2 to the kinetochore.

Third, we identified CENPV as a MAD2L1 associating protein (Figure 4A). CENPV was identified in a proteomic screen for novel components of mitotic chromosomes (58) and was later shown to localize to kinetochores early in mitosis and to have a major role in directing the chromosomal passenger complex (CPC) subunits Aurora B and INCENP to the kinetochore (50,59). Although BUB1 has been shown to be important for the recruitment of the CPC to kinetochores (60), we are unaware of any reports of MAD2L1 being involved in this process. Interestingly, MAD2L1 has been shown to regulate the relocation of the CPC from centromeres through its inhibition of MKLP2, which is essential for proper cytokinesis (61). Thus, it is possible

MAD2L1 could also be regulating CPC localization to kinetochores through its association with CENPV.

Fourth, components of the nuclear pore complex were found to associate with MAD1L1 and MAD2L1 (Figure S5). To better visualize these nuclear pore associated proteins, we performed a proximity protein mapping analysis for each of the core SAC proteins using the nuclear pore related GO annotations (see Table S8 for a list of nuclear pore related GO IDs) (Figure S16). This analysis revealed that MAD1L1 had associations with nuclear pore basket components including TPR, NUP153, NUP50, and other components of the nuclear pore that are in close proximity to the nuclear basket like ELYS/AHCTF1 (also known as MEL-28 in *C. elegans*) and NUP107 (Figure S16A). These data support previous studies in humans and other organisms that have shown that MAD1L1 associates with TPR, NUP153, ELYS, and NUP107 and is important for generating the MAD1L1-MAD2L1 complex in early mitosis to establish the SAC (62-68). Similarly, MAD2L1 was found to associate with TPR (previously verified in (63)), NUP50, Nup153, NUP210 and ELYS (Figure S16A). Of interest, we did not detect associations between other core SAC proteins (BUB1; BUB3; BUBR1) and nuclear pore basket proteins. These data are consistent with a model where MAD1L1 makes multiple direct contacts with the nuclear pore basket complex subunits and MAD2L1 is in close proximity to NUP153 and NUP50 due to its binding to MAD1L1. We note that ELYS was found in both the MAD1L1 and MAD2L1 proximity maps (Figure S16A). ELYS was discovered in a proteomic screen for NUP107-160 complex binding partners and was shown to localize to nuclear pores in the nuclear lamina during interphase and to kinetochores during early mitosis, similar to the NUP107-160 complex (69). More recently, ELYS was shown to function as a scaffold for the recruitment of Protein Phosphatase 1 (PP1) to the kinetochore during M-phase exit, which was required for proper cell division (70,71). Due to ELYS's roles at the kinetochore and an identified yeast two-hybrid interaction between *C. elegans* MEL-28 (ELYS in humans) and MDF-1 (MAD1L1 in humans) *(65)*,

we sought to determine if MAD1L1 and MAD2L1 were binding directly to ELYS. First, we performed MYC immunoprecipitations from mitotic protein extracts prepared from BioID2, BioID2-MAD1L1, and BioID2-MAD2L1 expressing cell lines that had been arrested in mitosis. Indeed, ELYS immunoprecipitated with both BioID2-MAD1L1 and BioID2-MAD2L1, albeit weakly, in these mitotic extracts (Figure 6A). Next, we sought to asses these interactions in a cell-free *in vitro* expression system. Although a validated full-length ELYS cDNA vector was not available and could not be generated, we were able to generate a MYC-tagged ELYS N-terminal fragment vector that expressed the first 46 amino acids of ELYS. This ELYS N-terminal fragment bound to FLAG-MAD1L1, but not FLAG-MAD2L1 (Figure 6B). Together, these data indicated that ELYS associated with MAD1L1 and MAD2L1 in mitotic cell extracts and that MAD1L1 bound to the ELYS N-terminal fragment *in vitro*.

Core SAC Proteins in Cellular Homeostasis

It's important to note that most of the core SAC proteins have been shown to have roles in cellular homeostasis independent of their role in the SAC, which are predominantly mediated through protein-protein interactions with non-kinetochore proteins. Many of these associations were present in the individual core SAC protein proximity maps where GO annotations were not applied (Figure S5). Consistently, Reactome pathway analysis of the core SAC protein proximity protein network showed that many of the SAC associated proteins had roles in numerous pathways important for cellular homeostasis including the cell cycle, DNA repair, and gene expression (Figure 4C). We encourage researchers interested in non-mitotic SAC protein functions to explore the SAC protein proximity association networks to gain further insights into these pathways.

CONCLUSIONS

The SAC is an important signaling pathway that is critical for proper cell division, which functions with great precision in a highly orchestrated manner (2). Due to the dynamic nature of the associations between core SAC proteins and the complexes and subcomplexes that they form, it has been difficult to generate a proteomic network view of the proteins that are in close proximity and that interact with core SAC proteins. Here, we have established an inducible BioID2-tagging system that allowed for the transient expression of BioID2-tagged core SAC proteins (BUB1, BUB3, BUBR1, MAD1L1, and MAD2L1), which bypasses issues associated with long-term overexpression of key cell division proteins that can compromise cellular homeostasis. We coupled this system to a proximity labeling proteomic approach to systematically define a proximity protein association map for each of the core SAC proteins. These proximity maps were integrated to generate a core SAC protein proximity protein network. The coupling of the proximity maps/network with curated functional databases like CORUM, GeneOntology, BioGRID, and Reactome allowed for a systems level bioinformatic analysis of the associations within these maps/network. To our knowledge this is the first systematic characterization of the core SAC proteins by proximity-based proteomics.

Our analysis recapitulated many of the core SAC protein-protein interactions, sub-complexes, and complexes that had been previously described. Importantly, it also identified numerous novel associations that warrant further examination. Among these is ELYS, which associated with MAD1L1 and MAD2L1. Although an interpretation of these associations could be that MAD1L1 and MAD2L1 associate with ELYS at the nuclear pore in preparation for mitotic entry and SAC activation, we favor a model where ELYS may be important for the recruitment of SAC proteins to the kinetochore and/or for checkpoint activation. Future studies aimed at addressing these models should bring clarity to the potential role of ELYS in SAC functioning and cell division. Of interest, previous studies had shown the importance of BUB1 for the localization

of the Astrin-Kinastrin minor complex proteins to the kinetochore (51-54) and our analysis further determined that the BUB1 kinase activity was important for this function. Together, these data indicate that BUB1 may have a central organizing role not only in SAC activation and function, but in SAC silencing and mediating the transition from metaphase to anaphase through its association with the Astrin-Kinastrin minor complex (Figure 5H).

We note that there are limitations to the BioID2 approach (for review see (72)). Although our analysis was conducted from mitotic-enriched populations of cells to enrich for mitotic protein associations, the biotinylation process is conducted over the time-frame of hours and some identified associations could represent associations that take place outside of mitosis. These associations could inform on the non-mitotic functions of core SAC proteins, which is a rapidly growing field. Moving forward recent developments in BioID2 technology such as the mini-turboID system should help to resolve proximity associations in a time-dependent manner, as labeling occurs within minutes (73). Our analysis also employed N-terminal BioID2-tagging and a similar approach using C-terminal tagging of core SAC proteins could lead to different results. Additionally, it is important to note that BioID systems do not identify all known interactions of any specific bait protein. For example, we did not identify the MAD1L1-MAD2L1 interaction in our BioID2 analysis, which is consistent with a previous BioID analysis of MAD1L1 (41). Interestingly, we were able to detect the MAD1L1-MAD2L1 interaction when we performed immunoprecipitations with BioID2-MAD1L1 and BioID2-MAD2L1 and immunoblotted for endogenous MAD1L1 or MAD2L1 (Figures S4B and 6A). This indicates that BioID2-MAD1L1 is capable of binding to MAD2L1, but is not able to biotinylate it efficiently. There are many reasons why similar phenomena may occur with other protein pairs and these include a low abundance of surface exposed lysines on prey proteins (whether absent from the protein surface or buried within a protein complex) and the orientation of the protein interaction could preclude access to lysines

on prey proteins (72). Nonetheless, BioID systems have been invaluable to understanding cellular process and the architecture of cellular structures (14,19,74-76).

To facilitate the use and interrogation of the core SAC protein proximity maps/network generated in this study, all mass spectrometry data and R scripts used to analyze the data have been deposited in open access databases that are freely available to the scientific community (see Experimental Procedures). These tools will enable researches to define novel associations and to generate testable hypotheses to further advance the current understanding of SAC protein function and regulation.

SUPPORTING INFORMATION

The Supporting Information is available free of charge at: (link provided by ACS)

Workflow for generating BioID2 vectors and cell lines; workflow of mass spectrometry data acquisition and analysis; supporting data characterizing cell lines and biochemical purification controls; combined Cytoscape protein association maps of selected SAC proteins with no GO terms applied; Cytoscape protein association maps for each SAC protein with applied GO terms; kinetochore protein enrichment analysis; uncropped immunoblots for all figures (PDF)

List of reagents used (XLSX)

List of primers used (XLSX)

List of vectors generated (XLSX)

Summary of all identified peptides from all BioID2 purifications (XLSX)

Summary of all identified proteins from all BioID2 purifications (XLSX)

Summary of peptides for all proteins that were identified with one peptide sequence (XLSX)

Summary of significant SAC protein proximity associated proteins (XLSX)

List of Gene Ontology (GO) annotations used in the core SAC protein proximity association network analyses (XLSX)

NOTES

The authors declare no competing financial interest. The pGBioID2-27 and pGBioID2-47 vectors have been deposited at Addgene (Addgene IDs: 140276 and 140277 respectively) and are available to the scientific community. All raw mass spectrometry files can be accessed at the UCSD Center for Computational Mass Spectrometry MassIVE datasets ftp://MSV000084975@massive.ucsd.edu. All R scripts used in this study are freely available at GitHub https://github.com/uclatorreslab/MassSpecAnalysis.

ACKNOWLEDGEMENTS

This material is based upon work supported by the National Institutes of Health NIGMS grant numbers R35GM139539 and R01GM117475 to J.Z.T., any opinions, findings, and conclusions or recommendations expressed in this material are those of the authors and do not necessarily reflect the views of the National Institutes of Health NIGMS. Y.A.G. and K.M.C. were supported by the UCLA Tumor Cell Biology Training Program (USHHS Ruth L. Kirschstein Institutional National Research Service Award # T32CA009056). This work was supported in part by a grant to The University of California, Los Angeles from the Howard Hughes Medical Institute through the James H. Gilliam Fellowships for Advanced Study Program (E.F.V), by a UCLA Molecular Biology Institute Whitcome Fellowship (E.F.V.) and a NIH P30DK063491 grant (J.P.W.).

FIGURES

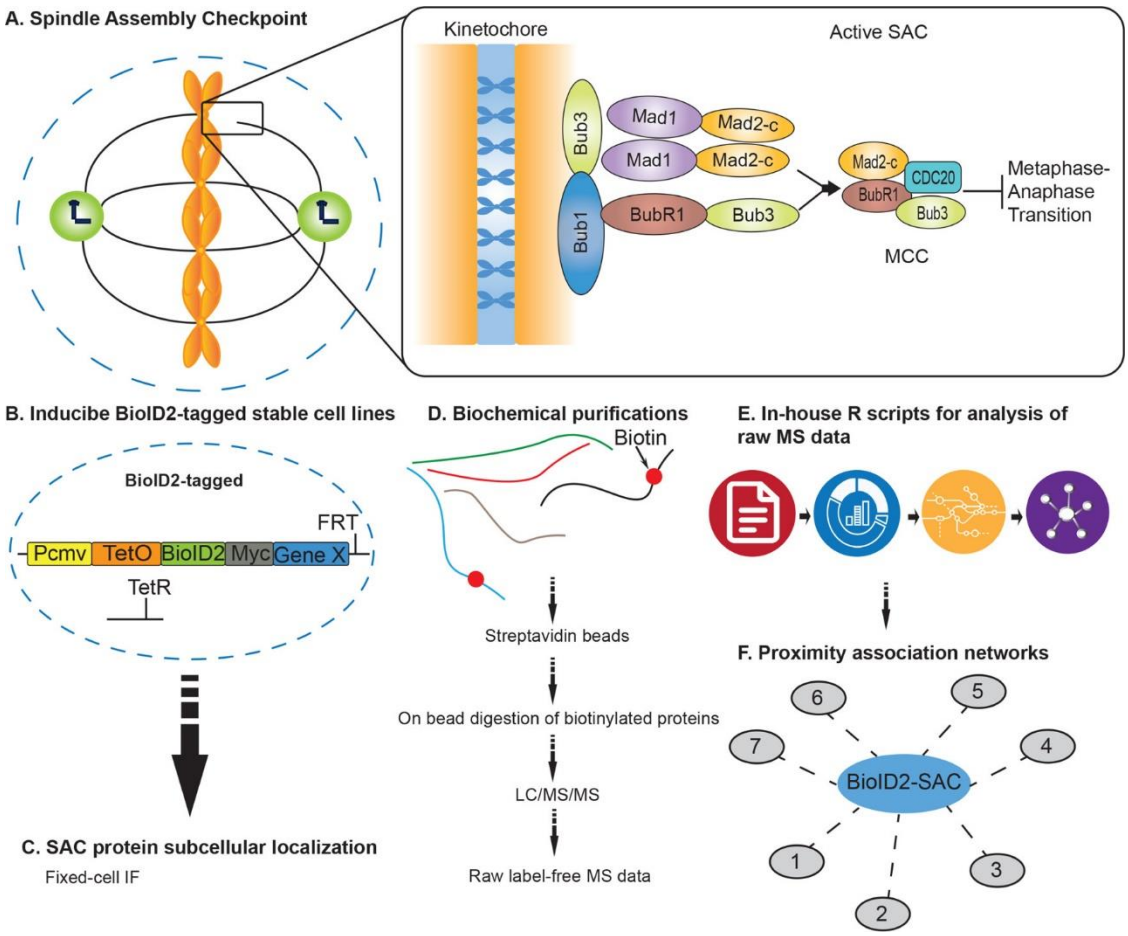

Figure 1. Overview of the approach to generate core SAC protein BioID2 proximity association networks. (A) Schematic of the core spindle assembly checkpoint (SAC) components BUB1, BUB3, BUBR1, MAD1L1, and MAD2L1 that localize to the kinetochore region during early mitosis. MCC denotes mitotic checkpoint complex. (B) Generation of inducible BioID2-tagged stable cell lines for each core SAC protein. (C) Fixed-cell immunofluorescence microscopy to analyze BioID2-tagged SAC protein subcellular localization in time and space. (D) Biochemical purifications; affinity purification of biotinylated proteins and identification of proteins by LC/MS/MS. (E) Computational analysis of raw mass spectrometry data using in-house R scripts. (F) Generation of high-confidence SAC protein proximity association networks.

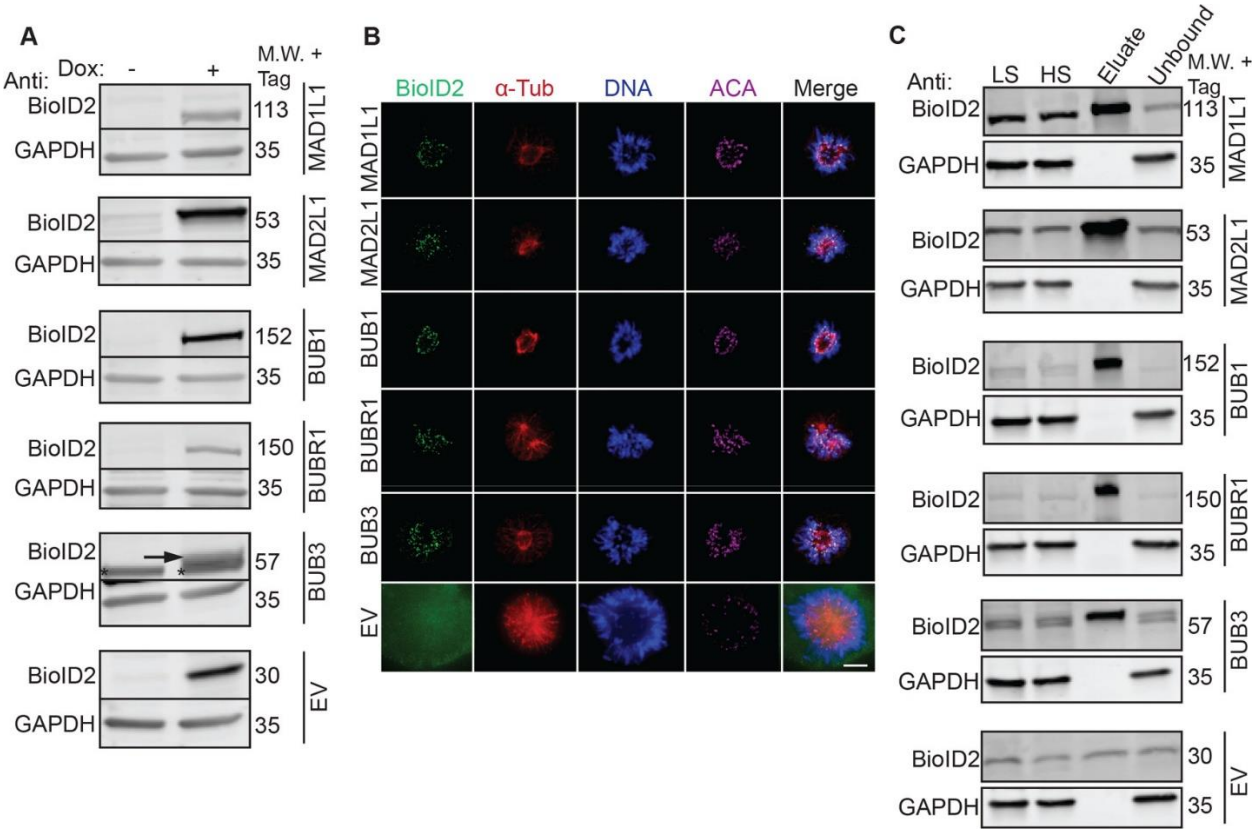

Figure 2. Establishment of inducible BioID2-tagged SAC protein (BUB1, BUB3, BUBR1, MAD1L1 and MAD2L1) stable cell lines and biochemical purifications. (A) Immunoblot analysis of extracts from doxycycline (Dox)-inducible BioID2-tag alone (EV, empty vector) or BioID2-tagged SAC protein (BUB1; BUB3; BUBR1; MAD1L1; MAD2L1) expression cell lines in the absence (-) or presence (+) of Dox for 16 hours. For each cell line, blots were probed with anti-BioID2 (to visualize the indicated BioID2-tagged SAC protein) and anti-GAPDH as a loading control. M.W. indicates molecular weight. Note that BioID2-tagged SAC proteins are only expressed in the presence of Dox. The arrow points to the induced BioID2-BUB3 protein band and the asterisk denotes a non-specific band recognized by the anti-BioID2 antibody. (B) Fixed-cell immunofluorescence microscopy of the BioID2-tag alone (EV) or the indicated BioID2-

tagged SAC proteins during prometaphase, a time when the SAC is active. HeLa BioID2-tagged protein expression cell lines were induced with Dox for 16 hours, fixed and stained with Hoechst 33342 DNA dye and anti-BioID2, anti-α-Tubulin and anti-centromere antibodies (ACA). Bar indicates 5μm. Note that all BioID2-tagged SAC proteins localize to the kinetochore region (overlapping with the ACA signal), whereas the BioID2-tag alone (EV) was absent from kinetochores. (C) Immunoblot analysis of BioID2 biochemical purifications from cells expressing the indicated BioID2-tagged SAC proteins or the BioID2-tag alone (EV). For each cell line, blots were probed with anti-BioID2 (to visualize the indicated BioID2-tagged SAC protein) and anti-GAPDH as a loading control. M.W. indicates molecular weight. LS indicates low speed supernatant, HS indicates high speed supernatant. Uncropped immunoblots are provided in Figures S17 and S18.

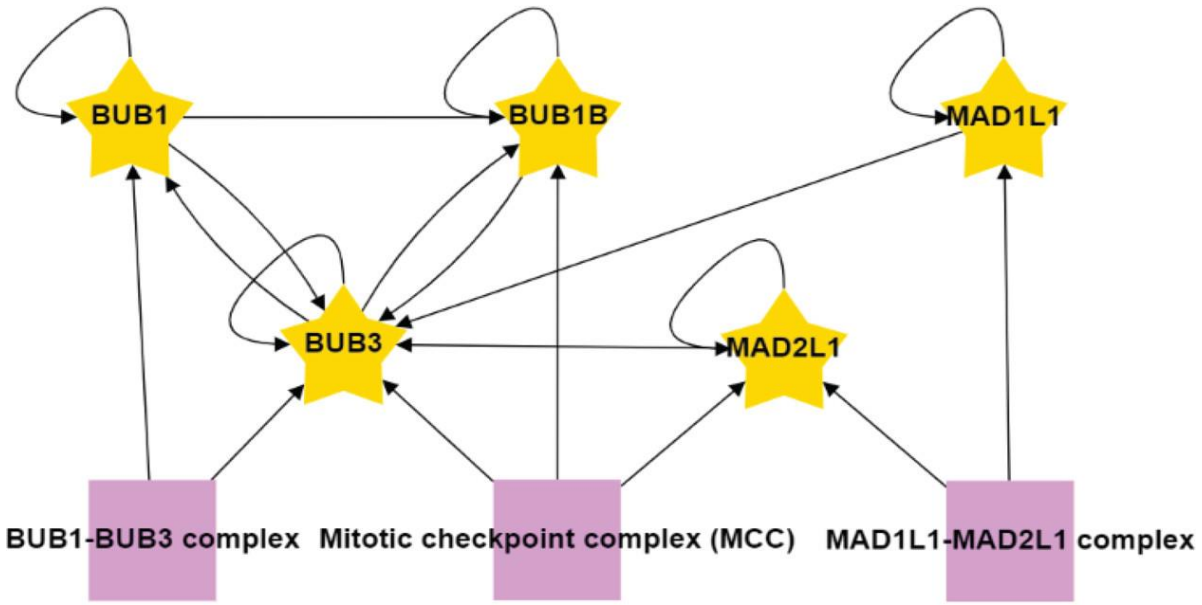

Figure 3. Associations among the core SAC proteins identified in the proximity protein network. The associations between each of the core SAC proteins (BUB1; BUB3; BUBR1; MAD1L1; MAD2L1) were isolated from the unified core SAC protein proximity association network (Figure S6). Purple boxes highlight protein complexes known to assemble with core SAC proteins as annotated by the CORUM database. Arrows indicate the direction of the detected associations.

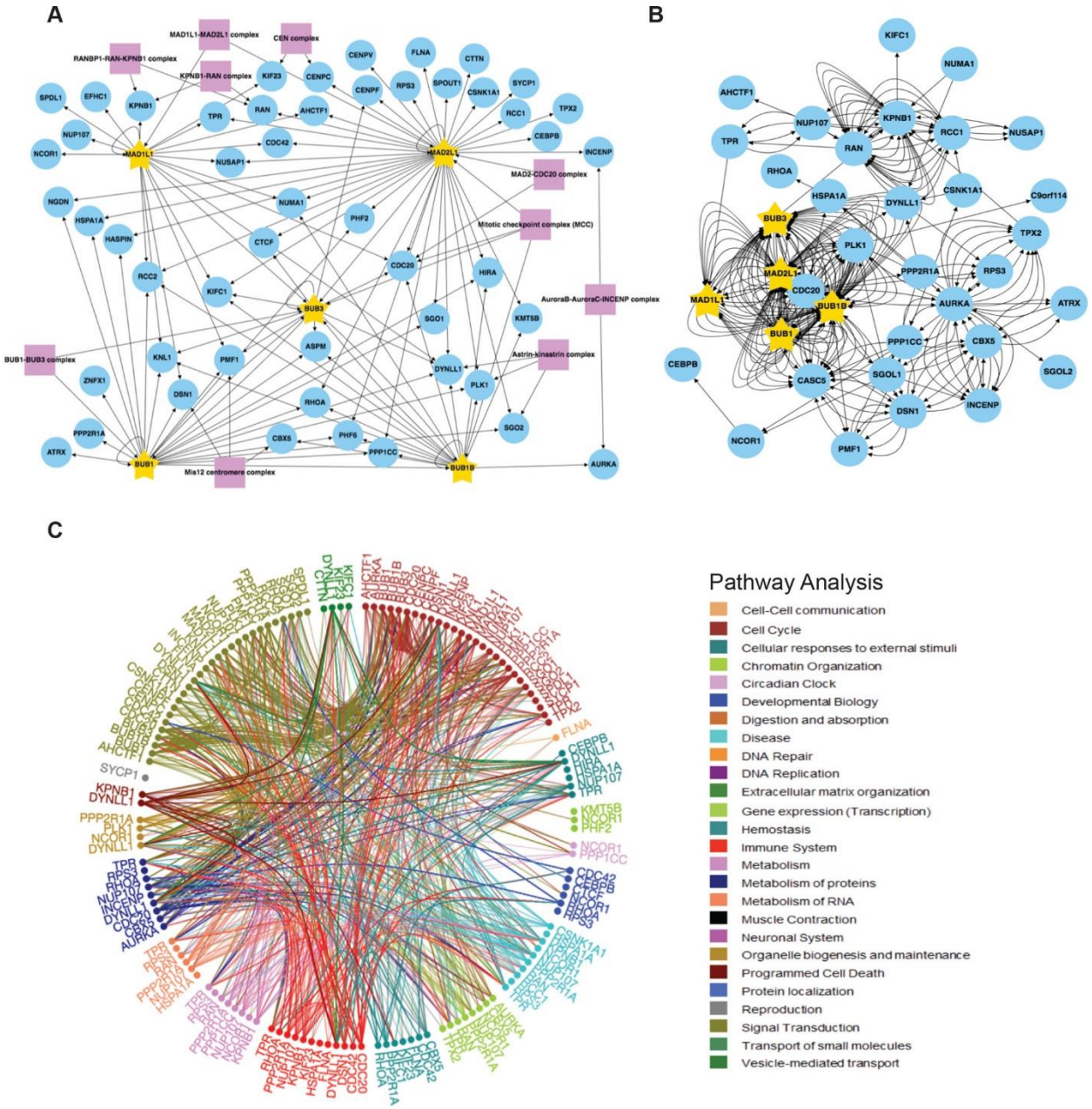

Figure 4. SAC protein BioID2 kinetochore/mitotic spindle assembly/centromere proximity association network. (A) Individual core SAC protein (BUB1; BUB3; BUBR1; MAD1L1; MAD2L1) proximity protein maps were compiled and subjected to kinetochore, mitotic spindle assembly, and centromere GO annotation analysis along with a COURM complex annotation analysis to generate a core SAC protein kinetochore/mitotic spindle assembly/ centromere proximity association network. Purple boxes highlight kinetochore, mitotic spindle assembly, and

centromere associated protein complexes present in the network. Arrows indicate the direction of the detected interactions. For a list of GO terms used see Table S8. (B) The core SAC protein kinetochore/mitotic spindle assembly/ centromere proximity association network was analyzed with BioGRID to reveal previously verified protein associations. Each arrow indicates an experimentally annotated interaction curated in the BioGRID database. Direction of arrows indicate an annotated interaction from a bait protein to the prey. (C) Reactome pathway analysis of the core SAC protein kinetochore/mitotic spindle assembly/ centromere proximity association network. The Reactome circular interaction plot depicts the associations between the identified proteins within the SAC protein kinetochore/mitotic spindle assembly/centromere proximity association network and the corresponding pathways in which they function. Legend presents the color-coded pathways that correspond to the circular interaction plots.

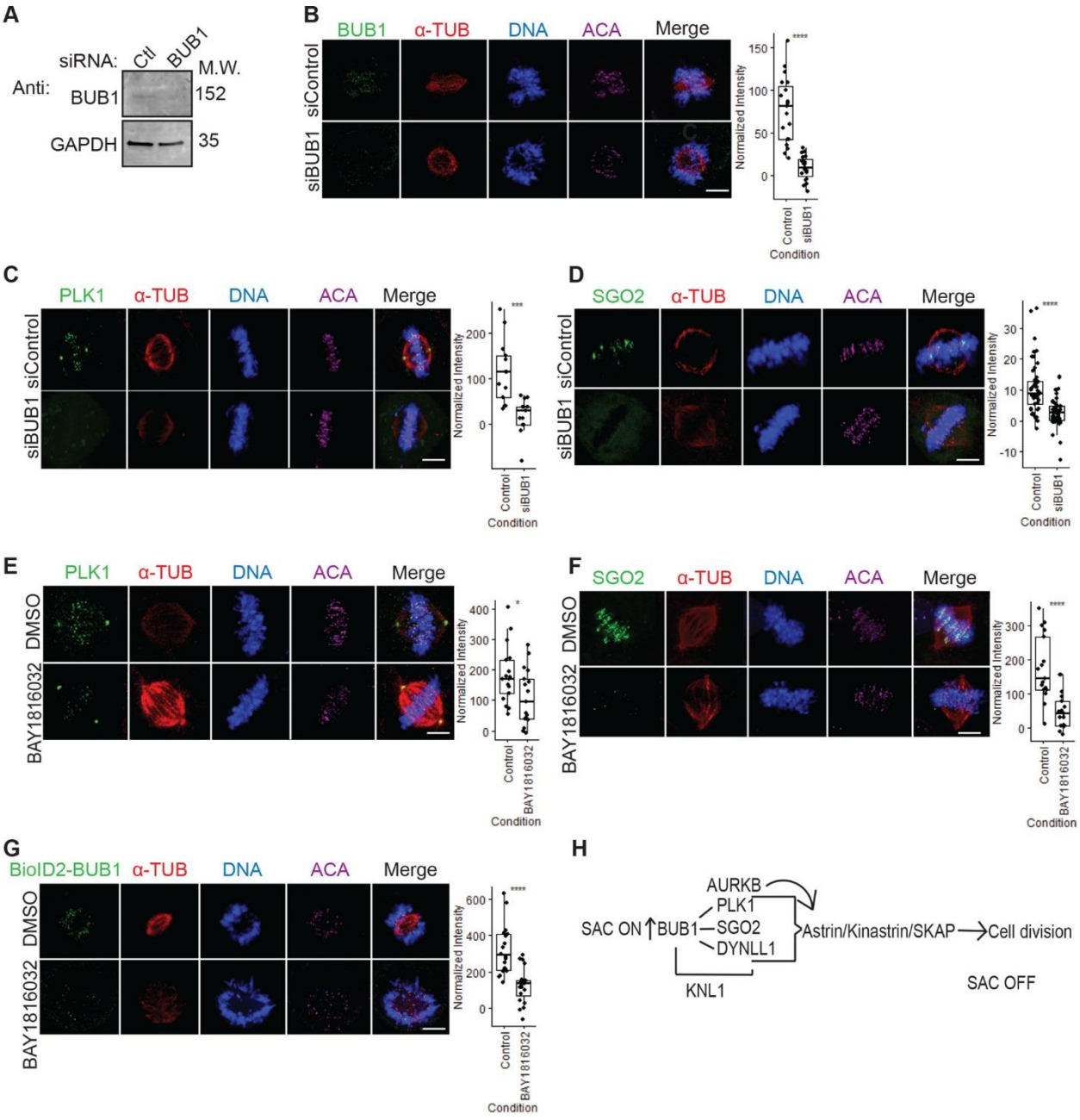

Figure 5. BUB1 as a hub for organizing the metaphase to anaphase transition. (A) Immunoblot analysis of protein extracts isolated from HeLa cells treated with control (Ctl) or BUB1 siRNA. GAPDH was used as a loading control. (B-D) Fixed-cell immunofluorescence microscopy of mitotic HeLa cells treated with control siRNA (siControl) or siRNA targeting BUB1 (siBUB1). Cells were fixed and stained with Hoechst 33342 DNA dye and anti-BUB1 (B), anti-PLK1 (C), or anti-SGO2 (D) antibodies, along with anti-α-Tubulin and anti-centromere antibodies (ACA). Bars

indicate 5μm. Box plots on the right of each panel show the quantification of the normalized fluorescence intensity for kinetochore-localized BUB1 (B), PLK1 (C), or SGO2 (D) and **** denotes a P-value < 0.001. (E-F) Same as in A, except that RPE cells were used and treated with control DMSO vehicle or the BUB1 kinase inhibitor BAY 1816032. Note that the levels of kinetochore-localized PLK1 (E) and SGO2 (F) decrease in BAY 1816032-treated cells. Bars indicate 5μm. Box plots on the right of each panel show the quantification of the normalized fluorescence intensity for kinetochore-localized PLK1 (E, * indicates P-value of 0.027) or SGO2 (F, **** indicates P-value < 0.001). (G) Same as in E-F, except that a HeLa BioID2-BUB1 expressing cell line was used. Bar indicates 5μm. Box plot shows the quantification of the normalized fluorescence intensity for kinetochore-localized BioID2-BUB1, **** indicates P-value < 0.001. (H) Model of BUB1 as an organizer of the metaphase to anaphase transition. BUB1 is critical for SAC protein binding to KNL1 to establish the SAC response and is also critical for the recruitment of the Astrin-Kinastrin minor complex, which is essential for the metaphase to anaphase transition.

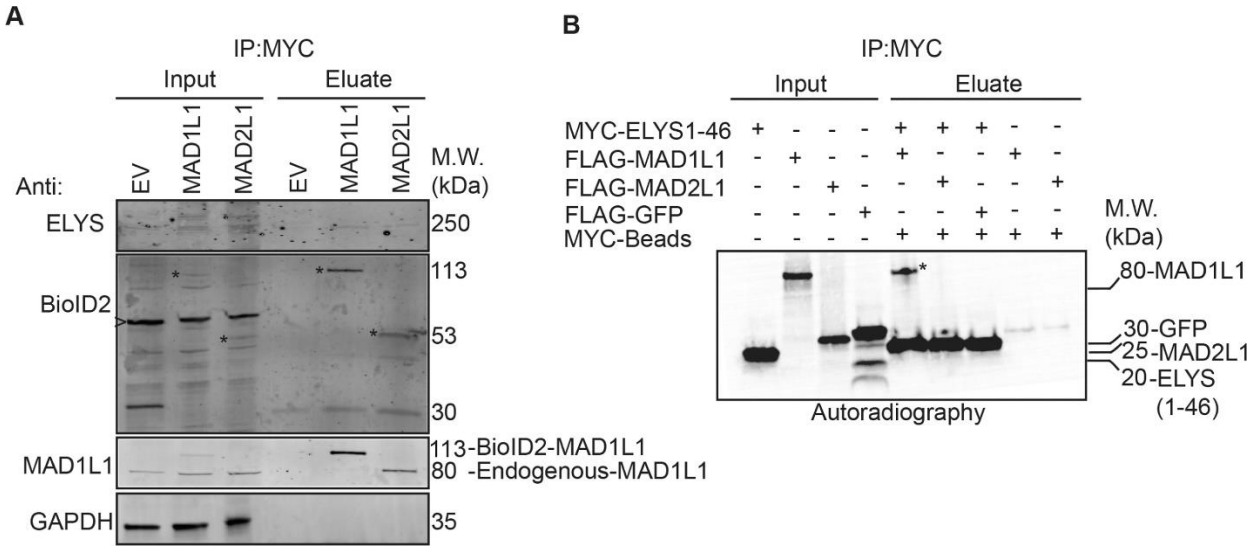

Figure 6. ELYS binds to MAD1L1 and MAD2L1 in mitotic cell lysates and to MAD1L1 *in vitro*. (A) BioID2-Myc (empty vector, EV), BioID2-Myc-MAD1L1, or BioID2-Myc-MAD2L1 inducible HeLa stable cell lines were induced with Dox and treated with 100 nM Taxol to arrest cells in mitosis. Mitotic cell lysates were then used for Myc immunoprecipitations and subjected to immunoblot analysis with the indicated antibodies. Note that endogenous ELYS immunoprecipitates with BioID2-Myc-tagged MAD1L1 and MAD2L1. Asterisks indicate BioID2-Myc-MAD1L1 or BioID2-Myc-MAD2L1 in the inputs or eluates. Arrow head indicates non-specific background band recognized by the anti-BioID2 antibody. (B) ^{35}S-radiolabeled Myc-ELYS N-terminal fragment (ELYS1-46, first 46 amino acids), FLAG-MAD1L1, FLAG-MAD2L1, and FLAG-GFP (control) were used in *in vitro* binding assays. Myc immunoprecipitations were resolved by western blotting and the blots were analyzed by autoradiography. Note that the ELYS N-terminal fragment binds to MAD1L1 and not MAD2L1.

REFERENCES

1. Holland, A. J., and Cleveland, D. W. (2009) Boveri revisited: chromosomal instability, aneuploidy and tumorigenesis. *Nat Rev Mol Cell Biol* **10**, 478-487
2. Musacchio, A., and Salmon, E. D. (2007) The spindle-assembly checkpoint in space and time. *Nat Rev Mol Cell Biol* **8**, 379-393
3. Gelens, L., Qian, J., Bollen, M., and Saurin, A. T. (2018) The Importance of Kinase-Phosphatase Integration: Lessons from Mitosis. *Trends Cell Biol* **28**, 6-21
4. Foley, E. A., and Kapoor, T. M. (2013) Microtubule attachment and spindle assembly checkpoint signalling at the kinetochore. *Nat Rev Mol Cell Biol* **14**, 25-37
5. Liu, S. T., and Zhang, H. (2016) The mitotic checkpoint complex (MCC): looking back and forth after 15 years. *AIMS Mol Sci* **3**, 597-634
6. Sudakin, V., Chan, G. K., and Yen, T. J. (2001) Checkpoint inhibition of the APC/C in HeLa cells is mediated by a complex of BUBR1, BUB3, CDC20, and MAD2. *J Cell Biol* **154**, 925-936
7. Stemmann, O., Zou, H., Gerber, S. A., Gygi, S. P., and Kirschner, M. W. (2001) Dual inhibition of sister chromatid separation at metaphase. *Cell* **107**, 715-726
8. Matson, D. R., and Stukenberg, P. T. (2011) Spindle poisons and cell fate: a tale of two pathways. *Mol Interv* **11**, 141-150
9. Ricke, R. M., and van Deursen, J. M. (2011) Correction of microtubule-kinetochore attachment errors: mechanisms and role in tumor suppression. *Semin Cell Dev Biol* **22**, 559-565

10. Hauf, S. (2013) The spindle assembly checkpoint: progress and persistent puzzles. *Biochem Soc Trans* **41**, 1755-1760

11. Corbett, K. D. (2017) Molecular Mechanisms of Spindle Assembly Checkpoint Activation and Silencing. *Prog Mol Subcell Biol* **56**, 429-455

12. Musacchio, A. (2015) The Molecular Biology of Spindle Assembly Checkpoint Signaling Dynamics. *Curr Biol* **25**, R1002-1018

13. Dou, Z., Prifti, D. K., Gui, P., Liu, X., Elowe, S., and Yao, X. (2019) Recent Progress on the Localization of the Spindle Assembly Checkpoint Machinery to Kinetochores. *Cells* **8**

14. Go, C. D., Knight, J. D. R., Rajasekharan, A., Rathod, B., Hesketh, G. G., Abe, K. T., Youn, J.-Y., Samavarchi-Tehrani, P., Zhang, H., Zhu, L. Y., Popiel, E., Lambert, J.-P., Coyaud, É., Cheung, S. W. T., Rajendran, D., Wong, C. J., Antonicka, H., Pelletier, L., Raught, B., Palazzo, A. F., Shoubridge, E. A., and Gingras, A.-C. (2019) A proximity biotinylation map of a human cell. *bioRxiv*, 796391

15. Firat-Karalar, E. N., and Stearns, T. (2015) Probing mammalian centrosome structure using BioID proximity-dependent biotinylation. *Methods Cell Biol* **129**, 153-170

16. Roux, K. J., Kim, D. I., and Burke, B. (2013) BioID: a screen for protein-protein interactions. *Curr Protoc Protein Sci* **74**, Unit 19 23

17. Mehus, A. A., Anderson, R. H., and Roux, K. J. (2016) BioID Identification of Lamin-Associated Proteins. *Methods Enzymol* **569**, 3-22

18. Kim, D. I., Jensen, S. C., Noble, K. A., Kc, B., Roux, K. H., Motamedchaboki, K., and Roux, K. J. (2016) An improved smaller biotin ligase for BioID proximity labeling. *Mol Biol Cell* **27**, 1188-1196

19. Gupta, G. D., Coyaud, E., Goncalves, J., Mojarad, B. A., Liu, Y., Wu, Q., Gheiratmand, L., Comartin, D., Tkach, J. M., Cheung, S. W., Bashkurov, M., Hasegan, M., Knight, J. D., Lin, Z. Y., Schueler, M., Hildebrandt, F., Moffat, J., Gingras, A. C., Raught, B., and Pelletier, L. (2015) A Dynamic Protein Interaction Landscape of the Human Centrosome-Cilium Interface. *Cell* **163**, 1484-1499

20. Senese, S., Cheung, K., Lo, Y. C., Gholkar, A. A., Xia, X., Wohlschlegel, J. A., and Torres, J. Z. (2015) A unique insertion in STARD9's motor domain regulates its stability. *Mol Biol Cell* **26**, 440-452

21. Siemeister, G., Mengel, A., Fernandez-Montalvan, A. E., Bone, W., Schroder, J., Zitzmann-Kolbe, S., Briem, H., Prechtl, S., Holton, S. J., Monning, U., von Ahsen, O., Johanssen, S., Cleve, A., Putter, V., Hitchcock, M., von Nussbaum, F., Brands, M., Ziegelbauer, K., and Mumberg, D. (2019) Inhibition of BUB1 Kinase by BAY 1816032 Sensitizes Tumor Cells toward Taxanes, ATR, and PARP Inhibitors In Vitro and In Vivo. *Clin Cancer Res* **25**, 1404-1414

22. Torres, J. Z., Miller, J. J., and Jackson, P. K. (2009) High-throughput generation of tagged stable cell lines for proteomic analysis. *Proteomics* **9**, 2888-2891

23. Bradley, M., Ramirez, I., Cheung, K., Gholkar, A. A., and Torres, J. Z. (2016) Inducible LAP-tagged Stable Cell Lines for Investigating Protein Function, Spatiotemporal Localization and Protein Interaction Networks. *J Vis Exp* **118**, 54870

24. Rappsilber, J., Mann, M., and Ishihama, Y. (2007) Protocol for micro-purification, enrichment, pre-fractionation and storage of peptides for proteomics using StageTips. *Nat Protoc* **2**, 1896-1906

25. Cheung, K., Senese, S., Kuang, J., Bui, N., Ongpipattanakul, C., Gholkar, A., Cohn, W., Capri, J., Whitelegge, J. P., and Torres, J. Z. (2016) Proteomic Analysis of the Mammalian Katanin Family of Microtubule-severing Enzymes Defines Katanin p80 subunit B-like 1 (KATNBL1) as a Regulator of Mammalian Katanin Microtubule-severing. *Mol Cell Proteomics* **15**, 1658-1669

26. Ishihama, Y., Oda, Y., Tabata, T., Sato, T., Nagasu, T., Rappsilber, J., and Mann, M. (2005) Exponentially modified protein abundance index (emPAI) for estimation of absolute protein amount in proteomics by the number of sequenced peptides per protein. *Mol Cell Proteomics* **4**, 1265-1272

27. Baez-Saldana, A., Zendejas-Ruiz, I., Revilla-Monsalve, C., Islas-Andrade, S., Cardenas, A., Rojas-Ochoa, A., Vilches, A., and Fernandez-Mejia, C. (2004) Effects of biotin on pyruvate carboxylase, acetyl-CoA carboxylase, propionyl-CoA carboxylase, and markers for glucose and lipid homeostasis in type 2 diabetic patients and nondiabetic subjects. *Am J Clin Nutr* **79**, 238-243

28. Giurgiu, M., Reinhard, J., Brauner, B., Dunger-Kaltenbach, I., Fobo, G., Frishman, G., Montrone, C., and Ruepp, A. (2019) CORUM: the comprehensive resource of mammalian protein complexes-2019. *Nucleic Acids Res* **47**, D559-D563

29. Stark, C., Breitkreutz, B. J., Reguly, T., Boucher, L., Breitkreutz, A., and Tyers, M. (2006) BioGRID: a general repository for interaction datasets. *Nucleic Acids Res* **34**, D535-539

30. Ashburner, M., Ball, C. A., Blake, J. A., Botstein, D., Butler, H., Cherry, J. M., Davis, A. P., Dolinski, K., Dwight, S. S., Eppig, J. T., Harris, M. A., Hill, D. P., Issel-Tarver, L., Kasarskis, A., Lewis, S., Matese, J. C., Richardson, J. E., Ringwald, M., Rubin, G. M., and Sherlock, G. (2000) Gene ontology: tool for the unification of biology. The Gene Ontology Consortium. *Nat Genet* **25**, 25-29

31. Jassal, B., Matthews, L., Viteri, G., Gong, C., Lorente, P., Fabregat, A., Sidiropoulos, K., Cook, J., Gillespie, M., Haw, R., Loney, F., May, B., Milacic, M., Rothfels, K., Sevilla, C., Shamovsky, V., Shorser, S., Varusai, T., Weiser, J., Wu, G., Stein, L., Hermjakob, H., and D'Eustachio, P. (2020) The reactome pathway knowledgebase. *Nucleic Acids Res* **48**, D498-D503

32. Shannon, P., Markiel, A., Ozier, O., Baliga, N. S., Wang, J. T., Ramage, D., Amin, N., Schwikowski, B., and Ideker, T. (2003) Cytoscape: a software environment for integrated models of biomolecular interaction networks. *Genome Res* **13**, 2498-2504

33. Franz, M., Lopes, C. T., Huck, G., Dong, Y., Sumer, O., and Bader, G. D. (2016) Cytoscape.js: a graph theory library for visualisation and analysis. *Bioinformatics* **32**, 309-311

34. Xia, X., Gholkar, A., Senese, S., and Torres, J. Z. (2015) A LCMT1-PME-1 methylation equilibrium controls mitotic spindle size. *Cell Cycle* **14**, 1938-1947

35. Joglekar, A. P. (2016) A Cell Biological Perspective on Past, Present and Future Investigations of the Spindle Assembly Checkpoint. *Biology (Basel)* **5**

36. Zhang, G., Mendez, B. L., Sedgwick, G. G., and Nilsson, J. (2016) Two functionally distinct kinetochore pools of BubR1 ensure accurate chromosome segregation. *Nat Commun* **7**, 12256

37. Kulukian, A., Han, J. S., and Cleveland, D. W. (2009) Unattached kinetochores catalyze production of an anaphase inhibitor that requires a Mad2 template to prime Cdc20 for BubR1 binding. *Dev Cell* **16**, 105-117

38. Taylor, S. S., Ha, E., and McKeon, F. (1998) The human homologue of Bub3 is required for kinetochore localization of Bub1 and a Mad3/Bub1-related protein kinase. *J Cell Biol* **142**, 1-11

39. Overlack, K., Primorac, I., Vleugel, M., Krenn, V., Maffini, S., Hoffmann, I., Kops, G. J., and Musacchio, A. (2015) A molecular basis for the differential roles of Bub1 and BubR1 in the spindle assembly checkpoint. *Elife* **4**, e05269

40. De Antoni, A., Pearson, C. G., Cimini, D., Canman, J. C., Sala, V., Nezi, L., Mapelli, M., Sironi, L., Faretta, M., Salmon, E. D., and Musacchio, A. (2005) The Mad1/Mad2 complex as a template for Mad2 activation in the spindle assembly checkpoint. *Curr Biol* **15**, 214-225

41. Zhang, G., Kruse, T., Lopez-Mendez, B., Sylvestersen, K. B., Garvanska, D. H., Schopper, S., Nielsen, M. L., and Nilsson, J. (2017) Bub1 positions Mad1 close to KNL1 MELT repeats to promote checkpoint signalling. *Nat Commun* **8**, 15822

42. Maskell, D. P., Hu, X. W., and Singleton, M. R. (2010) Molecular architecture and assembly of the yeast kinetochore MIND complex. *J Cell Biol* **190**, 823-834

43. Petrovic, A., Pasqualato, S., Dube, P., Krenn, V., Santaguida, S., Cittaro, D., Monzani, S., Massimiliano, L., Keller, J., Tarricone, A., Maiolica, A., Stark, H., and Musacchio, A. (2010) The MIS12 complex is a protein interaction hub for outer kinetochore assembly. *Journal of Cell Biology* **190**, 835-852

44. Kline, S. L., Cheeseman, I. M., Hori, T., Fukagawa, T., and Desai, A. (2006) The human Mis12 complex is required for kinetochore assembly and proper chromosome segregation. *J Cell Biol* **173**, 9-17

45. Screpanti, E., De Antoni, A., Alushin, G. M., Petrovic, A., Melis, T., Nogales, E., and Musacchio, A. (2011) Direct Binding of Cenp-C to the Mis12 Complex Joins the Inner and Outer Kinetochore. *Curr Biol* **21**, 391-398

46. Obuse, C., Iwasaki, O., Kiyomitsu, T., Goshima, G., Toyoda, Y., and Yanagida, M. (2004) A conserved Mis12 centromere complex is linked to heterochromatic HP1 and outer kinetochore protein Zwint-1. *Nat Cell Biol* **6**, 1135-1141

47. Ghongane, P., Kapanidou, M., Asghar, A., Elowe, S., and Bolanos-Garcia, V. M. (2014) The dynamic protein Knl1 - a kinetochore rendezvous. *J Cell Sci* **127**, 3415-3423

48. Rodriguez-Rodriguez, J. A., Lewis, C., McKinley, K. L., Sikirzhytski, V., Corona, J., Maciejowski, J., Khodjakov, A., Cheeseman, I. M., and Jallepalli, P. V. (2018) Distinct Roles of RZZ and Bub1-KNL1 in Mitotic Checkpoint Signaling and Kinetochore Expansion. *Curr Biol* **28**, 3422-3429 e3425

49. Krenn, V., Wehenkel, A., Li, X., Santaguida, S., and Musacchio, A. (2012) Structural analysis reveals features of the spindle checkpoint kinase Bub1-kinetochore subunit Knl1 interaction. *J Cell Biol* **196**, 451-467

50. Mora-Santos, M. D., Hervas-Aguilar, A., Sewart, K., Lancaster, T. C., Meadows, J. C., and Millar, J. B. (2016) Bub3-Bub1 Binding to Spc7/KNL1 Toggles the Spindle Checkpoint Switch by Licensing the Interaction of Bub1 with Mad1-Mad2. *Curr Biol* **26**, 2642-2650

51. Dunsch, A. K., Linnane, E., Barr, F. A., and Gruneberg, U. (2011) The astrin-kinastrin/SKAP complex localizes to microtubule plus ends and facilitates chromosome alignment. *J Cell Biol* **192**, 959-968

52. Thein, K. H., Kleylein-Sohn, J., Nigg, E. A., and Gruneberg, U. (2007) Astrin is required for the maintenance of sister chromatid cohesion and centrosome integrity. *J Cell Biol* **178**, 345-354

53. Kern, D. M., Monda, J. K., Su, K. C., Wilson-Kubalek, E. M., and Cheeseman, I. M. (2017) Astrin-SKAP complex reconstitution reveals its kinetochore interaction with microtubule-bound Ndc80. *Elife* **6**

54. Ikeda, M., and Tanaka, K. (2017) Plk1 bound to Bub1 contributes to spindle assembly checkpoint activity during mitosis. *Sci Rep* **7**, 8794

55. Asghar, A., Lajeunesse, A., Dulla, K., Combes, G., Thebault, P., Nigg, E. A., and Elowe, S. (2015) Bub1 autophosphorylation feeds back to regulate kinetochore docking and promote localized substrate phosphorylation. *Nat Commun* **6**, 8364

56. El Yakoubi, W., Buffin, E., Cladiere, D., Gryaznova, Y., Berenguer, I., Touati, S. A., Gomez, R., Suja, J. A., van Deursen, J. M., and Wassmann, K. (2017) Mps1 kinase-dependent Sgo2 centromere localisation mediates cohesin protection in mouse oocyte meiosis I. *Nat Commun* **8**, 694

57. Baron, A. P., von Schubert, C., Cubizolles, F., Siemeister, G., Hitchcock, M., Mengel, A., Schroder, J., Fernandez-Montalvan, A., von Nussbaum, F., Mumberg, D., and Nigg, E. A. (2016) Probing the catalytic functions of Bub1 kinase using the small molecule inhibitors BAY-320 and BAY-524. *Elife* **5**

58. Gassmann, R., Henzing, A. J., and Earnshaw, W. C. (2005) Novel components of human mitotic chromosomes identified by proteomic analysis of the chromosome scaffold fraction. *Chromosoma* **113**, 385-397

59. Tadeu, A. M., Ribeiro, S., Johnston, J., Goldberg, I., Gerloff, D., and Earnshaw, W. C. (2008) CENP-V is required for centromere organization, chromosome alignment and cytokinesis. *EMBO J* **27**, 2510-2522

60. Boyarchuk, Y., Salic, A., Dasso, M., and Arnaoutov, A. (2007) Bub1 is essential for assembly of the functional inner centromere. *J Cell Biol* **176**, 919-928

61. Lee, S. H., McCormick, F., and Saya, H. (2010) Mad2 inhibits the mitotic kinesin MKlp2. *J Cell Biol* **191**, 1069-1077

62. Scott, R. J., Lusk, C. P., Dilworth, D. J., Aitchison, J. D., and Wozniak, R. W. (2005) Interactions between Mad1p and the nuclear transport machinery in the yeast Saccharomyces cerevisiae. *Mol Biol Cell* **16**, 4362-4374

63. Lee, S. H., Sterling, H., Burlingame, A., and McCormick, F. (2008) Tpr directly binds to Mad1 and Mad2 and is important for the Mad1-Mad2-mediated mitotic spindle checkpoint. *Genes Dev* **22**, 2926-2931

64. Lussi, Y. C., Shumaker, D. K., Shimi, T., and Fahrenkrog, B. (2010) The nucleoporin Nup153 affects spindle checkpoint activity due to an association with Mad1. *Nucleus* **1**, 71-84

65. Rodenas, E., Gonzalez-Aguilera, C., Ayuso, C., and Askjaer, P. (2012) Dissection of the NUP107 nuclear pore subcomplex reveals a novel interaction with spindle assembly checkpoint protein MAD1 in Caenorhabditis elegans. *Mol Biol Cell* **23**, 930-944

66. Rodriguez-Bravo, V., Maciejowski, J., Corona, J., Buch, H. K., Collin, P., Kanemaki, M. T., Shah, J. V., and Jallepalli, P. V. (2014) Nuclear pores protect genome integrity by assembling a premitotic and Mad1-dependent anaphase inhibitor. *Cell* **156**, 1017-1031

67. Gonzalez-Aguilera, C., and Askjaer, P. (2012) Dissecting the NUP107 complex: multiple components and even more functions. *Nucleus* **3**, 340-348

68. Mossaid, I., and Fahrenkrog, B. (2015) Complex Commingling: Nucleoporins and the Spindle Assembly Checkpoint. *Cells* **4**, 706-725

69. Rasala, B. A., Orjalo, A. V., Shen, Z., Briggs, S., and Forbes, D. J. (2006) ELYS is a dual nucleoporin/kinetochore protein required for nuclear pore assembly and proper cell division. *Proc Natl Acad Sci U S A* **103**, 17801-17806

70. Hattersley, N., Cheerambathur, D., Moyle, M., Stefanutti, M., Richardson, A., Lee, K. Y., Dumont, J., Oegema, K., and Desai, A. (2016) A Nucleoporin Docks Protein Phosphatase 1 to Direct Meiotic Chromosome Segregation and Nuclear Assembly. *Dev Cell* **38**, 463-477

71. Hattersley, N., and Desai, A. (2017) The nucleoporin MEL-28/ELYS: A PP1 scaffold during M-phase exit. *Cell Cycle* **16**, 489-490

72. Samavarchi-Tehrani, P., Samson, R., and Gingras, A. C. (2020) Proximity Dependent Biotinylation: Key Enzymes and Adaptation to Proteomics Approaches. *Mol Cell Proteomics* **19**, 757-773

73. Branon, T. C., Bosch, J. A., Sanchez, A. D., Udeshi, N. D., Svinkina, T., Carr, S. A., Feldman, J. L., Perrimon, N., and Ting, A. Y. (2018) Efficient proximity labeling in living cells and organisms with TurboID. *Nat Biotechnol* **36**, 880-887

74. Youn, J. Y., Dunham, W. H., Hong, S. J., Knight, J. D. R., Bashkurov, M., Chen, G. I., Bagci, H., Rathod, B., MacLeod, G., Eng, S. W. M., Angers, S., Morris, Q., Fabian, M., Cote, J. F., and Gingras, A. C. (2018) High-Density Proximity Mapping Reveals the Subcellular Organization of mRNA-Associated Granules and Bodies. *Mol Cell* **69**, 517-532 e511

75. Coyaud, E., Mis, M., Laurent, E. M., Dunham, W. H., Couzens, A. L., Robitaille, M., Gingras, A. C., Angers, S., and Raught, B. (2015) BioID-based Identification of Skp Cullin F-box (SCF)beta-TrCP1/2 E3 Ligase Substrates. *Mol Cell Proteomics* **14**, 1781-1795

76. Remnant, L., Booth, D. G., Vargiu, G., Spanos, C., Kerr, A. R. W., and Earnshaw, W. C. (2019) In vitro BioID: mapping the CENP-A microenvironment with high temporal and spatial resolution. *Mol Biol Cell* **30**, 1314-1325